

THE PRODUCTION OF ALGAL BIODIESEL USING HYDROTHERMAL CARBONIZATION  
AND IN SITU TRANSESTERIFICATION

by

Robert Bernard Levine

A dissertation submitted in partial fulfillment  
of the requirements for the degree of  
Doctor of Philosophy  
(Chemical Engineering)  
in The University of Michigan  
2013

Doctoral Committee:

Professor Phillip E. Savage, Chair  
Brian Goodall, Valicor Renewables  
Professor Nancy G. Love  
Professor Henry Y. Wang  
Distinguished University Professor Emeritus Walter J. Weber, Jr.

© Robert Bernard Levine 2013

## DEDICATION

To my mother Rita.

## ACKNOWLEDGEMENTS

This work would not have been possible without the mentorship provided by my advisor Phil Savage and the outstanding committee members who helped guide me towards its final form. These individuals generously shared with me wisdom gained over many years in their respective fields. I am grateful for their interest in my work as well as my professional development, and I thank them for giving freely of their time and ideas.

I also wish to acknowledge my fellow graduate students, both in the Savage Group and beyond, for creating a vibrant community of scholarship. In particular, my time at the University of Michigan was influenced by fellow group members Shujauddin Changi, Jacob Dickenson, Julia Faeth, Chad Huelsman, Tannawan Pinnarat, and Peter Valdez, as well as Michael Hoepfner, Aaron Shinkle, Elizabeth Stuart, and Huanan Zhang. I also want to thank the many undergraduates who I had the experience of working, including Alexandra Bollas, Matthew Durham, Anna Jenks, and Sita Syal.

My sincere gratitude also goes to the excellent staff of the Chemical Engineering Department. In particular, Pablo Lavallo was instrumental in helping me acquire much of the instrumentation required to carry out this work, and his creativity, willingness to share, and can-do attitude made working with him a pleasure. Likewise, Harald Eberhart, our glassblower, never ceased to amaze me with new solutions to my problems and his unwavering generosity. Finally, I wish to acknowledge the support of the administrative professionals who helped me in countless ways (Pam Bogdanski, Susan Hamlin, Shelley Fellers, Laurel Neff).

Finally, I acknowledge financial support from an NSF Graduate Research Fellowship, a University of Michigan Graham Environmental Sustainability Institute Fellowship, and a University of Michigan Rackham Graduate Fellowship. I also gratefully acknowledge financial support from the University of Michigan College of Engineering and from the U.S. National Science Foundation.

## TABLE OF CONTENTS

Dedication.....	ii
Acknowledgements.....	iii
List of Tables .....	vi
List of Figures .....	viii
List of Abbreviations .....	xi
Abstract.....	xii
CHAPTER 1 Introduction .....	1
1.1 The case for biofuels .....	1
1.2 Algae as a biofuel feedstock.....	4
1.3 Process overview and chapter summaries .....	7
CHAPTER 2 Feedstock Production and Characterization.....	9
2.1 Background.....	9
2.2 Materials and methods .....	17
2.3 Results and discussion.....	25
2.4 Conclusions.....	38
CHAPTER 3 Hydrothermal Carbonization .....	39
3.1 Background.....	39
3.2 Materials and methods .....	45
3.3 Results and discussion.....	47
3.4 Conclusions.....	78
CHAPTER 4 Supercritical In Situ Transesterification .....	80
4.1 Background.....	80
4.2 Materials and methods .....	84
4.3 Results and discussion.....	87
4.4 Conclusions.....	114
CHAPTER 5 Acid-catalyzed In Situ Transesterification.....	115
5.1 Background.....	115
5.2 Materials and methods .....	116

5.3	Results and discussion.....	117
5.4	Conclusions.....	129
CHAPTER 6 Triflate-Catalyzed In Situ Transesterification.....		131
6.1	Background.....	131
6.2	Materials and methods .....	132
6.3	Results and discussion.....	134
6.4	Conclusions.....	147
CHAPTER 7 Algal Growth on the Aqueous Co-product of HTC.....		148
7.1	Backgrounds.....	148
7.2	Materials and methods .....	151
7.3	Results and discussion.....	154
7.4	Conclusions.....	170
CHAPTER 8 The Energy Balance of Algal Biodiesel Processes .....		172
8.1	Background.....	172
8.2	Methodology and model descriptions .....	176
8.3	Results and discussion.....	182
8.4	Conclusions.....	188
CHAPTER 9 Summary and Engineering Significance .....		189
Appendix A.....		192
References .....		195

## LIST OF TABLES

Table 1.1. Feedstock oil yield .....	5
Table 1.2. Fertilizer consumption and non-oil product generation related to producing 20% of US transportation fuels from algae without nutrient recycling .....	5
Table 2.1. The metabolisms of algae .....	9
Table 2.2. Algae bioreactor apparatus.....	17
Table 2.3. Media compositions.....	19
Table 2.4. Fatty acid profiles for relevant microalgae .....	35
Table 3.1. Characterization of biomass feedstock and hydrochars for <i>C. vulgaris</i> HTC at 250 °C .....	50
Table 3.2. Hydrochar characterization from <i>C. vulgaris</i> HTC at 250 °C.....	53
Table 3.3. Hydrochar elemental analysis and energy content for <i>C. protothecoides</i> hydrochars at various temperatures and 60 min .....	57
Table 3.4. Lipid composition of hydrochars from HTC reactions containing <i>C. protothecoides</i> with and without acetic acid .....	59
Table 3.5. The effect of solids loading on lipid composition of <i>Chlorella</i> hydrochars.....	61
Table 3.6. Hydrothermal carbonization yields and hydrochar characteristics for <i>Nannochloropsis</i> .....	69
Table 3.7. Hydrochar yields and lipid information from HTC (200 °C, 15 min) of algae grown in bubble column reactors.....	71
Table 3.8. Hydrochar elemental composition and energy yields <sup>a</sup> .....	73
Table 3.9. Aqueous phase analysis from HTC of <i>C. protothecoides</i> biomass for 60 min at various temperatures .....	74
Table 3.10. Aqueous phase analysis from low-temperature HTC (200 °C x 15 min) with various feedstocks .....	76
Table 4.1. Characterization of algal hydrochars used in SC-IST.....	88
Table 4.2. Crude biodiesel yield and composition from the SC-IST of hydrochar A.....	90
Table 4.3. Fatty acid ethyl ester composition of biodiesel produced through SC-IST.....	94
Table 4.4. Fatty acid ethyl ester yield from SC-IST .....	96
Table 4.5. Reaction conditions and total ester yields for factorial experiment .....	102
Table 4.6. Second order regression model for supercritical in situ transesterification of hydrochar A.....	103
Table 5.1. Characterization of algal hydrochars used in AC-IST .....	118

Table 5.2. Mineral acid-catalyzed in situ transesterification factorial experiment.....	125
Table 5.3. Regression analysis of factorial experiment .....	126
Table 6.1 Non-catalytic oleic acid esterification .....	138
Table 6.2 Triflate-catalyzed hydrolysis of ethyl oleate .....	140
Table 6.3 Characterization of carbonized solids used in TC-IST .....	142
Table 7.1. C, N, and P content in the aqueous phase co-product from hydrothermal carbonization .....	156
Table 7.2. Media N content, biomass growth, and N uptake for the growth experiment shown in Figure 7.3.....	161
Table 7.3 Biomass and Lipid Productivities (mg/L-h) for Growth Experiments in Figure 7.6 .....	167
Table 7.4. Production model for algal biorefinery using two-stage growth scheme to produce about one million gallons of biodiesel annually.....	168
Table 8.1. Model productivity assumptions and land requirements .....	177
Table 8.2. Elemental composition and estimated energy content of process materials.....	178
Table 8.3. Elemental yields .....	178
Table 8.4. Process energy input assumptions .....	179
Table 8.5. Homogenization, extraction, and transesterification process assumptions .	181
Table 8.6. Mass flows in model algal biorefinery for 5 BGY biodiesel production.....	183
Table 8.7. Summary of energy use and generation.....	184
Table 8.8. Detailed summary of process energy inputs .....	186
Table 8.9. Energy required for traditional wet hexane extraction and transesterification .....	187



## LIST OF FIGURES

Figure 1.1. Shares of energy sources in total global primary energy supply in 2008.....	2
Figure 1.2. Consumption of N and P fertilizer by all of US agriculture in comparison to algal biofuel production with varying amounts of nutrient recycling. ....	6
Figure 2.1. <i>C. vulgaris</i> biomass density and media nitrate concentration over time.....	26
Figure 2.2. Light microscopy of <i>Chlorella vulgaris</i> .....	27
Figure 2.3. Fatty acid profile of phototrophic and heterotrophic <i>C. vulgaris</i> .....	28
Figure 2.4. Biomass density and lipid content over time in sterile fermentation of <i>C. protothecoides</i> . ....	29
Figure 2.5. Biomass density and lipid content over time in non-sterile carboy fermentation of <i>C. protothecoides</i> . ....	30
Figure 2.6. Light microscopy of <i>Chlorella protothecoides</i> grown heterotrophically. ....	31
Figure 2.7. Fatty acid profile of <i>C. protothecoides</i> over time during non-sterile fermentation on glucose.....	31
Figure 2.8. Biomass density over time in shaker flasks containing <i>C. protothecoides</i> grown in standard media containing glucose, glycerol, or cellulosic hydrolysate. . ....	33
Figure 2.9. Change in fatty acid profile for developing marine bi-culture immediately following introduction of metal stress.....	34
Figure 2.10. Light microscope image of bi-culture. ....	36
Figure 3.1. The properties of liquid and supercritical water. . ....	41
Figure 3.2. Hydrolysis of triglycerides.....	44
Figure 3.3. <i>Chlorella</i> hydrochar obtained from reaction at 250° C for 30 min.....	48
Figure 3.4. Lipid content of <i>C. vulgaris</i> biomass (time 0) and hydrochars . ....	49
Figure 3.5. Lipid composition and lipid retention in <i>C. vulgaris</i> biomass and hydrochars generated by reaction at 250 °C for various times.....	51
Figure 3.6. HT-GC-FID chromatogram showing FAs (9 to 12 min), MGs (13.5 to 16 min), DGs (20 to 21 min), and TGs (22 to 24 min) of <i>Chlorella</i> hydrochars processed at 250 °C. ....	52
Figure 3.7. Light microscopy of <i>Chlorella</i> biomass processed at 230 °C for (a) 0 min, (b) 5 min, (c) 15 min, or (d) 30 min. ....	54
Figure 3.8. HTC of <i>C. protothecoides</i> biomass at 220 °C, 235 °C, and 250 °C for 30, 60, and 90 min. . ....	56
Figure 3.9. Lipid retention for <i>C. protothecoides</i> hydrochars. ....	56

Figure 3.10. Solids yield in HTC reactions containing <i>C. protothecoides</i> with and without acetic acid. ....	58
Figure 3.11. Lipid retention in hydrochars from HTC reactions containing <i>C. protothecoides</i> with and without acetic acid.....	60
Figure 3.12. HTC of <i>C. protothecoides</i> at different solids contents at 235 °C for 60 min. 61	
Figure 3.13. HTC of <i>Nannochloropsis</i> biomass at 215 °C for 15, 30 or 45 min. ....	63
Figure 3.14. Filter cakes of <i>Chlorella</i> hydrochars reacted for 15 and 30 min at 215 °C. 63	
Figure 3.15. Solids yield from low-temperature HTC of <i>Nannochloropsis</i> . ....	65
Figure 3.16. Lipid retention in hydrochars formed by low-temperature HTC of <i>Nannochloropsis</i> .....	66
Figure 3.17. GC-FID analysis of <i>Nannochloropsis</i> hydrochar (200 °C x 30 min) compared to unreacted biomass. ....	67
Figure 3.18. GC-FID analysis of isomerization in commercial omega-3 ethyl ester product. ....	68
Figure 3.19. FT-ICR-MS spectra showing molecular weight distribution of organic matter in aqueous phase co-product obtained from reacting <i>N. oculata</i> biomass at 200 °C for 15 min. ....	77
Figure 3.20. van Krevelen plot of organic compounds detected by FT-ICR-MS. ....	78
Figure 4.1. Representative GC-FID chromatogram of fatty acid ethyl esters from supercritical in situ transesterification. ....	87
Figure 4.2. Reaction water content (wt.%) for supercritical in situ transesterification of hydrochars with various amounts of azeotropic ethanol (4.4 wt.% water)..	89
Figure 4.3. Supercritical esterification of oleic acid at 275 °C with 12:1 EtOH:FA molar ratio. ....	98
Figure 4.4. Supercritical in situ transesterification of wet and dry hydrochars at 275 °C.99	
Figure 4.5. Supercritical in situ transesterification of dry hydrochar B at 275–295 °C (~20 MPa). ....	100
Figure 4.6. Parity plot comparing experimental data with regression model.....	104
Figure 4.7. Supercritical in situ transesterification of partially dried hydrochar at 275 °C..	106
Figure 4.8. Comparing in situ transesterification under sub-critical and supercritical conditions with methanol and ethanol. ....	109
Figure 4.9. Proposed process flow diagram for supercritical in situ transesterification.111	
Figure 5.1. Total fatty acid ethyl ester yield from hydrochars reacted at 80, 90, and 100 °C for 15 to 120 min..	121

Figure 5.2. Total fatty acid ethyl ester yield from hydrochars reacted at 80 or 90 °C for 90 min. ....	123
Figure 5.3. Mechanism of acid-catalyzed transesterification.....	124
Figure 5.4. Acid catalyzed in situ transesterification of <i>Nannochloropsis</i> hydrochars...	128
Figure 6.1 Contour plots of ethyl oleate yield (%) from triflate-catalyzed esterification reactions.. ....	135
Figure 6.2. Oleic acid esterification with nominally 1 mol% Sc(OTf) <sub>3</sub> and 5% water.. ...	137
Figure 6.3. Oleic acid esterification using In(OTf) <sub>3</sub> . ....	138
Figure 6.4. The effect of water and stirring on triflate-catalyzed oleic acid esterification. ....	139
Figure 6.5. Triflate-catalyzed in situ transesterification of algal hydrochars A and B. ...	144
Figure 7.1. Schematic of the repeat batch growth system .....	155
Figure 7.2. Schematic of proposed two-stage growth system with one repeat batch seed reactor and three batch or fed-batch production reactors.....	158
Figure 7.3. Biomass density (a) and lipid content (b) over time in cultures containing control media or aqueous phase with and without supplemental nutrients.. ....	160
Figure 7.4. Bubble column reactors (BCRs) in a nutrient replete state (green) and nutrient-deprived state (yellow). ....	162
Figure 7.5. Biomass density (a) and lipid content (b) over time in cultures containing control media or aqueous phase with various seed sizes and recycled media.....	165
Figure 8.1. Simplified process flow diagram.....	177
Figure 8.2. Summary of energy use as a percentage of the total energy consumed.....	185

## LIST OF ABBREVIATIONS

Abbreviation	Meaning
AC-IST	acid-catalyzed in situ transesterification
AP	aqueous phase
BCR	bubble column reactor
BGY	billion gallons per year
BPD	barrels per day (oil)
CHG	catalytic hydrothermal gasification
CLE	crude lipid extract
DG	diglyceride
EIA	US Energy Information Administration
EPA	eicosapentaenoic acid (C20:5 fatty acid)
FA	fatty acid
FAEE	fatty acid ethyl ester
FAME	fatty acid methyl ester
FER	fossil energy ratio
FT-ICR-MS	Fourier transform ion cyclotron mass spectrometry
GC-FID	gas chromatography flame ionization detector
GHG	greenhouse gas
GREET	The Greenhouse Gases, Regulated Emissions, and Energy Use in Transportation Model (Argonne National Laboratory)
GWP	global warming potential
HHV	higher heating value
HIP	hexane:isopropanol mixture (3:2 v/v)
HTC	hydrothermal carbonization
HTL	hydrothermal liquefaction
IPCC	Intergovernmental Panel on Climate Change
IST	in situ transesterification
ISTD	internal standard
LCA	life-cycle assessment
LEC	lipid-extracted char
MG	monoglyceride
MT	metric ton
PTW	pump to well
RCF	relative centrifugal force (g-force)
SC-IST	supercritical in situ transesterification
SS	stainless steel
TC-IST	triflate-catalyzed in situ transesterification
TFF	tangential flow filtration
TG	triglyceride
USDA	US Department of Agriculture
WTP	well to pump
WTW	well to wheels

## ABSTRACT

Increasing demand for liquid transportation fuels and growing concerns about the impacts of our continued reliance on petroleum have encouraged the use of plant-based, alternative fuels. Recently, interest has grown in using oleaginous microalgae as a biofuel feedstock, largely on the promise of high oil yields and the ability to use abandoned or unproductive land along with brackish, salt, or wastewaters instead of freshwater. The production of biofuels from algae, however, is complicated by the fact that algae are commonly grown as a dilute suspension of biomass in water and require large amounts of nitrogen and phosphorus fertilizers. In this work, we developed a novel biorefinery concept for the production of algal biodiesel that incorporates nutrient recycling while obviating biomass drying and organic solvent use for lipid extraction.

We first grew algae, both photo- and heterotrophically, to produce biomass containing lipids suitable for conversion into biodiesel. This biomass was then dewatered to a 15–25% solids paste and reacted in and with subcritical liquid water (180–250 °C) in a process known as hydrothermal carbonization (HTC). During HTC, about half of the mass of the algae cell dissolves into the aqueous phase, forming a nutrient-rich co-product, while the remainder conglomerates into a hydrochar that can be recovered by filtration or centrifugation. Our work revealed that nearly all of the lipids present in the algae remain in the hydrochar and that this solid can be readily dried for downstream fuel conversion, if necessary. In growth experiments with a unique marine bi-culture developed in our laboratory, we found that the aqueous phase co-product supported algal growth and could replace roughly 50% of nitrogen and phosphorous fertilizers used in common media.

The lipids within hydrochars were then converted into fatty acid ethyl esters (FAEEs) without prior extraction by in situ transesterification (IST). We investigated uncatalyzed, supercritical IST as well as mineral acid and rare-earth triflate-catalyzed IST to determine

how best to achieve high biodiesel yields with low ethanol loadings. With *Chlorella* hydrochars containing 45–75% lipids, 80–90% yields were achievable at moderate ethanol loadings (5–20 ethanol:fatty acid molar ratios) in uncatalyzed reactions at 275 °C. Similarly high yields could be achieved with triflate catalysts at 215 °C and in mineral-acid catalyzed reactions at 80–100 °C, but the former is complicated by difficult catalyst recovery and the latter requires a substantial excess of ethanol (>100:1 ethanol:fatty acid molar ratios). Notably, both supercritical and triflate-catalyzed IST demonstrated a very high tolerance for feedstock moisture, which is helpful to reduce the energy associated with drying hydrochars. With all three IST routes, severe reaction conditions were found to reduce biodiesel yields due to the thermal degradation of unsaturated fatty acids. As a result, we focused on maximizing yields at temperatures that kept thermal losses to a minimum while using the least amount of ethanol. We also extended this work to the marine species *Nannochloropsis*, which is unique in that it produces both high-value oils (e.g., eicosapentaenoic fatty acid) as well as fatty acids suitable for biodiesel.

Based on our experimental work, we modeled the mass and energy flows associated with a hypothetical algal biorefinery capable of producing 5 billion gallons per year of biodiesel. These data suggest that HTC and supercritical IST can significantly reduce the energy associated with processing wet algal biomass relative to wet hexane extraction and traditional transesterification, perhaps by as much as 50%. In addition, this work highlighted the importance of effectively converting the non-lipid fraction of the biomass into usable nutrients as well as a source for on-site heat and power. Overall, this work provides new information related to hydrothermal processing of algal biomass at subcritical conditions and demonstrates that lipids within algal hydrochars can be extracted and converted into biodiesel in a single unit operation using ethanol.

## CHAPTER 1

### INTRODUCTION

#### 1.1 The case for biofuels

Worldwide energy demand, particularly for high-density liquid transportation fuels, continues to rise as populations grow and become more affluent. In 2008, about 500 EJ of total primary energy was consumed by Earth's 6.7 billion inhabitants (EIA, 2011). About 35% of this energy, equivalent to 86 million barrels per day (BPD), was in the form of liquid fuels. By 2035, a global population of over 9 billion is estimated to demand about 815 EJ of energy and 112 million BPD of liquid fuels (EIA, 2011). Just as fossil fuel consumption today contributes to climate change, ecosystem damage, and poor energy security for many nations, meeting future demands for energy by using more fossil fuels will only continue to exacerbate these consequences.

According to the Intergovernmental Panel on Climate Change (IPCC), the consumption of fossil fuels is the largest contributor to global anthropogenic greenhouse gas (GHG) emissions (IPCC, 2012). By some estimates, our planet has already warmed about 1 °C since pre-industrial times and will likely continue warming beyond a 2 °C increase unless the concentration of GHGs in the atmosphere stabilizes around 500 ± 50 parts per million (Pacala and Socolow, 2004; Arnell et al., 2013; Davis et al., 2013). This is the proposed range above which the more detrimental impacts of climate change, such as sea level rise, ocean acidification, drought, and severe weather events, are expected to significantly worsen. Considering that the EIA baseline model predicts global energy-related carbon emissions will rise from about 30 billion metric tons (MT) in 2008 to 43 billion MT in 2035, it is critical that we pursue disruptive and scalable technologies to reduce the environmental footprint of energy use.

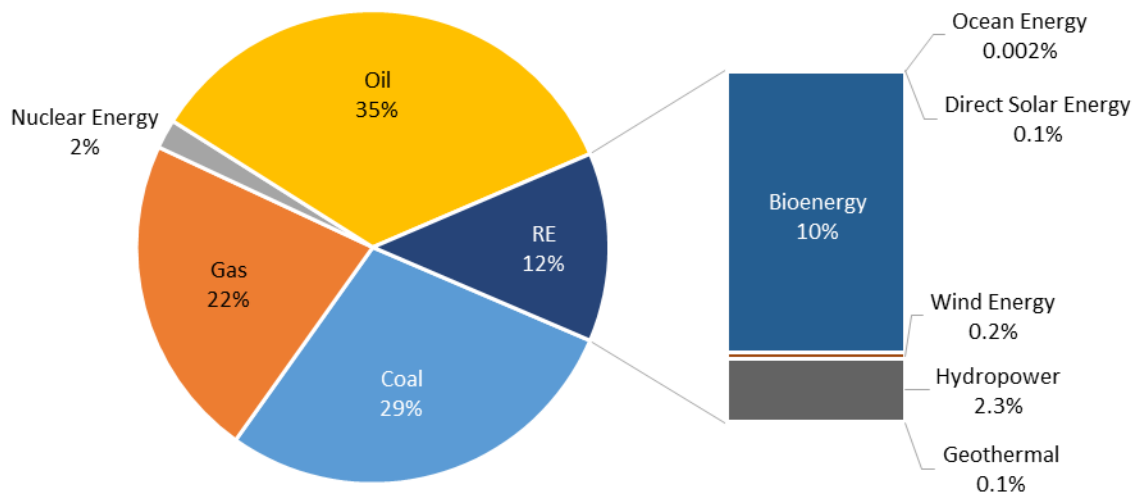


Figure 1.1. Shares of energy sources in total global primary energy supply in 2008 (492 EJ). Adapted from (IPCC, 2012).

One strategy to mitigate the rise in energy-related GHG emissions is to replace conventional fossil fuels with bioenergy. Bioenergy is defined here to include any biomass-derived energy source. It is assumed that carbon released during the combustion of these fuels is biogenic and therefore does not increase the net concentration of GHGs in the atmosphere over human time scales. As shown in Figure 1.1, bioenergy comprised only about 10% of global primary energy supply in 2008. Within this category, about 60% of the energy was derived from traditional biomass used for cooking and heating in developing countries. Liquid biofuels, which can be used to displace petroleum, only accounted for about 2% of global transportation fuels in 2008. In light of the significant reductions in GHG emissions required in the coming decades and considering that oil comprises the largest fraction of global energy use, extensive resources have been devoted to developing petroleum alternatives.

Today, the two most widely used liquid biofuels are ethanol, derived from fermenting sugarcane and corn, and biodiesel, produced by transesterifying vegetable oils from



soybean, rapeseed, palm, and similar oilseeds. Despite substantial investment and policy support, their production to date has been relatively small and resource intensive. For example, the US consumed about 56 thousand BPD of biodiesel and 844 thousand BPD of ethanol in 2012 compared to 3.7 million BPD of diesel and 8.7 million BPD of gasoline (EIA, 2013). In other words, biodiesel and fuel ethanol accounted for less than 2% and 10%, respectively, of the petroleum products they seek to replace. Although the volume of alternative fuels we currently produce is small in the context of petroleum use, the impacts associated with their production are quite large. For example, about 25% of all soybean oil produced in the US and 40% of the annual corn harvest were used for biofuels in 2012 (USDA, 2013a). To produce these feedstocks, more than 45 million acres of US farmland (or about 10% of total cropland) required water, fertilizer, and other energy inputs that limit the potential of these feedstocks to help reduce the environmental impacts of transportation (Nickerson et al., 2011). Moreover, competition with food grains, both real and perceived, has led to rising food prices and food shortages that limits the appeal of these biofuels (Gomiero et al., 2009). Finally, if one considers how forest and grassland throughout the world are converted to new cropland to replace grain diverted to fuel production, these terrestrial biofuels may actually increase GHGs. For example, it has been estimated that corn-based ethanol nearly doubles GHG emissions over 30 years and increases GHG emissions for 167 years as compared to gasoline (Searchinger et al., 2008). Although the impacts of indirect land-use change have been widely debated (Broch et al., 2013), these data nonetheless suggest that biofuels derived from grains produced on cropland currently used for food production cannot sustainably meet society's demand for fossil fuel alternatives.

If biofuel production is to help reduce our reliance on fossil fuels, new feedstocks must be developed. In the US, the Energy Policy Act of 2005 setup a Renewable Fuel Standard (RFS), which was later modified by the Energy Independence and Security Act of 2007, that now mandates 36 billion gallons per year (BGY) of renewable fuels be blended into transportation fuels by 2022. Of this total, it is expected that 15 BGY will be from first-

generation feedstocks (e.g., starch-based ethanol), while the remainder will come from biomass-based diesel, cellulosic biofuels, and other advanced alternative fuels that can demonstrate a 50% or greater reduction in life cycle emissions relative to the petroleum products they replace. Although evidence suggests that a sufficient quantity of cellulosic biomass is available in the conterminous US to meet this objective (US DOE, 2011), the technology required to convert it into liquid biofuels is only now reaching commercial scale. In fact, only about 155 million liters of cellulosic biofuels (~41 million gallons) were produced in 2012 worldwide (Bacovsky et al., 2013). One of the most promising alternatives to cellulosic biofuels being researched today is microalgae.

## 1.2 Algae as a biofuel feedstock

Interest has grown in using oleaginous microalgae as a non-edible biofuel feedstock, largely on the promise of high oil yields (Table 1.1) and the ability to use abandoned or unproductive land along with brackish, salt, or wastewaters instead of arable land and freshwater (Chisti, 2007; Hu et al., 2008; Schenk et al., 2008). Although algae exist in myriad forms, ranging from microscopic single cells on the order of 0.2-2.0  $\mu\text{m}$  in diameter to giant kelp that can reach 60 m in length, this work focuses exclusively on microalgae. Because these single cell organisms lack the high degree of differentiation found in terrestrial plants, such as roots, stems, and leaves, they can achieve about 2-fold higher photoconversion efficiency under typical growth conditions compared to the most productive terrestrial plant that fix carbon through the  $\text{C}_3$  and  $\text{C}_4$  pathways (Weyer et al., 2010). In addition, because some algae respond to certain chemical and physical stimuli by accumulating intracellular triglycerides (TGs), the most common parent material for producing biodiesel and renewable diesel, very high oil yields may be attainable (Hu et al., 2008).

Although promising in principle, microalgae present unique challenges in practice. For one, their cultivation can be nutrient intensive compared to some terrestrial bioenergy crops (Miller, 2010). A recent life-cycle assessment (LCA) estimated that fertilizer use

could account for approximately 50% of the energy and GHG emissions related to algal feedstock production (Clarens et al., 2010). In addition to becoming increasingly expensive, some fertilizer resources, such as phosphorus, are finite, mined resources (Cordell et al., 2009). If a meaningful amount of petroleum is to be displaced with algae-based fuels, N and P must be utilized efficiently.

**Table 1.1. Feedstock oil yield**

Crop	Oil Yield (L/ha-y)
Soybean	450
Camelina	560
Sunflower	955
Rapeseed	1,190
Jatropha	1,890
Oil Palm	5,950
Microalgae	3,800-50,800

Sources: (Chisti, 2007; Weyer et al., 2010)

**Table 1.2. Fertilizer consumption and non-oil product generation related to producing 20% of US transportation fuels from algae without nutrient recycling**

Fuel Type	Total US Consumption (1,000 barrels/yr)	Fertilizer Use for Algal Fuels 1,000 MT/yr (% of US total)		Non-Oil Product Generated 1,000 MT/yr (% of US total)
		Nitrogen	Phosphorus	
Motor Gasoline	3,185,312	12,000 (98)	3,000 (168)	224,800 (649)
Distillate Fuels	512,203	2,200 (18)	600 (31)	41,500 (120)
Jet Fuels	1,369,835	5,600 (45)	1,400 (78)	104,500 (302)
Combined	5,067,350	19,800 (161)	4,900 (276)	370,900 (1070)

Note. Algal biomass is assumed to contain 25% oil, 75% non-oil, 4% N, and 1% P. Volumetric petroleum consumption data for 2012 (EIA, 2013) was converted into weight by assuming densities of 740, 850, and 800 kg/m<sup>3</sup> for motor gasoline, distillate fuels, and jet fuels, respectively. Algae oil is assumed to directly replace each fuel with no change in mass and no losses during processing. The basis for percentages are the total use of N and P fertilizer in US agriculture (USDA, 2013b) and total oilseed meal consumed as animal feed in 2012 (USDA, 2013c).

Without nutrient recycling, the amount of N and P required to produce enough algal biomass to replace 20% of US transportation fuels is about 161 and 276%, respectively, of the total use of these fertilizer resources in the US today (Table 1.2). In addition, if the N and P-rich non-oil biomass is sold as animal feed, as many groups propose, this level of production would result in more than 10 times the amount of oilseed meal currently used in all US animal feeds today. These data suggest that algal biorefineries cannot afford to

export nutrients in the form of non-fuel co-products (e.g., feed and fertilizer), but rather must efficiently reuse nutrients while producing biofuels. As shown in Figure 1.2, however, even if 50% of the N and P within algal biomass is recycled, fertilizer use in the US would still need to almost double to make algal biofuels at this scale possible. Although wastewater may be able to fill this gap to some extent, these data highlight a significant challenge facing large scale commercialization of algal biofuels.

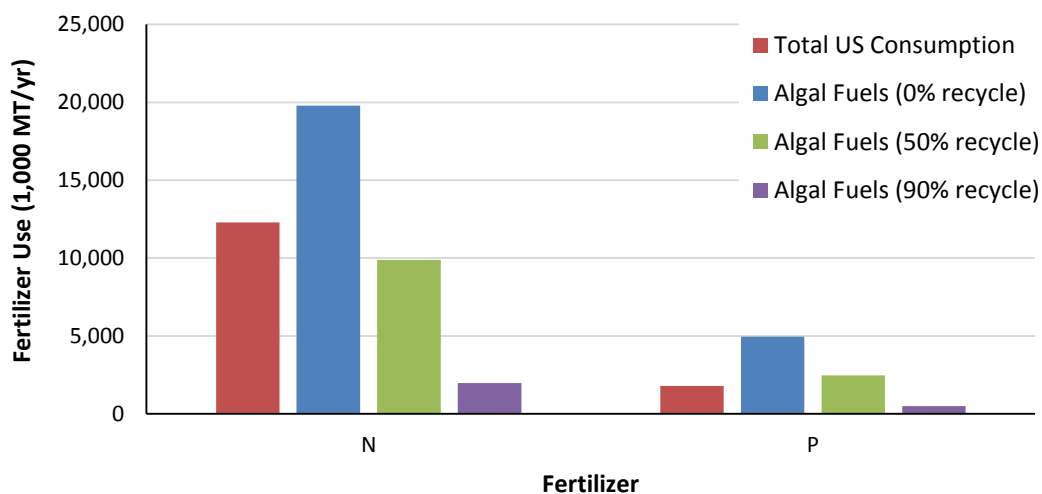


Figure 1.2. Consumption of N and P fertilizers by all of US agriculture in comparison to algal biofuel production to replace 20% of traditional petroleum fuels with varying amounts of nutrient recycling. Assumptions as given in the notes of Table 1.2.

In addition to being nutrient intensive, the dilute aqueous systems typically used to cultivate algae complicate biomass recovery and conversion into fuels. When grown outdoors in open raceway ponds, the most economical (Davis et al., 2011) and energy efficient (Jorquera et al., 2010) cultivation strategy for photosynthetic algae elucidated to date, biomass density and productivity typically ranges from 0.5–1 g/L dry cell weight and 10–30 g/m<sup>2</sup>-d, respectively. This contrasts sharply with terrestrial oilseed crops, which can be easily harvested using commercial farm equipment, dehulled, flaked, and dried to ~10% moisture prior to extraction with an organic solvent such as hexane. Although higher biomass densities (5–200 g/L) can be achieved in thin-plate photobioreactors (Carvalho et al., 2006) and fermenters (Xiong et al., 2008, 2010), dewatering and drying

algae remain energy- and cost-intensive processes (Golueke and Oswald, 1965; Molina Grima et al., 2003). A recent LCA of algal biodiesel production from *Chlorella vulgaris* indicated that drying and hexane extraction accounted for up to 90% of the total process energy inputs (Lardon et al., 2009). In addition, the US EPA has recognized oil extraction as a major source of the hazardous air pollutant n-hexane and has issued emissions standards to limit its release, which typically ranges from 0.8 to 8.3 L per MT of oil-bearing material processed (Johnson, 1997).

These data indicate that drying algal biomass and treating it as a substitute for terrestrial oilseeds in traditional solvent extraction and subsequent transesterification processes is not likely to be a net energy positive route towards biofuel production. Although disrupting cells in an aqueous environment and then using hexane for oil recovery may be a viable alternative, this approach still relies on a petroleum-based solvent and requires significant energy inputs for solvent recovery. Nevertheless, wet hexane extraction is a widely cited approach in modeling efforts to determine the life cycle impacts of algal biofuels and is discussed in greater detail in Chapter 8. In an effort to obviate biomass drying and organic solvent use for lipid extraction, as well as incorporate high levels of nutrient recycling, we set out to develop a new process to convert wet algal biomass in liquid transportation fuels.

### 1.3 Process overview and chapter summaries

Over the course of a five-year research effort, we developed a novel two-step process to convert wet algal biomass into biofuels using hydrothermal carbonization (HTC) and in situ transesterification (IST). Hydrothermal processing is uniquely suited to algae because they grow in water and still contain about 80% moisture after mechanical dewatering (e.g., filtration and centrifugation). During HTC, algal biomass reacts in and with subcritical water, yielding a lipid-rich, solid hydrochar and an aqueous phase co-product containing dissolved nutrients suitable for recycling. In the second step, lipids within the hydrochar are simultaneously extracted and transesterified to produce biodiesel in the

form of fatty acid ethyl esters (FAEEs). Biodiesel is an attractive replacement for petroleum diesel because it can be produced domestically and is compatible with existing diesel engines, reduces tailpipe emissions of most criteria air pollutants, and is biodegradable (Wu et al., 2009; Janaun and Ellis, 2010). Although most previous work on IST has focused on methanol, which is a less costly alcohol, we chose to work with ethanol because it has superior dissolving power for oils, is less toxic and renewably derived, and produces biodiesel with superior fuel properties (Stamenković et al., 2011).

The goal of this work was to demonstrate the feasibility of the proposed approach, gain engineering knowledge for process development, optimize each step by understanding its unique reaction chemistry, and complete a mass and energy balance on the system to validate its utility for net energy positive biofuel production. In Chapter 2, we introduce the algal species chosen for this work and our motivation for selecting them, as well as explain how biomass was produced for downstream processing. In Chapter 3, we focus on HTC and discuss how reaction conditions influence the yield of hydrochar, lipid retention within the hydrochar, and nutrient partitioning to the aqueous phase. In Chapters 4, 5, and 6, we summarize work done on IST of algal hydrochars in uncatalyzed, mineral acid-catalyzed, and triflate-catalyzed reactions, respectively. In Chapter 7, we demonstrate the capacity of algal cultures to use the nutrients within the aqueous phase co-product of HTC and produce lipids. In Chapter 8, we present an overview of the process and its mass and energy balances and compare it to other algae-to-biofuel pathways under consideration. Finally, we present conclusions in Chapter 9 and discuss opportunities for future work.

CHAPTER 2  
FEEDSTOCK PRODUCTION AND CHARACTERIZATION

2.1 Background

2.1.1 Algal metabolisms and production strategies

Throughout this work, we grew numerous species of algae to produce material for downstream processing. Although we experimented with various media recipes, cultivation conditions, and bioreactor designs, the overriding goal was to generate biomass containing lipids suitable for producing biodiesel. To this end, we made an effort to develop simple and low-cost media recipes that would facilitate use on a larger scale and reduce the environmental impact associated with fertilizer use. We also selected species that have been grown on a commercial scale before and show promise for future use.

In general, algae is a somewhat ambiguous term that represents a diverse and polyphyletic grouping of oxygen-evolving, photosynthetic organisms. Most algal divisions, however, contain some species that lack photosynthetic pigments entirely, instead obtaining organic carbon from dissolved compounds in their surrounding environment. Between the extremes of obligate phototrophy and obligate heterotrophy lie the majority of algae that use complex nutritional strategies in some form of mixotrophy (Table 2.1). In this work, we utilized algae capable of all of these metabolisms, both alone and in combination, to produce algal biomass.

Table 2.1. The metabolisms of algae

Metabolism	Carbon Source	Energy Source
Phototrophic	CO <sub>2</sub>	Light
Mixotrophic	CO <sub>2</sub> + Organic Carbon	Light + Organic Carbon
Photoheterotrophic	Organic carbon	Light
Heterotrophic	Organic carbon	Organic carbon

Adapted from: (Chen et al., 2011).

Although growing algae in the light without organic carbon represents the most direct conversion of solar energy to biofuel, the low biomass densities typically achieved in phototrophic cultures (1–2 g/L) and the limited culture volumes our laboratory could maintain and harvest made it difficult to produce sufficient material for our studies. As a result, we took advantage of the higher biomass densities (>10 g/L) and productivity (>1 g/L/d) that could be achieved in short times (<5 days) when algae are grown in the presence of an organic carbon source. Our work mainly utilized glucose, glycerol, and acetate, three of the most widely studied carbon sources for use in algal fermentation, but other non-traditional or waste sources have also been explored (Perez-Garcia and Escalante, 2011). Carbon sources are typically supplied at an initial concentration of 1–2% (10–20 g/L), as higher concentrations have been shown to be inhibitory (Perez-Garcia and Escalante, 2011), and then fed intermittently as their concentration drops below 5 g/L. Typically, the biomass yield (g biomass/g substrate) and lipid yield (g lipid/g substrate) are about 0.4–0.6 and 0.2–0.3, respectively (Xiong et al., 2010; O’Grady and Morgan, 2011). According to Ratledge & Cohen (2008), the maximum theoretical stoichiometric conversion for glucose to triglyceride is 33% (assuming no other cell material is produced) or about 22% in practice (Ratledge and Cohen, 2008). This means that about 5 tons of glucose is required to produce 1 ton of oil heterotrophically. Given the current price of vegetable oil (soybean oil is ~\$1,100/ton (Index Mundi, 2013a)) and sugar (~\$380/ton (Index Mundi, 2013b)), the necessity of using non-traditional and waste carbon sources to produce an economically competitive biofuel becomes readily apparent.

Beyond the economics, choosing a carbon substrate significantly impacts the energy balance and GHG emissions from a fermentation process. Our work, in collaboration with Nolan Orfield and Dr. Greg Keoleian from the School of Natural Resources and the Environment at the University of Michigan, has shown that fermentation-based algal biofuel production using sugarcane as the feedstock and energy-efficient aeration and mixing technologies can achieve significant reductions in the fossil energy ratio (FER) and



global warming potential relative to conventional diesel (Orfield et al., 2013). However, just as with terrestrial crops used for biofuels, indirect land use changes could easily erode this reduction in global warming potential. For example, if forest lands are cleared to plant more sugarcane in an equal amount to that used for algal biofuel production, the global warming potential could actually be much worse than petroleum. Moreover, the total occupied land for algal biofuels produced by fermentation is much greater than a phototrophic system, largely due to the lower efficiency of terrestrial crops (e.g., sugarcane or sugar beets) relative to algae. Our research, like that which promotes cellulosic ethanol, suggests it is critical to develop low-cost technologies to convert cellulosic biomass into fermentable sugars. To better understand the potential of this technology, we briefly examined the utility of a cellulosic hydrosylate generated by a new low-temperature steep delignification process (Bio-Process Innovation) as a carbon source for algal fermentation. We also used glycerol alone and in combination with glucose, since this carbon source has been shown to be utilized simultaneously with glucose by *Chlorella* and is metabolized similarly (O'Grady and Morgan, 2011; Perez-Garcia and Escalante, 2011). In general, the use of glycerol from transesterification reactions is preferable to glucose because it is a waste product with declining value, but it is ultimately not a scalable carbon substrate due to limited supply.

Our desire to produce large quantities of algae in fermenters instead of using less compact open ponds or tanks is similar to the approach taken by some leading companies in the algae industry, such as Solazyme and Martek Biosciences/DSM. Although both companies have expressed interest in developing biofuels, and Solazyme has successfully demonstrated the ability to do so, the majority of their revenue stems from higher-value products such as omega-3 oils (DHA and EPA), personal care products, and specialty oils. This is the direct result of the high cost of sugars, which will no doubt continue to limit the development of algal biofuels produced by fermentation.

Open raceway ponds are the common alternative to fermenters and permit the cultivation of algae in direct sunlight. Lacking access to an open pond-type production system, we utilized bubble column reactors and hanging plastic bags to produce algae in the light. These reactors were typically aerated with 1–2% CO<sub>2</sub> in air and illuminated either continuously or on a 14:10 hr light:dark cycle.

### 2.1.2 Species selection: *Chlorella*

Two species of *Chlorella* were selected as model organisms for this study due to their ability to grow both photo- and heterotrophically, previous use in algal biofuel research, and initial results indicating robust growth and high lipid content in artificial media. Moreover, *Chlorella* has been grown in outdoor ponds for decades to produce human nutraceutical products, so there is considerable commercial experience with this organism. Specifically, *C. vulgaris* (UTEX# 259 and UTEX# 395) was selected based on recommendations from the research staff at the National Renewable Energy Laboratory, who use it as a model organism in their own studies, as well as recent evidence that this species is capable of growth on glucose, glycerol, and acetate (Liang et al., 2009). In their work, lipid productivity ( $54 \pm 2$  mg/l/d) was greatest when cells were grown in the light with 1% glucose, though comparable productivity ( $31 \pm 2$  mg/l/d) was also obtained with 2% glycerol in the light.

*C. protothecoides* (UTEX #255) was selected based on a large amount of recent literature indicating the ability of this species to reach high cell density and lipid content during fermentation on various organic carbon sources (Kessler, 1982; Miao and Wu, 2004; Li et al., 2007; Cheng et al., 2009; O’Grady and Morgan, 2011). In addition to glucose and glycerol, *C. protothecoides* has also been grown on non-traditional carbon substrates, such as corn hydrosylate (Xu et al., 2006), the hydrosylate of Jerusalem artichoke tuber (Cheng et al., 2009), and sweet sorghum (Gao et al., 2010). Building on early work, which demonstrated that heterotrophic *C. protothecoides* contained substantially more lipid and less protein than autotrophic cells (Miao and Wu, 2006), this organism has been

exploited for biodiesel production. In 7-day fed batch experiments, lipid productivity was 0.95, 0.83, and 0.85 g/L-d at 5 L, 750 L, and 11,000 L (Li et al., 2007). In these experiments, cell densities ranged from 15.5 g/L to 14.2 g/L, although higher cell densities (51.2 g/L) with a comparable lipid content (~50%) have been reported for this organism (Xiong et al., 2008). Although relatively little has been published on its growth in purely photoautotrophic conditions, sequential phototrophic and heterotrophic growth phases have been shown to increase the biomass density, lipid productivity, and carbon substrate utilization efficiency of *C. protothecoides* culture (Xiong et al., 2010). Most likely, cells grown in the light and then transferred to an unlit fermenter containing dissolved organic carbon retain some capacity to take up dissolved CO<sub>2</sub> through Rubisco, thereby enhancing productivity and overall conversion of substrate to biomass. In addition, because the algae grown in the light requires CO<sub>2</sub>-enriched air and produces oxygen while the fermentation reactor requires oxygen and produces CO<sub>2</sub>, gas streams to and from both growth reactors can be appropriately integrated to further improve the conversion efficiency of organic carbon to lipid-rich biomass and limit the amount of external CO<sub>2</sub> required for cultivation (Santos et al., 2010).

In an attempt to elucidate the taxonomy of the genus *Chlorella*, Kessler et al. (1992) found that both *C. vulgaris* and *C. protothecoides* demonstrated tolerance to acidity (limit at pH 3.5–4.5), salinity (limit at 3–4 % NaCl), and had a similar DNA composition (58–63 mol% GC) (Kessler, 1976; Kessler and Huss, 1992). Kessler speculated that *C. protothecoides* may have evolved from *C. vulgaris* since the two species are very similar, with the exception that *C. protothecoides* has lost the ability to reduce nitrate and synthesize thiamine (Kessler, 1976). Overall, the ability of these two species to grow under a wide range of pH and salinity, in addition to their ability to utilize various organic carbon sources, makes them ideal model organisms for our study.

### 2.1.3 Species selection: *Nannochloropsis*

Over the course of this research effort, the eustigmatophyte *Nannochloropsis* became popular in the literature and the algae industry more broadly as a highly productive organism capable of growth in brackish and salt waters. From a biofuels perspective, Rodolfi et al. (2009) demonstrated that certain strains of *Nannochloropsis* maintained high total biomass productivities while accumulating lipids, a rare observation in algal cultures stressed by low N (Sheehan et al., 1998; Rodolfi and Zittelli, 2009). Recent work also demonstrated the large-scale cultivation of *Nannochloropsis* in submerged photobioreactors, where annual oil productivity averaged 10.7 m<sup>3</sup>/ha-yr or 1,150 gal/acre-yr (Quinn et al., 2012). Beyond biofuels, *Nannochloropsis* is commonly produced as a high value aquaculture feed ingredient and as a source of the omega-3 fatty acid eicosapentaenoic acid (EPA). We hypothesized that HTC and IST could be used to integrate production of both high-value omega-3 oils with lower value biodiesel, thereby permitting the near-term production of algal biofuels at prices competitive with petroleum. Although the market for omega-3 oils is small compared to that for fuels and would quickly become saturated should a large-scale algal biodiesel operation become operational, this may nevertheless present an opportunity to help refine algal growth and processing technologies to drive down costs.

Because *Nannochloropsis* is readily available from commercial sources, such as Reed Mariculture Inc., we purchased frozen algal biomass instead of growing it ourselves. We also received *Nannochloropsis* samples grown in outdoor ponds, courtesy of Valicor Renewables Inc.

### 2.1.4 Species selection: Marine bi-culture

Our original interest in *Nannochloropsis* stemmed from its ability to provide both a biofuel feedstock and a high value co-product, but we were also aware that its cultivation in outdoor ponds has been reported to suffer from sudden culture collapse due to predation by protozoa (e.g., *Paraphysomonas* sp.), contamination by bacteria (e.g., *Cytophaga* sp.),

and competition from cyanobacteria and other algae (Zittelli et al., 1999). These challenges have led many to pursue closed photobioreactors for the production of *Nannochloropsis* (Richmond and Cheng-Wu, 2001; Quinn et al., 2012), which is economically feasible when selling a high-value aquaculture feed or nutraceutical, but is ultimately too expensive for a large-scale biorefinery producing fuels. We hypothesized that it would be possible to stress an open pond culture containing predominantly *Nannochloropsis* and select for the hardiest strains present. To accomplish this, we cultured seed material from a pond in New Mexico in a typical saltwater media (f/2 media) containing ten times more trace metal stock solution than the standard recipe. Heavy metals are well known to cause oxidative stress in algae, typically by increasing the cellular concentration of reactive oxygen species and reducing the cellular antioxidant capacity (Pinto et al., 2003). Increased concentrations of metals have also been found to alter the fatty acid profile of some microalgae, typically resulting in reduced fatty acid desaturation and elongation that shunts more carbon to saturated or mono-unsaturated lipids, which are preferable for biodiesel (Harwood and Jones, 1989; McLarnon-Riches and Rolph, 1998; Guschina and Harwood, 2006). We hypothesized that metal-induced stress would help select for the most robust organisms present in the open pond culture and reduce the content of highly unsaturated fatty acids.

Following the stress period, a stable bi-culture was obtained that contained a green algae, tentatively identified as *Nannochloris*, and a cyanobacteria, tentatively identified as *Synechocystis*. This is the first time, to our knowledge, that a co-culture containing a green algae, which is known to accumulate lipids during periods of nutrient stress (Yamaberi et al., 1998; Takagi et al., 2000), and a cyanobacteria, which contains a basal lipid level and is most productive in nutrient replete conditions (Rittmann, 2008), has been explored for biofuel production. We hypothesized that a multi-species community would be able to consume a greater variety of dissolved organic nutrients in the aqueous phase co-product arising from HTC compared to a monoculture, so we chose this culture for the nutrient recycling experiments described in Chapter 7.

### 2.1.5 Biomass dewatering and preparation for HTC

Regardless of the cultivation strategy used, all algal cultures required dewatering prior to processing by HTC. At a large-scale facility, this is typically done using a combination of flocculation, dissolved air flotation, and centrifugation, although recently, tangential flow filtration (TFF) has appeared as a promising alternative (Danquah et al., 2009; Zhang et al., 2010). TFF involves pumping the algae-water mixture through pressurized ultrafiltration membranes (~500 kDa molecular weight cutoff) that remove water and some dissolved solids, resulting in concentration of the algal biomass. This approach has two major advantages: (1) biomass is completely retained during TFF, whereas about 5% is assumed lost during flocculation and dissolved air flotation; and (2) the liberated water is sterile and free of flocculants so it can be returned to the algal growth system free of contaminants. Recently, ultrafiltration has been found to be superior to chemical flocculation of microalgae from both an energy and economic perspective (Danquah et al., 2009), and has been used previously in high-density cultivations of *C. vulgaris* (Javanmardian and Palsson, 1991). Following concentration to about 6–10% solids in the TFF system, the biomass slurry is typically further dewatered with a centrifuge to about 20% solids.

Pall Corporation has pioneered work with TFF for algae harvesting, and they supplied a laboratory-scale filtration module we used for preliminary testing. Although this approach appeared to work well in our bench-top testing, the size of the filtration module we used was too small to permit the concentration of large volumes of dilute culture (>50 L) within a reasonable timeframe. In addition, the system hold-up volume was too large for use with smaller cultures (<5 L), making it difficult to use regularly. As a result, in most of the work presented here, centrifugation was used to concentrate algal cultures to about 15–20% solids. At this solids concentration, the biomass has a pasty consistency, like thick mud, and was typically reacted immediately or frozen for storage. Samples of

every harvest were also dried to measure the paste moisture content and analyze the lipid content of the biomass lipids.

## 2.2 Materials and Methods

### 2.2.1 Algal bioreactors

Algae were grown in a variety of bioreactors and other containers, from small shaker flasks to hanging bags to sterile fermenters. Each apparatus, along with a picture and basic description, is described below in Table 2.2.

Table 2.2. Algae bioreactor apparatus








Apparatus	Picture	Description
Shaker Flask		Volume: 50-250 mL Aeration: Shaking Sterile
Bubble Column Reactors		Volume: 4 L each Aeration: 1-2% CO <sub>2</sub> in air Non-sterile
Bubble Column Reactors (continuous flow)		Volume: 2 L each Aeration: 1-2% CO <sub>2</sub> in air Non-sterile

Table 2.2 continued. Algae bioreactor apparatus

Apparatus	Picture	Description
Large Flasks		Volume: 4 L each Aeration: 1-2% CO <sub>2</sub> in air Non-sterile
Hanging Bag Reactor		Volume: 50 L Aeration: 1-2% CO <sub>2</sub> in air Non-sterile
Carboy Fermenter		Volume: 10 L Aeration: air Non-sterile
Bioflo3000 (New Brunswick)		Volume: 3.5 L Aeration: air Sterile

Note. Cultures were typically maintained on agar plates and then inoculated into shaker flasks for scale-up. Inoculation at each subsequent scale was typically at 10% v/v or greater. Cultivation at each scale lasted approximately 3-6 d.

### 2.2.2 Media composition

Algae were grown in a variety of media throughout our research effort. The media used to produce the biomass that was subsequently used in HTC experiments is described in



Table 2.3. Typically, *C. vulgaris* was grown in a modified Bold's Basal Media (MBBM), containing either nitrate or urea as the nitrogen source. *C. protothecoides* was grown in a media based on Xiong's Basal Media (XBM) (Xiong et al., 2008), which was modified for cultures grown in the light and dark. Notably, this algae was found to do best when nitrogen was supplied by an organic source, such as yeast extract or glycine. Finally, the marine bi-culture we developed was cultivated in a modified f/2 recipe (Guillard, 1975) that contained either nitrate or urea as the nitrogen source. Additional nitrogen sources, such as NH<sub>4</sub>Cl and NH<sub>4</sub>SO<sub>2</sub> were examined in growth experiments, along with various modifications to these media recipes.

Table 2.3. Media compositions (mg/L)

Chemical	MBBM <sup>a</sup>	XBM-Light <sup>b</sup>	XBM-Dark <sup>c</sup>	f/2 <sup>d</sup>
NaNO <sub>3</sub>	750	0	0	425
Urea	0-100	0	0	0-100
Yeast Extract	0	2000	4000	0
K <sub>2</sub> HPO <sub>4</sub>	75	400	400	0
KH <sub>2</sub> PO <sub>4</sub>	175	600	600	0
NaH <sub>2</sub> PO <sub>4</sub> ·2H <sub>2</sub> O	0	0	0	60
MgSO <sub>4</sub> ·7H <sub>2</sub> O	75	400	400	0
CaCl <sub>2</sub> ·2H <sub>2</sub> O	25	0	0	0
NaCl	25	0	0	0
Na <sub>2</sub> EDTA·2H <sub>2</sub> O	4.5	0	0	4.36
H <sub>3</sub> BO <sub>3</sub>	2.86	4.29	4.29	0
FeCl <sub>3</sub> ·6H <sub>2</sub> O	0.58	0	0	3.15
FeSO <sub>4</sub> ·7H <sub>2</sub> O	0	1	0.5	0
MnCl <sub>2</sub> ·4H <sub>2</sub> O	0.25	0.27	0.27	0.18
CuSO <sub>4</sub> ·5H <sub>2</sub> O	0.079	2.7	2.7	0.01
ZnCl <sub>2</sub>	0.030	0	0	0
ZnSO <sub>4</sub> ·7H <sub>2</sub> O	0	0.33	0.33	0.022
CoCl <sub>2</sub> ·6H <sub>2</sub> O	0.012	0	0	0.01
Na <sub>2</sub> MoO <sub>4</sub> ·2H <sub>2</sub> O	0.024	0.06	0.06	0.0063
Vitamin B <sub>12</sub>	0.131	0	0	0.005
Biotin	0.024	0	0	0.005
Vitamin B <sub>1</sub> <sup>e</sup>	0.534	0.03	0.06	0.2
Glycine	0	100	100	0

Notes. Abbreviations: MBBM = modified Bold's Basal Medium. XBM = Xiong's Basal Medium.

<sup>a</sup> NaNO<sub>3</sub> was replaced by 100 mg/L urea in MBBM for *C. vulgaris* (UTEX #249) scale up in bubble column reactors. <sup>b</sup> Two versions of XBM were used for cultures grown phototrophically or heterotrophically. Growth was comparable on yeast extract and glycine as the major N sources. XBM contains 1.5 mL of A5 trace metals mix. <sup>c</sup> Sigma antifoam 204 (0.1 mL/L) and chloramphenicol (10 mg/L) were added to XBM media in fermenters to control foaming and reduce bacterial contamination, respectively. XBM-Dark media also contained 20-30 g glucose initially. <sup>d</sup> The original f/2 media recipe was slightly modified and typically contained urea instead of NaNO<sub>3</sub>. f/2 included 27 g/L Instant Ocean salt mix. <sup>e</sup> Thiamin HCl.

### 2.2.3 Production of *Chlorella* biomass

*C. vulgaris* was received on an agar slant and then grown in shakers flasks containing MBBM (Table 2.3). Once a dense culture was obtained, the flasks were used to seed a series of six glass bubble column reactors (BCRs) (3.8 cm diameter x 130 cm length each) continuously fed (approximately 60 mL/h) with MBBM. The synthetic medium was prepared with purified deionized water and adjusted to pH 7.2 with 1 N NaOH. All BCRs were sanitized with a bleach-water solution prior to use, but the media was not sterile filtered. A humidified 1-2% CO<sub>2</sub>-air mixture was delivered to each column (0.3 L/L-min) via a linear air pump (LT19, Whitewater) and a regulated CO<sub>2</sub> tank. Light was supplied continuously with cool-white fluorescent bulbs (SP-50 ECO, 32 W, GE), for a light output at the tube surface of approximately 250  $\mu\text{mol}/\text{m}^2\text{-s}$ . A PAR detector (MQ-303, Apogee Instruments) was used to measure irradiance. The apparatus was maintained at room temperature (23-25 °C). The mean hydraulic residence time in the reactor was 7 d. Reactor effluent (ca. 3.5 L) was collected in a 10 L HDPE carboy for 2 d, then transferred to a 4 L flask. Glucose (20 g/L) was added to the flask and the cells were then cultivated in the dark with aeration (1 L/L-min) and stirring for 7 d. The culture was centrifuged to obtain a paste, which was subsequently dried to obtain a powdery solid suitable for long term storage and use.

*C. vulgaris* was also grown phototrophically in hanging bags reactors containing about 50 L of MBBM and in 4 L polystyrene BCRs (12.2 cm diameter x 50 cm tall) illuminated on a 14:10 h light:dark cycle with fluorescent bulbs ( $\sim 300 \mu\text{mol}/\text{m}^2\text{-sec}$ ) and stirred at 60 rpm. MBBM used in these BCRs contained urea instead of NaNO<sub>3</sub>. The BCRs were sparged with sterile-filtered air containing  $\sim 1\%$  CO<sub>2</sub> during the light hours or air during the dark hours. These cultures were regularly harvested for HTC experiments.

*Chlorella protothecoides* (UTEX #255) was generously provided by John O'Grady (Purdue University) on an agar slant and grown up in shake flasks in the light on XBM (Table 2.3).

Exponentially growing phototrophic cultures were used to inoculate heterotrophic shake flasks. After 3 d incubation in the dark at 28 °C with shaking at 250 RPM, 0.8 L of combined shake flask culture was used to inoculate a 5 L bioreactor (Bioflo3000, New Brunswick) containing 3 L of the heterotrophic media. The fermenter was sterilized prior to inoculation by autoclaving at 121 °C. Glucose was fed intermittently and pH was controlled at 6.4 for 5 d until biomass was harvested by centrifugation (3000 RCF x 10 min) and immediately reacted. Three separate batches of 4 L total volume each were carried out in the Bioflo3000 to produce sufficient paste for experiments. In addition, some fermentations were carried out under less sterile conditions in plastic carboys, both in our lab as well as in collaboration with Toby Ahrens (Bioprocess Algae). Biomass density at harvest was typically 15-30 g/L with a total lipid content of 25-45% as FAMES on a dry weight basis. No attempt was made to optimize cell density or lipid productivity; rather, cultivation was carried out under conditions known to produce lipid-rich biomass for downstream processing experiments.

#### 2.2.4 Marine bi-culture production

A seed culture of *N. oculata* grown outdoors in open raceway ponds (94,625 L total capacity, 45,420 L typical culture volume) in Artesia, New Mexico was provided by the Center of Excellence for Hazardous Materials Management in conjunction with Valicor Renewables. This strain has reportedly been cultured continuously on f/2 media containing nitrate in brackish water for over 3 years and contained minor levels of contamination upon receipt. In our laboratory, this strain was initially cultured in brackish water (27 g/L Instant Ocean salt mix, Spectrum Brands) fortified with 425 mg/L NaNO<sub>3</sub>, 60 mg/L NaH<sub>2</sub>PO<sub>4</sub>·2H<sub>2</sub>O, and a commercial vitamin and trace metal solution (Micro Algae Grow Trace Pack™, Florida Aqua Farms, Inc.) containing the traditional f/2 recipe (Guillard, 1975). To select for the most stress-resistant algal community, some cultures received 10-fold higher concentrations of the trace metal and vitamin stock solution over a period of 4 weeks. After the stress induction period, the commercial f/2 vitamin and trace metal solutions were replaced with stocks prepared in our lab (Table 2.3). Three

different N supplemental sources were assessed (i.e., nitrate, urea, and ammonium) in preliminary experiments and urea was chosen for subsequent work because it is a nonionic N source (diminishing issues associated with pH increases and decreases over time in cultures containing nitrate and ammonium, respectively), contains the highest proportion of N by weight of the tested sources (46.6%, thereby reducing transportation costs), its production results in less environmental impacts relative to nitrates (Handler et al., 2012), and it supported strong growth. Cultures were maintained in 4 L plastic BCRs, as described above, and harvested by centrifugation to produce a paste.

#### 2.2.5 Biomass sampling

Throughout growth experiments and feedstock production, biomass density was determined gravimetrically by centrifuging a known volume of culture media, drying the pellet, and determining its weight. Typically, a 5-14.5 mL sample was removed and centrifuged (5,000 RCF x 5 min) and the cell-free supernatant was retained for analysis. The pH in the supernatant was measured immediately and then samples were typically frozen until further analysis. The pellet was washed with distilled H<sub>2</sub>O and transferred to a pre-dried, pre-weighed glass tube where it was dried (65 °C for at least 24 h), allowed to cool in a desiccator, and then weighed. The solids in the glass tube were used for lipid analysis, as described in the next section. Dry biomass samples were also assayed for elemental analysis by third-party laboratories.

#### 2.2.6 Total lipids analysis by in situ transesterification

Lipids from all classes in algal biomass, hydrochars, and lipid-extracted residues were simultaneously extracted and catalytically transesterified to determine their total lipid content. Because analytical-scale acid-catalyzed in situ transesterification, which is carried out with a methanol (MeOH) or ethanol (EtOH) to fatty acid ratio of >1500:1, has repeatedly been shown to recover more fatty acids than traditional two-step extraction and transesterification procedures (Rodríguez-Ruiz et al., 1998; Lewis et al., 2000), this procedure provided the theoretical maximum ester yield possible from process solids. Dry

solids (5-20 mg) were weighed into glass tubes (16 mm x 100 mm) with teflon-lined screw caps and reacted with 2 mL freshly prepared methanol (99%) containing 5% acetyl chloride at 100 °C for 90 min with vigorous stirring. Water (1 mL) was added to stop the reaction and FAMES were extracted into 2–4 mL total *n*-heptane containing 100-200 mg/L tricosanoic methyl ester (C23:0 FAME) as internal standard. About 2 mL of the heptane mixture was transferred to a vial for GC-FID analysis. In some instances, solids were reacted with various amounts of ethanol containing 5% H<sub>2</sub>SO<sub>4</sub> or 5% acetyl chloride to produce FAEE; the identical reaction workup was used in both cases.

Tricosanoic methyl ester was selected as an internal standard because it is not naturally present in algal biomass, does not co-elute with other FAs, and elutes near the majority of the FAMES in algae, minimizing the effects of different volatilities during split injection (Alves et al., 2009). In addition, Alves et al. (2009) found that the relative standard deviation of the area of the internal standard decreased with increasing of carbon chain length (cf. 8.3 for C15:0 to 1.9 for C21:0), suggesting that longer-chain FAs may serve as a better internal standard. Occasionally, when supplies of C23:0 were not available, pentadecanoic methyl ester (C15:0 FAME) was used as an internal standard. Typically, the relative standard deviation of the internal standard area was less than 2%.

Samples were injected (1µL; 10-100:1 pulsed split ratio; 260 °C inlet temperature) onto an HP-InnoWax column (30 m x 0.32 mm x 0.25 µm, J&W 1909BD-113) with an initial oven temperature of 150 °C. After a 3 min hold, the temperature was ramped at 6 °C min<sup>-1</sup> to 260 °C. Helium was the carrier gas at a constant flow rate of 1.0 mL min<sup>-1</sup>. The FID detector temperature was 300 °C and N<sub>2</sub> served as the make-up gas. The retention time of each FAME or FAEE was identified from standard mixes and peak area was converted into the mass quantity of each ester in the sample by the following formula:

mg ester<sub>x</sub> =

$$(\text{mg/L ISTD in solvent}/\text{area ISTD})(\text{L workup solvent})(\text{area ester}_x)(\text{RRF}_{\text{ISTD},x})$$

where ester<sub>x</sub> refers to the specific fatty acid group; ISTD refers to the internal standard used; and  $RRF_{ISTD,x}$  is the theoretical response factor for each ester<sub>x</sub> relative to the appropriate internal standard (Ackman and Sipos, 1964). This internal standard approach was adopted to improve the accuracy of quantification relative to direct area comparisons. In general, analyte weight percent is not equal to area percent on a GC chromatogram due to (i) inlet discrimination (ii) irreversible adsorption of analytes to the column (iii) analyte thermal instability, and (iv) unequal FID response towards esters with varying carbon length and degree of unsaturation (Ulberth et al., 1999; Dodds et al., 2005)

### 2.2.7 Lipid composition by extraction, derivatization, and high temperature GC-FID

Lipids within algal biomass and process solids were extracted and analyzed to determine their composition (relative amounts of FA, TG, DG, MG). Dry solids (~30 mg) were loaded into glass tubes (16 mm x 100 mm) with teflon-lined screw caps and extracted at 60 °C for 4 h with 6 mL of n-hexane or a mixture of n-hexane:isopropanol (HIP, 3:2 v/v). n-Hexane was chosen based on its commercial relevance in oilseed extraction and previous use to extract heterotrophic algal lipids (Miao and Wu, 2006; Xiong et al., 2008; Cheng et al., 2009; Shen et al., 2010), whereas HIP was used as a less toxic alternative to chloroform:methanol mixtures (Folch et al., 1957; Bligh and Dyer, 1959; Hara and Radin, 1978) In addition, isopropanol has been found to reduce lipid degradation caused by lipolytic enzymes in plant tissues (Christie, 1989). Upon cooling, the tubes were centrifuged (2000 RCF x 15 min) and 2 mL of the upper solvent layer (i.e. crude lipid extract, CLE) was transferred to a 2 mL GC-vial and stored at 4 °C prior to analysis.

The CLE (50 to 500 µL) was transferred to two pre-weighed GC vials using the Agilent 7693A Automated Liquid Sampler. The solvent was evaporated under N<sub>2</sub> (Visiprep Solid Phase Extraction Vacuum Manifold, Supelco) and the mass of the CLE was determined gravimetrically (XS205DU, Mettler Toledo, readability = 0.01 mg). Prior to analysis by high-temperature (HT) GC/FID, the CLE was derivatized with MSTFA to improve the volatility of lipid components containing free hydroxyl groups (e.g., FA, MG, DG). A

modified micro-scale EN14105 procedure was adopted to automate standard and sample preparation, include FA quantification, increase analysis throughput, and reduce experimenter exposure to hazardous solvents (EN14105, 2003; McCurry, 2009). Three internal standards (1,2,4-butanetriol, dodecanoic acid, and tricaprin) in pyridine (10  $\mu$ L each; 6,000-8,000 ppm) and MSTFA (20  $\mu$ L) were added to a vial, the vial was stirred for 1 min, and then allowed to react for 30 min at room temperature. The sample was diluted in *n*-heptane (700  $\mu$ L), stirred again, and injected in an Agilent 7890 GC-FID with an ASTM6584 column (15 m x 320 mm x 0.25  $\mu$ m, Agilent J&W). Injection (1.0  $\mu$ L) was made to a cool-on-column inlet in oven-track mode with an initial oven temperature of 50  $^{\circ}$ C. After a 1 min hold, the temperature was ramped to 180  $^{\circ}$ C at 15  $^{\circ}$ C/min, 230  $^{\circ}$ C at 7  $^{\circ}$ C/min, and 380  $^{\circ}$ C at 30  $^{\circ}$ C/min. Helium was the carrier gas at a constant flow rate of 3.0 mL/min. FID detector temperature was 380  $^{\circ}$ C and N<sub>2</sub> served as make-up gas (30 mL/min). Peaks corresponding to FA, MG, DG, and TG were identified by their retention time and quantified based on internal standard calibrations of oleic acid, monoolein, diolein, and triolein, respectively.

## 2.3 Results and Discussion

### 2.3.1 *C. vulgaris* production and characterization

In an effort to produce lipid-rich algal biomass, *C. vulgaris* was grown phototrophically in a series of continuously fed bubble column reactors and then heterotrophically in a single stirred tank. Lipid accumulation was promoted through N stress; nitrate in the phototrophic media was entirely consumed by the fourth bubble column reactor when the reactor was operated in continuous mode. When each of the six bubble columns were operated as batch cultures, *C. vulgaris* was able to consume all the N in the media in a similar time period (3-4 days) while continuing to increase in density (Figure 2.1). The lipid content of the phototrophic biomass collected in continuous mode or at the end of batch cultures lasting longer than 6 days was typically near 50% when measured as FAMES. Green cells collected at approximately 3 g/L were then grown on glucose in the dark for 7 days in large flasks, during which time they yellowed and biomass density

roughly doubled (Figure 2.2). A reduction in chlorophyll in the absence of external N has been hypothesized to correspond to intracellular scavenging of this N-rich compound (Piorreck et al., 1984; Li et al., 2008), and chlorophyll breakdown and chloroplast degeneration during heterotrophy have been linked to lipogenesis in *C. protothecoides* (Xiong et al., 2010). In general, the large flasks used for heterotrophic growth in this experiment were not optimized for the high oxygen demand these cultures would normally have, resulting in relatively slow growth rates during heterotrophy.

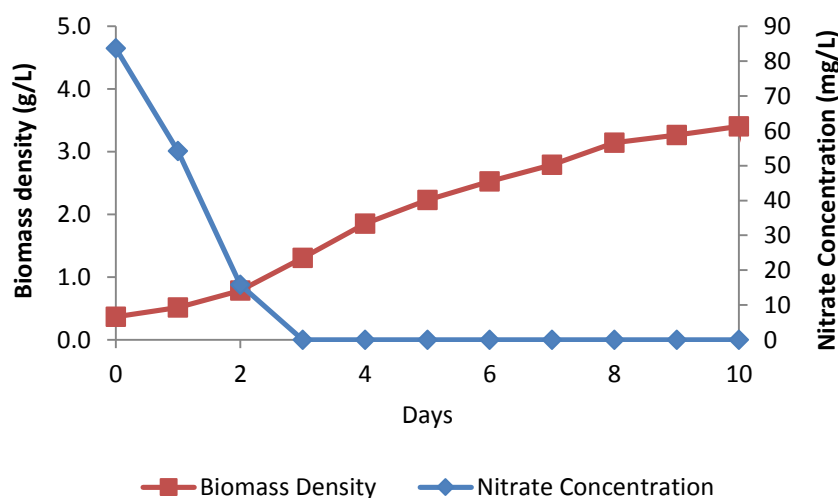


Figure 2.1. *C. vulgaris* biomass density and media nitrate concentration over time. Data represent the averages of two identical bubble column reactors containing MBBM.

Dry algal biomass after both the phototrophic and heterotrophic growth stages was thoroughly characterized. The biomass total lipid content, measured as FAEE by GC-FID, increased only slightly from 50% to 53% during heterotrophic cultivation. As expected, lipids in both samples were comprised almost entirely of TGs (95–96%) with minor amounts of DG (2–3%), MG (<1%), and FAs (1–2%). This total lipid content was higher than the previously reported range (21–36%) for *C. vulgaris* grown in media containing 1–2% of acetate, glycerol, or glucose (Liang et al., 2009), but similar to gravimetric lipid determinations reported for N-starved *C. vulgaris* grown phototrophically with CO<sub>2</sub> supplementation (40–50%) (Illman et al., 2000; Widjaja et al., 2009) and in a marine



medium supplemented with iron (56%) (Liu et al., 2008). The lipid content achieved also compares favorably to that measured in high-cell-density cultures of heterotrophic *C. protothecoides* (40–50%) (Li et al., 2007; Xiong et al., 2008).

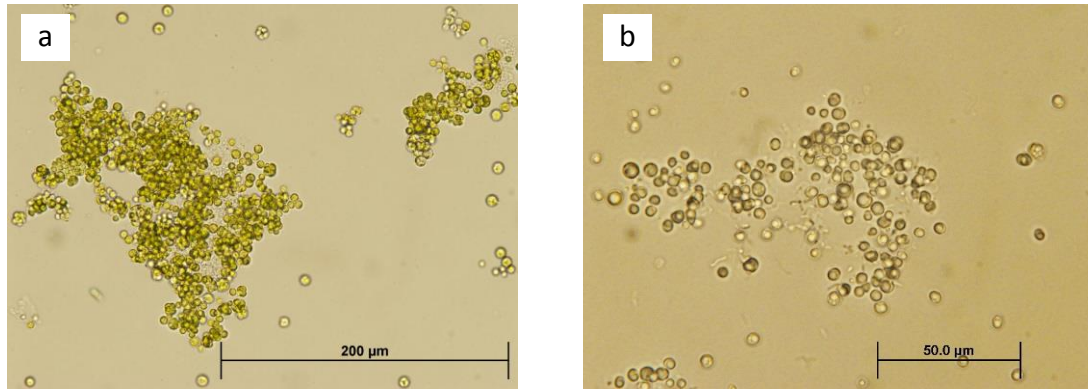


Figure 2.2. Light microscopy of *Chlorella vulgaris*. a) Cells grown phototrophically and b) Cells grown on glucose in the dark just prior to harvest for HTC. Note the large lipid bodies present in the heterotrophic cells, which contained about 53% lipids.

The FA profile of biodiesel feedstocks is an important determinant of fuel quality (Knothe, 2005, 2009). Figure 2.3 shows that the major FAs of harvested *C. vulgaris* were 46% oleic acid (C18:1), 18% palmitic acid (C16:0), 13% linolenic acid (C18:3), and 9% linoleic acid (C18:2). This FA distribution is similar to that reported for N-starved *C. vulgaris* (Piorreck et al., 1984), but with more oleic acid and less palmitic acid than some recent reports (Converti et al., 2009; Gouveia and Oliveira, 2009). Incubation with glucose in the dark decreased the percentage of C18:3 FA (cf. 18 and 13%) and increased the percentage of C18:1 FA (cf. 37 and 46%), resulting in a FA profile more likely to yield biodiesel with improved cold-flow properties and oxidative stability (Knothe, 2009). This finding corroborates evidence that FA biosynthesis in heterotrophic *C. vulgaris* stops at oleic acid (Nichols et al., 1967) and suggests that combined photo- and heterotrophic cultivation can be used to produce algal biomass with a suitable FA profile for biodiesel.

Elemental analysis showed that the N content of harvested cells was very low (1%) compared to reported values for the N content of microalgae (e.g. 5–9%), most likely

reflecting the decrease in protein and increase in lipids typically observed during N limitation and heterotrophy (Illman et al., 2000; Miao and Wu, 2006). In addition, because the N in the media was consumed by the fourth lit reactor, yet biomass density nearly doubled during heterotrophic growth, there must have been a concomitant decrease in the biomass N-to-lipid ratio. Such an effect is desirable because it indicates an efficient use of N to produce lipids and reduces the potential for N-containing fuel impurities (e.g., chlorophylls) that could lead to increased NO<sub>x</sub> emissions during combustion. The problem of NO<sub>x</sub> emissions was a critical factor in why we initially chose to produce liquid fuels from carbonized algal biomass, as opposed to investigate its direct combustion as was recently reported (Heilmann et al., 2010).

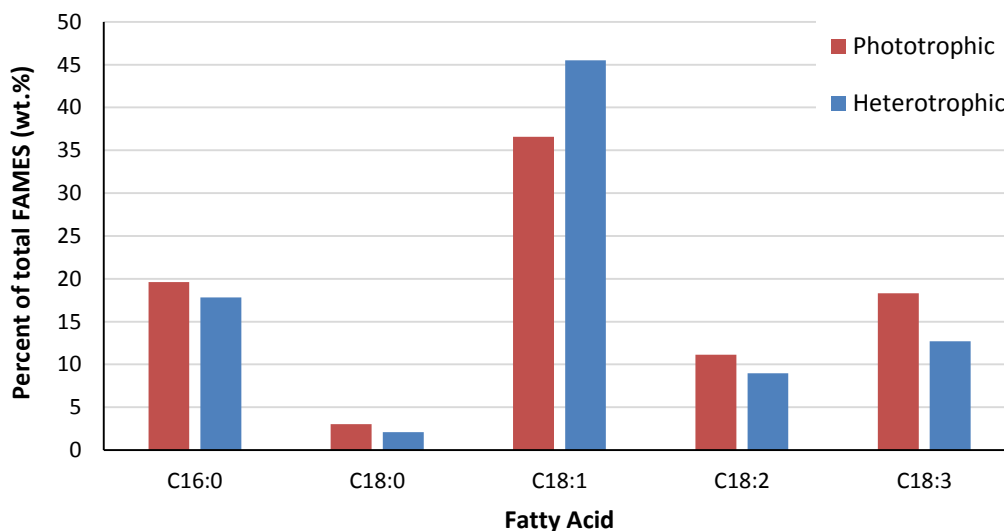


Figure 2.3. Fatty acid profile of phototrophic and heterotrophic *C. vulgaris*

### 2.3.2 *C. protothecoides* production and characterization

Sequential phototrophic and heterotrophic growth phases were also used to produce *C. protothecoides* biomass. Shaker flasks were used to seed either sterile (Figure 2.4) or non-sterile (Figure 2.5) fermenters at 5–10 vol%. Multiple batches lasting up to about 200 hours were carried out to produce biomass; the two shown here are representative of the performance we observed in each fermenter. Due to the more precise control of

pH, DO, agitation, and temperature, it is not surprising that about two-fold higher densities were achieved in the Bioflo3000 compared to the stirred and aerated plastic carboy. In addition, due the lack of sterility, there were low levels of background contamination in the carboy fermenter. By using low-cost antibiotics, however, the bacterial population could be maintained at very low levels, which is desirable to reduce their consumption of glucose and other media components. Although the use of antibiotics is generally undesirable, the development of bacterial resistance can be mitigated because all algae and media exposed to antibiotics will be reacted by HTC within 5 days of exposure, effectively destroying the antibiotic and any living organisms exposed to it. We used chloramphenicol at 10 mg/L in this work; other recent efforts with heterotrophic *Chlorella* have used a combination of chloramphenicol (5 mg/l), penicillin-G (62 mg/l), and streptomycin (100 mg/l) (Santos et al., 2010) or chloromycetin (10 m/L) (Li et al., 2007).

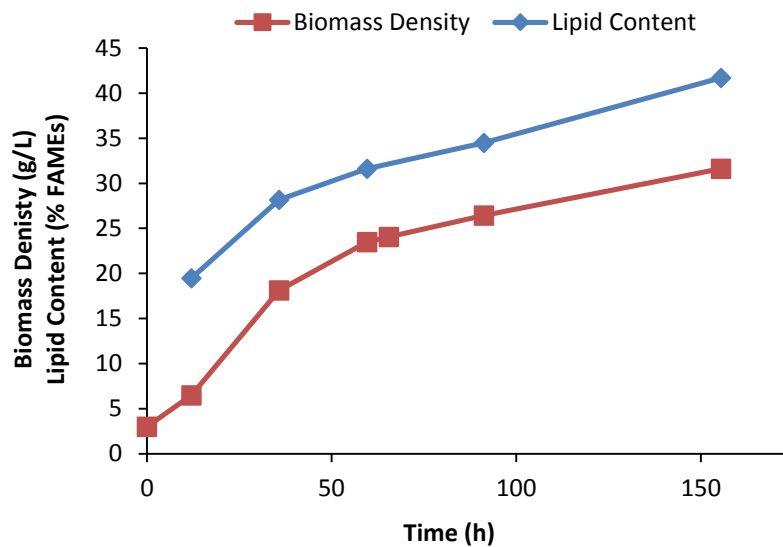


Figure 2.4. Biomass density and lipid content over time in sterile fermentation of *C. protothecoides* (3.5 L Bioflo 3000).

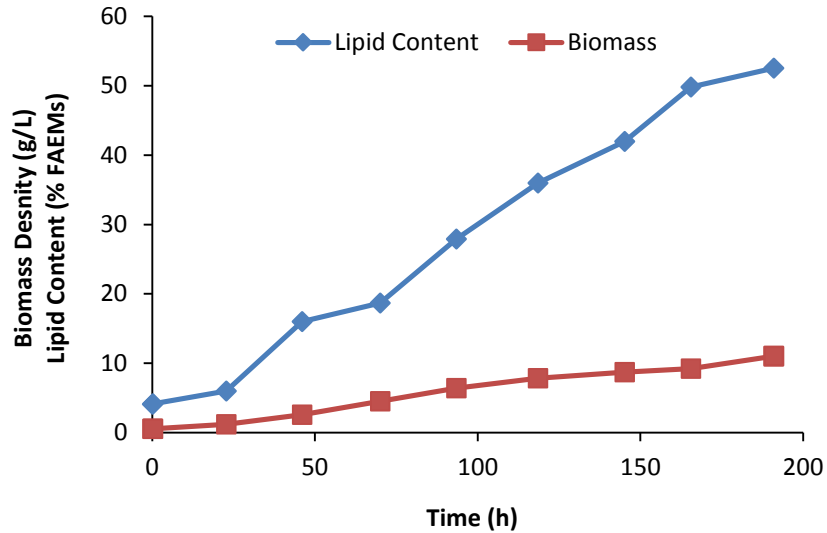


Figure 2.5. Biomass density and lipid content over time in non-sterile carboy fermentation of *C. protothecoides* (10 L plastic carboy).

In both fermenters, the lipid content of the biomass at the conclusion of the batch was between 40-50% when measured as FAMES. As expected, the vast majority (95%) of these lipids were TGs, with about 2% DG, 1% MG, and 2% FAs. Under light microscopy, it was easy to see large cytoplasmic lipid inclusion bodies (Figure 2.6). Notably, the FA profile during heterotrophic growth tended to change over time in a similar way as observed during cultivation of *C. vulgaris*. As shown in Figure 2.7, the proportion of oleic acid (C18:1) rose over time as the amount linoleic (C18:2) and linolenic (C18:3) FAs declined. These data suggest that *C. protothecoides* makes lipids well suited for biodiesel when grown heterotrophically.

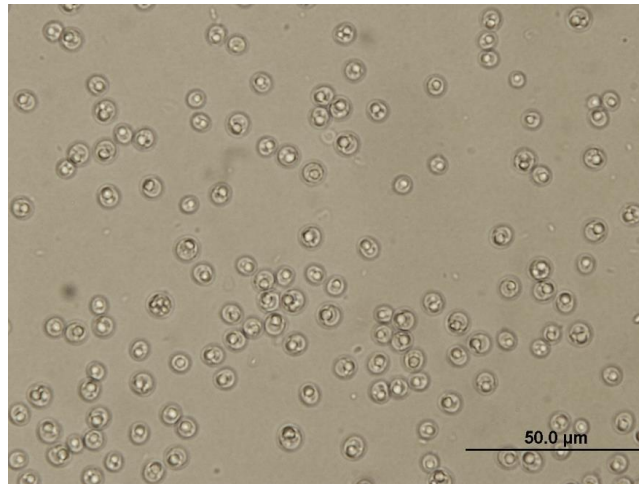


Figure 2.6. Light microscopy of *Chlorella protothecoides* grown heterotrophically. Note the large lipid droplets in most cells.

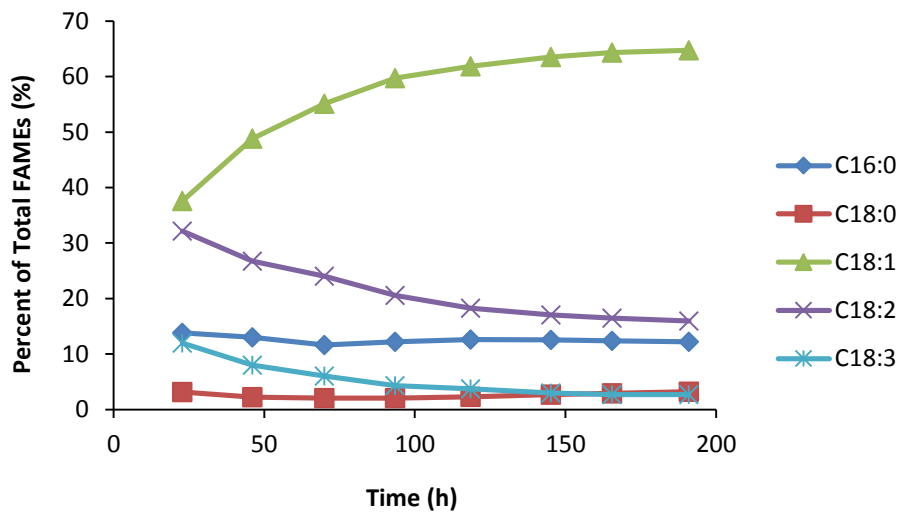


Figure 2.7. Fatty acid profile of *C. protothecoides* over time during non-sterile fermentation on glucose

Finally, in an effort to demonstrate that *C. protothecoides* is capable of growth on carbon substrates besides pure glucose, which is critical to reduce the environmental footprint associated with fermentation-based biofuels, we performed shake flask experiments to compare growth in XBM media containing glucose, glycerol, and cellulosic hydrolysate. As shown in Figure 2.8, biomass density reached the highest concentration after about 75

hrs in the cultures which contained 75% XBM media (30 g/L glucose, 4 g/L yeast extract) and 25% cellulosic hydrosylate. These data indicate that the hydrosylate more than compensated for the reduction in the amount pure glucose added to the flask and likely provided sugars that *C. protothecoides* could readily metabolize. Notably, however, when 50% of the standard media was replaced with the hydrosylate, very little growth occurred. Although this could be due to the presence of inhibitors, it is also likely that pH played a strong role in reducing growth rates. The hydrosylate had a pH near 4.5, causing the initial pH of this flask to be 4.8 compared to the 6.8 of the control flask containing 100% XBM with glucose. Experiments with even higher levels of the hydrosylate revealed similar pH-dependent growth inhibition. It is also possible that the superior growth of the culture that received 25% hydrosylate could be due to the hydrosylate's buffering capacity. Fermentation produces organic acids and carbonic acid from dissolved CO<sub>2</sub> that naturally drives down the culture pH over time. For example, the control flask had a pH of 3.9 at hour 75 compared to 5.8 for the flask with 25% hydrosylate. The complex matrix of the hydrosylate likely affords better capacity to absorb changes in pH, which may have supported higher growth rates for longer. This experiment also revealed that growth on glycerol was superior to that on glucose, but again pH effects may have played an important role. When grown on glycerol, cultures produce far less acid compared to growth on glucose, so the pH was 6.3 at hour 75. Taken together, these data suggest that cellulosic hydrosylates and waste glycerol are likely suitable substrates for *C. protothecoides* fermentation. Future work should examine the growth performance and lipid productivity of *C. protothecoides* when grown on these substrates in a controlled fermenter to remove pH as a confounding variable.

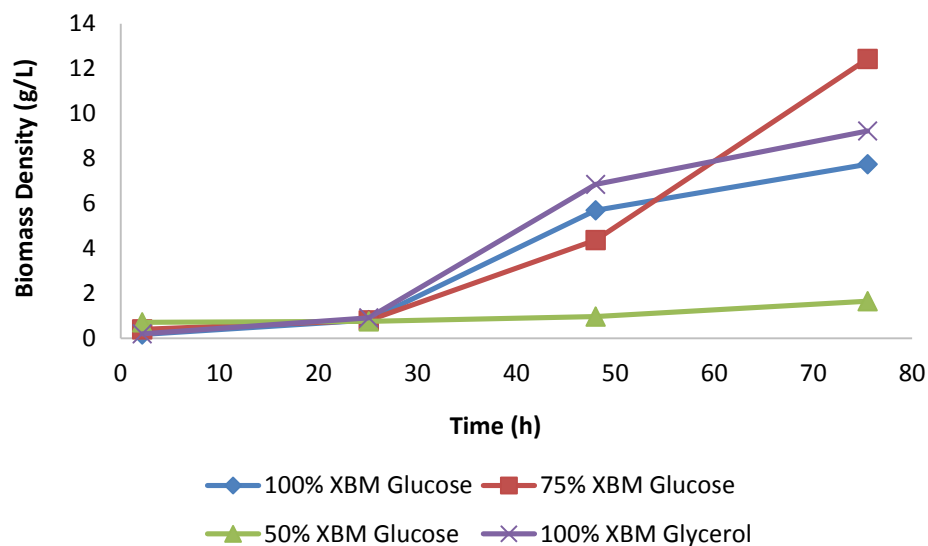


Figure 2.8. Biomass density over time in shaker flasks containing *C. protothecoides* grown in standard media containing glucose, glycerol, or cellulosic hydrosylate. The treatments containing 75% and 50% XBM contained 25% and 50% cellulosic hydrosylate provided by Bio Process Innovation, respectively.

### 2.3.3 Marine bi-culture

The seed culture from an open pond containing predominantly *Nannochloropsis* was grown in f/2 media containing 70 mg/L N as NaNO<sub>3</sub> and 13.5 mg/L P along with a ten-fold higher dose of trace metals and vitamins. Although biomass density increased over time during the initial batch (cf. 0.24 g/L to 0.71 g/L over the course of 5 days), the lipid content of the biomass remained very low (4–6% total FAMES on a dry weight basis). This was partly expected since nitrogen was supplied in excess and the cells were actively dividing; however, a surprising change in the fatty acid profile was observed during the days immediately following the first grow out of the seed culture (Figure 2.9). When the first lipid analysis was taken 3 days after inoculation, the fatty acid profile was similar to what would be expected for *Nannochloropsis* based on previous reports (Table 2.4): a high proportion of C16:0 and C16:1 fatty acids (30-50% of total fatty acids), moderate amounts of C18:1 (3-10%), very little C18:0, C18:2, or C18:3 (each less than 5% typically) and a large amount of EPA (15-35%). Within just a few days, the proportion of C16:0, C18:2, and C18:3 fatty acids rose while the amount of C16:1 and C20:5 fatty acids fell sharply.

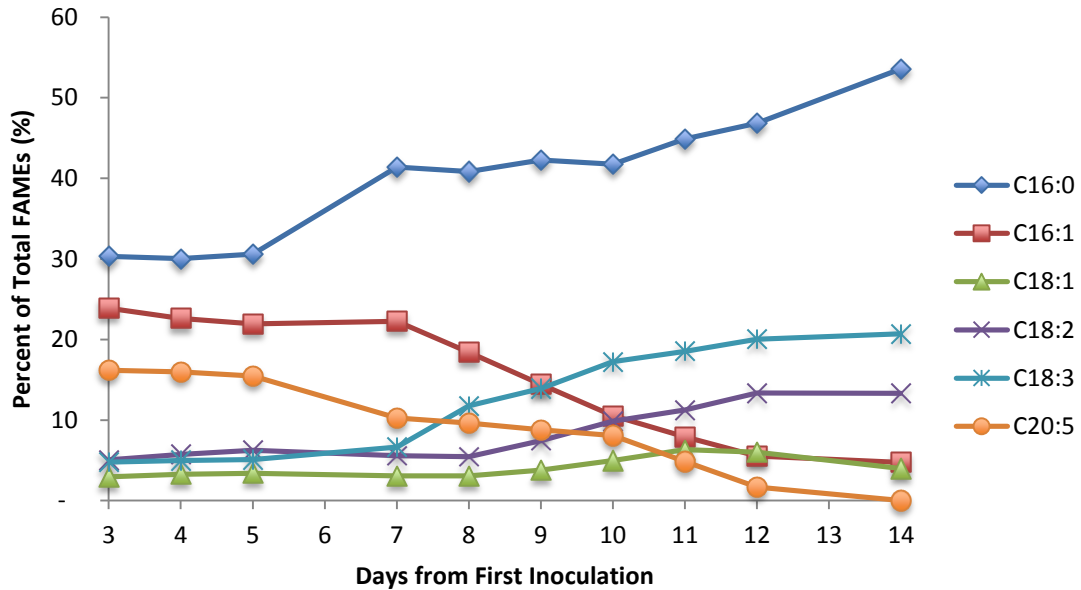


Figure 2.9. Change in fatty acid profile for developing marine bi-culture immediately following introduction of metal stress

At first we considered whether this observation could be due to the selective inhibition of enzymes responsible for fatty acid desaturation and elongation in *Nannochloropsis* as a result of the high metal concentrations. To our knowledge, no evidence in the literature suggests that this type of inhibition has been observed in *Nannochloropsis*, although work in marine brown algae (Harwood and Jones, 1989; Guschina and Harwood, 2006) and a freshwater green algae (McLarnon-Riches and Rolph, 1998) has demonstrated fatty acid profile changes due to high metal concentrations. If such inhibition had occurred, we would expect it to be reversible; yet, when cultures exposed to elevated metals were subsequently cultured in control media, no EPA and only trace amounts of C16:1 fatty acids were detected.



Table 2.4. Fatty acid profiles for relevant microalgae

Species	Fatty Acid (wt. % of total lipids)								Source
	C16:0	C16:1	C17:0	C18:0	C18:1	C18:2	C18:3	C20:5	
<i>Nannochloropsis oculata</i>	14.5	15.7	4.1	1.8	10.1	3.6	2.5	21.5	(Roncarati et al., 2004)
<i>Nannochloropsis oculata</i> (Reed)	21.4	24.2	0.7	0.3	4.6	0.1	0.9	36.4	This work
<i>Nannochloropsis</i> (From pond)	30.0	22.6	1.8	0.5	3.3	5.8	5.0	16.0	This work
<i>Nannochloris</i>	11.5	2.5	0.9	1.27	19.1	19.2	32.0	0.2	(Roncarati et al., 2004)
<i>Nannochloris oculata</i> <sup>a</sup>	31.5	n/a	n/a	0	2.3	26.1	31.2	0	(Park et al., 2012)
<i>Nannochloris oculata</i> <sup>b</sup>	35.7	n/a	n.a	2.8	11	31.2	14	0	(Park et al., 2012)
<i>Synechocystis</i> sp. PCC 6803	60.6	9.8	n/a	1.3	1.9	9.8	16.6	n/a	(Sheng et al., 2012)

Notes. <sup>a</sup> Fatty acid profile during nutrient replete growth. <sup>b</sup> Fatty acid profile during nutrient deprivation.

We considered too that *Nannochloropsis* may have mutated under the stress of high metal concentrations. Previously, *Nannochloropsis* has been mutated using ethyl methane sulfonate (EMS) in attempts to improve its lipid productivity. In one study, which also employed 4-fold more trace metals than recommended by the f/2 recipe, EMS-induced mutation did not lead to any significant changes in the fatty acid profile (Anandarajah et al., 2012). In another study, EMS-induced mutation of *Nannochloropsis* led to increased total lipid content with a smaller proportion as EPA, which the authors noted was ideal for biodiesel (Doan and Obbard, 2012). Given that previous work has had to rely upon a strong mutagenic agent like EMS and low survival rates to isolate new *Nannochloropsis* mutants, it appears unlikely that over the course of 10 days we selected for a mutant *Nannochloropsis* with irreversibly suppressed fatty acid desaturation and elongation capabilities.

Because the original seed culture came from an open pond that probably contained other algae species, it is more likely that the metal-induced stress selected for species that are more metal tolerant than *Nannochloropsis* and do not produce EPA. Light microscopy of the cultures over time revealed that the original seed culture, which appeared to contain predominantly one green spherical cell resembling *Nannochloropsis*, became a bi-culture

that included one larger green species and a smaller teal-colored species (Figure 2.10). The larger spherical cell was 5-8 microns in diameter with a green pigmentation, parietal chloroplasts, and some circular inclusions that look similar to, but not morphologically identical, to *Chlorella*. The other cell was smaller, 2-4 microns in diameter and was typically observed as a single cell or diploid and appeared without inclusions and with a teal color.

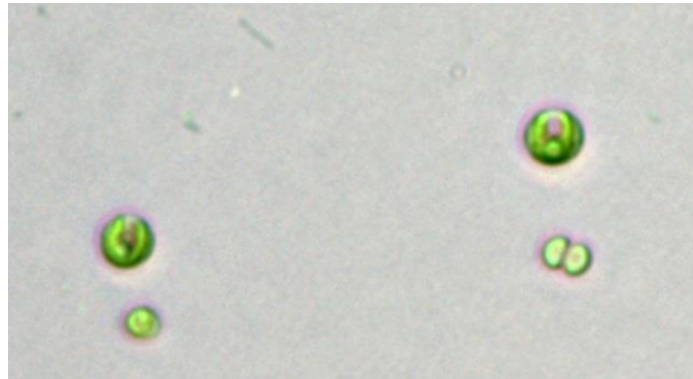


Figure 2.10. Light microscope image of bi-culture. Larger green algae cells were tentatively identified as *Nannochloris*, and smaller teal-colored cells, are suspected to be *Synechocystis*. The smaller spherical cells were commonly found to be dividing by fission, as shown on the right hand side. Minor bacterial contamination, typically in the form of rod-shaped cells, is evident in the upper left hand portion of the image.

Although it was not possible to ascertain the precise identity of these two species without a genetic analysis, which was beyond the scope of this work, we have compared our microscope observations and the measured fatty acid profile with previously published information to tentatively identify the larger cell as *Nannochloris* and the smaller cell as *Synechocystis*. *Nannochloris* is a green algae that is commonly found as a contaminant in cultures and has reportedly been found before in the pond growing *Nannochloropsis* used as the seed material for this study (Dr. Brian Goodall, personal communication). *Nannochloris* has previously been found to contain lipids rich in C16:0, C18:2, and C18:3 fatty acids (each greater than ~20% of total fatty acids) while being almost completely devoid of EPA (Table 2.4). In addition, like most green algae, *Nannochloris* has been found to accumulate storage lipids in response to N deprivation (Yamaberi et al., 1998; Takagi

et al., 2000). Finally, *Nannochloris* was previously found to be the dominant species in a eutrophic waterway and was successfully cultured outdoors with few contaminants for over 2 years (Witt et al., 1981). This work also demonstrated that *Nannochloris* was euryhaline and had a preference for ammonia-N over nitrate, which would indicate it is well suited to grow on the aqueous phase liberated during HTC and may be able to outcompete other organisms in its environment.

We suspect the smaller cells to be the gram-negative cyanobacterium *Synechocystis* sp., which has gained attention recently due to its physiological robustness, its ability to grow both heterotrophically and photosynthetically, and the ease with which it can be genetically transformed (Rittmann, 2008; Sheng et al., 2012). In contrast to algae, which typically accumulate lipid as a storage material during stressful conditions and slow growth rates, cyanobacteria accumulate lipids in thylakoid membranes, which are associated with high levels of photosynthesis and rapid growth rates (Rittmann, 2008) (Rittmann, 2008). As a result, cyanobacteria may have an advantage over algae in that they can produce lipids under nutrient replete conditions with higher overall productivity. *Synechocystis* has been reported to contain very high amounts of C16:0 fatty acid (~60%) while having only moderate amounts of C18:2 and C18:3 (10-16%), very little C18:1 (~2%), and no EPA (Table 2.4).

Although the lipid profile of the culture changed somewhat during each batch and over time as culture conditions varied, in general, it is likely that a combination of *Nannochloris* and *Synechocystis* cells contributed to overall lipid production. Although previous works have attributed the C18:3 content of *Nannochloropsis* cultures to contamination by other green algae such as *Tetraselmis* (Khozin-Goldberg and Boussiba, 2011; Quinn et al., 2012), the morphology of the cells observed in the BCRs were not consistent with this alga. Griffiths and Harrison (2009) collected data on the potential of 55 microalgae and cyanobacteria species to serve as biodiesel feedstocks and noted that *Synechococcus* and *Nannochloris* had lipid contents under nutrient replete conditions of about 11% and 28%,

respectively. Both species were also reported to have a very similar lipid productivity of about 75-77 mg/L/d under nutrient replete conditions (Griffiths and Harrison, 2009). In the first two batches, because biomass productivity and lipid content were most likely depressed by the high metal content, lipid productivity was very low (<12 mg/L/d); however, once the metal stress was removed, this bi-culture remained stable over time and demonstrated substantially higher productivities. These data are presented along with the nutrient recycling experiments in Chapter 7.

## 2.4 Conclusions

This work demonstrated that *C. vulgaris* and *C. protothecoides* are robust organisms for biofuel production and can be grown to accumulate large amounts of lipids (~50%) that are well suited for biodiesel. In particular, we corroborated previous work that demonstrated that sequential phototrophic and heterotrophic growth phases can be used to produce lipid-rich *Chlorella*. We extended this work to include both sterile and non-sterile fermenters, and demonstrated that glycerol and delignified cellulosic hydrolysate can serve as carbon substrates. These preliminary growth experiments warrant repeating under more controlled conditions to collect better data on the biomass and lipid productivity of heterotrophic *Chlorella*. Ultimately, our work suggests that fermenters may offer a route to significantly reduce the cost and environmental footprint of algal biofuels production, if low-cost and sustainably-sourced carbon feedstocks become available.

We also demonstrated the utility of a metal stress protocol to select for stresstolerant phototrophic organisms in an open pond culture. Although our initial goal was not to completely inhibit *Nannochloropsis* growth, we developed a stable marine bi-culture that consisted mostly of the green algae *Nannochloris* and the cyanobacteria *Synechocystis*. This co-culture did not produce EPA and had a fatty acid profile suitable for use in biofuels. Its ability to grow well on the aqueous phase co-product from HTC will be further discussed in Chapter 7.

## CHAPTER 3

### HYDROTHERMAL CARBONIZATION

#### 3.1 Background

##### 3.1.1 Introduction to hydrothermal processing

Hydrothermal processing, which involves the application of heat and pressure to biomass in an aqueous medium, mimics the conversion of ancient plant material into the crude oil, coal, and natural gas reservoirs we rely upon today. Hydrothermal processing is uniquely suited to algal biomass because algae grow in water and still contain about 80% moisture after mechanical dewatering (e.g., filtration and centrifugation). In this process, hot water serves as a solvent, a reactant, and even a catalyst or catalyst precursor.

Hydrothermal processing can occur over a continuum of temperature and pressure regimes to yield desired solid, liquid, and gaseous products (Savage et al., 2010). Under mild conditions (180–250 °C, 10–40 bar), bio-macromolecules hydrolyze and react in a process called hydrothermal carbonization (HTC), yielding a solid hydrochar or carbonized solid. This process has alternatively been called wet torrefaction, wet pyrolysis, or coalification (Titirici, Thomas, and Antonietti, 2007; Titirici, Thomas, Yu, et al., 2007). At elevated temperatures and pressures (250–350 °C, 40–165 bar), hydrothermal liquefaction yields a viscous bio-crude oil. If a suitable catalyst is used in this temperature range, it is possible to convert biomass to biogas, a mixture containing about 60% CH<sub>4</sub> and 40% CO<sub>2</sub>, through low-temperature catalytic hydrothermal gasification (CHG). Above the critical point of water (374 °C, 221 bar), biomass fragments decompose further, even without added catalyst, to form permanent gases. In this regime, the process is referred to as supercritical water gasification.

As outlined in recent reviews (Huber et al., 2006; Peterson et al., 2008; Savage et al., 2010), hydrothermal processing has unique advantages for wet biomass related to both

the chemistry (e.g., rapid hydrolysis, enhanced deoxygenation) and engineering considerations (e.g., higher energy efficiency). Importantly, hydrothermal processing requires less energy than drying the biomass because the energy penalty associated with the phase change from liquid water to vapor is avoided. For instance, the enthalpy change required to take liquid water at 25 °C to a liquid at 250 °C is less than half of that required to vaporize the water (i.e., dry the biomass). In addition, hydrothermal processing allows for integrated energy recovery because the hot reactor effluent stream can be used to preheat the ambient temperature feed stream, resulting in high process efficiencies (Goudriaan et al., 2000; Peterson et al., 2008). In comparison, conventional biomass conversion processes that use drying tend to use lower temperatures, making energy recovery from process streams more difficult.

### 3.1.2 The properties of water

Hydrothermal processing relies on the unique properties of water at elevated temperatures and pressures. As shown in Figure 3.1, higher temperatures diminish hydrogen bonding and reduce water's dielectric constant. As a result, many organic compounds, such as cellulose, become completely miscible in high temperature water, whereby they can be subject to hydrolytic attack (Kamio et al., 2007; Kumar and Gupta, 2008). From a solubility perspective, water under these conditions behaves much like a non-polar organic solvent. Furthermore, the ion product ( $K_w = [\text{OH}^-][\text{H}^+]$ ) for liquid water increases with temperature, being nearly three orders of magnitude higher at 250 °C than it is at ambient temperatures. Accordingly, high temperature water boasts higher  $\text{H}^+$  and  $\text{OH}^-$  concentrations than ambient liquid water, increasing the effectiveness of hydrolysis and dehydration reactions, which are known to be acid or base catalyzed.

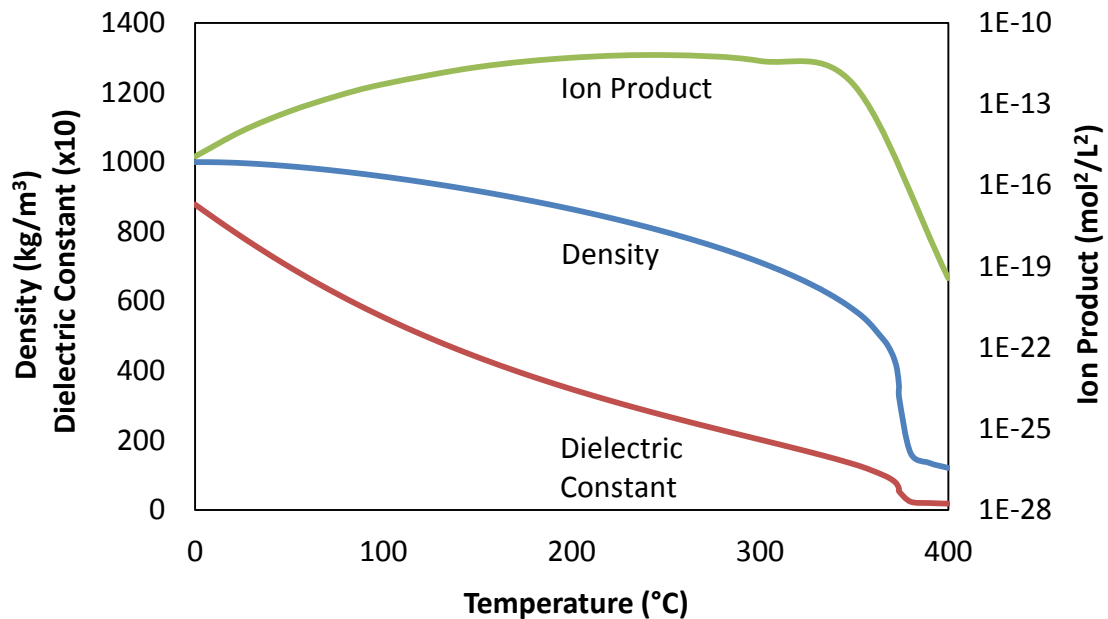


Figure 3.1. The properties of liquid and supercritical water. Data from: (Marshall and Franck, 1981; Haar et al., 1984; Green and Perry, 2008). For temperatures >374 °C, a pressure of 220 bar is assumed to calculate the density.

### 3.1.3 HTC of wet algal biomass

The advantages of processing algae in high temperature water led us to explore how HTC could be used to convert wet algal biomass into a lipid-rich hydrochar. Traditionally, HTC has been applied to lignocellulosic feedstocks as a way to increase energy density, reduce moisture content, and improve storability prior to thermochemical conversion processes (Titirici, Thomas, and Antonietti, 2007; Guiotoku et al., 2009; Yan et al., 2009; Yan, Hastings, et al., 2010). HTC has also been used for the synthesis of functional carbonaceous materials, such as carbon nanospheres, from carbohydrate precursors (e.g., glucose) using low temperatures (~200 °C) and long retention times (4–24 h) (Titirici, Thomas, Yu, et al., 2007). In both of these cases, the main focus has typically been on the solid hydrochar products, with little consideration given to the constituents of the biomass liberated to the aqueous phase or its potential nutrient value. In contrast, the application of HTC to municipal biosolids, the 10–15% solids material produced at wastewater treatment plants, is perhaps the most similar application of HTC to wet algae

processing and one in which the biological digestibility of the aqueous phase co-product has been seriously considered.

Thermal pre-treatment of biosolids from 150–200 °C has been shown to destroy the cellular structure of activated sludge flocs, greatly improve dewaterability, and increase biogas yields in downstream anaerobic digestion (Neyens and Baeyens, 2003). Several papers have highlighted that a temperature of 175 °C with a 30 min retention time appears to be ideal, gauged by high dewaterability (~40–50% solids in the cake) and a low amount of refractory chemical oxygen demand (COD) in the aqueous phase co-product. Notably, increasing temperatures to 180 °C and higher was found to increase the fraction of COD in the aqueous phase that was not removed during anaerobic digestion, suggesting that if the aqueous phase is going to be used as a nutrient source for algae, consideration should be given to how temperature affects the biological usability of these nutrients. This process is being carried out at commercial scale by several companies, referred to alternatively as the thermal hydrolysis process (Cambi AS, Norway) and SlurryCarb™ (EnerTech, USA). According to Cambi literature, waste-activated sludge is heated by steam injection at 150-165 °C for 20-30 min and then further disrupted by rapid pressure drop in a flash tank, producing an effluent stream well suited to anaerobic digestion and subsequent dewatering. In contrast, the SlurryCarb™ process is carried out at a “temperature sufficiently high so that cell structure is destroyed” (Dickinson et al., 2006) thereby liberating previously cell-bound water in sewage sludge and making it easier to dehydrate the hydrochar into a solid fuel (15 to 18.5 MJ/kg). EnerTech recently began operating a facility in Rialto, California that reportedly will produce 60,000 tons of carbonized solids annually for use as an environmentally-preferable alternative to coal at local cement kilns (EnerTech Environmental Inc., 2013).

From this previous literature, as well as our experience with hydrothermal liquefaction at more severe conditions, we hypothesized that it would be possible to carbonize wet algal biomass in a manner similar to cellulosic feedstocks by reacting a slurry of 15–20% solids



at 180–250 °C. The two primary goals of this process were to (1) retain all the lipids of the algal biomass within a solid hydrochar that would be easy to separate from its surrounding aqueous environment, and (2) to convert organic, non-lipid components of the algal biomass into soluble nutrients that would be usable by the algae for growth. At the outset of our work in 2009, we also sought to hydrolyze the lipids retained by the hydrochar to create fatty acids and smaller glycerides that would be more readily converted into biodiesel in subsequent transesterification reactions. We suspected that the properties of high-temperature liquid water could be tuned to engender the hydrolysis of intracellular lipids and organic sources of N and P (e.g., proteins and phospholipids), while also affecting the dehydration, condensation, polymerization, and aromatization of polysaccharides in the cell wall and extracellular matrix (mainly glucosamine, rhamnose, galactose, glucose, and mannose) that are thought to contribute to improved solids conglomeration (Takeda, 1991).

Our use of HTC on a lipid-rich algal biomass was unique in that we focused on whole biomass processing rather than follow the conventional route of first isolating and then purifying the lipid fraction of the algae. Prior to beginning our work, we were aware of only one previous paper that considered HTC of microalgae. Heilmann et al. (2010) heated wet algal biomass to temperatures between 190–210 °C to generate hydrochar suitable for co-generation with coal. Their work suggested that solids conglomeration of algae was possible with relatively high carbon and solids yields (55% and 39%, respectively, at 200°C and 90 min), but they did not focus on the production of liquid fuels and neglected to measure the lipid content of the reactant biomass or resulting hydrochar (Heilmann et al., 2010). Following our first publication on the subject (Levine et al., 2010), this group published a second paper focused on extracting lipids from the hydrochar using organic solvents, and presented preliminary data suggesting the aqueous phase co-product had utility as a growth media for algae (Heilmann, Jader, Harned, et al., 2011). Two other recent papers from the University of Minnesota highlighted HTC as a suitable pre-treatment for pyrolysis (Du, Mohr, et al., 2012), because it significantly reduces the energy

required to dry the biomass, and demonstrated the utility of the aqueous phase as a nutrient source for *C. vulgaris* (Du, Hu, et al., 2012). A review of the recent literature shows that HTC of microalgae is a relatively new subject, and though the technology has been used in other fields for decades, there is tremendous opportunity to learn more about its role in algal biomass processing.

With regards to lipid hydrolysis, previous work has been limited to studies concerned with subcritical water hydrolysis of pure vegetable oils (Holliday et al., 1997; King et al., 1999; Pinto and Lanças, 2006; Moquin and Temelli, 2008; Alenezi et al., 2009; King and Srinivas, 2009). To our knowledge, no previous work has investigated the in situ hydrolysis of cellular lipids by subcritical water. Work with pure vegetable oils indicated that hydrolysis is predominately a homogenous reaction in the oil phase (Lascaray, 1952), consisting of three reversible, stepwise reactions that convert TGs into diglyceride (DG), monoglyceride (MG), and finally glycerol, with each step liberating a FA molecule (Figure 3.2). Complete hydrolysis can be achieved quickly (15–20 min) in water at 270–280 °C with no degradation of saturated fatty acids but some reduction in the amount of polyunsaturated FA due to isomerization (*cis* to *trans*) and degradation (King et al., 1999). Considering the large excess of water present in wet algal biomass, we hypothesized that it would be possible to reach very high equilibrium conversions of TGs during HTC.

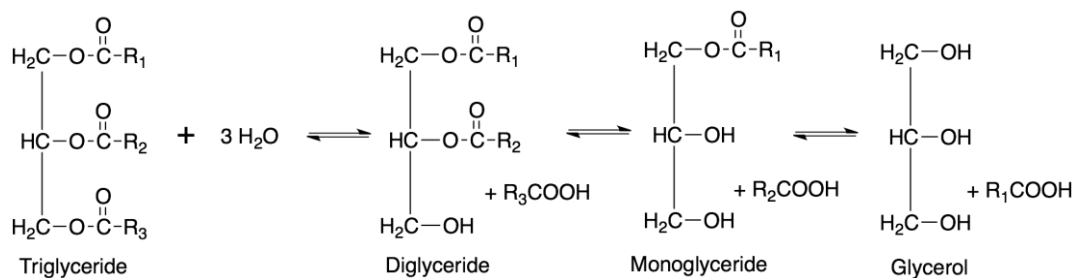


Figure 3.2. Hydrolysis of triglycerides

## 3.2 Materials and Methods

### 3.2.1 HTC

All carbonization reactions with wet algal biomass were carried out in 316 stainless steel (SS) reactors fashioned from Swagelok parts (2 caps and 1 port connector). All biomass samples were reacted as wet pastes with 15–25% solids contents, with the exception of heterotrophically grown *C. vulgaris*, which was first dried and then rehydrated. In exploratory experiments, no difference in the solids yield, elemental composition, or moisture content of hydrochar was found when reactions were completed with freshly harvested biomass or dried and rehydrated material. *Nannochloropsis oculata* biomass was special ordered from Reed Mariculture Inc. to be free of any preservatives and was stored as a ~32% solids clay prior to use. Previously frozen or freshly harvested biomass was loaded by mass into the Swagelok reactors such that the reactor headspace was less than 10% of the total reactor volume under reaction conditions. Small (4 mL) reactors were used for initial HTC factorial experiments while larger (28 mL) reactors were used routinely for processing larger quantities.

Once loaded, reactors were immersed in a preheated, isothermal fluidized sand bath for the desired amount of time and then promptly removed and cooled in water. Temperatures between 180 and 250 °C were explored with reaction times from 5 to 180 min. Upon cooling, the aqueous phase and solids were separated by filtering under light vacuum (pre-dried, pre-weighed 934-AH filter paper (Whatman) or Fisherbrand P2 paper) or by centrifugation. When centrifuging, the reactor contents were emptied into 50 mL centrifuge tubes and 25 mL of distilled water were used to rinse the reactor housing. The reaction mixture was centrifuged (10,000 RCF x 5 min) to pellet the hydrochar, and the supernatant (i.e., aqueous phase) was transferred to a new tube. The solids were rinsed with 5 mL of distilled H<sub>2</sub>O, briefly vortexed, and centrifuged again prior to storage (4 °C) or drying (65 °C for 1 or 24 h). In 28 mL reactions, the wash water was combined with the aqueous phase and the total volume of aqueous phase was diluted to 50 mL with distilled

H<sub>2</sub>O. Typically, multiple HTC reactions were pooled to produce enough diluted aqueous phase for the growth experiments detailed in Chapter 7.

The solids from each reaction were analyzed to determine the solids yield (g dry hydrochar/g dry biomass reacted), the lipid retention in the hydrochar (g lipid in hydrochar/g lipid in biomass reacted), and the elemental composition (C, H, N). From some reactions, a portion of the wet carbonized material collected by filtration or centrifugation was dried separately to accurately determine its moisture content. The higher heating value (HHV, MJ/kg) of the reactant biomass and each hydrochar was estimated based on the elemental analysis according the following formula (Friedl et al., 2005):

$$\text{HHV} = (3.55\text{C}^2 - 232\text{C} - 2230\text{H} + 51.2\text{C} \times \text{H} + 131\text{N} + 20,600)/1000$$

### 3.2.2 Aqueous phase analysis

Aqueous phase samples were analyzed for total organic carbon (TOC) using a Shimadzu TOC-V machine (50  $\mu\text{L}$  injection, replicate injections made if standard error of peak area > 0.2%). TOC was calculated by subtracting the inorganic carbon (IC) from total carbon (TC). Aqueous phase samples were further analyzed using HPLC (Agilent 2100 series, 5  $\mu\text{L}$  injection onto a Phenomenex ROA Organic Acids 7.8 mm x 300 mm column at 60 °C, 0.005 N H<sub>2</sub>SO<sub>4</sub> mobile phase, refractive index detector) and by GC-MS (Agilent 6890N and 5973N MSD, 1  $\mu\text{L}$  injection with 0 to 10:1 split ratio onto HP-InnoWax column J&W 1909BD-113; 260 °C inlet temperature, 40 °C initial column temperature with 5 °C/min rise to 250 °C). The total nitrogen (TN), ammonia-N (NH<sub>4</sub>-N), total phosphorus (TP), and reactive phosphorus (PO<sub>4</sub>-P) were measured spectrophotometrically using kits supplied by Hach.

The dissolved organic matter in the aqueous phase was further characterized using ultrahigh resolution Fourier transform ion cyclotron mass spectrometry (FT-ICR-MS).

Aqueous phase samples were diluted with 1:1 (v/v) methanol:water (LC-MS grade) and infused continuously into the Apollo II ESI ion source of a Bruker Daltonics 12 Tesla Apex Qe FT-ICR-MS at a rate of 2  $\mu\text{L}/\text{min}$  (COSMIC facility at Old Dominion University). Shield and capillary voltages were optimized for each sample to maintain constant and stable ion currents in negative ion mode. Ions were accumulated in a hexapole for 1 s before being transferred to the ICR cell, where 300 scans collected with a 4-MegaWord time domain were co-added in broadband mode from 200-1200  $m/z$ . The summed FID signal was zero-filled once and Sine-Bell apodized prior to fast Fourier transform and magnitude calculation using the Bruker Daltonics Data Analysis software. Polyethylene glycol was used to externally calibrate the instrument to an accuracy of  $<1$  ppm prior to analysis of samples. Internal calibration was performed on each sample using a peptide homologous series that was detected across all samples. Elemental formulae were assigned, with an accuracy of  $<1$  ppm, using a Matlab program developed and described previously (Stubbins et al., 2010).

### 3.2.3 Analysis of lipids within algal biomass and hydrochars

Lipids from all classes in algal biomass and carbonized solids were simultaneously extracted and catalytically transesterified to determine the total lipid content, as described previously (Section 2.2.6, page 22). Briefly, solids were reacted with methanol containing 5% acetyl chloride to produce FAMES, which were extracted into heptane containing internal standard (C23:0 FAME) and analyzed by GC-FID. Lipids were also extracted from some hydrochars using HIP (3:2 v/v) to determine the relative proportions of TG, DG, MG, and FA, as described in Section 2.2.7, page 24.

## 3.3 Results and Discussion

### 3.3.1 Early work in high-temperature HTC of *C. vulgaris* biomass

*C. vulgaris* biomass containing about 53% lipids was grown phototrophically and then heterotrophically as described in Section 2.2.3 (page 20) and subjected to hydrothermal

processing. In our initial studies of HTC, we sought to conglomerate the biomass into a filterable solid, hydrolyze intracellular lipids, and generate a sterile, nutrient-rich aqueous phase. In this early work, the lower temperature limit for HTC was determined in exploratory experiments that indicated formation of a black, charcoal-like filterable solid above 225 °C, but not at lower temperatures (Figure 3.3). The upper temperature limit for hydrolysis was selected to limit excessive FA trans-isomerization and potential degradation of unsaturated fatty acids that could impact fuel quality (Holliday et al., 1997; King et al., 1999; Kocsisová et al., 2006). Based on these reports, 250 °C was chosen for this initial investigation of how intracellular lipids changed during HTC.



Figure 3.3. *Chlorella* hydrochar obtained from reaction at 250° C for 30 min

Hydrochars produced at 250 °C and 15 to 60 min contained approximately 77–85% lipids when measured as the gravimetric yield of the HIP extraction or by quantifying the total amount of TG, DG, MG, and FA by HT-GC-FID (Figure 3.4). Typically, we found very good agreement between gravimetric analyses and GC quantification, indicating that the highly automated, micro-scale extraction and derivatization method we developed performed well. Likewise, lipid analysis by acid-catalyzed in situ transesterification revealed similar, albeit slightly lower, values (Table 3.1). The composition of the lipids in the unreacted biomass and each hydrochar is shown in Figure 3.5. It is evident that the lipids in the reactant biomass were almost exclusively TGs but that the TG content decreased and FA content increased with time as the biomass was reacted at 250 °C. This can also be

appreciated visually on the HT-GC-FID chromatogram shown in Figure 3.6. The content of MG also increased with time, while DG concentration increased up to 45 min, reached a maximum, and then declined. The trends apparent in Figure 3.5 are what one would expect for a series reaction like TG hydrolysis.

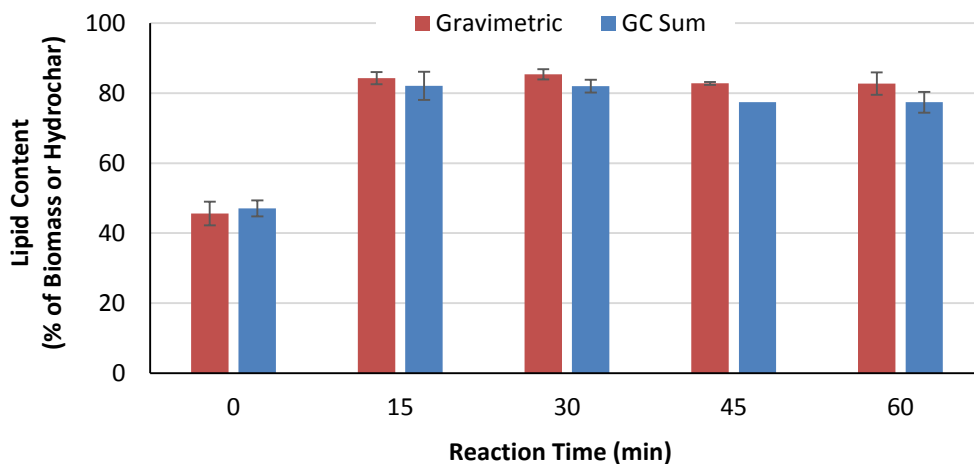


Figure 3.4. Lipid content of *C. vulgaris* biomass (time 0) and hydrochars (time 15–60 min) as measured by hexane:isopropanol extraction and quantified gravimetrically and by HT-GC FID. Error bars represent the mean  $\pm$  standard error of replicate extractions.

As also shown in Figure 3.5, the total lipid retention (wt.% of lipids in the dry algal feedstock loaded into the reactor that remained in the solids recovered after HTC) varied from 77 to 90%, with the highest retention occurring at the shortest reaction time. These data suggest that HTC at 250 °C may result in some loss of lipids from the hydrochar. We suspect most of these lipids reside within the aqueous phase, whether in their native forms (e.g., triglycerides, phospholipids, or glycolipids) or in hydrolyzed forms such as fatty acids. Our attempt to quantify the amount of lipid present in the aqueous phase by hexane extraction and subsequent transesterification of the extract rarely detected more than 5% of the original biomass lipid content in the aqueous phase. It is possible that the liquid-liquid extraction was incomplete, perhaps since lipids were present as fatty acid carboxylate anions that have been suggested to partition only weakly into the organic phase (Heilmann, Jader, Harned, et al., 2011). It is likely too that there were some losses

of lipid during the transfer of reactor contents and hydrochar solids. In a large-scale facility, we envision it may be possible to recover these lipids through a filtration and adsorption system prior to transferring the aqueous phase to the algal growth reactors. Overall, the net effect of this hydrothermal treatment for 60 min was to hydrolyze approximately 86% of the TGs in the feedstock and produce easy-to-recover solids containing ~80% of the total lipids, highly enriched in FA.

Table 3.1. Characterization of biomass feedstock and hydrochars for *C. vulgaris* HTC at 250 °C

Analysis	Biomass	HTC reaction time (min)			
		15	30	45	60
Ester yield (wt%)					
Gravimetric	52.9 ± 1.9	78.7 ± 4.1	70.8 ± 8.0	73.5 ± 2.8	73.0 ± 3.1
GC-FID	53.3 ± 1.3	77.1 ± 2.1	74.8 ± 1.1	73.1 ± 1.0	69.4 ± 0.4
Fatty acid (% of esters) <sup>a</sup>					
C14:0	0.4	0.5	0.2	bdl	bdl
C16:0	17.8	18.2	17.8	17.8	18.7
C18:0	2.1	2.1	2.3	2.0	2.2
C18:1	45.5	46.8	47.0	45.5	47.7
C18:2	9.0	9.2	9.1	8.7	9.0
C18:3	12.7	12.8	12.6	12.8	12.7

Note. Standard deviation is given for the mean of duplicate reactions/extractions; ester percentages all had a standard deviation less than 0.6%. <sup>a</sup>Other fatty acids detected, present at less than 5% of total fatty acids, included: C12:0, C16:1, C17:0, C20:0, C22:0, and C24:0. The percentages of C18:1, C18:2, C18:3 include all isomers. <sup>b</sup>Crude lipid extracted with hexane-isopropanol (3:2). <sup>c</sup>Replicate data was lost. <sup>d</sup>All elemental analysis data represent single analyses performed by Atlantic Microlab, Inc. (Norcross, GA). bdl = below detection limit.



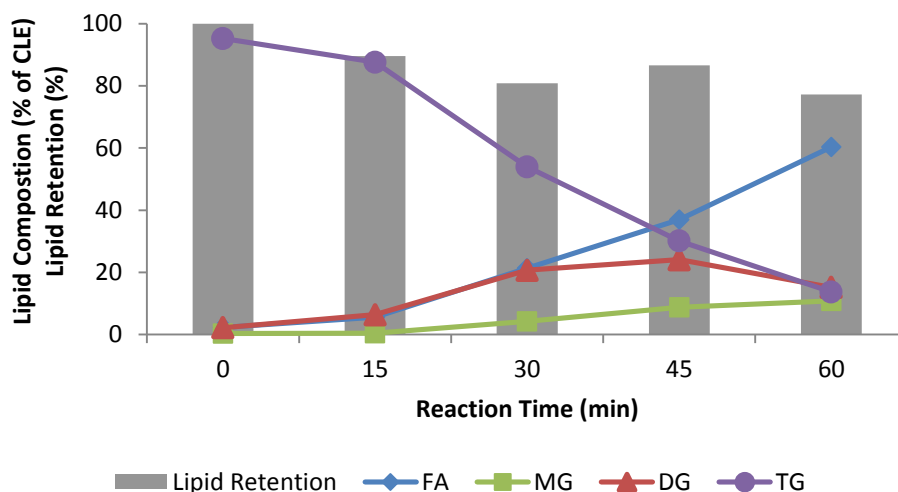


Figure 3.5. Lipid composition and lipid retention in *C. vulgaris* biomass and hydrochars generated by reaction at 250 °C for various times. Lipid composition is the proportion of fatty acids (FAs), monoglycerides (MGs), diglycerides (DGs), and triglycerides (TGs) in the crude lipid extract (CLE) obtained by hexane:isopropanol extraction. Lipid retention was calculated from the dry weight yield of hydrochar and the lipid content of both algal biomass and hydrochar solids as determined by their fatty acid ethyl ester composition from GC-FID analysis of acid catalyzed in situ transesterification. Time zero represents the heterotrophic algal biomass before HTC.

Table 3.1 also displays the FA profiles for the lipids in the reactant biomass and the hydrochar recovered at each reaction time. There was little variation in the distribution of the major FAEs with reaction time or in comparison to the original algal feedstock. This result indicates that there was no selective retention or rejection of certain FAs during the hydrothermal treatment; however, we did see evidence for isomerization and minor decomposition of linolenic acid (C18:3). About 10.4, 13.0, and 16.6% of the total C18:3 FAEE detected in reactions lasting 30, 45 and 60 min, respectively, were trans-isomerized. At 60 min, the percent difference between the yields of all C18:3 isomers and the average yield of saturated FAEE was 3.5%, suggesting some decomposition may have occurred at these longer times.

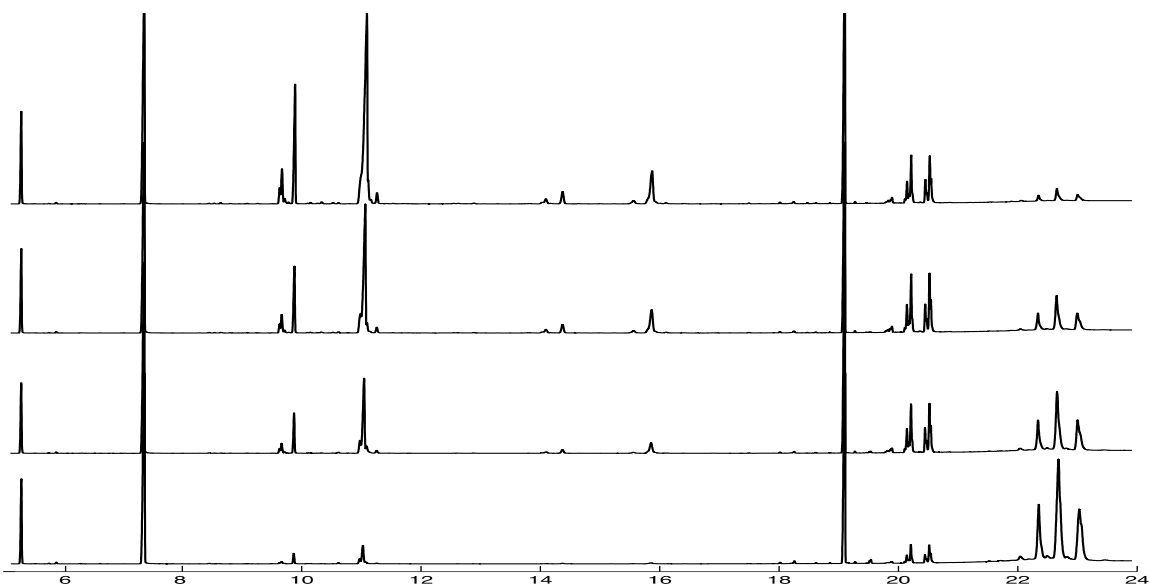


Figure 3.6. HT-GC-FID chromatogram showing fatty acids (9 to 12 min), monoglycerides (13.5 to 16 min), diglycerides (20 to 21 min), and triglycerides (22 to 24 min) of *Chlorella* hydrochars processed at 250 °C.

Table 3.2 provides the solids yield and elemental analysis of the hydrochars. The yield of hydrochar solids (% of mass in dry algal feedstock loaded into the reactor that remained in the solids recovered after HTC) was always about 60% regardless of the reaction time. These data compare favorably to the solids yields and C retention from hydrothermal reactions carried out on *Dunaliella salina* (5–25% solids) at 190–210 °C, which varied from 25 to 45% and 38 to 62%, respectively (Heilmann et al., 2010). The C, H, and N content also showed very little variation with time. The hydrochars were richer in C and H but had reduced amounts of N compared with the dry algal biomass feedstock. From 73–79% of the C and 41–52% of the N in the algal biomass feedstock was retained in the hydrochar solids. Carbon and nitrogen not retained in the hydrochar were most likely liberated as aqueous species. A similar enrichment in carbon has been observed for the hydrothermal carbonization of cellulose at 200–250 °C for 2 to 4 h; C increased from 44.4% in the parent material to 70.7–72.7% in the hydrochar, with solids yields and C retention in the range of 30–50% and 54–84%, respectively (Sevilla et al., 2011). Overall, the elemental composition of the hydrochar indicates a H/C ratio that is lower than that of the unreacted biomass. This result can be attained by either loss of material with a high H/C

ratio (e.g., glycerol lost to the aqueous phase) or by condensation of cellular material to form more hydrogen deficient moieties. During this process, we observed similar morphological changes to the algal biomass as has been described by others carbonizing cellulose and sugars (Sevilla and Fuertes, 2009). Mainly, the hydrochar appeared covered in microspheres that probably result from the severe chemical reactions affecting mostly the carbohydrate fraction of the cells (Figure 3.7).

Table 3.2. Hydrochar characterization from *C. vulgaris* HTC at 250 °C

Analysis	Feedstock	HTC reaction time (min)			
		15	30	45	60
Solids yield (wt%)		62	58	63	59
Elemental Analysis (wt %) <sup>d</sup>					
C	58.06	73.9	73.29	72.98	73.88
H	9.05	10.71	10.27	10.28	10.63
N	1.16	0.76	0.96	0.95	0.92
O	28.61	-	-	-	-
H/C	1.87	1.74	1.68	1.69	1.73
N/C	0.017	0.009	0.011	0.011	0.011
% C retained	-	78.8	72.7	79.3	75.5
% N retained	-	40.6	47.7	51.7	47.0
HHV (MJ/kg)	26	40	38	38	39
Energy densification	-	1.5	1.5	1.5	1.5
Energy yield	-	94	85	93	90

Note. Higher heating value (HHV) estimated from the CHN content (Friedl et al., 2005).

Beyond releasing nutrients to the aqueous phase, HTC also results in a densification of the algal biomass into a hydrochar with increased heating value. Another way to interpret these data is to calculate the energy densification ratio, which is the ratio of the heating value of the hydrochar product to that of the original biomass. For the conditions examined in Table 3.2, the energy densification ratio was about 1.5, which is comparable to the energy densification observed during the HTC of various algae (Heilmann et al., 2010) and lignocellulosic biomass (Lynam et al., 2012). Another important metric is the energy yield, which is defined as the solids yield multiplied by the energy densification ratio. Hydrochars contained between 85 and 94% of the energy content, estimated from the elemental composition, of the original biomass. These data suggest that nearly all of

the biomass energy is retained in the hydrochar, which could be expected considering its very high lipid content.

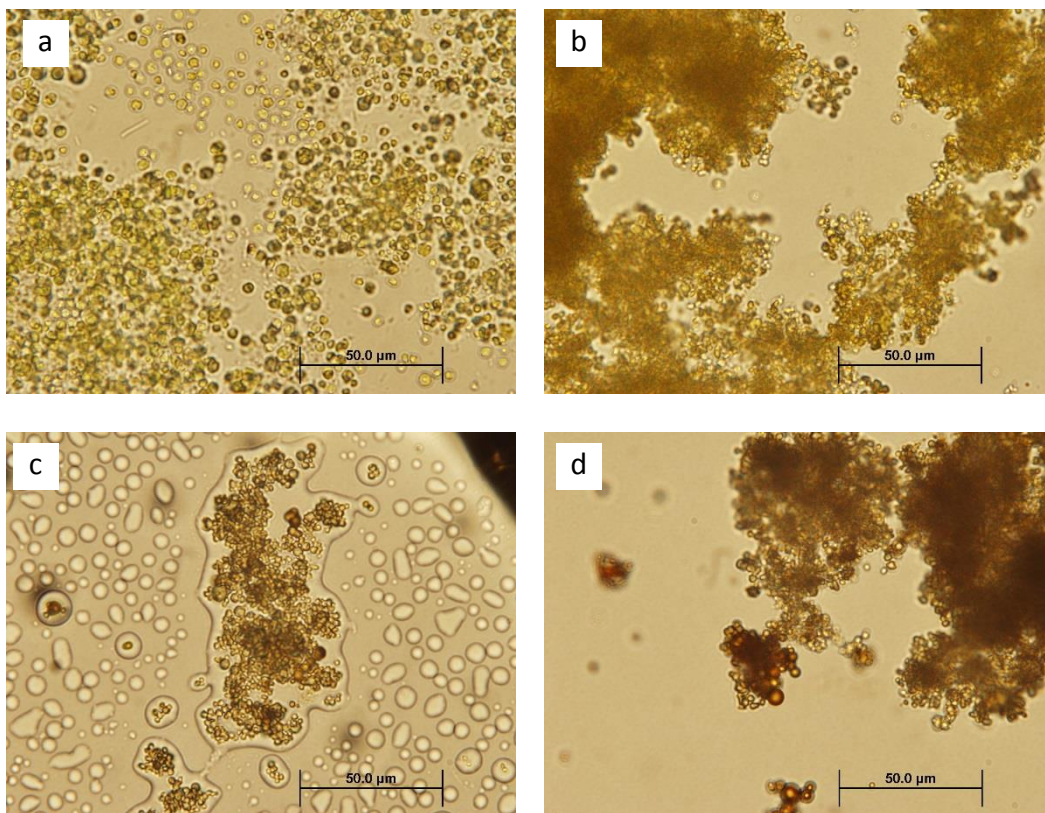


Figure 3.7. Light microscopy of *Chlorella* biomass processed at 230 °C for (a) 0 min, (b) 5 min, (c) 15 min, or (d) 30 min. Note the formation of microspheres as processing time increases.

### 3.3.2 The effect of time and temperature on HTC performance with *C. protothecoides* biomass

In follow-up studies with *C. protothecoides* grown heterotrophically, we sought to study lipid hydrolysis over a wider range of temperatures. In this work, biomass was reacted as a freshly harvested paste at about 25% solids at 220 °C, 235 °C, and 250 °C for 30, 60, and 90 min. As shown in Figure 3.8, the extent of lipid hydrolysis increased dramatically with temperature and time. These results are in agreement with findings that the rate of TG hydrolysis increases with temperature as water's ion product increases, dielectric constant decreases, and it becomes more soluble in the oil phase (Mills and Jiclain, 1949; Kusdiana and Saka, 2004a). Furthermore, the rate of oil hydrolysis is typically slow at first

and then increases as FAs are formed. This increase has been attributed to the increased solubility of water in FA compared to TG (Lascaray, 1952) and the autocatalytic effect of FA (Minami and Saka, 2006).

Kinetic effects are also important. The equilibrium conversion from hydrolysis increases with the water-to-oil ratio in the feed. Higher water-to-oil ratios, however, reduce TG and FA concentrations, which can decrease the initial reaction rate (Alenezi et al., 2009) and increase operating and capital costs because a larger volume of material must be processed. The wet algal biomass we reacted contained about 20% solids and 50% lipids on a dry weight basis. If we model the feedstock lipids as triolein and assume a pseudo-homogeneous reaction mixture, the water-to-oil ratio in our experiments was 6.8 (v/v), 8.0 (w/w), and 393 (molar). The large molar excess of water indicates that a very high equilibrium conversion should be attainable from hydrolysis under these conditions. The reaction mixture is not completely homogeneous, however, and equilibrium conversion will no doubt be affected by the relative proximity of intracellular lipids and water. Future work exploring how the concentration of water and glycerol (a hydrolysis product) vary within the lipid body and more widely across the cell could provide important information about how compositional heterogeneity and diffusion-limited transport affects the reaction. Overall, our data confirm that the trends typically observed in pure oil-water systems are similarly observed during in situ lipid hydrolysis of *Chlorella* biomass.

Because the retention of lipids within the hydrochar is of principal interest to maintaining high overall yields, we examined lipid retention for the same reactions described in Figure 3.8. Figure 3.9 shows that lipid retention appeared to increase with reaction temperature at each time, although this trend was less apparent at 90 min compared to shorter reaction times. These data are similar to those we observed with *C. vulgaris* biomass at 250 °C and suggest that lipid retentions between 80–90% can be expected for HTC at these conditions.

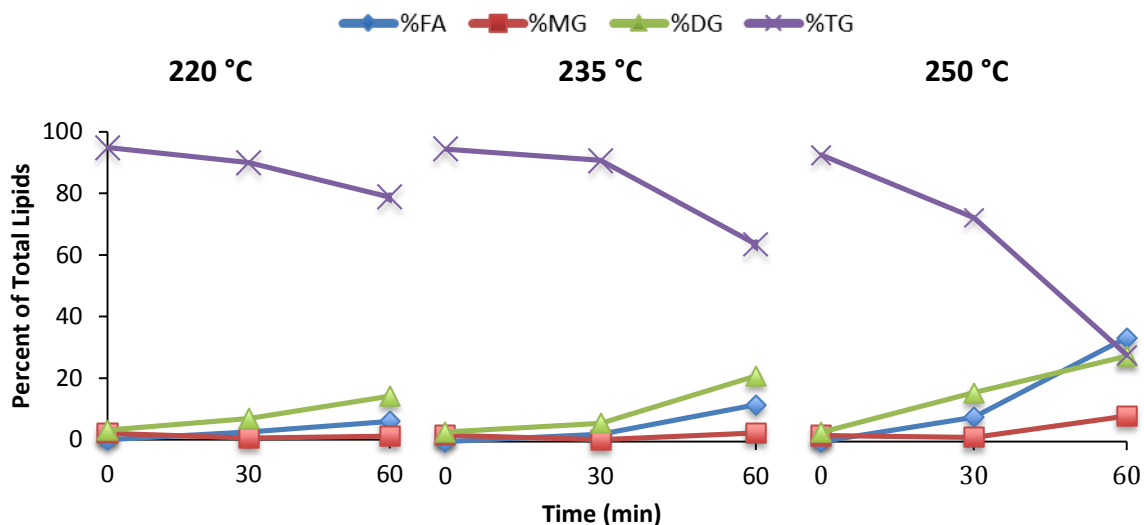


Figure 3.8. HTC of *C. protothecoides* biomass at 220 °C, 235 °C, and 250 °C for 30, 60, and 90 min. The data at 0 min correspond to the unreacted biomass.

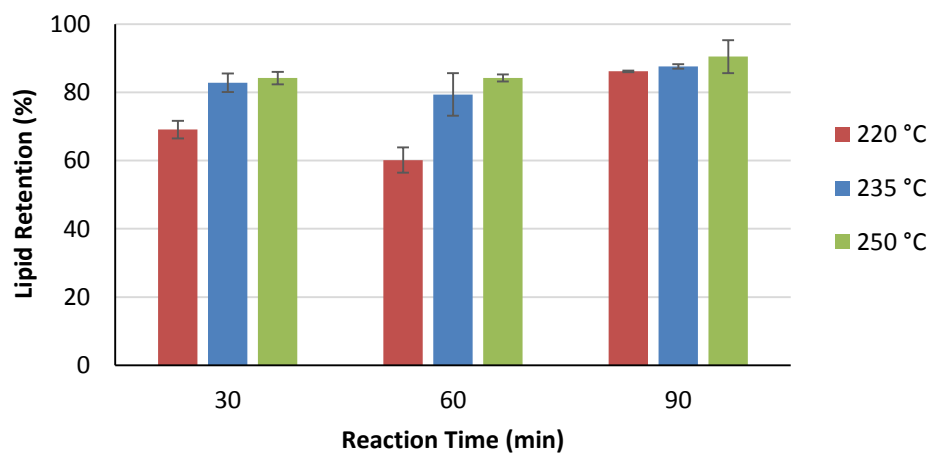


Figure 3.9. Lipid retention for *C. protothecoides* hydrochars. Error bars represent mean  $\pm$  standard error of replicate reactions.

In a similar manner to the analyses of *C. vulgaris* hydrochars, we selected the hydrochars produced at 60 min and 220, 235, and 250 °C for elemental analysis (Table 3.3). These data show very similar trends as were found before: hydrochar solids yields were 47-56% with retention of 60-70% of the C and 40-50% of the N in the hydrochar. The solids yield was, however, notably lower at 220 °C and 60 min, perhaps because hydrolysis reactions

outpace the repolymerization reactions responsible for hydrochar formation at this temperature. As a result of the lower solids yields, energy yield was somewhat reduced.

Table 3.3. Hydrochar elemental analysis and energy content for *C. protothecoides* hydrochars at various temperatures and 60 min

Analysis	Feedstock	HTC reaction temperature (°C)		
		220	235	250
Solids yield (wt%)	-	47.7	56.3	56.9
Elemental Analysis (wt %) <sup>d</sup>				
C	56.8	71.1	72.3	72.7
H	8.5	9.8	10.2	10.0
N	1.5	1.4	1.1	1.4
O	29.9	16.1	15.0	15.8
% C retained	-	59.7	71.7	72.8
% N retained	-	43.9	41.2	53.1
HHV (MJ/kg)	24.9	36.1	37.6	37.6
Energy densification	1.0	1.5	1.5	1.5
Energy yield		69.2	85.2	86.0

### 3.3.3 The effect of acid during HTC at 220 – 235 °C

Previous work has suggested that acidic conditions favor the formation of solid products and suppress gas formation during HTC, mostly by shifting the reaction chemistry towards dehydration reactions and coalification instead of hydride transfer and decarboxylation (Titirici, Thomas, Yu, et al., 2007; Funke and Ziegler, 2010). In general, very little if any gas is typically observed in HTC reactions near 200 °C and any gas that is formed is typically CO<sub>2</sub>. Recently, several works have used the addition of acid during HTC to increase solids yields and energy densification. For example, Heilmann et al. (2010) added 2-3 wt.% citric or oxalic acid to HTC reactions containing microalgae, and Lynam et al. (2011) investigated the effect of acetic acid on the HTC of pine (Lynam et al., 2011). In our work with *Chlorella*, the reactant biomass was usually slightly acidic (pH ~6-6.5) due to the conditions of fermentation. Nevertheless, we investigated the addition of acetic acid over a range of temperatures and times to determine how it affected solids yields and lipid hydrolysis. We chose acetic acid because it is the primary organic acid found in the aqueous phase following HTC and a suitable carbon substrate for algal growth. We hypothesized that if the addition of acetic acid could substantially improve the process outcome, the cost

would be justified if it also served as a carbon source for algal growth. In addition, we suspected that adding acetic acid might help elucidate whether recycling the aqueous phase, which is rich in acetic acid, would be beneficial to the process.

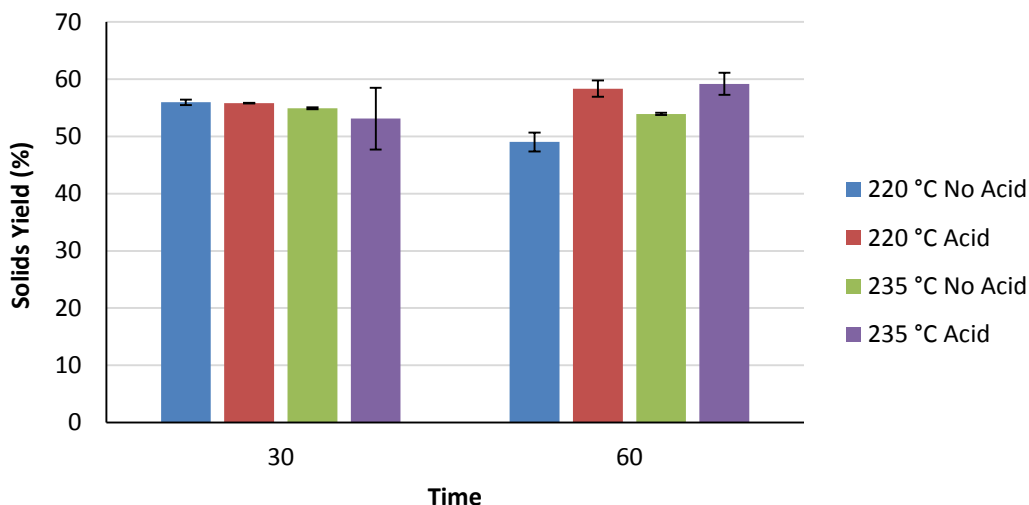


Figure 3.10. Solids yield in HTC reactions containing *C. protothecoides* with and without acetic acid. Reactions contained about 1.5 M acetic acid, equivalent to 0.4 g acetic acid/g reactant biomass dry weight. Error bars represent mean  $\pm$  standard error of replicate reactions.

Figure 3.10 shows the solids yields from HTC reactions containing *C. protothecoides* at 220 °C and 235 °C for 30 or 60 min both with and without acetic acid. Acetic acid was added such that its overall concentration in the reactant paste was about 1.5 M, equivalent to about 0.4 g acetic acid/g reactant biomass dry weight. These data show that acetic acid had very little effect at 30 min but increased solids yields moderately at 60 min for both temperatures. In contrast, Lynam et al. (2011) found that acetic acid added at 0.4 g/g biomass slightly decreased solids yields but resulted in more energy dense hydrochars at 200 °C, most likely due to precipitation of 5-hydroxymethyl furfural (5-HMF) in the pores of the solid. Unfortunately, we did not measure the higher heating value of these hydrochars or their elemental analysis, so it is not possible to know how acetic acid affected this property of the hydrochar. We did, however, observe 5-HMF in the aqueous phase of the HTC reactions containing heterotrophically grown *Chlorella*, which likely forms from the decomposition of residual glucose present in the reactant



biomass (Kruse and Dinjus, 2007). Therefore, it is possible that a similar mechanism to that observed by Lynam et al. (2011) could be occurring in our reactions, but this would need to be investigated in future work. It should be noted that 5-HMF is toxic to most algae, and we observed poor growth of *Chlorella* on aqueous phase containing 5-HMF. If the aqueous phase is recycled to algal growth systems without any kind of pre-treatment, selecting HTC conditions that reduce 5-HMF concentrations (e.g., lower temperatures and less acid) may be preferable.

Table 3.4. Lipid composition of hydrochars from HTC reactions containing *C. protothecoides* with and without acetic acid

Reaction Conditions			Lipid Composition (% of total lipids)			
Temp. (°C)	Time	Acid (M)	FA	MG	DG	TG
220	30	0	2.1	0.0	6.6	91
220	30	1.5	3.8	0.7	9.2	86
220	60	0	6.1	1.0	14	79
220	60	1.5	18	4.4	24	53
235	30	0	2.7	0.0	6.8	91
235	30	1.5	5.8	0.5	13	81
235	60	0	15	3.6	23	60
235	60	1.5	36	9.1	28	27

In addition to affecting the solids yield, acetic acid had a marked effect on lipid hydrolysis. As expected, reactions containing acid demonstrated significantly more hydrolysis than those without, with a stronger effect apparent at the highest temperatures and longest times (Table 3.4). Surprisingly, this had only a very minor impact on lipid retention, which was more strongly dependent on reaction temperature and time (Figure 3.11). The data at 220 °C show a similar trend to the one observed earlier with nearly identical biomass (Figure 3.9); that is, lipid retention improves from 30 to 60 min, perhaps as the solids conglomerate more completely. In this case, we observed much lower lipid retention at 235 °C and 30 min, but similarly high retention (80–85%) in 60 min reactions. Overall, these data suggest that lipid hydrolysis is likely not the strongest driving force behind lipid retention, as we originally hypothesized. In the next two sections, we address how the solids content of the reactant biomass and the lower temperatures may play a role.

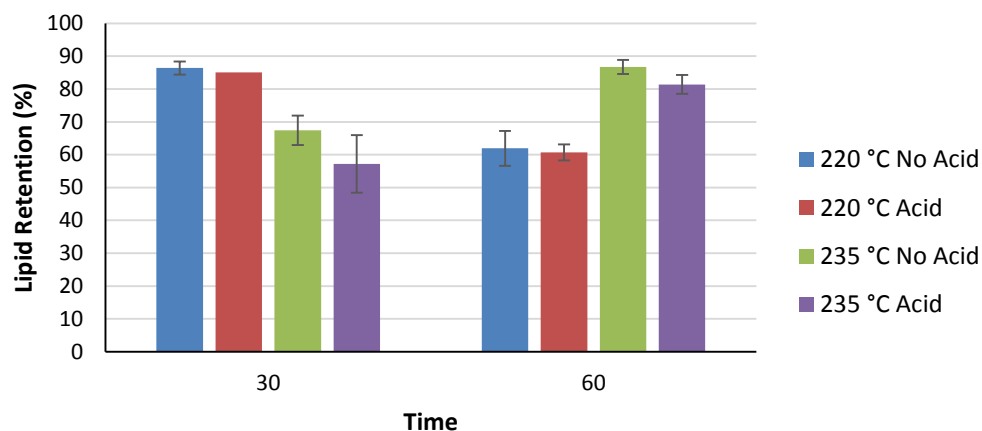


Figure 3.11. Lipid retention in hydrochars from HTC reactions containing *C. protothecoides* with and without acetic acid.

### 3.3.4 The effect of solids loading at 235 °C

Because dewatering is one of the most costly and energy-intensive components of algal biofuel production, we investigated the effects of reacting *C. protothecoides* biomass at different solids contents. On the one hand, being able to react 6% solids biomass would obviate an entire dewatering step, such as centrifugation, or possibly even permit the reaction of biomass directly from a fermenter without any dewatering. On the other hand, reacting a lower solids biomass entails heating up and reacting a significantly larger quantity of material for each unit of fuel produced, in addition to requiring larger reactors, pumps, and tanks. As shown in Figure 3.12, the solids yield is markedly lower with 6% solids reactant biomass compared to 12% or 25% (cf. 44% vs. 59% or 54%). Likewise, the lipid retention dropped from about 80–85% with 12 or 25% solids biomass to just 55% with the 6% solids biomass. These data are similar to the findings of Heilman et al. (2010), who rehydrated dry *Dunaliella salina* and reacted it at 5, 15, or 25% solids. They found that solids yields and carbon recovery in the hydrochar increased by about 25% when the solids content was increased from 5% to 25% in reactions at 190 and 210 °C lasting 30 or 120 min. One likely explanation is that algae cells in reactions containing less biomass experience more hydrolysis and do not contain sufficient concentrations of various substrates for the repolymerization reactions required to form hydrochar particles. In

addition, hydrochar formation may be inhibited by low biomass concentrations simply due to the limited frequency of particle-particle interactions during HTC.

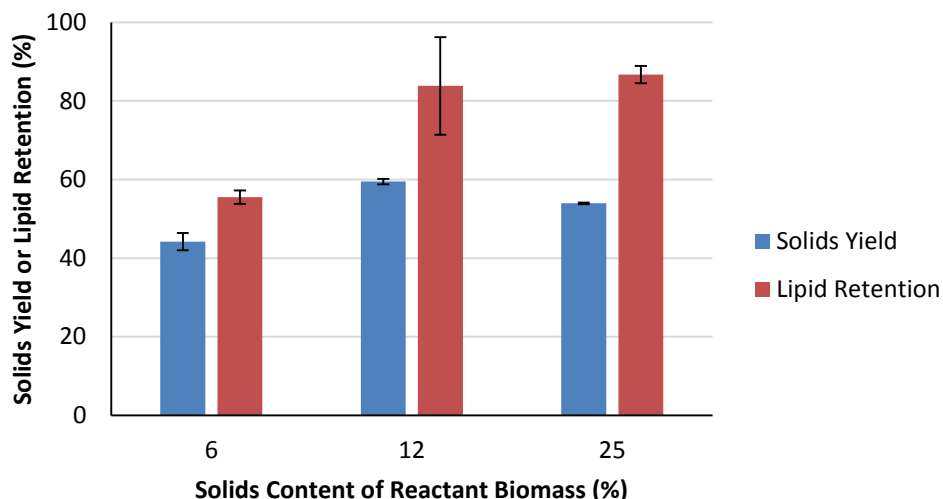


Figure 3.12. HTC of *C. protothecoides* at different solids contents at 235 °C for 60 min.

We also observed that solids loading affected lipid hydrolysis. Not surprisingly, the percentage of lipids hydrolyzed increased with biomass loading, as higher concentrations of reactants led to higher conversions (Table 3.5). Taken together, these data suggest that it is preferable to carry out HTC at the highest possible solids concentration in the reactant biomass. In addition to higher solids yields and superior lipid retention, this will reduce the capital required for reactors and associated pumping equipment. Because most commercial centrifuges or belt-filter presses output algae paste containing 20-30% solids, this type of dewatering should be considered upstream of the HTC process.

Table 3.5. The effect of solids loading on lipid composition of *Chlorella* hydrochars

Solids (%)	Lipid Composition (% of total lipids)			
	FA	MG	DG	TG
6	4.2	1.0	11	84
12	8.5	1.4	17	74
25	15	3.6	23	56

Note. Lipid composition determined by hexane:isopropanol (3:2) extraction and HT-GC-FID.

### 3.3.5 Filtration of hydrochars and the motivation for lower temperatures

In all of the work involving *Chlorella* hydrochars at 220–250 °C, HTC reactions were analyzed by filtration of the product mixture using laboratory filter papers. In addition to the type of data presented above, the extent of carbonization was evaluated through a qualitative assessment of filterability. This was considered an important process variable because the reaction mixture following HTC would need to undergo solid-liquid separation, and filtration is likely to be less energy and cost-intensive than centrifugation. The character of the hydrochar solids and the ease at which they dewatered when vacuum filtered were easy to assess visually, as shown in Figure 3.13. This exploratory work at 215 °C for 15, 30, or 45 min demonstrated how reaction time has an effect on solids conglomeration and likewise on filterability. Similarly, we observed that dewaterability improved with reaction time for hydrochars reacted at 220-250 °C; however, after completing filtration studies in collaboration with Pall Corporation, we learned that commercial-scale metal filter materials (i.e., Rigimesh K, 18 µm) perform very differently than cellulose laboratory filters. For example, a hydrochar produced from *Chlorella* biomass reacted at 215 °C for 30 min showed somewhat better filterability than a hydrochar produced at 215 °C for 15 min (cf. 0.005 vs. 0.003 kg/min flow rates), but both formed a suitable filter cake (Figure 3.14). In contrast, both appeared equally difficult to filter on 0.45 µm cellulose filter papers, leading us at first to erroneously conclude that HTC at lower temperatures conditions were unsuitable.

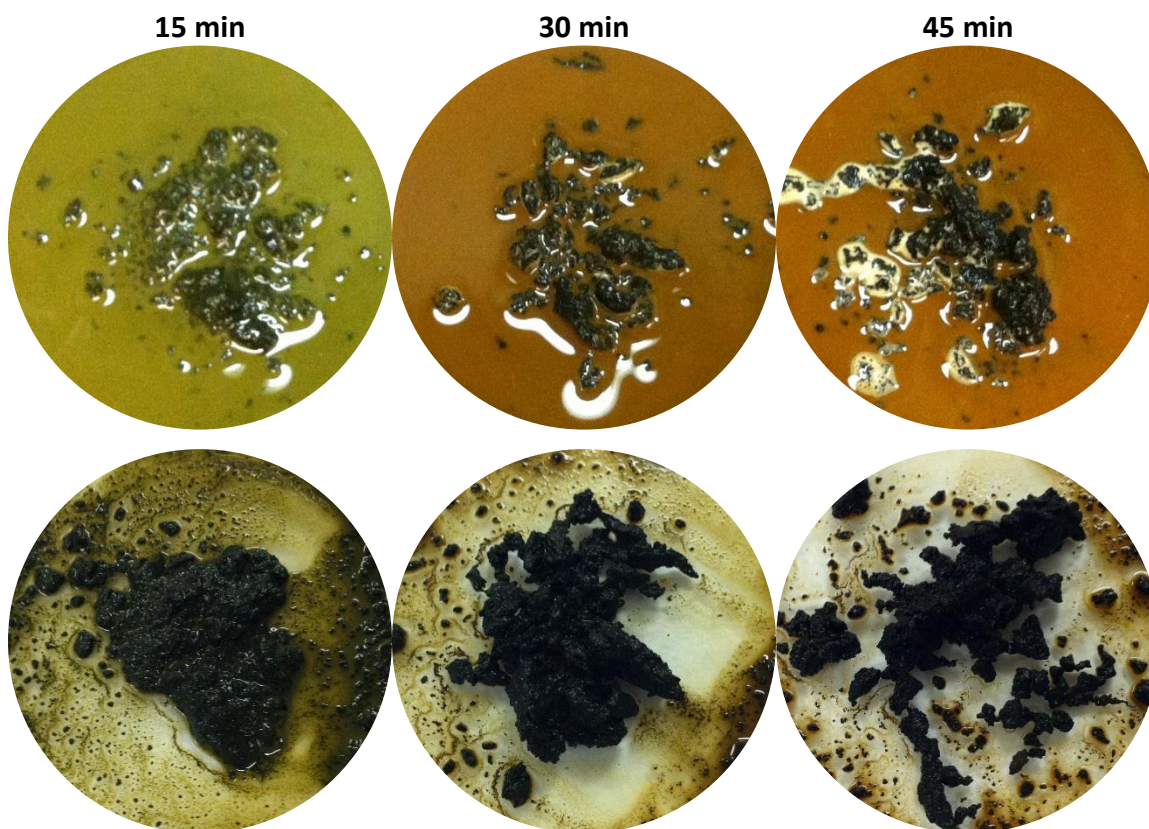


Figure 3.13. HTC of *Nannochloropsis* biomass at 215 °C for 15, 30 or 45 min. Top row shows undiluted reactor contents following HTC. The bottom row highlights the solids characteristics after the aqueous phase has been poured off.

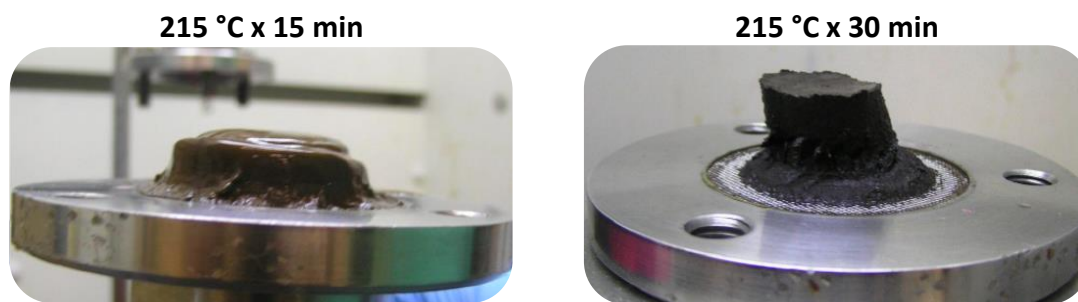


Figure 3.14. Filter cakes of *Chlorella* hydrochars reacted for 15 and 30 min at 215 °C. Testing carried out by the Pall's Scientific and Laboratory Services to determine the feasibility of using Pall Corporation's ZHF Centrifugal Discharge Filter technology for separation of hydrochar and aqueous phase. A 47mm filter disk of Rigimesh K (18  $\mu$ m) media was used.

To reduce bias in solid-liquid separation and focus on other important aspects of the HTC reaction, such as lipid retention and nutrient reusability, we decided to use a centrifuge for separation of hydrochars and aqueous phase in all future HTC work. Although we consider this a laboratory convenience, it may be a suitable alternative to filtration for large-scale implementation because the energy expenditure of centrifugation once the biomass is concentrated and reacted is only a small fraction of the total biomass energy. Use of centrifugation, especially large decanter-style units, is commonplace at wastewater treatment plants and is already used in HTC-like processes treating biosolids.

### 3.3.6 Low temperature HTC of *Nannochloropsis*

By using a centrifuge for hydrochar separation, we were able to explore lower reaction temperatures for HTC (180–210 °C) that may be more appropriately called subcritical water hydrolysis. Some benefits of lower reaction temperatures include reduced energy demand for heating and pressurizing reactants, potentially lower material costs for tanks and piping, and diminished concentration of inhibitory compounds in the aqueous phase that may form due to unwanted side reactions. Moreover, these conditions were suspected to maximize the potential reusability of nutrients in the aqueous phase because hydrolysis, rather than repolymerization, has been found to dominate in this temperature regime (Garcia Alba et al., 2012). Finally, we hypothesized that it would be possible to carbonize *Nannochloropsis* containing EPA at lower temperatures without damaging this valuable omega-3 fatty acid.

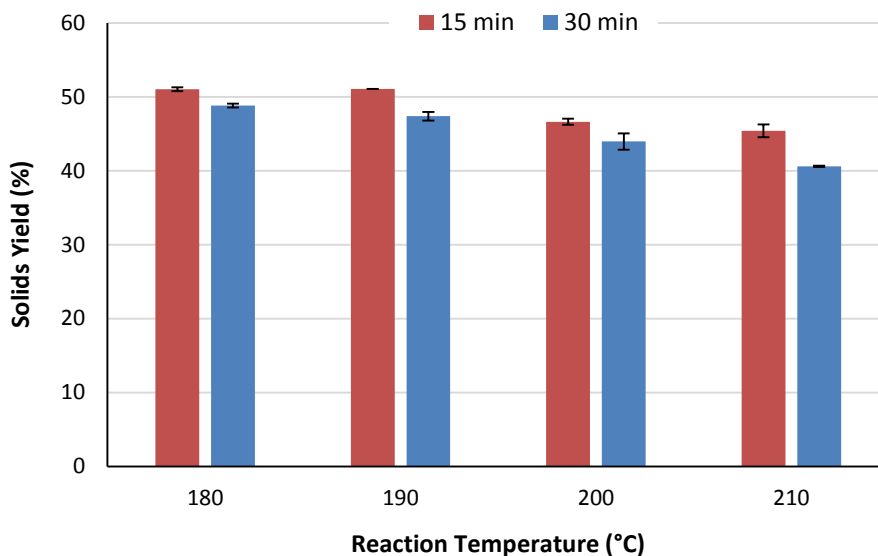


Figure 3.15. Solids yield from low-temperature HTC of *Nannochloropsis*. Error bars are the mean  $\pm$  standard error of replicate reactions.

As shown in Figure 3.15, HTC of *N. oculata* biomass (15% solids) resulted in solids yields ranging from 41 to 51%. The solids yield tended to decrease with increasing temperature and reaction times, likely as a result of increased hydrolysis of biomass constituents. Lipid retention, on the other hand, increased with reaction severity up to 200 °C but showed a slight decline at 210 °C and 30 min (Figure 3.16). Overall, this experiment showed very high lipid retentions, with an average of 100% retention at 200 °C. These data compare favorably to the lipid retention (~80–90%) reported for similar carbonization experiments at 200 °C with *Nannochloropsis* (Du, Mohr, et al., 2012). Importantly, our analysis showed that EPA, a valuable omega-3 lipid, was not selectively lost during HTC and had nearly identical retention values to the values reported in Figure 3.16 for the total lipid fraction.

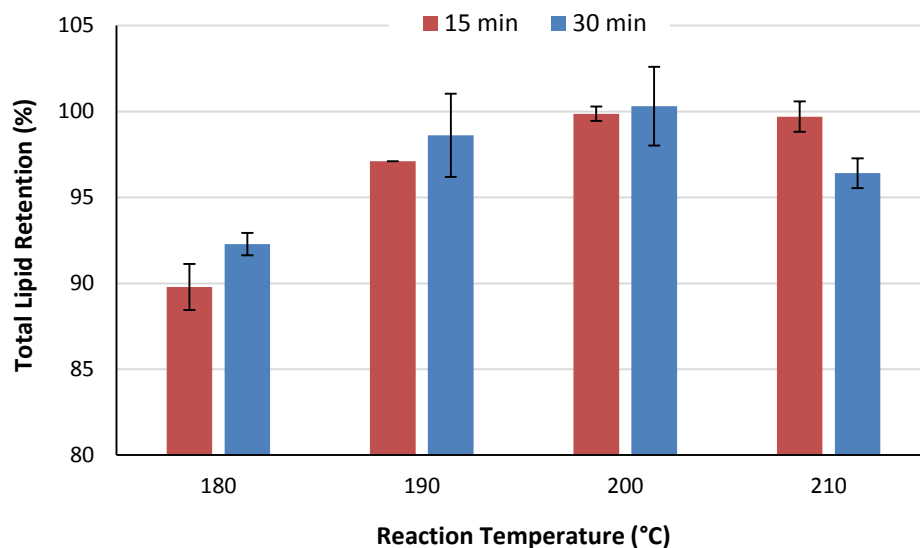


Figure 3.16. Lipid retention in hydrochars formed by low-temperature HTC of *Nannochloropsis*.

To confirm that the EPA was not thermally degraded (e.g., isomerized, oxidized, and polymerized) we estimated its total recovery as well as the amount of isomerization by integrating the all-*cis* EPA peak as well as any nearby peaks that were suspected to correspond to geometrical isomers (Fournier et al., 2006; Berdeaux et al., 2007). In the unreacted biomass, detected isomers had a combined peak area equivalent to about 1.6% that of the all-*cis* EPA peak. Our analysis showed that HTC at 180-210 °C can induce very mild alterations of EPA, from about 0.5 to 3% increased isomerization, and highlight the importance of using mild HTC conditions to minimize this damage. This nearly undetectable amount of isomerization can be visually appreciated in Figure 3.17. In an effort to better understand the issue of EPA isomerization in the context of commercial products, as well as determine whether our lipid analysis procedure may introduce potential artifacts, we examined two commercially available fish oil supplements: Nordic Naturals Omega-3 Purified Fish Oil (in liquid form) and a supercritical-CO<sub>2</sub> extracted ethyl ester preparation of omega-3 FAs called PUR 3 produced by K.D.-Pharma Bexbach GmbH. Because the fish oil product was composed of triglycerides, we reacted it using our standard protocol, which uses methanol at 100 °C for 90 min with 5% acetyl chloride. The



ethyl ester product was first analyzed directly on the GC-FID and then reacted to convert the ethyl esters into FAMES. As shown in Figure 3.18, both the unreacted PUR 3 sample and the esterified sample appear to contain very little isomerization, which we estimated at about 1-2%. This indicates that our lipid analysis protocol did not introduce isomers into samples and that the quality of EPA in *Nannochloropsis* hydrochars after HTC is quite similar to commercially available products. Because many fish oil products are prepared by hexane extraction, which can leave residues in the final product, the combination of HTC and IST to produce algae-derived EPA may have significant advantages.

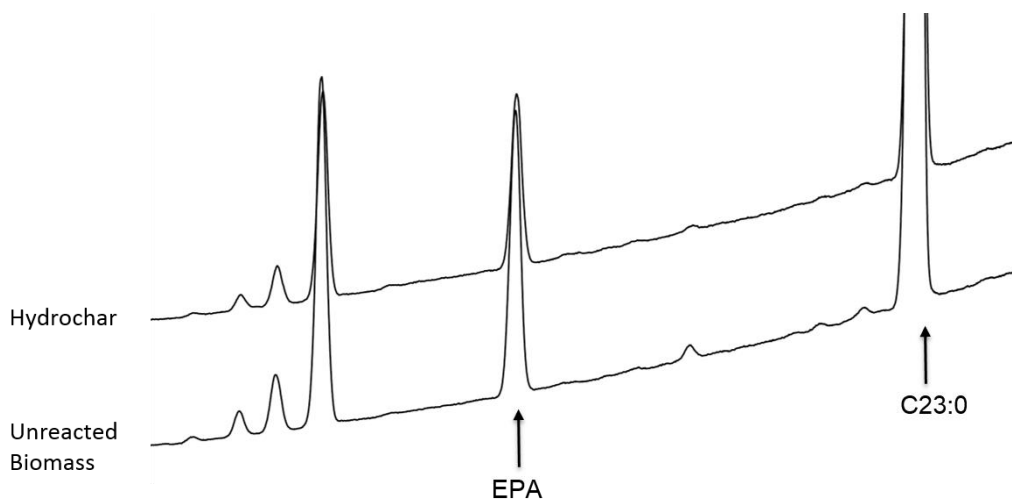


Figure 3.17. GC-FID analysis of *Nannochloropsis* hydrochar (200 °C x 30 min) compared to unreacted biomass. The biomass and hydrochar in these spectra were estimated to contain about 1.6% and 3.9% EPA in an isomerized form, respectively.

The elemental composition of the reactant biomass and the hydrochars from each reaction was used to calculate the retention of C, N, and P in each hydrochar. As shown in Table 3.6, the hydrochars produced under the conditions investigated retained about 50-60% and 30-49% of the C and N, respectively, of the original biomass. Compared to the high-temperature HTC performed on *Chlorella* biomass (Table 3.2), more C and N partitioned into the aqueous phase during low-temperature HTC with *Nannochloropsis*. Although nutrient retention is calculated on a relative basis, the elevated partitioning of N to the aqueous phase observed in *N. oculata* HTC may have been due to its substantially higher N content compared to the *Chlorella* biomass (cf. 8.5% vs. 1.1%). It is also possible

fewer aromatic and larger molecular weight C and N compounds, which are more likely to precipitate or adsorb onto the surface of the hydrochar, are formed at lower temperatures. The phosphorus content of *Nannochloropsis* biomass and the hydrochar produced at 200 °C x 15 min was measured by inductively coupled plasma mass spectrometry (ICP-MS), showing a P retention of 45%. Because processing of this same algae biomass at even harsher conditions (250 °C) resulted in <1 wt % of the biomass converted into gas-phase products (Valdez et al., 2012), we assume that any C, N, and P not retained in the hydrochar becomes dissolved in the aqueous phase.

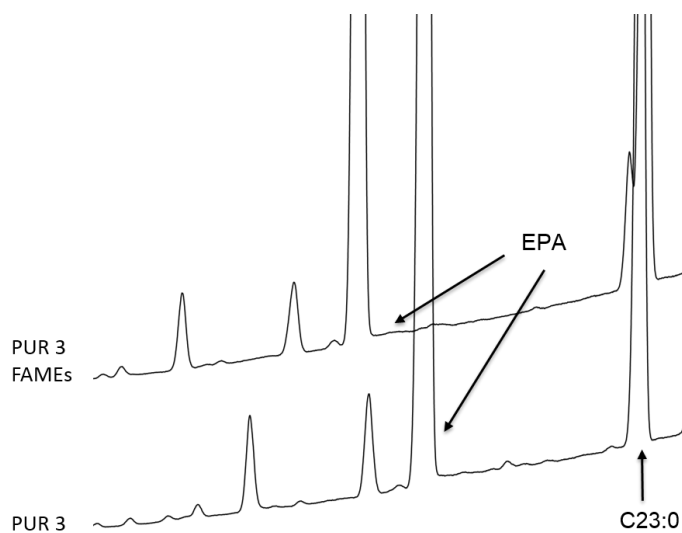


Figure 3.18. GC-FID analysis of isomerization in commercial omega-3 ethyl ester product (PUR 3). Both the original and reacted samples contain about 1-2% isomerization by our estimation methods.

These results are similar to work performed by Du et al. (2012), who also showed that the retention of C and N in *Nannochloropsis* hydrochars decreased with increasing temperatures or longer times. Working with the same biomass as we have, Valdez et al. (2012) showed that in liquefaction experiments at 250 °C for 20-90 min, about 30-40%, 66-82% and 76-85% of the initial biomass C, N, and P, respectively, ended up in the aqueous phase (Valdez et al., 2012). Although a similar amount of C and N dissolved in the aqueous phase during reactions at 250 °C and 190-210°C, our estimate of phosphorus partitioning to the aqueous phase after a reaction at 200°C for 15 min was notably lower.

Valdez et al. (2012) found that P partitioning to the aqueous phase decreased at temperatures above 250 °C; however, the lower temperatures used in our work may have reduced the hydrolysis of compounds containing P (such as phospholipids) and thereby increased the likelihood that the hydrochar retained more P.

Table 3.6. Hydrothermal carbonization yields and hydrochar characteristics for *Nannochloropsis*

Temp. (°C)	Time (min)	Elemental Composition (wt. %)			Retention (%)		Energy Content (MJ/kg), Yield (%) and Densification		
		C	H	N	C	N	HHV	Yield	Densification
Reactant Paste		49.9	8.0	8.5	-	-	21.6	-	-
180	15	57.8	8.5	8.1	60	49	26.3	63	1.22
180	30	58.8	8.6	7.6	58	44	26.9	61	1.25
190b	15	58.7	8.6	7.4	60	44	26.8	64	1.24
190	30	59.2	8.6	7.2	56	40	27.1	59	1.26
200	15	59.8	8.5	6.8	55	37	27.3	59	1.27
200	30	59.7	8.4	6.9	51	35	27.3	54	1.26
210	15	60.5	8.7	7.0	56	38	28.0	60	1.30
210	30	61.2	8.7	6.5	50	31	28.4	53	1.32

Note. <sup>a</sup> According to the supplier, *N. oculata* biomass contains 58.6% protein, 14.5% lipids (10.5 % total fatty acids), 20% carbohydrates, and 5.9% ash. <sup>b</sup> Lipid content reported as total fatty acid methyl esters. <sup>b</sup> Solids yield and lipid data are averages ± standard error for replicate reactions carried out in 4 mL reactors.

Another factor that must be considered when comparing data across experiments is the effect of pH on nutrient sorption to the hydrochars and the extent to which hydrochars were processed prior to drying (Libra et al., 2011). Acidic pH is likely to counteract the sorption of nutrients, particularly P, and additional water or solvent rinsing of hydrochars may remove aqueous phase components that would otherwise be dried with the solid hydrochar. Because we performed a mild water rinse of the hydrochars, while Valdez et al. (2012) used dichloromethane to separate liquefaction products into organic, aqueous, and solid fractions, N and P partitioning to the aqueous phase were likely affected as much by the workup procedure as the reaction conditions. The same issue arises when comparing hydrochar data between different labs, and consideration should be given to the implications of hydrochar handling at a large-scale facility. For example, separation of the hydrochar from the HTC reaction mixture by filtration and performing a thorough

water wash would help reduce the amount of N and P in the hydrochar as well as any subsequent fuel products while capturing the most nutrients for recycling.

For the conditions examined in Table 3.6, the energy densification ratio ranged from 1.2 to 1.3 and increased with temperature and reaction time. Hydrochars contained between 53 and 63% of the energy content, estimated from the elemental composition, of the original biomass. These data suggest that a sizeable amount of the biomass energy is released as dissolved components in the aqueous phase. Because *Nannochloropsis* contained significantly fewer lipids than *Chlorella* (cf. ~10% vs. 50%), and because lipids do not participate in hydrochar formation reactions during HTC (Heilmann, Jader, Sadowsky, et al., 2011), it is not surprising that *Nannochloropsis* hydrochars retained less of the energy content of the original biomass relative to *Chlorella* hydrochars. Overall, these data highlight the importance of capturing the energy value of the aqueous phase when processing biomass containing fewer lipids. In this work, we attempted to accomplish this by using the aqueous phase as a nutrient source for algal growth, but a more reliable method may involve catalytic hydrothermal gasification (CHG), which is further explained in Chapter 8.

### 3.3.7 Low-temperature HTC of BCR-grown algal biomass (*C. vulgaris* and marine bi-culture)

After experimenting with low temperature HTC with *Nannochloropsis*, we decided to expand this work to algal biomass we produced in our own bubble column reactors. In addition to producing biomass for HTC studies, this work facilitated experiments on nutrient recycling. Out of the dozens of HTC experiments we carried out, we have highlighted three for presentation here to describe how *C. vulgaris* and the marine bi-culture we developed performed in low-temperature HTC. We chose to carry out this work at 200 °C for 15 min with freshly harvested paste because these appeared to be optimal conditions from the work done with *Nannochloropsis*.

Table 3.7. Hydrochar yields and lipid information from HTC (200 °C, 15 min) of algae grown in bubble column reactors

Lipids	<i>C. vulgaris</i> <sup>a</sup>		Marine bi-culture (N-replete) <sup>b</sup>		Marine bi-culture (Aqueous Phase) <sup>c</sup>	
	Algae	Char	Algae	Char	Algae	Char
Hydrochar yield (wt.%)	-	56	-	52	-	51
Solids content (wt.%) <sup>d</sup>	16	35	13	39	16	31
Total FAMES (wt.%)	27.2	48.5	8.8	15	18	34
Lipid Retention (%)	-	100	-	87	-	99
Fatty Acid Profile (% of total FAMES)						
C16:0	17.0	16.6	19	20	21	21
C16:1	1.1	1.1	1.7	1.9	1.7	1.7
C17:0 + C17:1	7.1	7.1	12	12	8.1	7.8
C18:0	1.3	1.3	0.87	0.86	3.6	3.6
C18:1	40.4	40.8	2.3	2.4	25	26
C18:2	11.4	11.5	17	17	17	16
C18:3n3 + C18:3n6	17.9	17.8	35	34	17	16

Note. <sup>a</sup> Bubble column reactor culture (BCR) grown on MBBM with urea (93 mg/L N) for 5 days to about 1 g/L density. <sup>b</sup> BCR-grown marine bi-culture on f/2 media with 93 mg/L N (urea) for 5 days to about 1 g/L density. <sup>c</sup> BCR-grown marine bi-culture with 1 L seed culture from harvest of N-replete culture (data reported in middle two columns of this table) and grown on aqueous phase for 6 days to about 1.5 g/L density. <sup>d</sup> Solids content (wt.%) given for algae paste as reacted and for wet hydrochar immediately following the reaction after centrifugation.

As shown in Table 3.7, *C. vulgaris* biomass produced by phototrophic growth in a BCR contained about 27% total lipids when harvested. This biomass is highly representative of the material harvested from open ponds used in the modeling described in Chapter 8, which assumes a 25% lipid content. As with *C. protothecoides*, this biomass contained a high proportion of C18:1 FA, suggesting its lipids are ideally suited for biodiesel. After reaction at 200 °C for 15 min, nearly 100% of the lipids were retained in the hydrochar with no apparent loss in any specific FAs. Analysis of these lipids showed very little hydrolysis (<10%) occurred during the reaction. The marine bi-culture grown under phototrophic, N-replete conditions in a BCR contained about 8% lipids when harvested and demonstrated a hydrochar solids yield of 52% with a lipid retention of about 87%. When a seed culture of this N-replete biomass was then grown for 5 days in the presence of diluted aqueous phase, the density reached about 1.5 g/L density and the biomass lipid

content was 17% at harvest. Following HTC, the hydrochar solids yield was about 51% with a lipid retention of about 99%.

Based on our work with *Nannochloropsis*, the biomass grown in the BCRs, as well as high lipid *Chlorella* biomass, we believe that lipid retention tends to improve with biomass lipid content. One explanation for this may be that lipid accumulation results in the buildup of triglyceride-rich oil bodies within the cytoplasm that may be more likely to be retained within the structure of the hydrochar or somehow adsorbed to it. On the other hand, when a cell is rapidly growing and only contains ~10% lipids, a higher percentage of these are amphipathic polar lipids, such as phospholipids and glycolipids, which are typically membrane constituents and may be more likely to be hydrolyzed or partition into the polar aqueous phase during HTC. This hypothesis is supported in part by comparing the fatty acid profile of the low-lipid biomass, which contains very little C18:1 but is enriched in C18:3 fatty acids, to the higher lipid biomass, which contains more C18:1 (Table 3.7). Cytoplasmic oil bodies are more likely to contain TGs rich in oleic acid, whereas C18:3 fatty acids are typically associated with polar lipids in the chloroplast and other membranes (Piorreck et al., 1984; Thompson, 1996).

Table 3.8 details the elemental composition and estimated energy content for the solids in these three reactions. For the two reactant biomass samples that contained higher lipid contents, the N content of this biomass was lower (cf. about 4% vs. 8%) and as a result more was retained in the hydrochar. This is similar to what we observed with the *C. vulgaris* biomass that contained about 1.5% N and indicates that N partitioning to the aqueous phase tends to be somewhat lower in low-N biomass feedstocks when calculated on a relative basis. All three reactions resulted in hydrochars with an energy densification of about 1.3 to 1.4, although the *C. vulgaris* hydrochar demonstrated the highest energy yield and densification, most likely due to its higher lipid content. Overall, these data suggest that low temperature HTC can be used to produce hydrochars from a variety of microalgae and cyanobacteria feedstocks, resulting in about 30-40% of the C and 45-55%

of the N being released to the aqueous phase while most of the lipids are retained in the solid char.

Table 3.8. Hydrochar elemental composition and energy yields<sup>a</sup>

Analysis	<i>C. vulgaris</i>		Marine bi-culture (N-replete)		Marine bi-culture (Aqueous Phase)	
	Algae	Char	Algae	Char	Algae	Char
Elemental Analysis (wt.%)						
C	51.1	63.2	51.2	62.2	50.2	60.9
H	7.8	9.3	7.4	7.9	7.6	8.6
N	4.4	4.2	8.1	6.9	4.3	4.5
% C retained	-	69.5	-	62.6	-	62.1
% N retained	-	54.2	-	44.4	-	57.7
HHV (MJ/kg)	21.6	30.0	21.9	28.4	21.1	27.9
Energy densification	-	1.38	-	1.29	-	1.32
Energy yield	-	78.2	-	66.7	-	67.8

Note. <sup>a</sup> Columns refer to the same samples described in Table 3.7.

### 3.3.8 Aqueous phase characterization

The aqueous phase produced by HTC was thoroughly characterized to determine the concentration of C, N, and P, as well as the major chemical constituents of the dissolved organic matter. In general, the aqueous phase was amber in color, had a pH from 4 to 6 and emitted a foul odor. The odor most likely arose from volatile components, such as short chain fatty acids. From our early work with *Chlorella* hydrochars, we selected three representative samples to study in more depth (Table 3.9). We normalized the concentrations of each nutrient to the amount of biomass reacted to better compare across treatments. This analysis affords us the opportunity to better understand how reaction temperature affected aqueous phase characteristics. First, it is evident by comparing the N retention given in Table 3.3 with the amount of N recovered as TN in the aqueous phase that both analyses are in fairly close agreement and suggest that about 40-50% of the biomass N partitions to the aqueous phase under these HTC conditions. Considering the error associated with these replicate analyses, there is no clear trend of increasing N and P in the aqueous phase with temperature, as one might expect. This may be due to the already very low N content of this biomass (~1.5% N). There was,

however, a moderate increase in the percentage of N in the ammonia form as temperature increased. With regards to P, our data corroborate earlier reports that nearly all of the P in the biomass partitions into the aqueous phase and that a high percentage is reactive phosphorus (Heilmann, Jader, Harned, et al., 2011; Garcia Alba et al., 2012). As expected, the aqueous phase was rich in C, measured in this case by chemical oxygen demand (COD).

Table 3.9. Aqueous phase analysis from HTC of *C. protothecoides* biomass for 60 min at various temperatures (mg/L in undiluted aqueous phase per 1 g biomass dry weight reacted)

Assay	Temperature (°C)		
	220	235	250
TN	270 ± 60	210 ± 0	310 ± 40
NH <sub>4</sub> -N	20 ± 3	30 ± 3	50 ± 0.1
TP	380 ± 60	430 ± 20	460 ± 10
PO <sub>4</sub> -P	260 ± 40	300 ± 30	300 ± 10
COD	6100 ± 600	6900 ± 1100	6100 ± 600
N recovered as TN (%)	40 ± 9.8	50	40.5 ± 7.1
N recovered as NH <sub>4</sub> -N (%)	3.6 ± 0.5	4.7 ± 0.6	5.9 ± 0.3
P recovered as TP (%)	85 ± 17	89 ± 1.1	89 ± 6.8
P recovered as PO <sub>4</sub> -P (%)	59 ± 10	62 ± 2.9	58 ± 4.9
TN as NH <sub>4</sub> -N (%)	9.2 ± 1.0	11	15 ± 1.8
TP as PO <sub>4</sub> -P (%)	70 ± 2.0	69 ± 2.4	65 ± 0.5
Dissolved Solids (wt.%)	4.0 ± 0.7	3.9 ± 0.0	3.8 ± 0.1

Note. Mean ± standard error given for replicate reactions. N and P values given in mg/L N and mg/L P, respectively. Aqueous phase was collected from reactions containing about 23 g of paste at 25% solids; no extra rinse water was used to remove the hydrochar solids from the reactor so the aqueous phase remained undiluted. P content in the *Chlorella* hydrochars was not measured but is estimated at 1%.

We also selected some representative aqueous phase samples from HTC experiments at lower temperatures for additional analysis (Table 3.10). These data are presented as mg of nutrient per 1 g dry of dry weight biomass reacted because the aqueous phase was diluted upon reactor unloading. These data also correspond well to elemental analyses of the biomass and hydrochars that indicate that about 40–50% of the biomass N is recovered in the aqueous phase. Likewise, P recovery was similar to the higher temperature reactions. Perhaps the most striking difference we observed was that the fraction of TN appearing as ammonia was significantly higher for these samples, about



55–65%. This is in contrast to what Du et al. (2012) reported for HTC of *Chlorella* at 200 °C for 40 min (about 15% of TN as ammonia) and more in line with what is typically seen for hydrothermal liquefaction reactions at 300–350 °C. For example, Valdez et al. found that at 250 °C and 20 min, about 65% of the initial biomass N partitioned to the aqueous phase and about 20% was in the ammonia form (Valdez et al., 2012). At longer times, the ammonia content increased to 45–50% of TN. The ammonia fraction of TN was similar at 300 °C but increased to about 65% at 350 or 400 °C and 45 min reactions. Biller et al. (2012) reported similarly high fractions of TN in the ammonia form at 300–350 °C (Biller et al., 2012).

One explanation for our observation of high ammonia fractions at low temperatures and short times is that hydrolysis outpaces the aromatization and polymerization reactions that bind N into larger molecular weight compounds frequently seen at higher temperatures and longer times. Although we observed some of these compounds as well (see discussion below), it is possible that we selected for conditions that interrupted the formation of N-containing organic compounds and therefore we observed a high percentage of ammonia. This may also explain why we observed such a low fraction of ammonia-N in the *Chlorella* reactions carried out at 220-250 °C. This theory, however, does not then explain why several groups have observed high ammonia fractions during hydrothermal liquefaction, unless we assume that the rates of hydrolysis of organic N into ammonia and its subsequent incorporation into organic compounds change non-linearly across the temperature range of 200-350 °C. Another plausible explanation is that something in the aqueous phase interfered with the TN and ammonia-N kits we used from Hach, biasing the data. If this were the case, however, we would expect to have seen a similar bias in the data obtained from reactions carried out at 220-250 °C, which contained a very low fraction of ammonia. Overall, these data suggest that low temperature HTC produces an aqueous phase rich in ammonia-N and contains a majority of the biomass P in the form of reactive phosphate. Future work should seek to develop better analytical tools for quantifying TN and ammonia-N in this difficult matrix.

Table 3.10. Aqueous phase analysis from low-temperature HTC (200 °C x 15 min) with various feedstocks (mg in aqueous phase per 1 g dry weight reacted)

Assay	Feedstock		
	<i>N. oculata</i> (Reed)	Marine Bi-culture	<i>Chlorella</i>
TN	34	44	36
NH <sub>4</sub> -N	19	26	23
TP	8	9	12
TOC	124	169	n/a
N recovered as TN (%)	39	54	47
N recovered as NH <sub>4</sub> -N (%)	21	32	31
P recovered as TP (%)	82	86	116
TN as NH <sub>4</sub> -N (%)	54	58	65

Note. Single analyses only using Hach kits. Reactive phosphate measurements for these samples were slightly higher than the TN values, indicating poor assay performance. Only TP values reported here. P measured by ICP for Reed Mariculture *Nannochloropsis* but estimated at 1% for the marine bi-culture and *Chlorella* samples.

To further identify components of the aqueous phase, we used HPLC, GC-MS, and FT-ICR-MS. HPLC detected various hydrolysis and decomposition products, mainly acetic acid, lactic acid, citric acid, pyroglutamic acid, glycerol, and limited amounts of furfurals. GC-MS showed volatile organic acids (acetic, formic, propionic, and butanoic acids), short chain amides such as acetamide, heterocyclic compounds, such as 2-pyrrolidinone and butyrolactone, and several larger molecules tentatively identified as long chain crown ethers. By far, the largest peak detected on the GC-MS chromatogram and by HPLC was acetic acid, which corresponds to its refractory nature in hydrothermal environments (Meyer et al., 1995). Previous HTC work with loblolly pine has also found acetic acid to be the most prominent organic acid in the aqueous phase (Yan et al., 2010). Fortunately, acetic acid is also a common carbon and energy source for mixotrophic and heterotrophic algal growth (Perez-Garcia et al., 2011), and was previously found to be readily consumed in various algae growing on aqueous phase from hydrothermal liquefaction (Biller et al., 2012).

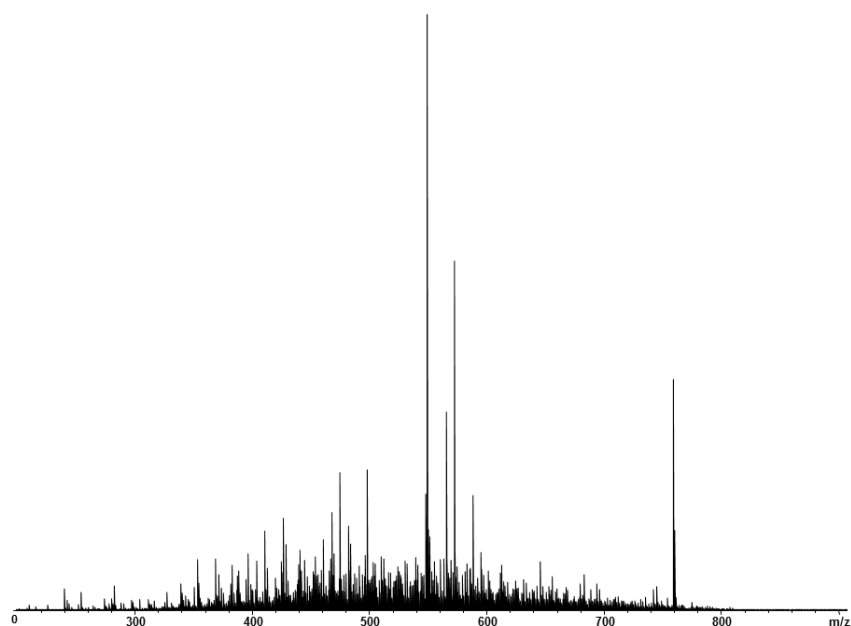


Figure 3.19. FT-ICR-MS spectra showing molecular weight distribution of organic matter in aqueous phase co-product obtained from reacting *N. oculata* biomass at 200 °C for 15 min.

To gain a deeper understanding of the dissolved organic matter in the aqueous phase, FT-ICR-MS was used. This analysis showed a distribution of compounds with molecular weights ranging from 200 – 800 m/z (Figure 3.19). Further molecular characterization of the compounds showed that >86% of the peaks in each analyzed aqueous phase had molecular formulas containing the elements C, H, O, and N. It is quite notable that such a large percentage of the detected compounds contained N. The extent to which algae can utilize organic N components is not precisely known, although several amino acids (e.g., glycine and glutamate) can serve as the sole N and C source for several algae. We have observed the growth of many algae species on yeast extract alone, which is a mixture of material derived from lysing and heating yeast cells. In many ways, the use of aqueous phase to grow algae is analogous to the use of yeast extract in many yeast media. The growth experiments presented in Chapter 7 would likewise suggest that the community of organisms present in the BCRs was adept at utilizing the N within the aqueous phase.

Placing the elemental composition of each compound detected on a van Krevelen plot helps to visualize that the major component of the organic matter in the aqueous phase appears to be protein-like compounds (Figure 3.20). Further analysis of the elemental ratios for the molecular formulas show that the majority of the compounds lie within the following ranges: 0.2-0.6 O/C, 1.5-2.2 H/C, and  $>0.05$  N/C, which are typical for proteins. The small fraction of compounds that contained the elements C, H, O, N, S, and P are likely to be phosphate or sulfate adducts.

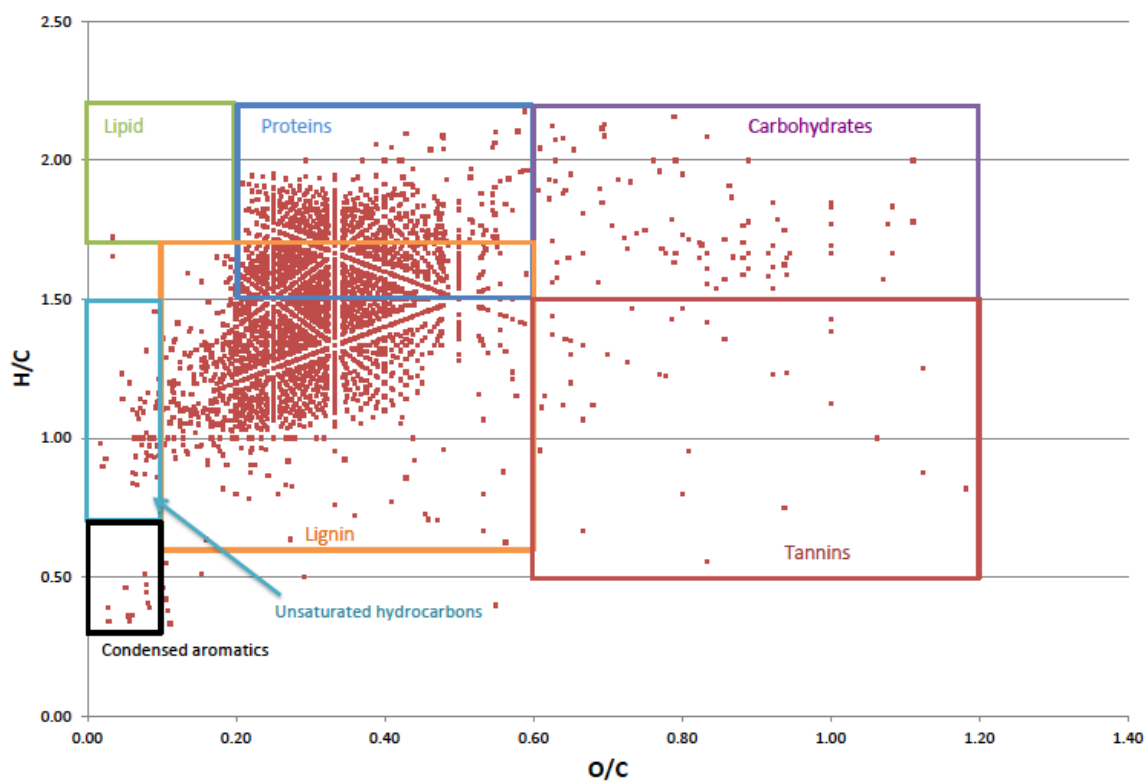


Figure 3.20. van Krevelen plot of organic compounds detected by FT-ICR-MS. The boundaries corresponding to representative compounds are highlighted.

### 3.4 Conclusions

Our work has demonstrated the utility of HTC as a thermal processing strategy to convert wet algal biomass into hydrochar. We envision this as the first step in a two-part process to produce biodiesel from algae. In addition to reducing the energy required to dry the

biomass, should that be desired, HTC reduces the amount of dry solids by about half, meaning less material must be subsequently transported, heated, and reacted during AC-IST. This may make it possible to perform carbonization at individual algal farms across a geographic region and then transport dried hydrochar to a centralized biodiesel processing facility. During HTC, roughly 40–60% of the N and 60–80% of the P partition into the aqueous phase, producing a sterile fertilizer for recycling to algae growth systems. The remainder of the N and P, contained in the hydrochar, can be liberated during in situ transesterification and can also potentially be recycled. Our work is the first to process high lipid algal biomass at a wide range of conditions and measure the lipid retention—a key parameter for maintaining high overall biodiesel yields. Based on the reduced energy and cost associated with performing HTC at temperatures near 200 °C, as well as the high measured amount of ammonia-N as a fraction of TN, which indicates the aqueous phase will be readily amenable to algal growth, we recommend future work continue to investigate low-temperature HTC. This may be of particular interest when producing algal biomass containing both high value co-products, such as EPA and biofuel feedstocks.

## CHAPTER 4

### SUPERCRITICAL IN SITU TRANSESTERIFICATION

#### 4.1 Background

In an effort to convert the lipids within hydrochars into biodiesel without first extracting them, we investigated various methods of in situ transesterification (IST). IST obviates the use of organic solvents like hexane and typically results in higher yields than traditional two-step extraction and transesterification procedures due to the conversion of lipids in all classes to esters as well as a reduction in losses from incomplete extraction (Lepage and Roy, 1984, 1986; Carrapiso and García, 2000; Lewis et al., 2000). To date, most work has focused on base- and acid-catalyzed IST of oilseeds occurring at moderate temperatures (30–120 °C) and with high molar ratios of alcohol to oil (~300–1200:1 MeOH:TG). In addition to using a large amount of alcohol, IST at subcritical alcohol temperatures is typically highly sensitive to water and requires long reaction times. Considering the costs and energy inputs associated with drying and processing the biomass prior to subcritical IST, as well as recovering the excess alcohol following the reaction, we have chosen to explore supercritical ethanol ( $T \geq 240.9$  °C,  $P \geq 6.1$  MPa) as a reaction medium for IST.

Supercritical IST (SC-IST) may benefit from reduced costs because it does not require catalysts or their recovery and generally has a higher tolerance for feedstock water and fatty acids. Although supercritical methanol and ethanol have been well studied as a medium for catalyst-free biodiesel production from pure vegetable oils (Pinnarat and Savage, 2008), relatively little work has explored SC-IST. Patil et al. (2010, 2011) demonstrated the conversion of lipids within wet *Nannochloropsis* to biodiesel using supercritical methanol, but MeOH:FA molar ratios above 1600 were used (Patil, Ganeswar, Mannarswamy, Cooke, et al., 2011; Patil, Ganeswar, Mannarswamy, Deng, et al., 2011). In another work, dry rice bran was reacted with ~90:1 MeOH:FA molar ratio and CO<sub>2</sub> as a co-solvent at 300 °C, but ester yields were unsatisfactorily low (~50%) (Kasim

et al., 2009). Finally, there have been reports on the thermochemical liquefaction of dry algal biomass, as well as other feedstocks, in supercritical alcohols (Huang et al., 2011; Zhou et al., 2012).

From our perspective, liquefaction in alcohol to produce bio-oil and IST to produce biodiesel describe the same process. Both bio-oil and biodiesel yields are determined after removing solids from the reaction mixture and evaporating excess alcohol, and in both cases, some form of upgrading or cleanup will be required before the fuel is engine-ready. From the literature available, liquefaction work tends to focus mostly on pre-dried, low-lipid feedstocks, favoring the presentation of total bio-oil yields over ester yields, while qualitatively identifying reaction products by GC-MS and ignoring the excessive use of alcohol (estimated >1500:1 EtOH:FA molar ratio). On the other hand, in situ transesterification work typically uses GC-FID to quantitatively determine ester yields while neglecting other components in the crude biodiesel (e.g., nitrogen-rich compounds derived from the biomass) and what measures must be taken to remove them.

Although a number of factors affect reaction performance (e.g., temperature, pressure, residence time, alcohol loading, feedstock composition), the ratio of alcohol to TG or FA is particularly important because alcohol recovery is energy and cost-intensive (Kiwjaroun et al., 2009). Typically, the equilibrium conversion to esters increases with ethanol loading, but high EtOH:FA molar ratios (>15-30) can result in lower ester yields (Minami and Saka, 2006; Chen et al., 2010), likely because of dilution effects that reduce reaction rates. Most work to date at supercritical conditions has been carried out at MeOH:TG ratios around 40:1 (Pinnarat and Savage, 2008; Sawangkeaw, 2010), and recent work on supercritical methylation of FAs was completed at a MeOH:FA ratio of about 24 (Chen et al., 2010). For reference, a biodiesel facility operating at subcritical temperatures and using base catalysts with pure vegetable oils typically uses a MeOH:TG ratio of 6:1, equivalent to a 2:1 MeOH:FA molar ratio. Early work on the supercritical process showed that methyl esterification occurs more quickly than transesterification, and that low molar

ratios (e.g., MeOH:FA of 3) could result in high FAME yields (Kusdiana and Saka, 2004a). Work at Syracuse University, recently patented, shows that supercritical transesterification can be accomplished at high temperatures (375–400°C), very short residence times (90–180 s), and low alcohol-to-oil molar ratios (5–6), suggesting supercritical transesterification may be a promising route to simplify biodiesel production and reduce costs substantially (Anitescu et al., 2008; Deshpande et al., 2010; Marulanda et al., 2010a, 2010b). We hypothesized that it would be possible to apply the lessons learned from these studies carried out with pure FA or oil feedstock to convert the lipids within hydrochars into biodiesel while using low ethanol loadings (EtOH:FA ratios 5-20).

In addition to the alcohol to feedstock ratio, perhaps the next most important factor in transesterification chemistry is water. Subcritical alcohol reactions are nearly completely inhibited by water, which can lead to soap formation in base-catalyzed reactions and catalyst removal in acid-catalyzed reactions. In contrast, early work showed that rapeseed oil was converted almost completely to FAMES in the presence of methanol (42:1 molar ratio) and water (as high as 36% on basis of oil mass) after 4 min at 350°C (Kusdiana and Saka, 2004a). It was suggested that water may act as an acid catalyst more strongly than methanol itself, thereby promoting TG hydrolysis. This liberates FAs, which are more soluble in alcohol than TGs and react more quickly to form esters (Warabi et al., 2004; Chen et al., 2010). The effect of water in supercritical alcohol transesterification has been explored in ethanol systems as well. The time required to reach maximum FAME yields increased with water content (cf. 28 min for 0% to 42 min for 10%) and total yield decreased (cf. 77.5% to 68.1 %) (Vieitez, Silva, Borges, et al., 2008). In general, longer residence times favor thermal degradation of fatty acids, in particular C18:2 and C18:3 fatty acids (Vieitez, Silva, Alckmin, et al., 2008). This work corroborated earlier findings that temperature should be kept below 300°C to avoid fatty acid degradation (Imahara et al., 2008), but showed that increasing water content from 0% to 10% of the reaction decreased degradation and increased conversion of TGs. Because hydrochar contains about 50–70% moisture after being mechanically separated from the HTC reaction



mixture, we hypothesized that it may be possible to react this material without prior drying and that some water would actually be beneficial by promoting TG hydrolysis.

In an effort to reduce the severity of supercritical alcohol reaction conditions, a two-step method of methyl ester production was proposed by Kusdiana and Saka (Kusdiana and Saka, 2004b). In this process, oils or fats are first hydrolyzed to fatty acids in a molar excess of water at 270 °C ( $P > 7$  MPa) for 20 min. Following water removal, fatty acid esterification with supercritical methanol takes place at 270 °C for 20 min. For a total reaction time of 40 min, this two-step method yielded near complete conversion to FAME, whereas the one step SC-MeOH method (both with and without water; at 270 °C and 40 min) demonstrated lower conversions and the presence of reaction intermediates (e.g., TG, MG, DG). This work, in addition to others that showed FA esterification occurs more quickly than TG transesterification (Warabi et al., 2004), motivated our early decision to pursue lipid hydrolysis during HTC. In many ways, our work on in situ lipid hydrolysis during HTC and SC-IST of hydrochar is analogous to this two-step method developed by Kusdiana and Saka, with the key difference being that we process lipids within a solid matrix as opposed to pure vegetable oils. This has an advantage in that we avoid the water-FA separation step, which is often a challenge. For example, Kusdiana and Saka (2004) reportedly dried the upper phase containing FA in a vacuum evaporator, while Holliday et al. (1997), who studied oil hydrolysis in subcritical water, observed milky white emulsions to which they had to add  $\text{NaSO}_4$  and then diethyl ether (which was later evaporated) to obtain the FA product (Holliday et al., 1997). Similar challenges with de-emulsification have hindered the adoption of enzyme-assisted aqueous extraction processing of oilseeds (Rosenthal et al., 1998; Zhang et al., 2007; Moura et al., 2008; Jung et al., 2009). To avoid difficulties in recovering FA from aqueous suspensions, our process retains lipids within a filterable solid matrix and then utilizes SC-IST to generate biodiesel.

Ultimately, the goal of SC-IST is to convert the lipids within algal hydrochars into biodiesel. To be a commercially viable process, we hypothesize that SC-IST must achieve high ester

yields while using as little ethanol as possible. In this work, we examined the impact of reaction conditions on the ability to meet these two requirements in single isothermal batch reactions containing wet, partially dried, or completely dried hydrochars (Levine et al., 2013).

## 4.2 Materials and Methods

### 4.2.1 Feedstock cultivation and hydrothermal carbonization

*Chlorella vulgaris* (UTEX #249) and *Chlorella protothecoides* (UTEX #255) were grown as biodiesel feedstocks as described in Section 2.2. The *C. vulgaris* biomass was harvested, dried, and then rehydrated to a 20% solids mixture prior to carbonization at 250 °C for 45 min. Freshly harvested *C. protothecoides* biomass (~20% total solids) was carbonized directly at 215–235 °C for 15–60 min. Upon cooling, hydrochars were recovered by filtering under light vacuum (P2 Glass microfiber filter, Whatman). The wet hydrochar was then either reacted directly, stored at 4 °C prior to reaction, or dried (65 °C for 1 h or 24 h) and then reacted. A complete description of the HTC conditions used and the hydrochar lipid content can be found in Table 4.1. Each hydrochar is designated with a letter in the second row of Table 4.1 that is referenced throughout this chapter. For one experiment, multiple 28 mL reactions (215 °C for 30 min) were pooled and the reaction mixture was sent to Pall Corporation’s Scientific and Laboratory Services for filtration tests on commercial equipment (hydrochar B).

### 4.2.2 Supercritical in situ transesterification

SC-IST was carried out in 1.6 mL SS Swagelok reactors with wet or dry hydrochars. Reactors were loaded with hydrochars and alcohol (methanol or ethanol containing a known water content) at the desired proportions and quantities such that the system was estimated to reach the target reaction pressure at the reaction temperature. The mass of each reactant was recorded to the nearest 0.01 mg (XS205DU, Mettler Toledo). Once loaded, reactors were submersed in an isothermal fluidized sand bath. The reaction time

was calculated as the total time in the sand bath (including a 5 – 8 min heat-up period). After the desired amount of time, reactors were removed from the sand bath and quenched in cold water.

An exploratory 2<sup>3</sup> factorial experiment with wet hydrochar was carried out to determine the effects of reaction temperature (275 and 325 °C), reaction time (60 and 120 min), and ethanol loading (~2 and 8 w/w dry solid) on the yield and composition of crude biodiesel. Following the reaction, reactor contents were filtered, and ethanol (95%; 15 mL) was used to wash the out the reactor. Hexane (1 mL) was added to the empty reactor to ensure complete ester recovery without exposing the lipid-extracted char to this solvent. The ethanol-biodiesel mixture was collected in a round bottom flask and ethanol was evaporated under vacuum at 70 °C. The crude biodiesel was resuspended in hexane (5 mL), combined with the 1 mL hexane reactor wash, centrifuged to remove any remaining fine particles, and transferred to a sample vial. The hexane-biodiesel mixture was analyzed for FAEs directly by gas chromatography with flame ionization detection (GC-FID) and the mass of the crude biodiesel was determined gravimetrically, as described in Section 4.2.3. The crude biodiesel (5-10 mg) was then analyzed for FAs, MGs, DGs, TGs, and glycerol following derivatization with N-trimethylsilyl-N-methyl trifluoroacetamide (MSTFA, Sigma), as described in Section 3.2. Each reaction condition was analyzed in duplicate.

Additional factorial experiments were carried out to determine the effects of reaction temperature, time, ethanol loading, water content of the reaction, and pressure on the yield of ethyl esters. To simplify the reactor work-up procedure, we forcefully emptied the reactor contents into plastic centrifuge tubes, and ethanol or heptane was used to wash out the reactor housing. In some cases, the reaction mixture contained a hexadecane internal standard, but in most reactions, hexadecane, methyl pentadecanoate (C15:0 FAME), or methyl tricosanoate (C23:0 FAME) was included as an internal standard only in the solvent used to wash out the reactor. The diluted reaction

mixture was centrifuged (10,000 RCF x 5 min) to pellet the lipid-extracted char, and 2 mL of the solvent mixture was transferred to a GC vial for analysis. The total volume of solvent used to recover the esters and the concentration of internal standard used to quantify the total ester product were as described in Section 4.2.3.

#### 4.2.3 Analysis of lipids within algal biomass, hydrochars, lipid-extracted residues, and biodiesel

Lipids from all classes in algal biomass, hydrochars, and lipid-extracted residues were simultaneously extracted and catalytically transesterified to determine their total lipid content, as described in Section 2.2.6. A representative GC-FID chromatogram is shown in Figure 4.1. Reaction ester yields were calculated by dividing the mass of FAME or FAEE recovered in the product by the theoretical maximum mass of ester that could form from the hydrochars. FAs were quantified on the basis of a calibration curve created with oleic acid and each internal standard. Control experiments with mixtures of ethyl oleate, oleic acid, ethanol, and water loaded into reactors placed only at room temperature demonstrated recoveries of ethyl oleate and oleic acid >95%.

#### 4.2.4 Statistical analysis

Minitab (v. 16.1.0) was used to design and analyze factorial experiments. The significance of regression coefficients was determined with a *p*-value of < 0.05. Results from additional experiments in which only one factor was varied at a time were compiled and analyzed using Microsoft Excel.

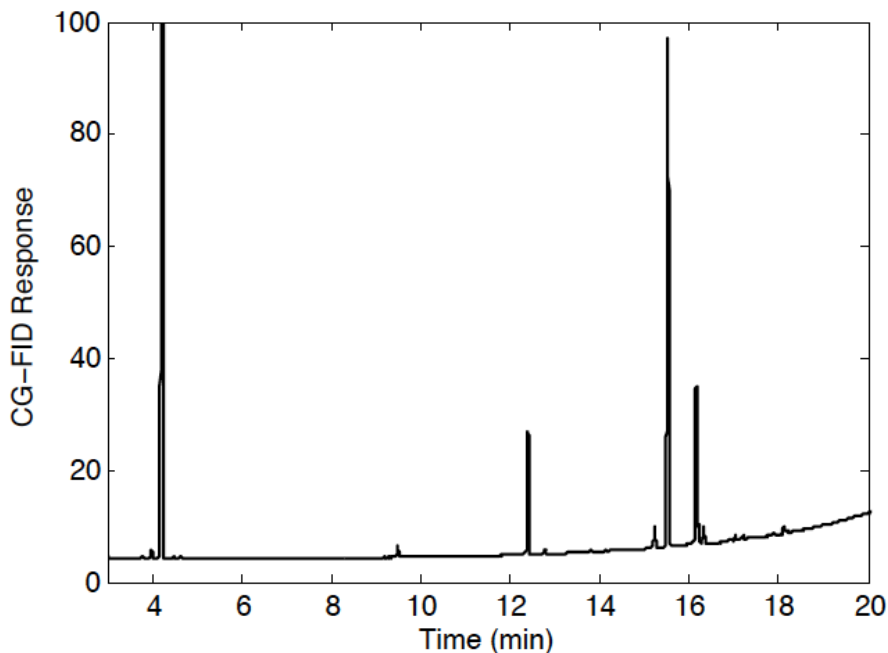


Figure 4.1. Representative GC-FID chromatogram of fatty acid ethyl esters from supercritical in situ transesterification. Reaction conditions were: 275 °C, 180 min, 20:1 EtOH:FA molar ratio, as described in Figure 4.7. The following peaks were quantified: hexadecane (internal standard, 4.2 min) C14:0 FAEE (9.4 min), C16:0 FAEE (12.3 min), C18:0 FAEE (15.3 min), C18:1 FAEE (15.5 min), C18:2 FAEE (16.2 min, minor isomer at 16.3 min), and C18:3 FAEE (isomers, 16.9-17.2 min). The isomerization of C18:2 and C18:3 FAEEs was due to the long reaction time at 275 °C.

### 4.3 Results and Discussion

#### 4.3.1 Feedstock production and hydrothermal carbonization

*Chlorella* biomass was grown, harvested, and carbonized under a variety of conditions to produce lipid-rich hydrochar. Many different hydrochars were used throughout this work; the four selected for presentation here (lettered A through D) are described in Table 4.1. Hydrochars contained about 50-75% total lipids on a dry weight basis when measured as FAEE and contained a mixture of FA, MG, DG, and TG. As expected, more severe HTC reaction conditions resulted in a greater percentage of lipids being hydrolyzed. Hydrochars C and D were derived from the same biomass harvest, whereas the parent material for hydrochar A and B each came from separate harvests. Slight variations in the growth protocol and the time at which the biomass was harvested

resulted in the differences in the lipid profile that is apparent in Table 4.1. Because the reaction conditions of HTC may impact the physical properties of the hydrochar (e.g., porosity, hydrophobicity) as well as the lipid composition based on the extent of hydrolysis, we selected these carbonized solids to represent the range of typical HTC processing conditions. In some reactions, hydrochars were reacted wet, exactly as they were recovered by filtration following HTC. In other reactions, hydrochars were partially dried prior to reaction or completely dried and then rehydrated with the desired amount of water to investigate the effects of water on the reaction.

Table 4.1. Characterization of algal hydrochars used in SC-IST

Parameter	Hydrochar			
	A	B	C	D
Carbonization Temp. (°C)	250	215	220	235
Carbonization Time (min)	45	30	60	60
Total FAEEs (wt.%) <sup>a</sup>	53	75	58	51
Fatty acid (% of FAEEs) <sup>b</sup>				
C16:0	18	13	13	13
C18:0	2	3	2	2
C18:1	46	65	57	57
C18:2	9	16	24	24
C18:3	13	2	2	2
Lipid Composition				
FA	37	4	9	28
MG	9	trace	2	8
DG	241	7	19	28
TG	30	89	71	37

Note. <sup>a</sup>Total fatty acid ethyl esters (FAEEs) were determined by acid-catalyzed in situ transesterification and quantified by GC-FID considering only the amount of each FAEE listed in the table; other FAEEs were detected but typically made up <5% of the hydrochar mass. FAEE yields from supercritical in situ transesterification were computed only on the basis of these five esters. <sup>b</sup>Sum of percentages does not total to 100 due to rounding. <sup>c</sup>The percentage of fatty acids (FA), monoglycerides (MGs), diglycerides (DGs), and triglycerides (TGs) in the total lipid extract was determined by hexane-isopropanol extraction and quantification by high temperature GC-FID.

#### 4.3.2 Early work on SC-IST with wet hydrochar

At first we focused exclusively on processing wet hydrochars, under the assumption that the supercritical reaction medium could tolerate a high moisture content and that drying hydrochars prior to SC-IST would be a significant energy burden. As shown in Figure 4.2, the moisture content of the entire reaction mixture is highly dependent on the hydrochar moisture content and decreases with increasing ethanol loading. Throughout this work,

we report the ethanol loading during SC-IST on either a molar basis with respect to the total number of FA groups present in the hydrochar or on a mass basis to the dry hydrochar. For the conditions shown in Figure 4.2, a 2, 15, 30, or 50 EtOH:FA molar ratio is equivalent to a 0.2, 1.2, 2.4, or 4 EtOH:hydrochar (w/w) ratio, respectively. Based on prior work done with pure oil feedstocks, we hypothesized that low water contents might increase the conversion of glycerides to FAEE at 250–325 °C, most likely through increased glyceride hydrolysis prior to esterification and decreased decomposition of unsaturated FAEE (Vieitez, Silva, Borges, et al., 2008). On the other hand, a high water content can dilute the reaction mixture, thereby reducing reaction rates, encouraging FAEE hydrolysis (Changi et al., 2011), and increasing the total mass that must be heated.

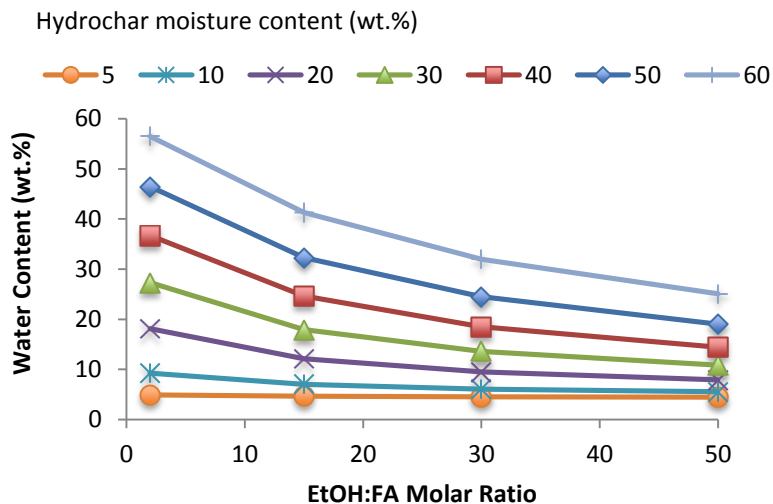


Figure 4.2. Reaction water content (wt.%) for supercritical in situ transesterification of hydrochars with various amounts of azeotropic ethanol (4.4 wt.% water). Hydrochars are assumed to contain 50% total lipids (average molecular weight of 285 g/mol).

Hydrochar A (reacted at 250 °C and 45 min) was selected for an initial factorial experiment to examine the effects of reaction temperature, time, and ethanol loading in wet hydrochars (Table 4.2). Notably, a significant fraction of the TGs originally in the reactant biomass were hydrolyzed in this hydrochar, leading to a high percentage of FA. Hydrochar A was not dried prior to SC-IST and contained approximately 46 wt.% water. As shown in Table 4.2, longer reaction times and higher temperatures led to higher crude biodiesel yields and significantly fewer non-FAEE components therein, particularly FA and MG. In

contrast, the higher ethanol loading led to significantly greater gravimetric yields of crude biodiesel but with concomitant increases in its non-FAEE content. According to an analysis of covariance, which determined the statistical significance of time, temperature, and ethanol loading as main predictors of crude biodiesel yield and composition using linear regression, only ethanol loading was found to significantly affect the yield. However, the influence of all predictors on the aggregated amount non-FAEE components in the crude biodiesel was significant.

Table 4.2. Crude biodiesel yield and composition from the SC-IST of hydrochar A

Reaction conditions and loading					Crude biodiesel composition (wt%)						
Run #	Temp (°C)	Time (min)	EtOH (w/w) <sup>a</sup>	H <sub>2</sub> O (%) <sup>b</sup>	Crude biodiesel yield (%) <sup>c</sup>	FAEE	FA	MG	DG	TG	Other
1	275	60	2.2	21.0	56.4	53.5	11.7	10.1	2.1	2.1	20.5
2	275	60	8.3	8.4	80.5	39.8	14.0	16.7	6.7	2.7	20.1
3	275	120	2.3	20.4	68.3	79.2	9.3	5.3	1.7	1.3	3.1
4	275	120	7.5	9.1	94.0	56.6	9.7	13.2	2.2	0.8	17.5
5	325	60	2.1	21.6	65.8	33.4	9.9	3.2	0.8	0.6	52.2
6	325	60	7.2	9.4	87.7	52.0	13.9	10.7	0.8	0.4	22.3
7	325	120	2.3	20.4	58.7	58.6	8.6	2.0	0.6	0.1	30.1
8	325	120	6.6	10.1	100	58.7	9.0	4.3	0.3	0.1	27.6

Note. <sup>a</sup>Ethanol loading is the mass ratio of ethanol to dry hydrochar. <sup>b</sup>H<sub>2</sub>O % is the mass percentage of water in the reactor. <sup>c</sup>Crude biodiesel yield is a gravimetric determination (average standard deviation for the mean of at least two gravimetric determinations was less than 6%) and is reported as a percentage of total lipids (hexane-isopropanol extraction) in the reactant hydrochar on a dry basis. The crude biodiesel was analyzed directly for fatty acid ethyl esters (FAEEs) and for fatty acids (FAs), monoglycerides (MGs), diglycerides (DGs), and triglycerides (TGs) following derivatization with MSTFA.

In this complex, multiphase reaction system, lipids were both extracted from the hydrochar and transesterified. The crude biodiesel yield, which indicates overall extraction efficiency, ranged from about 56 to 100% (relative to the total lipids in the hydrochar as determined by HIP extraction). As shown in Table 4.2, yields from reactions lasting 120 min with an EtOH:solids mass ratio of 6.6-7.5 were from 94 to 100%, suggesting that lipid removal from the solids was nearly complete under these conditions. This result was confirmed by examining the residual solids after SC-IST (i.e. lipid-extracted char, LEC) and finding the FAEE content to range from 1 to 4% on a dry weight basis.



Although nearly all lipids may have been removed from the hydrochar during these reactions, total FAEE yields (60-66%) indicate that transesterification was somewhat inhibited. In the discussion that follows, the influence of key process parameters on lipid extraction and conversion is elucidated through an analysis of the yield and composition of biodiesel.

Table 4.2 provides information about the composition of the crude biodiesel. In general, its ester content decreased with ethanol loading at 275 °C, while at 325 °C, ester content increased or remained the same. Ester content increased with time, although with a less pronounced effect at the higher temperature. The highest ester content (79.2%) was achieved at 275 °C, 120 min, and a low (2.3) EtOH:solids mass ratio. The ester contents reported here compare well with data reported for SC-EtOH transesterification of soybean oil in systems containing 10% water: at 275 °C, the ester content of the recovered product was approximately 10, 40, or 50% at 21, 42, or 52.5 min residence times, respectively, and 58, 69, 70.8% esters at 325 °C (Vieitez, Silva, Alckmin, et al., 2008). In addition, the ester contents compare favorably to a previous report regarding in situ transesterification of dry rice bran containing 17.4% total oil (comprising 73.7% TG and 12.3% FA): the FAME yield was 51% and FAMEs composed 52.5% of the product mixture following reaction with SC-MeOH and a CO<sub>2</sub> co-solvent (300 °C, 30 MPa, 5 min, 271 MeOH:oil molar ratio) (Kasim et al., 2009).

As detailed in Table 4.2, the crude biodiesel contained unreacted glycerides and FA in addition to esters. TGs and DGs were typically present in low amounts, especially at 325 °C. At both temperatures, increasing the amount of ethanol resulted in crude biodiesel containing a higher percentage of FA and MG. For example, in runs 4 and 8, FAEE accounted for only 57–59% of the crude biodiesel product; a significant amount of FA (9.0–9.7%) and MG (4.3–13.2%) were present. The prevalence of MGs can be explained by their increased stability relative to other glycerides, and previous work demonstrates that their conversion is the rate-limiting step in TG transesterification (Warabi et al.,

2004). Likewise, FA in the crude biodiesel most likely resulted from incomplete esterification or from FAEE hydrolysis. Because EN14214 mandates that esters comprise more than 96.5% of biodiesel and limits the amount of FA, MG, DG, and TG in biodiesel to 0.4, 0.8, 0.2, and 0.2 (w/w), respectively, the crude biodiesel produced by SC-IST under the conditions examined herein does not meet the specifications for finished biodiesel. In general, non-FAEE components could be removed with a warm alkaline water wash followed by centrifugation (Haas and Scott, 2006) or with new techniques that require less water (Mazzieri et al., 2008; Wang et al., 2009). FA and glycerides recovered from the crude biodiesel could be recycled back to the supercritical reactor, generating additional FAEE.

Both the ethanol and water content of SC-IST reactions may have impacted the yield and quality of biodiesel produced. Water may play both beneficial and detrimental roles during supercritical transesterification. The benefit arises from low water contents increasing the conversion of glycerides to FAEE at 250–325 °C, most likely through increased glyceride hydrolysis prior to esterification and decreased decomposition of unsaturated FAEE (Vieitez, Silva, Alckmin, et al., 2008). The detriment arises from higher water contents diluting the system (thereby reducing reaction rates) and facilitating FAEE hydrolysis (loss of desired product). These phenomena are likely responsible for the reduced ester yields reported from SC-EtOH transesterification reactions done in the presence of water (Kusdiana and Saka, 2004a; Pinnarat and Savage, 2008; Vieitez, Silva, Borges, et al., 2008).

Likewise, the ethanol loading can have positive and negative impacts on the FAEE yield. The equilibrium conversion to esters increases with ethanol loading, but high EtOH:FA molar ratios (>15-30) can result in lower ester yields (Minami and Saka, 2006; Chen et al., 2010), perhaps because of dilution effects that reduce reaction rates. In the SC-IST reactions we ran, the molar ratio of EtOH to total FA groups ranged from about 20:1 at the lower loading to 60-75 at the higher loading. In all of the reactions in Table 4.2, the

initial water-to-oil ratio was constant (~1.1 w/w water to HIP CLE of hydrolysis solids). Therefore, reactions with a higher ethanol loading necessarily had a lower water content on a total mass basis (cf. 8–10% to 20–21%). This conflation of the effects of ethanol loading and water content makes it difficult to isolate the effect of either component in our experiments, but given the large excess of water and ethanol, relatively long residence times, and the prevalence of FA in the product mixtures, it is likely that dilution of the reactant mixture and FAEE hydrolysis limited ester yields. These data were the basis for further work that considered lower ethanol loadings and the removal of some or all of the water from hydrochar (Sec. 4.3.5). In addition to improving the ester yield from SC-IST, these process changes may also reduce process costs and energy inputs.

Previously, supercritical alcohol treatment has been noted to cause trans-isomerization and decomposition or polymerization of unsaturated FA (Kusdiana and Saka, 2001; He, Wang, et al., 2007; Imahara et al., 2008). Although some have suggested that isomerization reduces fuel stability (Gui et al., 2009) and negatively impacts cold flow properties (Imahara et al., 2008), there is little conclusive evidence that trans-isomers of unsaturated FAEE are actually detrimental to fuel quality. Nevertheless, we estimated the extent to which isomerization occurred by examining GC retention time shifts in the elution of unsaturated FAEE. Note that both isomerization and decomposition can contribute to changes in the FAEE profile of the synthesized crude biodiesel. Because no isomerization of C18:2 was detected in the hydrochar, the appearance of C18:2 isomers following exposure to SC-EtOH permitted a useful analysis of the effects of time, temperature, and ethanol loading on isomerization.

Table 4.3 shows that at 275 °C, between 6 and 8% of the C18:2 synthesized was in a non-native form, with the exception of the reaction lasting 60 min with high ethanol, in which no isomerization was detected. Significantly more C18:2 isomerized at 325 °C; from 34–44% and 56–57% of the C18:2 synthesized was in a non-native form after 60 or 120 min, respectively. At both temperatures, higher amounts of ethanol led to a reduction in isomerization, with a more prominent effect evident at shorter times. Similar but more

pronounced trends were observed for C18:3 FAEE. Although analysis of C18:3 isomerization is complicated by the fact that the hydrolysis solids already contained some isomerized linolenic FA, about 35–60% and 77–83% of C18:3 FAEE detected in the crude biodiesel was isomerized at 275 °C and 325 °C, respectively. In summary, higher temperatures and longer reaction times resulted in greater trans-isomerization of C18:2 and C18:3 FAEE, in agreement with previous reports (He, Wang, et al., 2007; Vieitez, Silva, Borges, et al., 2008).

Table 4.3. Fatty acid ethyl ester composition of biodiesel produced through SC-IST

Run #	Fatty acid profile (% of total FAEE)						Percent isomerized (% of total species)	
	C14:0	C16:0	C18:0	C18:1	C18:2	C18:3	C18:2	C18:3
1	0.0	19.3	2.2	47.7	9.3	11.8	8.0	42.2
2	0.0	18.5	2.3	48.1	9.0	12.4	0.0	34.9
3	0.5	20.1	2.3	50.4	8.4	9.8	8.4	59.1
4	0.4	19.1	2.2	49.6	8.9	11.4	6.3	53.9
5	0.6	23.2	2.9	57.1	6.1	3.4	43.8	77.2
6	0.5	20.1	2.4	52.1	8.6	7.7	34.5	83.6
7	0.7	24.9	3.5	59.4	4.1	0.0	57.1	- <sup>a</sup>
8	0.4	21.0	2.6	54.3	8.3	5.4	55.9	80.7

Note. Isomerized ethyl esters correspond to both positional and geometric isomers, which demonstrated earlier (typically *trans*) and later (typically *cis*) retention times compared to compounds with the same chain length and number of double bonds in unreacted algal biomass where only single peaks were detected. C18:1, C18:2, and C18:3 data include all isomers detected, with the percent isomerized indicated in the two rightmost columns. <sup>a</sup>No C18:3 FAEE was detected in this reaction.

In addition to isomerization, unsaturated FA can undergo a variety of reactions that may impact their usefulness as fuel components and cause them to be unaccounted for in our ester analysis. Decomposition is indicated when the yield of all isomers of an unsaturated FAEE is less than the yield of saturated FAEEs, which are assumed to be thermally stable under these conditions (Imahara et al., 2008). Previous work has shown that unsaturated FA can polymerize into higher molecular weight compounds and may decompose into gaseous products in the presence of alcohols near or above 300 °C, thereby reducing ester yields. For example, saturated FAMES were found to be stable in methanol up to 300 °C (19 MPa) for 60 min, whereas C18:1 and C18:2 FAMES were stable at 270 °C (17 MPa) but showed ~10% losses after 60 min at 300 °C and C18:3 FAME showed minor losses at 270

°C but 20% loss after 60 min at 300 °C (Imahara et al., 2008). He et al. (2007) found that supercritical transesterification yields increased with time at 280 °C up to 50 min, but at 300°C, yields peaked at 82% at 25 min and then decreased to about 67% at 50 min. Similar trends in decomposition were found for FAEE reacted in ethanol and ethanol-water mixtures (Vieitez, Silva, Alckmin, et al., 2008; Vieitez et al., 2011), as well as our previous work with hydrochars in ethanol at 275 and 325 °C. In recent work on the decomposition of soybean oil during supercritical transesterification with methanol, an unidentified peak eluting near the diglycerides was suspected of corresponding to thermal decomposition products arising from unsaturated fatty acids (Quesada-Medina and Olivares-Carrillo, 2011). These authors suggested that monounsaturated FAMES could suffer thermal linear dimerization to form acyclic dimers, while polyunsaturated FAMES may generate a mixture of monocyclic and six-membered cyclic dimers. Considering the elution of this unidentified peak near the diglycerides, which contain two fatty acid groups with a glycerol backbone, it seems plausible that dimerization may contribute to ester losses, especially when quantifying yield based on GC-FID results with polar columns. A review of the chromatograms generated in our work at 275 and 325 °C confirmed the presence of this unidentified peak, which we at first mistakenly identified as a diglyceride. As expected, the area of this peak increased with temperature and reaction time.

We examined the decomposition of unsaturated FAs during SC-EtOH treatment of hydrochars. We implicitly assume that the transesterification rates in SC-EtOH are identical for both saturated and unsaturated FAs. The data in Table 4.4 show that decomposition was most prevalent in the polyunsaturated FAEE at higher temperatures and longer times. For example, the difference between the C18:3 yield and the yield of saturated FAEE increased from 3–5 and 1.2–1.5 fold from 275 to 325 °C and 60 to 120 min, respectively. In addition, yields of C18:2 and C18:3 FAEE, inclusive of all isomers, were closer to the average yield of saturated FAEE in reactions containing more ethanol, with the exception of those carried out at 275 °C and 60 min. In contrast, the yield of native C18:1 was within 2% of the average yield of saturated FAEE in all treatments, with

the exception of reactions at 325 °C containing low amounts of ethanol. Here, C18:1 yields were about 4.4 and 10% less than the average yield of saturated FA at this temperature and 60 or 120 min, respectively. These data suggest that thermal reactions consume unsaturated FAEE, generating compounds that were not detected in this study.

**Table 4.4. Fatty acid ethyl ester yield from SC-IST**

Run #	Ester yield		Yield reduction <sup>b</sup>		
	Total	Saturated <sup>a</sup>	C18:1	C18:2	C18:3
1	34.2	37.2	1.4	1	9.3
2	36.3	39.7	1.4	2.3	8.5
3	49.5	55.4	0.6	8	21.9
4	60.2	65.1	-0.5	3.6	17.5
5	43.0	58.4	4.4	28.5	48.2
6	51.6	59.7	0.7	8.7	32.3
7	38.9	60.6	9.9	42.3	60.6
8	66.4	81.3	2.1	18.2	56.5

Note. All yields based on GC-FID determinations of FAEE from the acid catalyzed in situ transesterification of hydrolysis solids and of FAEE recovered from supercritical in situ transesterification. <sup>a</sup>Saturated FAEE yield is the average yield of C16:0 and C18:0 FAEEs.

<sup>b</sup>The difference between the average yield of saturated FAEE and the yield of all isomers of either C18:1, C18:2, or C18:3.

Some of these products, such as glycerol decomposition products and short chain FAEE, may still contribute to the biodiesel as fuel components and may even improve the biodiesel viscosity and cloud/pour point (Anitescu et al., 2008). Recall from Table 4.2 that in most reactions, about 20–30% of the gravimetric mass of the crude biodiesel remained unidentified by GC-FID. This result is consistent with findings of Kasim *et al.* (2009), who suggested unidentified matter was most likely degradation products of proteins, carbohydrates, and hydrocarbons (Kasim et al., 2009). Although biodiesel may be narrowly defined by international specifications to contain only long-chain mono-alkyl esters, we suggest that the total fuel yield from SC reactions may contain non-FAEE components that are still valuable. In addition, exposing feedstocks rich in polyunsaturated FA to SC-EtOH may be a useful way to generate biodiesel that meets EN14103 specifications (i.e., C18:3 content < 15% of esters).

In general, the FAEE yield from both SC oil transesterification and FA esterification tends to increase with residence time until a critical point, after which it decreases. The competing phenomena of conversion and decomposition define this optimum time, which tends to occur earlier at higher temperatures (He, Wang, et al., 2007). Because isomerization and thermal decomposition were less pronounced at 275 °C, the longer reaction time increased crude biodiesel and FAEE yields. At 325 °C, increasing the reaction time from 60 to 120 min decreased both crude biodiesel and FAEE yields at the lower ethanol loading but increased yields at the higher ethanol loading. These data highlight how the decomposition of unsaturated FAEE, evidenced in part by the complete absence of C18:3 FAEE in run 7, can influence fuel yields when considering esters only. Because data in the factorial experiment was collected at only two time points, little can be inferred about whether a maximum in yield occurred at intermediate times; however, in additional SC-IST experiments carried out for 60, 90, and 120 min at 290 °C, crude biodiesel and FAEE yields were highest at 90 min by 10-20%. Taken together, these data suggest that reaction time must be chosen wisely to optimize conversion and limit decomposition.

#### 4.3.3 Additional studies on SC-IST in the presence of water

The factorial experiment presented in the previous section suggested that ester yields from wet hydrochars of about 60% were achievable at 275 °C when using a ~70:1 EtOH:FA molar ratio and relatively long reaction times (120 min, run 4, Table 4.4). We next sought to better understand the impact of water on supercritical transesterification when using lower alcohol loadings that would be more realistic for a commercialized process.

First, reactions were carried out with oleic acid as a model compound to study supercritical esterification. As shown in Figure 4.3, oleic acid is converted into ethyl oleate in high yields in reactions at 275 °C lasting 30 and 60 min with a 12:1 EtOH:FA molar ratio and no water initially present. As expected, the ethyl oleate yield increased with reaction time, reaching 97% after 60 min. When water was added to the reaction mixture at 26-

32 wt.%, the reaction was severely impeded, and ethyl oleate yields dropped to 32-45%. Correspondingly, the amount of oleic acid recovered from the reaction mixture rose, indicating that the fatty acid remained unreacted.

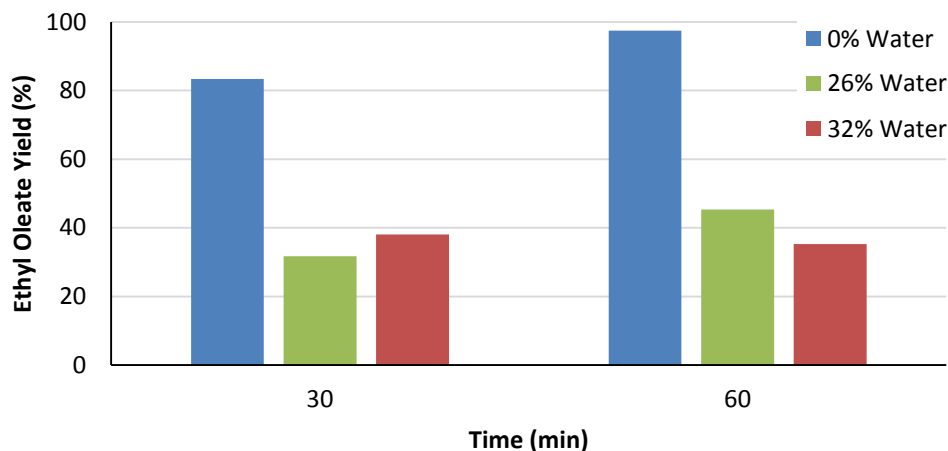


Figure 4.3. Supercritical esterification of oleic acid at 275 °C with 12:1 EtOH:FA molar ratio. Reactions contained 0%, 26%, or 32% water on a total reaction weight basis. Single reactions only.

Although the data from oleic acid esterification at high water contents were not promising, reactions with wet hydrochars were attempted to determine if high ester yields could be achieved without an additional drying step. Hydrochar D was reacted immediately following carbonization, when it contained 46% water, or after being oven dried at 65°C for 24 hrs. Figure 4.4 shows the total ethyl ester yields of reactions lasting 30 or 60 min that contained pure ethanol in a 5:1 or 10:1 EtOH:FA molar ratio. Yields increased with reaction time regardless of ethanol loading or water content, though reactions containing dry hydrochar with the least amount of ethanol showed the smallest change with time (cf. 39% to 43%). In reactions containing wet hydrochars, yield almost doubled from 30 to 60 min at both ethanol loadings, but the highest yield was less than 40%. In contrast, when dry hydrochar was reacted with ethanol at a 10:1 EtOH:FA molar ratio for 60 min, the yield was almost 70%. These data suggest that reacting wet hydrochars with supercritical ethanol at moderate to low ethanol loadings is unlikely to produce high ester yields. Considering that hydrochars typically contain 40–60%



moisture and the energy required to remove most of this water is equivalent to less than 15% of their total energy content, subsequent work used oven-dried hydrochars only. In most cases, hydrochars were dried for 1 h to approximately 5–10% moisture content to realistically model how a commercial facility might process them and reduce the energy required for evaporation. As shown in Figure 4.2, hydrochars with this amount of moisture can be reacted with relatively low amounts of azeotropic ethanol while maintaining the overall reaction water content below 10 wt.%.

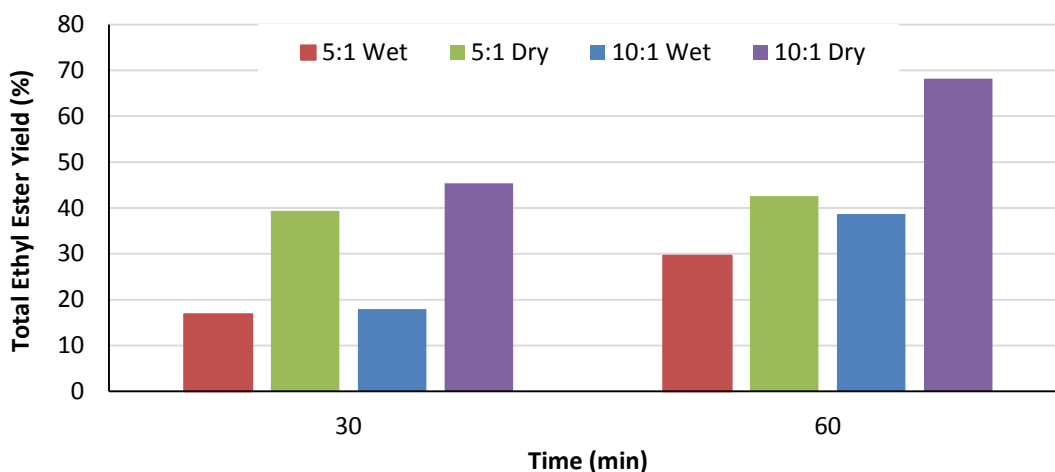


Figure 4.4. Supercritical in situ transesterification of wet and dry hydrochars at 275 °C. Reactions contained pure ethanol at a ~5:1 or 10:1 EtOH:FA molar ratio. Hydrochar D was reacted immediately following carbonization (46% moisture) or oven dried at 65 °C for 24 h and then reacted. Reactions with wet hydrochar contained 30-36 wt.% water overall. Single reactions only.

#### 4.3.4 Effect of reaction temperature

As described in Section 4.3.2, we observed that the transesterification of hydrochar lipids and the degradation of unsaturated FAs occur simultaneously in reactions at or above 275 °C (Levine et al., 2010). In an effort to determine if it was possible to reduce the time required to reach high conversion without incurring ester losses, we examined the influence of reaction temperature from 275–295 °C for 5–90 min at ~20 MPa. Hydrochar B, which was produced at mild HTC conditions, commercially filtered, and oven dried for 24 h, was used in these experiments as well as the factorial experiments described in Section 4.3.5. As shown in Figure 4.5, the highest overall yields were observed at 275 °C and 90 min. Although after 15 min, reactions carried out at 295 °C had almost 3 times

greater yield than those at 285 °C, and a similar trend of increasing yield with reaction time was observed at 30 min, yields at 285 °C and longer times were lower than those at 275 °C. This trend was more pronounced at even higher temperatures, where very low ester yields were observed in preliminary experiments carried out at 325 °C and 375 °C and shorter reaction times (3–12 min).

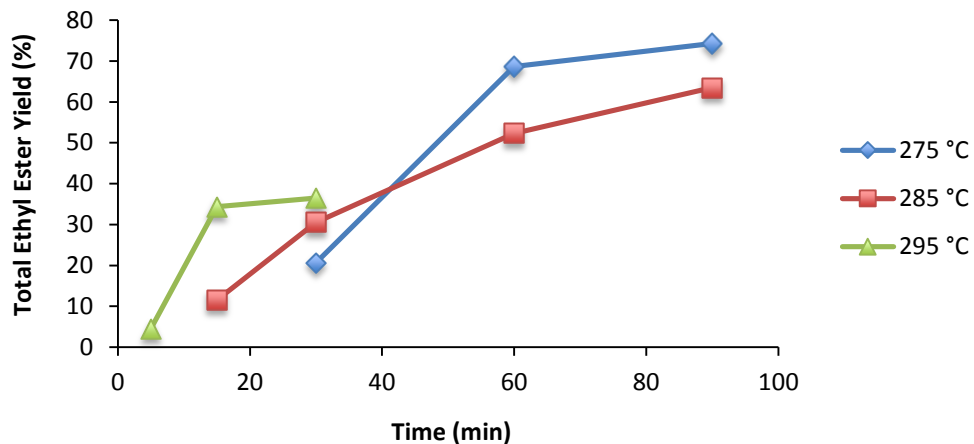


Figure 4.5. Supercritical in situ transesterification of dry Hydrochar B at 275–295 °C (~20 MPa). Reactions contained azeotropic ethanol at a ~5:1 EtOH:FA molar ratio. Single reactions only.

The most likely explanation for these observations is that higher temperatures lead to the disappearance of unsaturated FAs through a variety of thermal degradation pathways.

It is notable that the reduction in yield observed for SC-IST at 275 °C and above seems elevated in comparison to the aforementioned literature that studied oil or ester feedstocks. Thermal decomposition is indicated when the yield of all isomers of an unsaturated FAEE is less than the yield of saturated FAEEs (e.g., C16:0), which are assumed to be thermally stable under these conditions. For instance, for the reactions performed at 275 °C in Figure 4.5, the estimated reductions in yield for 30 to 90 min for C18:1, C18:2, and C18:3 were 0.2–1.3%, 2.1–9.3%, and 7.1–25.3%, respectively. Considering the lipid profile of this feedstock (shown in Table 4.1), the losses observed over this time range at 275 °C equate to about a 2–3% overall reduction in yield due to

thermal degradation of unsaturated FA. It is plausible that non-lipid components of the hydrochars may serve to accelerate the decomposition of unsaturated FAs at temperatures and retention times below those previously observed for pure feedstocks. This may be due to a catalytic effect, provided perhaps by acidic or metallic components in the hydrochar, or by the virtue of supplying additional compounds that can react with unsaturated FAs to produce higher molecular weight aggregates that are not detectable by GC-FID. Because the aqueous phase recovered from HTC is typically acidic (pH ~6), the solids may have some acidic properties that accelerate reaction rates. We have observed a similar trend when performing in situ transesterification at sub-critical conditions using an acid catalyst; yields decrease at 100 °C and long batch holding times whereas no loss in yield is seen at 85 °C (Section 5.3). These data suggest that lower temperatures than previously found for pure feedstocks may be necessary to avoid ester losses due to degradation when performing in situ transesterification. In an effort to compromise between fast reaction rates and thermal degradation, subsequent work was carried out at 275 °C.

#### 4.3.5 Factorial experiment with dry hydrochar

A factorial experiment was designed to concurrently investigate the effects of time (30 to 120 min), ethanol loading (4.5 to 18 EtOH:FA molar, equivalent to 0.5 to 2 EtOH:hydrochar w/w), reaction water content (0 to 4 wt.%), and reaction pressure (10 to 20 MPa) at 275 °C. As shown in Table 4.5, 20 runs were carried out with hydrochar B, comprising a full 2<sup>4</sup> factorial as well as a replicated center point and replicated reactions at the center point but without water. The range of reaction water content explored in this experiment corresponds to the use of dry solids with pure ethanol or azeotropic ethanol at these EtOH:FA molar ratios. While keeping the desired EtOH:FA molar ratios, the total reaction volume was scaled based on the density of ethanol at 275 °C and 10 or 20 MPa (about 0.2 and 0.4 g/mL, respectively). This corresponded to reactors being loaded about 30-45% (10 MPa) or 55–70% (20 MPa) full at room temperature. These pressures were chosen

because yields have previously been found to increase with pressure up to about 25 MPa (He et al., 2007b).

Table 4.5. Reaction conditions and total ester yields for factorial experiment

Run	Temp. (°C)	Time (min)	EtOH:FA (mol/mol)	Water (wt.%)	Pressure (MPa) <sup>a</sup>	Ester Yield (%)
1	275	30	4.5	2.0	10	40
2	275	30	4.5	0.0	10	21
3	275	30	4.5	2.1	20	24
4	275	30	4.5	0.0	20	44
5	275	30	18	0.0	10	40
6	275	30	18	4.0	10	19
7	275	30	18	0.0	20	20
8	275	30	18	4.0	20	13
9	275	75	11	1.7	15	35
10	275	75	11	1.7	15	46
11	275	75	11	0.0	15	59
12	275	75	11	0.0	15	43
13	275	120	4.5	0.0	10	69
14	275	120	4.5	2.1	10	63
15	275	120	4.5	0.0	20	59
16	275	120	4.5	2.0	20	68
17	275	120	18	0.0	10	68
18	275	120	18	4.0	10	64
19	275	120	18	0.0	20	65
20	275	120	18	4.0	20	58

Note. <sup>a</sup>Pressure estimated from Peng-Robinson equation of state. All reactions used hydrochar B.

Table 4.5 presents the reaction conditions and corresponding total FAEE yields for each run. The mean yield and its standard error for the replicated center point reactions with and without water were  $40 \pm 5.5$  % and  $51 \pm 8.1$  %, respectively. The variation observed was most likely due to the heterogeneous nature of the hydrochar, which was not ground or otherwise processed after drying. As a result, loading small quantities into each reactor likely resulted in differences in the lipid and moisture content between runs. A similar finding was reported for the in situ transesterification of dried distillers grains, which tended to have much higher run-to-run variability than when processing a more homogenous feedstock like flaked soybeans (Haas et al., 2007). Nevertheless, these data

provide useful information regarding the relationship of reaction parameters to ester yield, which can be described through a regression analysis. An equation containing the main factors and second-order interaction terms was satisfactory to capture the important trends in the data (Table 4.6) and had an  $R^2$  value of 88%, indicating a reasonably good fit with the experimental data (Figure 4.6). This regression analysis revealed that time had a strong positive impact on ester yield ( $p < 0.05$ ) while increasing reaction water content was predicted to reduce yields. Higher ethanol loadings were also predicted to increase yields, though the effect was not as strong as the impact of reaction time. In the case of reaction pressure, the average ester yield for all runs at the high level (20 MPa) was slightly lower than the average yield for all runs at the low level (10 MPa) (cf. 44% vs. 48%), indicating a slight reduction in yield with rising pressure.

Table 4.6. Second order regression model for supercritical in situ transesterification of hydrochar B.

Terms	Coeff.	p-value
Constant	20.92	0.00
Time	0.301	0.00
EtOH:FA	0.570	0.45
H <sub>2</sub> O	-1.086	0.42
P	0.249	0.42
Time*EtOH:FA	0.005	0.57
Time* H <sub>2</sub> O	0.021	0.55
Time*P	0.001	0.91
EtOH:FA*H <sub>2</sub> O	-0.151	0.59
EtOH:FA*P	-0.065	0.41
Water*P	-0.015	0.96

Note. Coefficients given for uncoded units: time (min), EtOH:FA (mol/mol), H<sub>2</sub>O (wt.%), and pressure (MPa).  $R^2 = 87.7$ .

Notably, the highest yield observed (69%) occurred at the longest time investigated in a reaction with the lowest amount of ethanol, no water, and low pressure (run 13). Similar yields were also achieved in run 16, which contained the same amount of ethanol but also included water and was carried out at twice the pressure, as well as run 17, which was identical to run 13 except it contained more ethanol. Although yields increased significantly with time, degradation of unsaturated FAs was slightly more pronounced at

longer reaction times. Overall computed yield losses were 1.8, 2.2, and 3.4% on average for reactions lasting 30, 75, and 120 min, respectively.

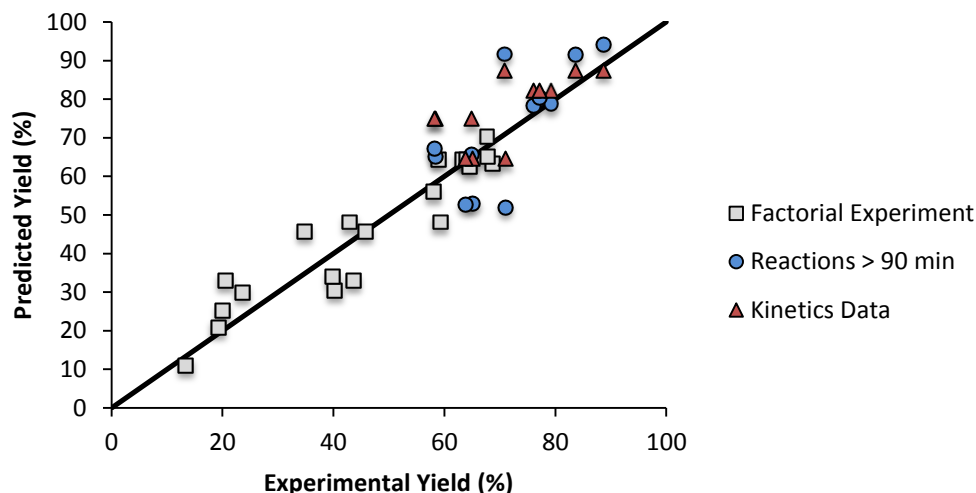


Figure 4.6. Parity plot comparing experimental data with regression model. Includes data from the factorial experiment (20 runs, Table 4.5), reactions performed for 90-180 min (Figure 4.7), and the data collected for kinetics analysis (Figure 4.5).

These data support the concept that it is possible to increase yields with time when performing reactions at a temperature that minimizes ester losses. Furthermore, it corroborates previous reports that have documented an increase in ester yield with higher alcohol loadings between 10:1 and 40:1 MeOH:oil molar ratio. For example, yields from supercritical transesterification of soy bean oil (300 °C, 25 min residence time) were about 39, 64, 71, and 76% at 5, 10, 17, 23, and 30 MeOH:oil molar ratio (He et al., 2007a). In this factorial experiment, EtOH:FA ratios varied from 4.5:1 to 18:1, equivalent to EtOH:oil ratios of 13.5:1 to 54:1. Higher ethanol loadings are expected to shift the equilibrium towards products, thereby increasing yields, but can also dilute the reaction mixture and decrease initial reaction rates. Likewise, although there are mixed reports about the effects of pressure on yield, with some concluding that higher pressures increase yields (He, Sun, et al., 2007), at least one group found very little influence of pressures between 7 and 20 MPa at 350 °C with ethanol and soybean oil (Silva et al.,

2007). These authors suggested that reaction rates increase at lower pressures due to favorable transport properties of the fluid, such as greater diffusivity and lower viscosity. In addition, in reactions at 250 °C with ethanol and oleic acid, lower pressures led to higher esterification yields for times shorter than 40 min (Pinnarat and Savage, 2010). Fortunately, our data suggest that high yields can be achieved at low ethanol loadings and pressures, both of which are cost factors we seek to limit.

#### 4.3.6 The effect of ethanol loading at long reaction times (> 90 min)

Longer reactions were attempted with a partially dried hydrochar because time was determined to be a major driver of ester yields. As shown in Figure 4.7, reactions with hydrochar C containing ethanol at a 5:1, 10:1, or 20:1 EtOH:FA molar ratio that lasted 90-180 min achieved yields between 58 and 89%. Although the highest yields were observed at the longest reaction time, there was not a clear trend of increasing yield with time as previously observed between 30 and 60 min (Figure 4.4). The most likely reason for this is experimental variability; the data shown represent single reactions and as explained earlier, hydrochars are somewhat heterogeneous in nature. Nevertheless, it is noteworthy that relatively high yields (79%) were accomplished with 5:1 EtOH:FA molar ratio at 150 min, a 22% improvement over the yield observed at 90 min. In addition, with the exception of the reactions carried out for 180 min, ethanol loading had a very minor impact on total ester yield. This result mirrors what was found in the factorial experiments (cf. run 13 and 17) and suggests that high yields can be accomplished with only a small excess of ethanol. These data, however, suggest that at long reaction times where equilibrium is approached, yields may be improved somewhat at higher ethanol loadings. Another explanation may be that high ethanol volumes inhibit polymerization and thermal degradation, perhaps by diluting reactants or through free radical stabilization. As can be seen in Figure 4.6, the second order regression model generated from the factorial experiment can be used to predict total ester yields from these reactions, even though some of the reactions lasted longer than the reactions used to produce the model.

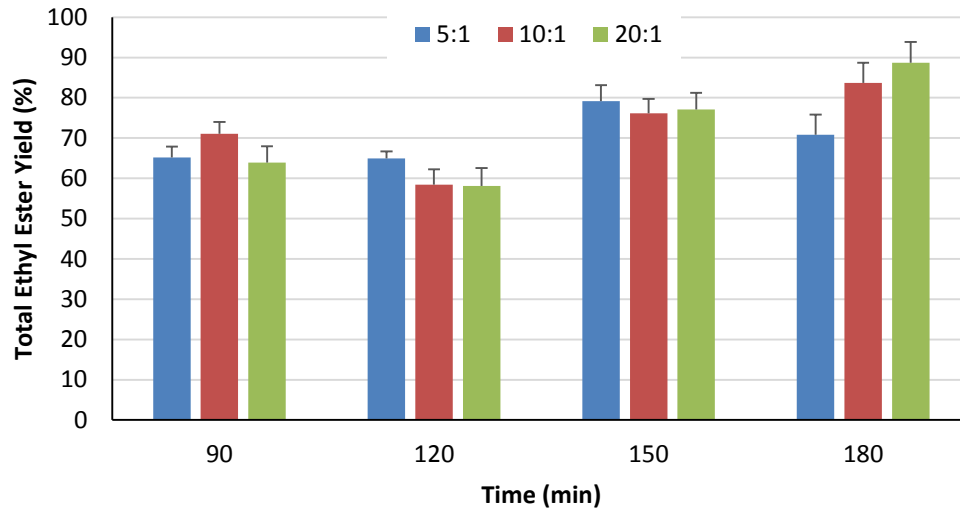


Figure 4.7. Supercritical in situ transesterification of partially dried hydrochar at 275 °C. Hydrochar C was oven dried to 7% moisture and reacted 90–180 min with 5–20 EtOH:FA acid molar ratios. The positive error bars show the yield of ethyl palmitate, which when considered independently was higher than the total yield as a result of decomposition of unsaturated fatty acids. The GC-FID chromatogram for the reaction at 180 min and 20:1 EtOH:FA molar ratio is given in Figure 4.1.

The positive error bars on Figure 4.7 do not represent experimental uncertainty; rather, they indicate the yield of ethyl palmitate (C16:0) obtained in each experiment. The yield of the saturated ester always exceeded the total ester yield, suggesting that a small amount of unsaturated FA decomposition occurred that reduced total ester yields. The difference between the ethyl palmitate yield and the total ester yield, which was from 3 to 5% and increased with reaction time, confirms that these reaction conditions are suitable to avoid substantial losses. However, considering that ethyl palmitate yields as high as 94% were observed (180 min, 20:1 EtOH:FA) and some losses can be expected during product workup due the small reactor sizes and adsorbent nature of the hydrochars, it is likely that near theoretical maximum yields can be achieved if the decomposition of unsaturated FAs is reduced or prevented. One possible method to accomplish this may be gradual heating of the reaction from ~100 to 320 °C, which has



been shown to achieve 96% overall yields in soybean oil transesterification (He et al., 2007a).

#### 4.3.7 Reaction kinetics and modeling

The kinetics of transesterification has been well studied in both the subcritical and supercritical regimes for systems containing pure oils or fatty acids (He, Sun, et al., 2007; Silva et al., 2007; Changi et al., 2011); however, less work has explored the kinetics of in situ transesterification, and, to our knowledge, no attempt has been made to describe quantitatively the rates of SC-IST. First, we compared the results obtained from the supercritical esterification of oleic acid (Figure 4.3) with predictions from the autocatalytic model of Changi et al. (2011). We found our ester yields for reactions containing no water to be within 5%, on average, of the value calculated by their model, whereas in reactions containing large amounts of water, the model overpredicted yields by 60-130%. Likewise, yields were overpredicted by the model for the 20 runs of the factorial experiment with hydrochar. This comparison corroborates the model posited by Changi et al. (2011) when little or no water is present during pure FA esterification, but highlights the inadequacy of the model when water content is as high as 20-30 wt.% or mixtures of lipids are processed within biomass solids. This outcome could be expected because such high water contents were not used in the experiments done to develop the model and because lipid mixtures, which contain both FAs and other glycerides, are likely to react slower than pure fatty acid feedstocks.

To better understand the kinetics of supercritical in situ transesterification, the data presented in Figure 4.5 was analyzed to determine the relevant kinetics parameters. A simple model was created based on the concentration of lipid initially within the hydrochar and the amount that remained unreacted following the reaction. The final concentration of unreacted lipid was determined by difference based on the measured conversion to FAEE. In all cases, ethanol was assumed to be in excess. We assumed pseudo-first order kinetics, in agreement with previous work (He et al., 2007b), and used

least squares linear regression to determine the reaction rate constant ( $k$ ) at each temperature based on the following formula:

$$\ln(C_{Lipid,0}) - \ln(C_{Lipid,t}) = kt$$

The rate constants at 275, 285, and 295 °C were 0.012, 0.014, and 0.016 min<sup>-1</sup>, respectively, and the energy of activation ( $E_a$ ) was determined to be 44 kJ/mol. These values are in line with previous reports on the kinetics of supercritical transesterification. For instance, Pinnarat and Savage (2010) reported the  $E_a$  for supercritical oleic acid esterification with EtOH to be 56 kJ/mol while He et al. (2007) reported the identical  $E_a$  value for soybean oil transesterification with methanol. Notably, however, monounsaturated FAs in soybean oil were found to react most quickly, with the  $E_a$  value for methyl oleate being the lowest observed at 39 kJ/mol. Meanwhile, the reaction rate constants and the corresponding  $E_a$  values for the transesterification of soybean oil were determined to be 0.006 min<sup>-1</sup> and 92.9 kJ/mol or 0.0127 min<sup>-1</sup> and 78.7 kJ/mol at 270 °C (20 MPa) for reactions containing 20:1 or 40:1 EtOH:oil molar ratios, respectively (Silva et al., 2007). Considering the various factors that can influence reaction rates and  $E_a$  values, including alcohol type and quantity, the feedstock's FA profile and lipid composition, and reaction pressure, we believe our estimate of  $E_a$  is a reasonable approximation, especially considering the very high oleic acid content in the hydrochar lipids.

#### 4.3.8 Comparison to catalyzed in situ transesterification and alcohol selection

The ability to achieve high ester yields in the presence of low alcohol loadings is a major advantage of the SC-IST process. To demonstrate this advantage, acid-catalyzed in situ transesterification of hydrochar was carried out at a subcritical temperature of 60 °C with a 3:1 or 6:1 EtOH:FA molar ratio and 5% H<sub>2</sub>SO<sub>4</sub> and compared to a 120 min noncatalytic reaction under supercritical conditions with either ethanol or methanol. Both supercritical alcohol reactions resulted in ester yields of ~60% whereas the subcritical reactions demonstrated ester yields between 5 and 10% (Figure 4.8). These data

demonstrate that for identical times and ethanol loadings, the uncatalyzed supercritical reaction can achieve significantly higher conversions than the acid-catalyzed reaction. To achieve yields greater than 70% with subcritical ethanol and 5% H<sub>2</sub>SO<sub>4</sub>, temperatures between 80–100 °C and 50–100 EtOH:FA molar ratios are required for reactions lasting 30–120 min (Section 5.3).

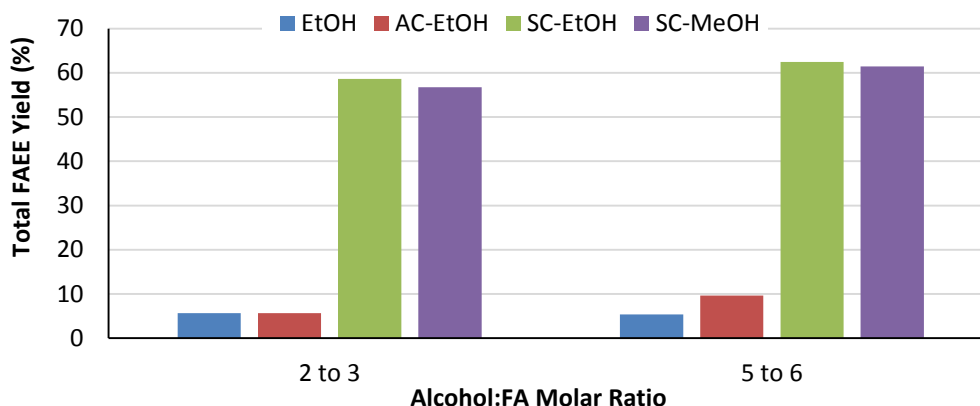


Figure 4.8. Comparing in situ transesterification under sub-critical and supercritical conditions with methanol and ethanol. The sub-critical reactions were carried out at 60 °C for 120 min with or without 5% H<sub>2</sub>SO<sub>4</sub> and stirred vigorously. The supercritical reactions were carried out without catalyst at 275 °C for 120 min. Hydrochar C was used in all experiments. The EtOH:FA molar ratio varied slightly for each type of reaction, but all reactions fell within a range of 2 to 3 or 5 to 6.

Besides the faster kinetics that occur at elevated temperatures, the supercritical method benefits from a significant reduction in the density of ethanol and the formation of a single, nearly homogenous fluid phase during the reaction, thereby enhancing mass transfer and the reaction of lipids with the hydrochar. In contrast, hydrochar solids in subcritical reactions with these amounts of ethanol are not even fully submerged in the alcohol. It is also apparent that using ethanol resulted in slightly higher yields than when using methanol, although reaction conditions varied slightly when using each alcohol so a broad conclusion is not justified. Similar results have been observed in the supercritical transesterification of pure oils (Madras et al., 2004; Varma et al., 2010), most likely because ethanol has superior dissolving power for oils compared to methanol. Although

methanol is usually less expensive, we chose to work principally with ethanol because it is less toxic, renewably derived, and produces biodiesel with improved fuel properties (Stamenković et al., 2011). Nevertheless, these data suggest that if the alcohol cost is a major consideration, high yields can also be achieved with methanol.

#### 4.3.9 Process engineering

A proposed process flow diagram for how SC-IST may work at an industrial facility is shown in Figure 4.9. The significant reduction in alcohol use made possible through the higher temperatures and pressures used during SC-IST should provide a major reduction in the cost and energy required to recycle alcohol. Traditional biodiesel production relies on distillation to recycle excess alcohol (Marchetti et al., 2008) whereas the supercritical process will likely be able to utilize adiabatic flash drums to separate azeotropic ethanol from the reaction mixture. In Figure 4.9, this is shown as a single flash drum that achieves perfect separation; in reality a single stage flash operation will not achieve such definitive separation, potentially requiring additional unit operations. The liquid effluent of the flash drum, containing FAEE, unreacted glycerides and FA, as well as water and the lipid-extracted char (LEC), would then be separated into organic and aqueous fractions. The organic phase would be processed to remove the unreacted glycerides and any remaining impurities to produce engine-ready biodiesel. The unreacted lipids would be returned to the SC-IST reactor for conversion to FAEE. The aqueous phase would be reacted by catalytic hydrothermal gasification to produce biogas, a mixture typically comprised of 60% CH<sub>4</sub> and 40% CO<sub>2</sub>. In this way, any carbonaceous material in the hydrochar that is not converted to biodiesel is processed to generate on-site energy. A more in-depth discussion of CHG is described in Section 7.1.

Although a complete techno-economic analysis is beyond the scope of the present work, previous assessments of supercritical transesterification have suggested that this technology can outperform traditional catalyzed processes and produce biodiesel from vegetable oils that is cost competitive with petroleum diesel (Van Kasteren and Nisworo,

2007; Deshpande et al., 2010). It seems unlikely that modifying the processes detailed in these works to perform SC-IST of algal hydrochars instead of supercritical transesterification of hexane-extracted soybean oil would dramatically affect the production costs. For example, dried hydrochar could be mixed with alcohol and pumped as a slurry into the SC-IST reactor, just as soybean oil is. In addition, D'Ippolito et al. (2007) validated the concept of using a flash drum to remove methanol if the alcohol:FA ratio is low enough (e.g., < 20 MeOH:TG) (D'Ippolito et al., 2007). Finally, the use of CHG to convert the lipid-extracted hydrochar into biogas is similar to how Deshpande et al. (2010) proposed that a fraction of the biodiesel could be combusted to provide process power.

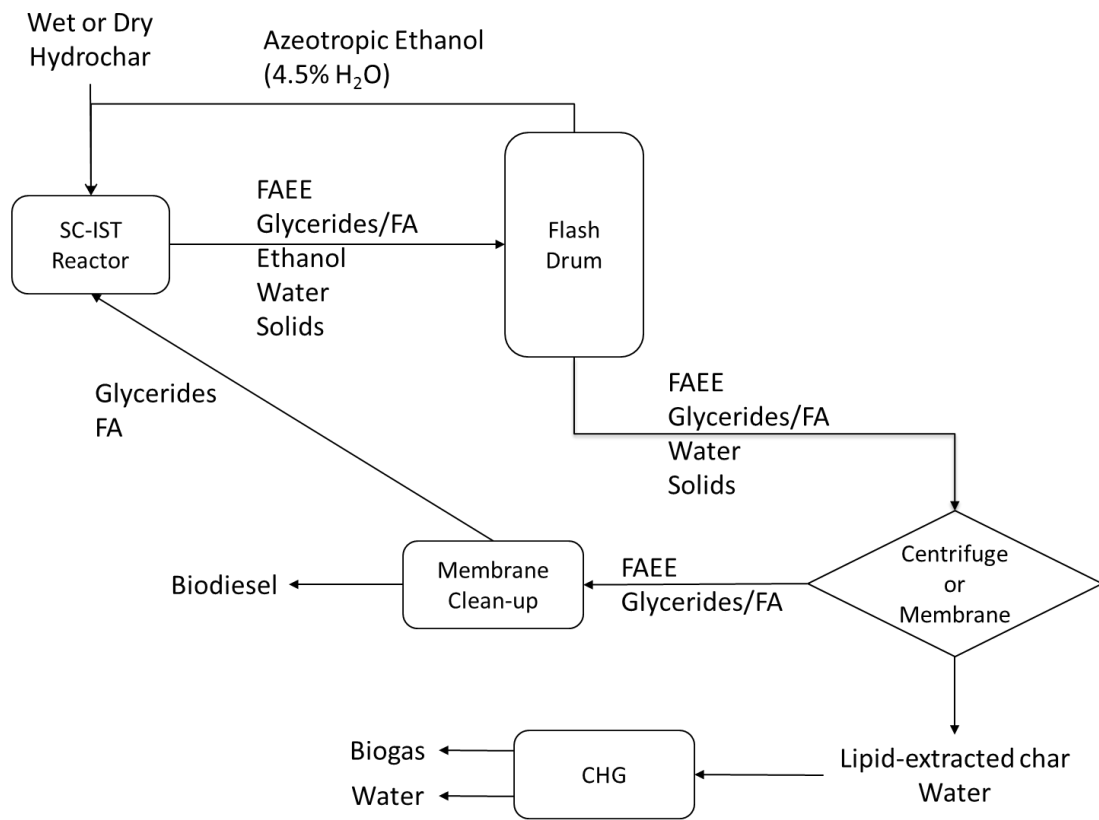


Figure 4.9. Proposed process flow diagram for supercritical in situ transesterification.

Complete dehydration of ethanol is not possible in a single distillation column because ethanol forms an azeotrope with water (95.6 wt.% or 97.2 vol.% at 78.15 °C). Typically, 92.4wt.% ethanol is obtained through ordinary distillation, with additional (more costly)

measures taken to obtain anhydrous ethanol (azeotropic distillation, extractive distillation, liquid–liquid extraction, adsorption, or some complex hybrid separation methods) (Huang et al., 2008). In an effort to reduce costs and energy requirements, we have assumed ethanol containing 7.6% water will be recycled in the SC-IST process.

Other ethanol recovery strategies besides distillation or flash evaporation should also be considered. Liquid-liquid extraction to recover ethanol has been investigated; it is possible that fatty acids could be used to recover ethanol, while contributing to the FAEE yield as well (Boudreau and Hill, 2006). It is also possible that biodiesel could serve as a liquid-liquid extractant for ethanol (Adhami et al., 2009), with the possibility that some loss in ethanol could go towards ethanol-biodiesel-diesel fuel blends (Lapuerta et al., 2009) in a similar way that gasoline is used to extract ethanol and produce gasohol (Huang et al., 2008).

During SC-IST, under conditions that led to high ester yields, hydrochars typically lost 5-10 wt.% more mass than corresponded solely to the weight of FAEE recovered. This could be because a small amount of other components like proteins and carbohydrates dissolved in the alcohol as well, or because the hydrochar was only partially dry to start with and moisture was lost, as observed by Haas et al. (2004) in subcritical reactions with flaked soybeans (Haas et al., 2004). This finding is also supported by ethanol liquefaction work, in which the crude bio-oil has been found to contain 6-9 wt.% N comprised of protein decomposition products (e.g., amino acids), Maillard reaction products, and other heterocyclic compounds and esters (Zhou et al., 2012). We also found that the lipid extracted hydrochar typically contained less than 5% lipids when overall conversion was greater than 80%, suggesting that nearly all lipids were extracted from the solids yet some remained unreacted in the liquid phase. Because any remaining lipids in the LEC will be reacted by CHG, maximizing the yield of biodiesel comes at the expense of electrical and heat production on-site. As discussed in Section 8.3, many factors can influence the

energy balance of the process and change the percentage of total energy output that is in a liquid form.

Besides CHG, other options for use of the lipid-extracted char are as a soil amendment or environmentally preferable alternative to coal that can be burned to produce power. A third-party analysis of the heavy metal content of a representative lipid extracted hydrochar did not detect mercury (<0.05 mg/kg), lead (<0.30 mg/kg), or cadmium (<0.20 mg/kg), and only very low levels of arsenic (0.37 mg/kg) and chromium (4.5 mg/kg). These data, together with a predicted heating value of about 17 MJ/kg for a LEC derived from a biomass originally containing 25% oil, suggest lipid-extracted char may be a suitable material for on-site power generation at algal biorefineries.

In the two-step process we are investigating, overall biodiesel production efficiency is predicated on lipid retention in the hydrochar during HTC as well as the lipid conversion to biodiesel during SC-IST. Depending on HTC reaction conditions, lipid retention can vary widely. In the present work, the lipid retention observed was about 86% for hydrochar A, 98% for hydrochar B, and about 65-70% for hydrochars C and D. These data highlight the importance of selecting moderate HTC conditions that result in high lipid retention.

Haas et al. 2003 suggested that current biodiesel production processes using soy achieve about 92% overall efficiency due to losses during hexane extraction, refining, bleaching, and deodorizing as well as incomplete transesterification (Haas et al., 2004). The most recent GREET analysis for algal biofuel production assumes homogenization and wet hexane extraction have a combined efficiency of 85.5% whereas transesterification of the extracted oil is 99% efficient (ANL et al., 2012). For the sake of comparison, if we use the lipid retention achieved with hydrochar B (98%) and assume SC-IST achieves 95% of the theoretical maximum conversion possible, overall efficiency for the process may approach 93%. The potential to achieve this overall efficiency without prior extraction of lipids from the hydrochar in a process that is tolerant of 5-10 wt.% moisture, which would

permit the use of rectified ethanol and partially dried hydrochars, may offer opportunities to reduce the cost and environmental impact of algae biodiesel production.

#### 4.4 Conclusions

This work investigated the effect of process conditions on biodiesel yield from the supercritical in situ transesterification of algal hydrochars. By performing reactions at temperatures that limited the thermal degradation of unsaturated FAs, we achieved overall FAEE yields from partially dried hydrochars as high as 79% with 5:1 EtOH:FA molar ratio (150 min, 275 °C) and 89% with 20:1 EtOH:FA molar ratio (180 min, 275 °C). Reactions containing wet hydrochars (45-50% moisture) achieved lower ester yields (40–60%), but our data suggest that with appropriate water management throughout the SC-IST process, complete drying of algal hydrochars can be avoided. Overall, yields were limited by incomplete transesterification, decomposition and polymerization of unsaturated FA, hydrolysis of FAEE, or incomplete lipid extraction from the solid. To further improve yields, future work should focus on eliminating the thermal loss of unsaturated FAs in addition to recovering and reacting lipids that were extracted from the hydrochars but not transesterified.



## CHAPTER 5

### ACID-CATALYZED IN SITU TRANSESTERIFICATION

#### 5.1 Background

Acid-catalyzed in situ transesterification (AC-IST) has been the most commonly studied form of IST with algal biomass because this feedstock typically contains a higher percentage of fatty acids than traditional oilseeds. To date, high conversions have only been observed at high alcohol loadings (>100-200:1 MeOH:FA) and with dry algal biomass (Johnson and Wen, 2009; Ehimen et al., 2010; Haas and Wagner, 2011a; Wahlen et al., 2011). For example, Ehimen et al. (2010) found that when *Chlorella* containing 0.7 wt.% moisture (dry weight basis; equivalent to ~0.16 wt.% water in the total reaction mixture) was reacted at 60 °C for 6 h with ~105 MeOH:FA molar ratio and 100 wt.% H<sub>2</sub>SO<sub>4</sub> (oil basis), equilibrium conversion to FAME was reduced by ~20%, compared to reactions with dry biomass. When biomass moisture content exceeded 31.7% (dry basis) or water constituted more than ~9.5 wt.% of the reaction mixture, transesterification was totally inhibited. These data suggest that acid-catalyzed IST (AC-IST) may only be successful on carbonized solids containing very little water (<5%), especially if lower amounts of alcohol are used. It may be energetically favorable to dry the carbonized solids, especially if they exit the reactor hot and are allowed to undergo evaporative cooling.

The recent work on IST of dry algal biomass parallels earlier efforts to perform IST on traditional oilseeds. For example, flaked soybeans containing 7.4 wt.% moisture were reacted at 23 °C for 8 hours with alkaline methanol (~180:1 methanol:fatty acid (MeOH:FA) molar ratio) to achieve 93% conversion of lipids to biodiesel (Haas et al., 2004). Subsequent work demonstrated that by reducing the moisture content (Haas and Scott, 2006) and physically pre-treating the biomass (Haas and Wagner, 2011b), high yields could be obtained in shorter times (~1.5-5 hours) and with less methanol (~9-25:1 MeOH:FA). Although improved, methanol use was still much higher than commercial transesterification of oils, which is typically carried out at a 2:1 MeOH:FA molar ratio.

Excess alcohol is required in most cases to submerge the biomass (e.g., 7.5 mL MeOH was required to cover 5 g of flaked soybeans, equivalent to ~45:1 MeOH:FA molar ratio), with a secondary effect being the dilution of any water present to below inhibitory concentrations (Haas et al., 2004).

We seek to convert the lipids within algal hydrochars directly to usable biodiesel in a single step. To better understand how hydrochars react in subcritical ethanol in the presence of a homogeneous acid catalyst, factorial experiments were carried out at different temperatures, reaction times, alcohol loadings, and catalyst concentrations. Our experiments were designed to identify conditions that result in high biodiesel yields while using the least amount of alcohol. Moreover, in an effort to promote near-term adoption of algal biodiesel, we demonstrated how the process could be carried out with feedstocks containing both high value omega-3 fatty acids and lower value fatty acids for fuels. Furthermore, regression analysis was used to create a predictive model for biodiesel yield based on reaction temperature, time, and ethanol loading. To our knowledge, this is the first work to explore the in situ transesterification of algal hydrochars at subcritical conditions.

## 5.2 Materials and Methods

### 5.2.1 Hydrothermal carbonization

*Chlorella* and *Nannochloropsis* hydrochars were produced by reactions at 200-215 °C and then oven dried (65 °C for 24 h) prior to use. A complete description of the HTC conditions used and the hydrochar lipid content can be found in Table 5.1. Each hydrochar is designated with a letter in the second row of Table 5.1 that is referenced throughout this chapter.

### 5.2.2 Acid-catalyzed in situ transesterification

Hydrochars were weighed into glass tubes (16 mm x 100 mm) with teflon-lined screw caps and reacted with varying amounts of ethanol containing 1–8% H<sub>2</sub>SO<sub>4</sub> or 5% acetyl chloride at 80–100 °C for 30–120 min with vigorous stirring. Water (1 mL) was added to stop the reaction and FAEEs were extracted into 2–4 mL total *n*-heptane containing 100–200 mg/L C23:0 FAME as an internal standard. About 2 mL of the heptane mixture was transferred to a vial for GC-FID analysis. Reaction ester yields were calculated by dividing the mass of FAEE recovered in the product by the theoretical maximum mass of ester that could form from the hydrochars, as determined by the typical AC-IST analysis described in Section 2.2.6.

### 5.2.3 Statistical analysis

Minitab (v. 16.1.0) was used to design and analyze experiments. AC-IST was investigated as a function of four factors using a factorial design. Significance of regression coefficients was determined with a *p*-value of < 0.05. Results from additional experiments in which only one factor was varied at a time were compiled and analyzed using Microsoft Excel.

## 5.3 Results and Discussion

### 5.3.1 Feedstock production and hydrothermal carbonization

Algal biomass for carbonization was produced in a fermenter and outdoor ponds for *C. protothecoides* and *Nannochloropsis*, respectively. Biomass was obtained by centrifugation of the culture broth and reacted as a 15-20% solids paste. Both *C. protothecoides* and *Nannochloropsis* were successfully carbonized to produce a hydrochar that retained most of the lipids in the original biomass. For example, reactions at 215 °C for 30 min resulted in lipid retention of > 95% for *C. protothecoides* and reactions at 200 °C for 15 min resulted in lipid retentions near 100% for *Nannochloropsis* (Figure 3.16, pg. 66). Because AC-IST requires dry biomass, it is interesting to note that the process of HTC significantly reduces the amount of energy required to dehydrate wet algal

biomass. For example, in a 20% solids algae slurry, 4 kg of water must be evaporated for every kg of dry biomass obtained. If this same slurry is reacted by HTC, half of the solids dissolve in the aqueous phase and the remaining hydrochar contains only ~40% moisture. As a result, only 0.33 kg of water must be evaporated to obtain a dry hydrochar containing nearly all of the lipids of the original biomass. This represents about a 12-fold reduction in drying costs for the relatively low energy inputs associated with HTC.

Table 5.1. Characterization of algal hydrochars used in AC-IST

Parameter	Hydrochar		
	A	B	C
Parent Material Species	<i>C. protothecoides</i>	<i>C. protothecoides</i>	<i>Nannochloropsis oculata</i> (Reed)
Carbonization Temp. (°C)	200	215	200
Carbonization Time (min)	30	30	15
Total FAEs (wt.%)	45.0	76.0	11.5
Fatty acid (% of FAEs) <sup>a</sup>			
C14:0	1.1	1.3	5.5
C16:0	16	13	30
C16:1	0	0	33
C18:0	3.3	3.3	0.8
C18:1	54	65	6.7
C18:2	19	16	4.8
C18:3	6.9	2.4	1.6
C20:4	0.0	0.0	1.9
C20:5	0.0	0.0	16

Note. Hydrochar B in this table is the same material as hydrochar B in Table 4.1.

As shown in Table 5.1, the lipid content of each hydrochar varies widely (11.5-76%) depending on the feedstock species and growth conditions. For example, hydrochar A and B are both derived from *C. protothecoides* biomass, but the parent material for each hydrochar differed, based on when it was harvested during fermentation. The fatty acid profile of these hydrochars, which showed a high content of C18:1 fatty acids and relatively low levels of polyunsaturated fatty acids, suggests that they will yield high quality biodiesel (Knothe, 2005). The *Nannochloropsis* hydrochar, which contained about 11% total lipids when measured as FAE, is notable for its high content of eicosapentaenoic acid (EPA, C20:5). Typically, hydrochars produced from the *Nannochloropsis* supplied by Reed Mariculture contained closer to 20% total lipids with

30% EPA; however, this hydrochar had a lower lipid and reduced percentage of EPA because it was stored at room temperature for several weeks prior to use in AC-IST experiments. We frequently observed a decline in EPA content in stored hydrochars, most likely because HTC destroys natural antioxidants present in the algae cell that inhibit oxidation of this polyunsaturated FA. This observation suggests that *Nannochloropsis* hydrochars should be reacted immediately after HTC in order to preserve their EPA content. Nevertheless, this hydrochar still served as a useful feedstock for AC-IST experiments. In general, the lipid profile of this hydrochar suggests that following AC-IST, the esters could be fractionated based on chain length to obtain a higher value product (omega-3 fatty acid ethyl esters) and lower value biodiesel. The suitability of this process to *Nannochloropsis* will be further discussed in section 5.3.6.

### 5.3.2 Acid catalyzed in situ transesterification

By reacting hydrochars with ethanol in the presence of sulfuric acid, we seek to convert lipids from all classes within algal hydrochars into biodiesel. Based on previous attempts to perform AC-IST on dry algal biomass and other oilseeds, we chose reaction conditions suspected to produce high yields while using as little ethanol as possible. Although some studies have used methanol at temperatures below its boiling point (65 °C), ostensibly to reduce the cost of pressurizable reactors, higher temperatures lead to faster reaction rates and reduce the batch holding times required to reach high conversions (Ehimen et al., 2010; Haas and Wagner, 2011a; Wahlen et al., 2011). Considering that ethanol's boiling point is 78.4 °C and we routinely run AC-IST using methanol at 100 °C for analytical purposes, we chose to explore the reaction space at 80, 90, and 100 °C. The corresponding vapor pressures for ethanol are approximately 108, 158, and 225 kPa respectively, which are well within the limits for common industrial reactors. With regards to ethanol loading, preliminary experiments at 100 °C showed that FAEE yield was highly dependent on this variable. Previous work has shown optimal FAME yields from various dry algal biomass at MeOH:FA molar ratios of about 520:1 (Wahlen et al., 2011), 300:1 (Haas and Wagner, 2011a), and 105:1 (Ehimen et al., 2010). We chose to begin our

investigation of AC-IST near the lowest previously reported value by using an EtOH:hydrochar (w/w) ratio of about 7.5, which is equivalent to a 110:1 EtOH:FA molar ratio for hydrochar A. Recall that hydrochar lipid content varied, so reactions containing different hydrochars with an equivalent EtOH:hydrochar (w/w) loading will have different EtOH:FA molar ratios. For this reason, maximizing hydrochar lipid content without increasing the EtOH:hydrochar (w/w) loading will help reduce ethanol use on a biodiesel-produced basis. Finally, we chose to work with sulfuric acid because it is a low cost mineral acid and widely used industrially.

### 5.3.3 Effect of reaction time and temperature

Hydrochar A, which contained about 45% total lipids, was selected for initial experiments to study the effect of reaction time (15–120 min) and temperature (80, 90, or 100 °C). All reactions contained ethanol with 5% H<sub>2</sub>SO<sub>4</sub> and a EtOH:FA molar ratio of 110:1. As shown in Figure 5.1, higher temperatures led to increased reaction rates, and yields at 15 and 30 min were highest at 100 °C; however, at reaction times longer than 30 min, yields at 100 °C began to decline. In previous work with transesterification using supercritical ethanol, a similar reduction in yield was observed at high temperatures ( $\geq 275$  °C), most likely due to thermal degradation of unsaturated fatty acids or polymerization of esters into higher molecular weight compounds that were not detected (Levine et al., 2010; Quesada-Medina and Olivares-Carrillo, 2011; Vieitez et al., 2008b; Vieitez et al., 2010).

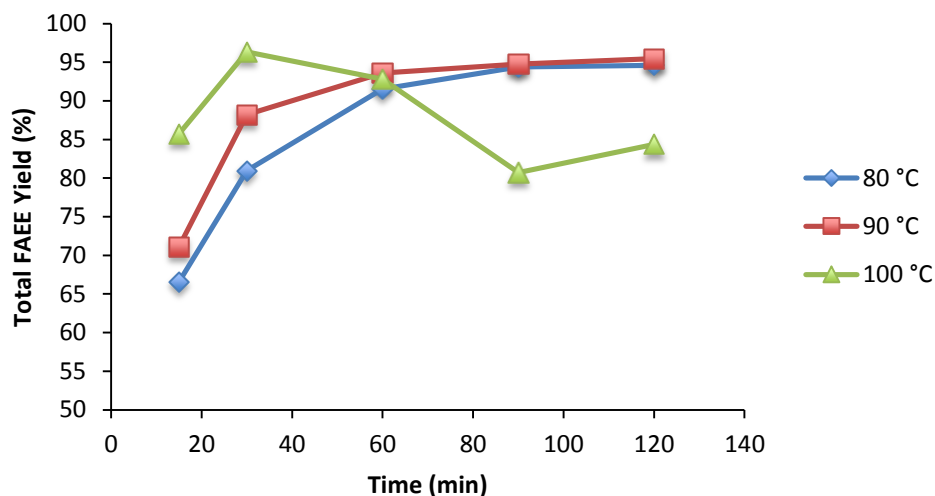


Figure 5.1. Total fatty acid ethyl ester yield from hydrochars reacted at 80, 90, and 100 °C for 15 to 120 min. All reactions contained dry hydrochar A (45% FFAE content) and ethanol containing 5% H<sub>2</sub>SO<sub>4</sub> at a 110:1 EtOH:FA molar ratio (equivalent to 7.5:1 EtOH:solids ratio). Reactions at four select conditions were replicated and the average standard error was 0.6%.

In contrast, yields at 80 and 90 °C continued to increase with time, reaching a plateau around 95% of the theoretical maximum ester content of the hydrochar after 90 min. These data suggest that at this ethanol loading and acid concentration, similar hydrochar FFAE yields can be obtained at 100 °C for 30 min, 90 °C for 60 min, or 80 °C for 90 min. The choice of reaction temperature and time then becomes one of process economics, where reactor capital costs must be weighed against differences in operating expenses at each temperature. Nevertheless, the high yields obtained under these conditions, using significantly less ethanol than in most previously reported works on AC-IST of algal biomass, suggest the relative ease with which lipids within hydrochars can be transesterified. Although no dried *Chlorella* biomass was reacted under identical conditions for comparison, it is likely that the reduction in non-lipid solids and the variety of hydrolysis reactions that occur during HTC permit greater diffusion of alcohol and lipid within the solid matrix. It has not been definitively proven whether lipids first diffuse out of the solid and are then transesterified in the liquid phase or if they react within the solid and diffuse out as FFAE (Haas and Wagner, 2011a), In either case, however, we suspect

the structure of the hydrochar is likely to facilitate improved mass transfer relative to the unreacted biomass. This is analogous to several reports that have detailed how cell wall disruption of microalgae can improve solvent extraction of lipids, including microwaving and thermal pre-treatments (Kita et al., 2010; Lee et al., 2010). In addition, AC-IST of hydrochars may benefit from some self-catalysis given their acidic nature, which is evidenced by the acidic aqueous phase (pH 5-6) in which they are generated.

#### 5.3.4 Effect of acid concentration

To better understand the effect of acid catalyst concentration on FAEE yield, Hydrochar A was reacted with ethanol containing 1, 2, 4, 5, and 8%  $\text{H}_2\text{SO}_4$  (v/v) at a 110:1 EtOH:FA molar ratio for 90 min at 80 or 90 °C. Given the amount of hydrochar in each reaction, this corresponds to 0.4, 0.8, 1.6, 2, and 3.25  $\text{H}_2\text{SO}_4$ :FA (w/w) and 1.25, 2.5, 5, 6.3, and 10  $\text{H}_2\text{SO}_4$ :FA (mol/mol). As shown in Figure 5.2, yields at both temperatures increased with acid concentration from 1 to 2%, but reactions at 90 °C plateaued at 90% yields and then declined with acid concentrations of 5% and above. In contrast, yields from reactions carried out at 80 °C continued to increase until acid concentration reached 4%, but then fell as acid concentration was further increased. Interestingly, yields from reactions carried out at 90 °C with 1% and 2% acid were higher than the yields obtained at 80 °C, though this trend reversed itself at acid concentrations of 4% and higher.



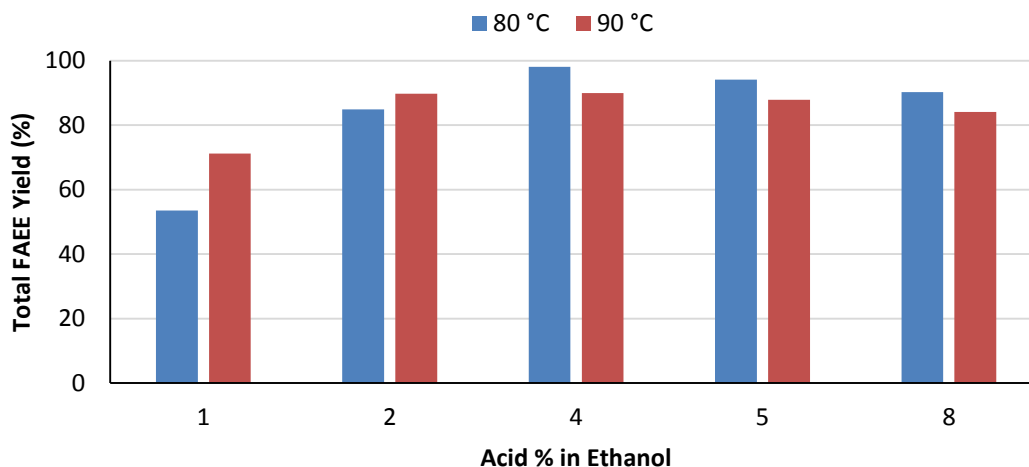


Figure 5.2. Total fatty acid ethyl ester yield from hydrochars reacted at 80 or 90 °C for 90 min. All reactions contained dry hydrochar A (45% FFAEE content) and ethanol at about 110:1 EtOH:FA molar ratio (equivalent to 7.5:1 EtOH:solids ratio). Reactions at six select conditions were replicated and the average standard error was 1.3%.

These data are similar to those in Figure 5.1, where yields increased with reaction temperature for short batch reaction times but then decreased as reaction time was extended. In this case, acid seems to play a role similar to temperature in that it accelerates both the in situ transesterification reaction as well as whatever reaction is consuming esters and resulting in diminished yields. Although these data suggest that higher acid concentrations could be used in place of increasing the reaction temperature, 1% and 2% acid at both 80 and 90 °C did not result in yields above 90%. Lower yields at these acid concentrations may be due to the catalytic effect of  $H_2SO_4$  on the transesterification of lipids, which begins with the protonation of the carbonyl group in the triglyceride molecule or fatty acid, forming a carbocation intermediate (Figure 5.3). In the case of triglyceride transesterification, the alcohol present then initiates a nucleophilic attack on the carbocation center, resulting in a tetrahedral intermediate that splits into the desired ester product and a diglyceride. The acid catalyst ( $H^+$ ) is regenerated, and the reaction occurs twice more to completely convert a triglyceride into three fatty acid alkyl esters. Although reactions with 1 and 2% acid contained more than a 1:1 acid:FA molar ratio, higher acid concentrations may have still improved reaction rates and led to higher yields. Another plausible explanation is that the acid plays a critical

role in hydrolyzing non-lipid components of the hydrochar, such as cell wall components, and thereby promotes enhanced lipid or alcohol diffusivity through the solid.

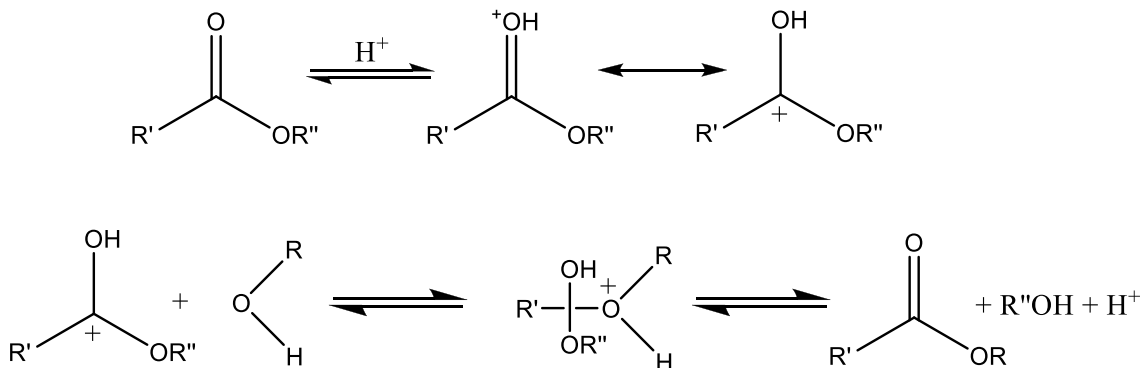


Figure 5.3. Mechanism of acid-catalyzed transesterification. R'' corresponds to the structure of a diglyceride within the triglyceride molecule; R' corresponds to the carbon chain of the fatty acid that is not part of R''; R corresponds to the alkyl group of the alcohol.

In contrast to reactions with 1% or 2% acid, 98% of the theoretical maximum ester content was obtained at a 4% acid concentration (80 °C, 90 min). This acid concentration is similar to previous work on the AC-IST of dried algal biomass, which was carried out over the range of 3.8% to 17.6% H<sub>2</sub>SO<sub>4</sub> (v/v) (Haas and Wagner, 2011a), at 2% H<sub>2</sub>SO<sub>4</sub> (v/v) (Ehimen et al., 2010), and at about 3.4% H<sub>2</sub>SO<sub>4</sub> (v/v) (Wahlen et al., 2011). Ideally, catalyst use will be minimized both to reduce operational costs as well as the requirement to neutralize the reactor effluent prior to product recovery and ethanol recycling.

### 5.3.5 Factorial experiment and regression modeling

Given the promising results obtained with hydrochar A in the previous two experiments, a *Chlorella* biomass was carbonized to produce a lipid-rich hydrochar (Table 5.1, hydrochar B) that was commercially filtered using an energy-efficient dewatering and drying system (i.e. Pall Corporation's ZHF Centrifugal Discharge Filter). A factorial experiment was carried out to better explore the reaction space between 80 and 100 °C, 30 and 120 min, and ethanol loadings around 40:1 to 80:1 EtOH:FA molar ratio (Table 5.2). For this experiment, we chose to use ethanol containing 5% H<sub>2</sub>SO<sub>4</sub>, because 4% acid

concentrations were found to be ideal in a hydrochar containing about 40% fewer lipids. Twelve individual runs were completed, with a replicated center point at 90 °C, 75 min, and 62:1 EtOH:FA molar ratio that showed a standard error of 1.7% (Table 5.2).

Table 5.2. Mineral acid-catalyzed in situ transesterification factorial experiment

Run	Temperature (°C)	Time (min)	EtOH:Solids (g/g)	EtOH:FA (mol/mol)	Overall FAEE Yield (%)
1	80	30	4.7	41	70
2	80	30	9.5	83	91
3	80	120	4.8	41	93
4	80	120	9.5	83	90
5	90	30	7.1	62	89
6,7	90	75	7.1	62	94 ± 1.7
8	90	90	7.1	62	94
9	100	30	9.5	83	93
10	100	30	4.7	41	85
11	100	120	4.7	41	94
12	100	120	9.4	82	96

Note. Ethanol contained 5% H<sub>2</sub>SO<sub>4</sub> and loadings corresponded to 40:1 or 80:1 EtOH:FA molar ratios. All reactions contained dry hydrochar B (75% FAEE content). Single reactions only.

When these data are analyzed using a least squares regression approach, as shown in Table 5.3, it is apparent by comparing the magnitude and sign of the coded, or standardized coefficients, that temperature, time, and ethanol loading all had a similar impact on total FAEE yield. Compared to the uncoded coefficients, which signify how the yield is expected to change due to a one-unit increase or decrease in a given factor (assuming all other factors are held constant), the coded coefficients represent the change in yield in terms of a one standard deviation change in that factor. For example, although the coded coefficients were all similar for temperature, time, and ethanol loading, the uncoded coefficient for ethanol loading was quite large relative to the other factors due to the units of this measurement. Based on the *p*-values, which indicate the likelihood that a change in a given factor impacted yield, all three main factors were significant at the *p* ≤ 0.1 level (signifying that there is a greater than 90% probability that the observed effects were not due to chance).

Interestingly, all the second-order terms in the model, which correspond to the interactive effects of the variables, were negative. The negative effect on yield in reactions carried out for long times and high temperatures was previously observed (Figure 5.1), but the strongest interactive effect observed here was time and ethanol loading. This is apparent by comparing the yields obtained in runs 3 and 4, which suggests that more ethanol slightly reduced yields when reactions were carried out for 120 min. This trend, however, is not apparent at 100 °C, where more ethanol led to a slight increase in yield (cf. runs 11 and 12). In other experiments carried out at 100 °C for 90 min and longer, we have also observed higher yields with increased ethanol loadings beyond 110:1 EtOH:FA molar ratios (data not shown). One likely explanation for these observations is that increased ethanol loadings reduced the concentration of water, thereby diminishing rates of ester hydrolysis. Because reactions carried out at 80 °C appear less sensitive to the backward hydrolysis reaction, the increased ethanol loading in these reactions could reduce transesterification yields as a result of diluting the reactants. In either case, the difference in yield appears relatively small and is within the standard error measured for replicate reactions at the center point, so the trends here must be considered in light of the experimental uncertainty in the data.

Table 5.3. Regression analysis of factorial experiment

Term	Coded coefficient	Uncoded coefficient	<i>p</i> -value
Constant	90.5	-114	0.00
Temperature	3.2	1.9	0.07
Time	3.9	1.9	0.03
EtOH:FA	3.5	21.4	0.06
Temperature*Time	-1.2	-0.02	0.41
Temperature* EtOH:FA	-1.0	-0.02	0.49
Time* EtOH:FA	-3.8	-0.02	0.05
Temperature*Time* EtOH:FA	2.2	2.3E-04	0.18

Note. EtOH:FA (mol/mol).  $R^2=89.7\%$

Overall, the regression model generated by this factorial experiment is most appropriate for a hydrochar containing about 75% lipids and indicates that even lower alcohol loadings

than previously studied can still result in very high FAEE yields. Although a 40:1 EtOH:FA molar ratio is still 20-fold higher than what is used in a typical commercial transesterification reaction with vegetable oils, AC-IST obviates hexane extraction and is capable of converting lipids from all classes into FAEE. In addition, there are simple methods that may permit a further reduction in ethanol consumption. For example, the ethanol-FAEE effluent from one batch reaction could be used without any processing in a second batch reaction with fresh hydrochar. Although some amount of water may build up in this liquid phase as a result of FA esterification or due to moisture in the hydrochars, it is possible that multiple batches could be carried out prior to evaporating the ethanol for recovery.

#### 5.3.6 Acid catalyzed in situ transesterification of *Nannochloropsis* hydrochars

Given that HTC and AC-IST were successful with *Chlorella* biomass grown in a freshwater media, we sought to demonstrate the utility of these two processes for a marine species of green algae that is currently grown commercially. When AC-IST is applied to carbonized *Nannochloropsis* biomass, lipids from all classes are converted to FAEE and can later be fractionated based on chain length to separate the C20 omega-3 esters (mainly EPA). A variety of techniques, such as adsorption chromatography, fractional or molecular distillation, enzymatic splitting, low-temperature crystallization, supercritical fluid extraction and urea complexation, have all been studied for this application (Shahidi and Wanasundara, 1998; Rubio-Rodríguez et al., 2010). AC-IST is an attractive alternative to traditional lipid extraction in this case because the ethyl ester form of EPA is typically preferred for fractionation, particularly when using of supercritical CO<sub>2</sub> (Riha and Brunner, 2000; Perretti et al., 2007), and is also a biologically active form that is commonly marketed today as supplements (e.g., fish oil concentrates) and pharmaceuticals (e.g., Lovaza®).

We next sought to determine the ideal conditions for AC-IST of a *Nannochloropsis* hydrochar produced at 200°C in a 15 min reaction. These reaction conditions were

chosen because the total lipid and EPA yield were near 100% and because EPA isomerization was estimated to increase by only about 1% at these conditions (Section 3.3.6). Preliminary experiments with unreacted *Nannochloropsis* biomass, as well as the *Chlorella* hydrochar, helped us narrow the reaction space. For example, we observed that the highest yields in *Nannochloropsis* biomass were attained at 100 °C and 60 min and that yields improved with temperature (relative to 70 or 85 °C), time (relative to 15 and 30 min), and ethanol loadings (4:1 and 30:1 EtOH:solids w/w). We also found that yields increased with acid concentrations from 1 to 2% H<sub>2</sub>SO<sub>4</sub>, but higher acid concentrations had no positive effect and led to minor increases in EPA isomerization. These findings, along with the knowledge that 100 °C for 90 min with 5% acetyl chloride in methanol appeared to induce very minor if any isomerization, led us to examine the AC-IST of *Nannochloropsis* hydrochars at 100 °C for 30 to 60 min with 5% acetyl chloride, 1 and 2% H<sub>2</sub>SO<sub>4</sub>, and various amounts of ethanol (~7.5:1, 15:1, and 20:1 EtOH:hydrochar w/w ratio). Because the *Nannochloropsis* hydrochar contained fewer lipids than the *Chlorella* hydrochar (cf. 11% vs. 45% or 75%), similar EtOH:solids ratios result in much higher EtOH:FA molar ratios. In this case, the examined ethanol loadings were equivalent to ~450:1, 900:1, and 1300:1.

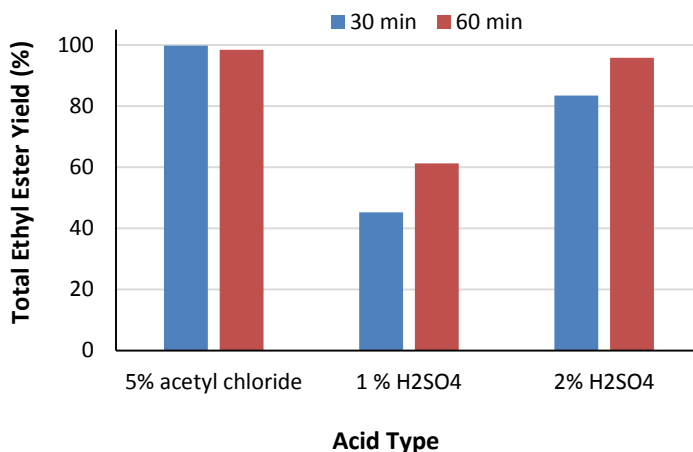


Figure 5.4. Acid catalyzed in situ transesterification of *Nannochloropsis* hydrochars. Single reactions at 7.5:1 EtOH:solids ratio (~450 EtOH:FA) at 100 °C.

As shown in Figure 5.4, reactions containing 7.5:1 EtOH:solids (w/w) with 5% acetyl chloride reached about 100% of the theoretical maximum yield regardless of time. In contrast, reactions containing 1% H<sub>2</sub>SO<sub>4</sub> achieved only 45 or 61% yields at 30 and 60 min, respectively. With 2% H<sub>2</sub>SO<sub>4</sub>, yields also increased with time, from 83% at 30 min to 96% at 60 min. These data were in line with our previous observations, as well as literature that suggests the transesterification capacity of a 5% acetyl chloride solution is about equivalent to a 1–2% H<sub>2</sub>SO<sub>4</sub> solution (Christie, 1989). The data for reactions containing 7.5:1 and 15:1 EtOH:solids ratio were very similar, though slightly higher yields were observed at both time points for reactions containing H<sub>2</sub>SO<sub>4</sub>.

Just as isomerization of EPA was carefully measured during HTC (Section 3.3.6), here too we measured EPA isomerization. Reactions with acetyl chloride showed little if any change from the baseline values we observed using the analytical lipid analysis protocol (which utilized methanol containing 5% acetyl chloride at 100 °C for 90 min). Reactions with 7.5:1 EtOH:solids ratio containing 1% and 2% H<sub>2</sub>SO<sub>4</sub>, however, showed about a 5% and 1% increase in EPA isomerization, respectively. Because it seems odd that higher acid concentrations would lead to reduced isomerization, we believe the data collected at 1% H<sub>2</sub>SO<sub>4</sub> is biased high due to the lower overall conversion of lipids to FAEE. In general, these data suggest that a mineral acid like H<sub>2</sub>SO<sub>4</sub> with strong oxidizing properties may not be suitable for processing *Nannochloropsis* hydrochars if minor isomerization cannot be tolerated (Christie, 1989). Although acetyl chloride and related acids may be somewhat more expensive than H<sub>2</sub>SO<sub>4</sub>, the value of the EPA should offset this cost.

#### 5.4 Conclusions

This work is the first to explore the acid-catalyzed in situ transesterification of algal hydrochars. By virtue of the HTC process, the costs associated with drying algal biomass are substantially reduced, thereby making AC-IST an alternative to traditional wet hexane extraction and transesterification worth studying. In accordance with our work on SC-IST, we found that thermal degradation of FA could diminish yields at temperatures of 100 °C

and reaction times >30 min but that this phenomenon did not occur at lower temperatures. By extending reaction times at 80 °C or 90 °C, yields >95% of the theoretical maximum were obtained at ethanol loadings <10:1 EtOH:solids (w/w). Although high yields were achievable in our experiments, the substantial amount of ethanol required to perform the reaction, and the high energy burden associated with its recycling, may hinder commercial adoption of this technology for feedstocks containing FA profiles similar to common oilseeds. For a feedstock like *Nannochloropsis*, however, which contains both high value omega-3 oils and FAs well suited to biodiesel, the costs associated with this approach may be justified. By working with a feedstock like *Nannochloropsis*, we hope to better understand how to reduce the costs associated with IST and then apply this engineering knowledge to other feedstocks.



## CHAPTER 6

### TRIFLATE-CATALYZED IN SITU TRANSESTERIFICATION

#### 6.1 Background

In the previous two chapters we demonstrated that the lipids within the hydrochar could be converted into biodiesel without prior solvent extraction by use of supercritical ethanol or mineral acids at subcritical conditions. Here we report on an alternative method of in situ transesterification using rare-earth metal triflate catalysts at subcritical temperatures and in the presence of water (Levine et al., 2012).

Lower rare-earth metal triflate (trifluoromethanesulfonate, Tf = SO<sub>2</sub>CF<sub>3</sub>) catalysts (e.g., Sc(OTf)<sub>3</sub>) are Lewis acids known for being highly active, inexpensive, non-toxic, reusable, and insensitive to air, moisture, and common heteroatoms (e.g., N, P, S) (Kobayashi et al., 2002; Rebacz and Savage, 2010). Compared to traditional Lewis acid catalysts (e.g., AlCl<sub>3</sub>), which decompose when exposed to water and are usually required in stoichiometric amounts, and common heterogeneous acid catalysts (e.g., heteropolyacids), which tend to be expensive and rarely outperform conventional methods using H<sub>2</sub>SO<sub>4</sub> (Yan, Dimaggio, et al., 2010; Stamenković et al., 2011), metal triflates may be a promising alternative for biodiesel production. Although metal triflates have been extensively used in organic synthesis, including the esterification of carboxylic acids with alcohols (Ishihara et al., 1996), only one study in the literature indicates their use in transesterification reactions to produce FAMES (Socha and Sello, 2010). In that study, transesterification of pure triglycerides was 82-99% complete after 20-30 min at 150 °C in a microwave reactor (0.2–2.0 mL, stirred) with 10 mol% Sc(OTf)<sub>3</sub> or Bi(OTf)<sub>3</sub> and a 48-fold molar excess of methanol. FA esterification was nearly complete in 1 min under the same conditions with just 1 mol% catalyst. In both cases, FAME yields increased significantly with alcohol loading (from 6:1 to 48:1 methanol:FA ratio), and Sc(OTf)<sub>3</sub> and Bi(OTf)<sub>3</sub> showed similar activity. Catalyst recovery from esterification reactions was reportedly ~80% with no significant loss in activity during 6 sequential reactions.

This initial literature report shows that metal triflate catalysts offer a potential pathway to fast reaction rates at conditions milder than those used in the uncatalyzed, supercritical IST approach. It is this potential that motivates our interest in these catalysts. Although related work demonstrated that several different metal triflates are effective catalysts for making and breaking C-O bonds in an aqueous-phase medium at ~200 °C (Rebacz and Savage, 2010), no previous work has explored the efficacy of these catalysts for biodiesel production in the presence of water. In addition, the literature contains no reports on the use of these catalysts with ethanol rather than methanol. Although methanol is usually less expensive, we chose to work with ethanol because it is less toxic and renewably derived, has superior dissolving power for oils, and produces biodiesel with improved fuel properties (Stamenković et al., 2011). Finally, metal triflates have never been used with lipid-rich biosolids produced from real biomass nor with the lower alcohol:FA ratios that would be desired for a viable commercial process. The potential benefits of triflate catalysts for biodiesel production from high FA and high moisture feedstocks together with our previous green chemistry research with these compounds leads us to hypothesize that these catalysts might lead to a transformative technology for biodiesel production.

## 6.2 Materials and Methods

### 6.2.1 Triflate-catalyzed in situ transesterification

Pure oleic acid and hydrochars were reacted with ethanol in the presence of varying amounts of metal triflate catalysts (i.e., Sc(OTf)<sub>3</sub> and In(OTf)<sub>3</sub>) and H<sub>2</sub>O. All catalysts and pure lipids were purchased from Sigma Aldrich and Nu-Check Prep, Inc., respectively, and used as received. Reactions were performed to identify the effects of reaction temperature, reaction time, catalyst type and loading, ethanol loading, water content, and stirring on the molar yield of FAEEs (defined as moles of ethyl ester formed per mol of FA initially present). Reactants were loaded into SS Swagelok reactors (0.6 mL total volume) at the desired proportions and quantities such that the reactors were 85% full at

reaction temperatures. The mass of each reactant was recorded to the nearest 0.01 mg (XS205DU, Mettler Toledo). In stirred reactors, Teflon-coated micro stir bars were included (2 mm long x 2.5 mm diameter, Fisher). Once loaded, reactors were submerged in either an isothermal fluidized sand bath (unstirred reactions only) or within 16 mm diameter openings in an aluminum heating block (Dynabloc, ACE Glass) placed atop a stirring hot plate. Both heating elements were controlled by thermocouples inserted into modified reactors loaded with water. Heat-up times were on the order of 2 and 10 min for the sand bath and DynaBloc, respectively.

After cooling to room temperature, reactors were unloaded and the reaction mixture was prepared for GC-FID analysis. Hexadecane was used in initial reactions as an internal standard to control for potential losses introduced during reactor unloading. In these reactions, 5–30 mg of hexadecane were loaded along with the reactants, and 6 mL of *n*-heptane and 1 mL of 1 N H<sub>2</sub>SO<sub>4</sub> were used to recover and dilute the reaction mixture. Product yields were corrected for hexadecane recovery, which typically ranged from 85–98%. Reactions in which the hexadecane recovery was below 85% were excluded from further analysis. In an effort to eliminate possible unintended effects caused by hexadecane acting as a co-solvent in the reaction, as well as to simplify reactor unloading by using a one-phase solvent system, reactions were carried out that contained no internal standard in the reactor and utilized 10–20 mL of ethanol (containing ~6,000 mg/L hexadecane) for product recovery and dilution. Control experiments with mixtures of ethyl oleate, oleic acid, triflate catalyst, ethanol, and water loaded into reactors placed only at room temperature demonstrated recoveries of ethyl oleate and oleic acid exceeding 90%. In both reactor unloading procedures, the diluted reaction mixture was centrifuged to remove fine particles (3000 RCF x 10 min) and then analyzed by GC-FID to determine the amount of FAEE and FA (Section 2.2.6, pg. 22). To simplify reporting and reduce error associated with the comparison of multiple calibration curves, FAEE yields for reactions containing carbonized solids are given on the basis of oleic acid and ethyl oleate only.

### 6.2.2 Statistical analysis

Minitab (v. 16.1.0) was used to design and analyze experiments. Oleic acid esterification was investigated as a function of five factors using a response surface methodology (RSM) and factorial experiments. Significance of regression coefficients was determined with a p-value of  $< 0.05$ . Results from additional experiments in which only one factor was varied at a time were compiled and analyzed using Microsoft Excel.

## 6.3 Results and Discussion

### 6.3.1 Triflate-catalyzed esterification of model compounds

Prior to investigating triflate-catalyzed IST/E of carbonized solids, we sought to better understand how FA esterification occurs under a variety of reaction conditions. To our knowledge, the only previous report on transesterification of TGs and FAs with  $\text{Sc}(\text{OTf})_3$  or  $\text{Bi}(\text{OTf})_3$  involved microwave-heated reactions carried out at 50–150 °C for 1–25 min with 6:1–48:1 methanol:FA molar ratio (Socha and Sello, 2010). To further probe the potential reaction space we used a response surface methodology as well as factorial designs to concurrently investigate the effects of reaction temperature (150 to 235 °C), time (5 to 45 min), catalyst loading (1 to 10 mol%), ethanol loading (1 to 20 EtOH:FA molar ratio), and water content (0 to 20 wt.% of the total reaction mixture). The data from 55 independent oleic acid esterification reactions were combined and analyzed using Minitab to better understand how reaction conditions influence ethyl oleate yield (see Table A.1 in Appendix A for complete data table).

A linear regression of the molar yield of ethyl oleate as a function of the main independent variables was found to have a low correlation value ( $R^2 = 0.57$ ); therefore, a quadratic equation including the main factors, squared terms, and their interactions was used for further analysis (Table A2). This model was found to have a correlation value of 0.87, meaning 87% of the variability in the yield could be attributed to the factors investigated.

In this model, the coefficients corresponding to the main independent variables were all positive except for reaction water content. This means that increasing the amount of water in the reaction was the only factor that consistently led to a reduction in yield. This was expected considering the strong reversibility of the esterification reaction at these temperatures (Changi et al., 2011).

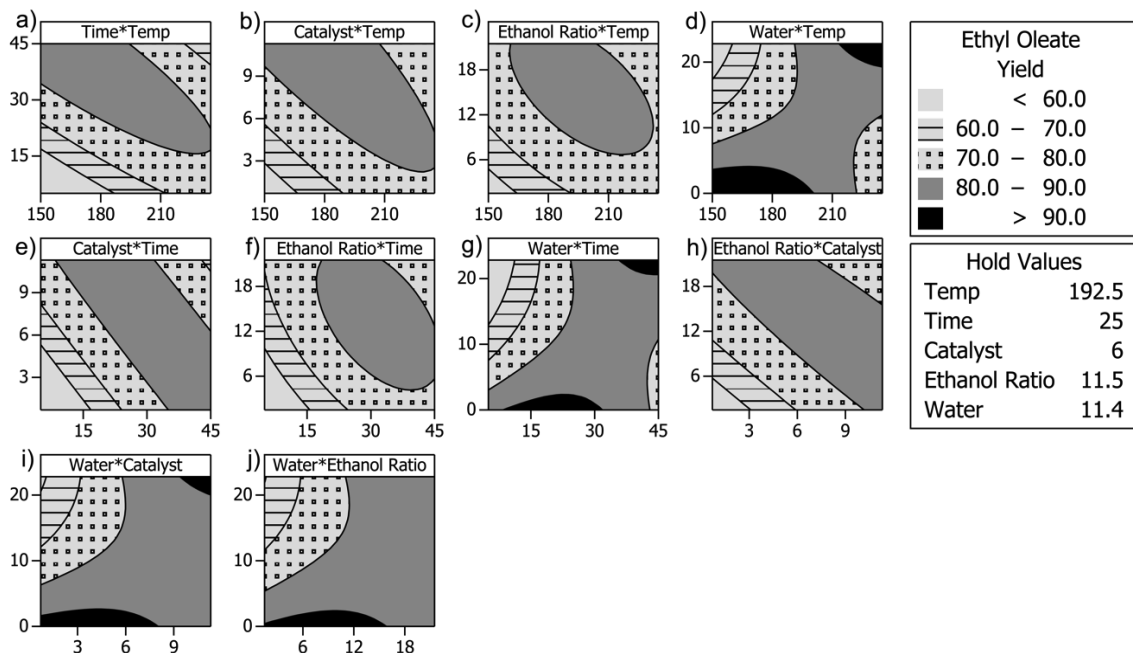


Figure 6.1 Contour plots of ethyl oleate yield (%) from triflate-catalyzed esterification reactions. The molar yield of ethyl oleate is given based on the shading scheme indicated in the upper right box. Each figure (labeled with a-j) shows ethyl oleate yield for two variables (y axis\*x axis given in figure title) with all other variables held at the values shown in the lower right box. Units are: temperature (°C), time (min), catalyst loading (mol%), ethanol ratio (mol EtOH/mol oleic acid), and water content (wt.% of total reaction mixture).

Contour plots of ethyl oleate yield were constructed on the basis of this quadratic model to more easily interpret trends in the data (Figure 6.1). In these plots, ethyl oleate yield is shown as a factor of two variables, while the remaining three variables are held at mid-point values. Ideally, we seek to find the conditions that result in the highest yield while minimizing the temperature, time, catalyst loading, and ethanol required for the reaction. The water content is controlled mostly by the water present in the reactants, water

generated during the reaction, and the combined volume of all reactants, which is most strongly influenced by the ethanol to FA ratio. As shown in Figure 6.1a-c, yields tend to increase with temperature at short reaction times, low catalyst loadings, and low ethanol ratio. In other words, higher temperatures appeared to compensate for a reduction in reaction time, catalyst use, and ethanol loading. In general, these plots suggest that temperatures above 210 °C are required to achieve yields greater than 80% in the presence of water if time, catalyst loading, and ethanol ratio are set to about 15 min, 3 mol%, and 6 EtOH:FA molar ratio. In Figure 6.1d, it is also apparent that 210 °C is a temperature at which yields greater than 80% should be achievable at any water content investigated. Just as higher temperatures led to increased yields (Figure 6.1a-c), data presented in Figure 6.1e-f suggest that higher yields can be achieved at low catalyst loadings and ethanol ratios when reaction time is extended. Similarly, Figure 6.1h demonstrates that in reactions containing more catalyst, higher yields can be achieved at lower ethanol ratios. Finally, Figure 6.1d,g,i,j show that in reactions containing very little to no water, high yields can be obtained at temperatures below 200 °C, times between 5 and 30 min, catalyst loading between 1 and 8 mol%, and with an EtOH:FA molar ratio between 6 and 15. Conversely, at the highest water content investigated, Figure 6.1d,g,i show the highest temperature, longest time, and greatest catalyst loading are required to achieve yields above 90%. In general, the contour plots with water on one axis suggest that yields above 80% are achievable as long as temperature, time, catalyst loading, and ethanol ratio increase correspondingly with water content.

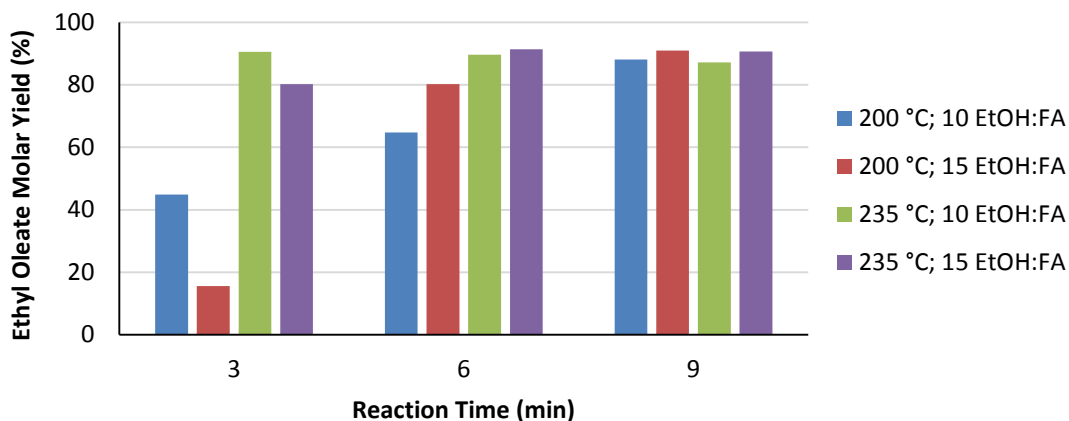


Figure 6.2. Oleic acid esterification with nominally 1 mol%  $\text{Sc}(\text{OTf})_3$  and 5% water. The average loadings were:  $1.2 \pm 0.2$  mol% catalyst,  $15.2 \pm 0.4$  or  $10.2 \pm 0.2$  EtOH:FA molar ratio, and  $5.4 \pm 0.6$  wt.% water. The average standard error in the molar yield for replicate reactions was 2.5%.

Additional experiments were carried out at 200 and 235 °C to better determine the influence of short reaction times, moderate ethanol loadings, and a reaction water content similar to the expected percentage of water to FA in reactions containing wet hydrochar. As shown in Figure 6.2, ethyl oleate yield increased with reaction time from 3 to 9 min except in reactions at 235 °C, which showed no increase after 6 min. Increasing the ethanol loading from 10:1 to 15:1 EtOH:FA molar ratio led to reduced yields in reactions lasting 3 min, most likely due to dilution of the FA reactant. This apparent reduction in reaction rate due to ethanol dilution was no longer observed at 6 or 9 min, where reactions with a 15:1 EtOH:FA ratio demonstrated very similar or higher yields than reactions with a 10:1 EtOH:FA ratio. At 9 min, yields for all reactions were from 88–90%.

Previously,  $\text{In}(\text{OTf})_3$  was found to be even better than  $\text{Sc}(\text{OTf})_3$  for organic syntheses involving the cleavage and formation of C-O bonds (Rebacz and Savage, 2010); therefore, additional experiments were carried out with 1 mol%  $\text{In}(\text{OTf})_3$  and a 15:1 EtOH:FA molar ratio. The yields of ethyl oleate from reactions at 200 and 235 °C for 6 and 9 min were very similar to yields achieved in identical reactions with 1 mol%  $\text{Sc}(\text{OTf})_3$  (Figure 6.3). In comparison to similar reactions carried out without catalyst (Table 6.1), which showed

yields at 230 °C of 61, 73 and 78% at 60 min, 120, and 240 min, respectively, Sc(OTf)<sub>3</sub> and In(OTf)<sub>3</sub> clearly enhanced the reaction rate.

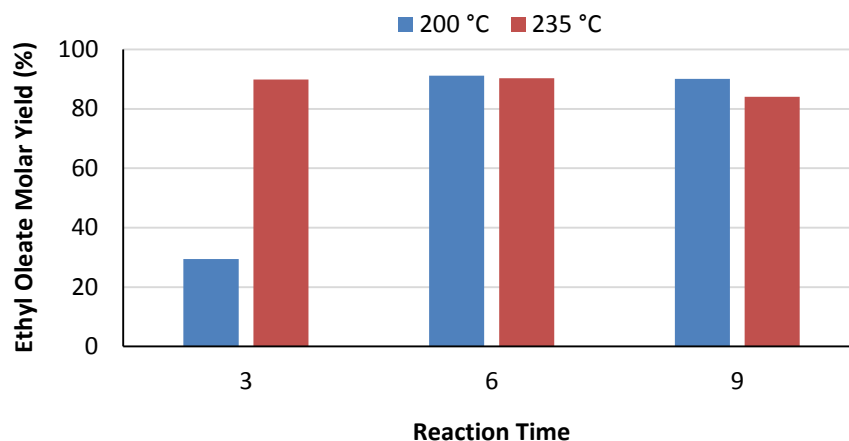


Figure 6.3. Oleic acid esterification using In(OTf)<sub>3</sub>. All reactions were carried out with 1 mol% In(OTf)<sub>3</sub> and 15:1 EtOH:FA molar ratio. The average loadings were: 1.1 ± 0.3 mol% catalyst, 15.3 ± 0.2 EtOH:FA molar ratio, and 4.8% ± 0.1 wt% water. Single reactions only.

Table 6.1 Non-catalytic oleic acid esterification

Temp. (°C)	Time (min)	Ethanol:FA molar ratio	Water (wt.%)	Ethyl Oleate Yield (mol %)
200	60	10	0	61.4
200	60	10	5	51.7
200	120	10	0	68.7
200	120	10	5	64.7
200	240	10	0	80.2
200	240	10	5	73.0
215	60	10	0	58.7
215	60	10	5	65.6
215	120	10	0	66.0
215	120	10	5	59.2
215	240	10	0	75.1
215	240	10	5	76.7
230	60	10	0	61.1
230	60	10	5	54.6
230	120	10	0	73.1
230	120	10	5	67.5
230	240	10	0	78.0
230	240	10	5	87.3

Note. Single reactions only.



To determine whether the reactions may have been mass transfer limited due to the insufficient solubility of ethanol in oleic acid, we performed reactions in a heating block set atop a stirring hotplate (Figure 6.4). Stirring appeared to increase yields in reactions without water and with 5% water, but did not cause a significant change in yield in reactions containing 2.5% water. Although additional experiments should be performed to better elucidate how mixing may affect reaction yields, these data suggest that the reactor geometries and loading rates utilized in this work most likely did not lead to significant mass transfer limitations in reactions with pure oleic acid. Notably, this set of experiments again demonstrated that water up to approximately 5% of the reaction mixture has only a minor impact on yield under these conditions. This outcome is an important consideration because water will be present in reactions with partially or completely dried carbonized solids and rectified ethanol (4.4 wt.% H<sub>2</sub>O).

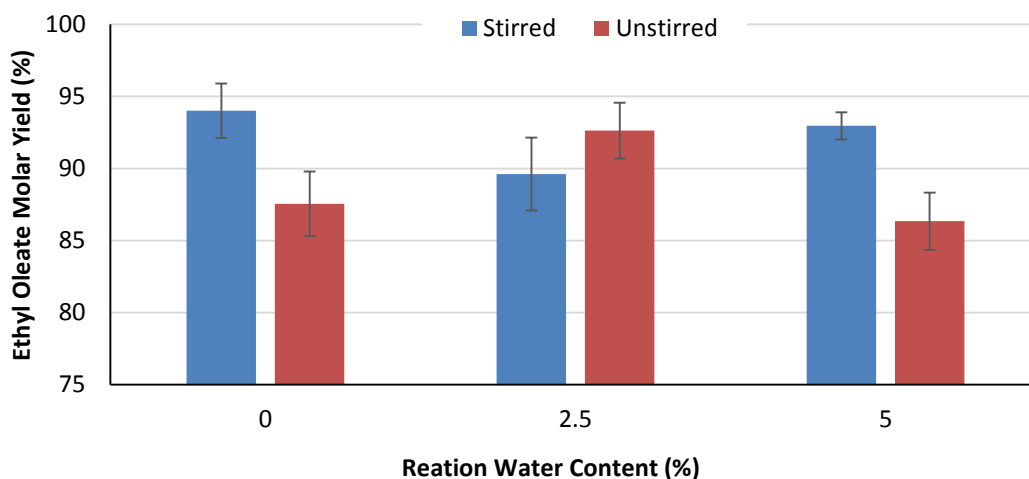


Figure 6.4. The effect of water and stirring on triflate-catalyzed oleic acid esterification. Nominal reaction conditions were carried 215 °C for 9 min with 1 mol% Sc(OTf)<sub>3</sub> and 15:1 EtOH:FA molar ratio. The average loadings were:  $1.2 \pm 0.2$  mol% catalyst,  $15.2 \pm 0.3$  EtOH:FA molar ratio, and  $2.3 \pm 0.1$  wt.% or  $4.7\% \pm 0.1$  wt.% water. Error bars are given for the standard error of replicate reactions.

Although Sc(OTf)<sub>3</sub> and In(OTf)<sub>3</sub> were found to be beneficial in increasing the rate of oleic acid esterification, the observation of decreasing yields with longer times at severe reaction conditions and high catalyst loadings (Figure 6.1) led us to investigate the

stability of ethyl oleate under these reaction conditions. Reactors were loaded with mixtures of ethyl oleate, ethanol (8.5-10:1 EtOH:FA), Sc(OTf)<sub>3</sub> (3.5 or 7 mol%) and water (0 or 12.5-13.5 wt.%) in the desired percentages and reacted for 10, 30 or 60 min at 150, 170, 190, 210, and 215 °C.

Table 6.2. Triflate-catalyzed hydrolysis of ethyl oleate

Temperature (°C)	Time (min)	Catalyst (mol %)	EtOH:FA molar ratio	Water (wt.%)	Ethyl Oleate Yield (mol %)
150	30	7	10	13.5	84 ± 2.1
150	30	3.5	10	13.5	83 ± 0.2
170	30	7	10	13.5	80 ± 1.4
170	30	3.5	10	13.5	84 ± 1.0
190	30	7	10	13.5	78 ± 0.3
190	30	3.5	10	13.5	77 ± 0.4
210	30	7	10	13.5	73 ± 1.7
210	30	3.5	10	13.5	77 <sup>a</sup>
215	10	6.5	8.5	0	91 ± 0.5
215	10	6.5	8.5	12.5	83 ± 1.0
215	60	6.5	8.5	0	76 ± 3.6
215	60	6.5	8.5	12.5	73 ± 0.4

Note. Ethyl oleate yield is the moles of ethyl oleate recovered following the reaction divided by the number of moles of ethyl oleate loaded. Oleic acid was detected in all reactions; the average total molar recovery of ethyl oleate and oleic acid was 94%. The average yield and standard error of replicate reactions are given. <sup>a</sup> Single reaction only.

As shown in Table 6.2, at 215 °C and 10 min, approximately 91% of the ethyl oleate loaded in the reactor was recovered in reactions containing no water whereas only 83% was recovered in similar reactions containing 12.5 wt.% water. Although less than 100% recovery would be expected even in the case of no hydrolysis due to some error associated with unloading the reactors and the quantification of ethyl oleate, these data suggest hydrolysis was indeed occurring even when no water was purposefully added to the reactors. Attempts were made to limit this introduction of moisture, however, it is possible that trace amounts of water were present given the hygroscopic nature of both the Sc(OTf)<sub>3</sub> catalyst and ethanol. When similar reactions were carried out for 60 min at 215 °C, the difference between ethyl oleate recovery in reactions containing water and those without was less apparent (cf. 73% and 76% on average) but the overall recoveries

were lower, suggesting that hydrolysis increases with reaction time regardless of reaction water content. As expected, ethyl oleate recoveries for reactions carried out for 30 min at lower temperatures (150–210 °C) in the presence of 13.5 wt.% water indicated that hydrolysis increases with temperature; however, hydrolysis was relatively unresponsive to a doubling in catalyst loading. Finally, it is noteworthy that in all reactions carried out at 215 °C except those run for 10 min with 12.5 wt.% water, an unidentified peak appeared in the chromatogram with a retention time intermediate between ethyl oleate and oleic acid. Attempts to positively identify the peak using GC-MS were unsuccessful, but based on its molecular ion and our knowledge of triflate-catalyzed acetylation reactions, it is likely that this peak corresponds to an ethyl substituted FAEE. In addition, in exploratory reactions at 250 °C and 60 min, the ethyl oleate peak was no longer singular in nature; rather, it was an amalgamation of one large peak surrounded by numerous smaller peaks suggestive of isomerization. Taken together, these data suggest that ethyl oleate is subject to hydrolysis, isomerization, and substitution reactions under the reaction conditions investigated. As a result, esterification reactions should be carried out under the mildest conditions possible and with the least amount of catalyst that will result in high yields to avoid these undesirable reaction products.

### 6.3.2 Hydrothermal carbonization

*C. protothecoides* was reacted as a wet paste (~25% solids) in 30 mL Swagelok reactors to produce hydrochars. Because the reaction conditions of HTC may impact the physical properties of the hydrochar (e.g., porosity, hydrophobicity) as well as the lipid composition based on the extent of hydrolysis, we selected carbonized solids produced from reactions carried out at two different sets of temperatures and times to use in IST experiments (Table 6.3). When analyzed for total lipids and lipid composition, the hydrochars selected for this work contained 46–58% FAMES on a dry weight basis and a mixture of mostly TG, DG, MG, and FA. Each hydrochar is designated with a letter in the second row of Table 6.3 that is referenced throughout this chapter. In some reactions, hydrochars were reacted wet, exactly as they were recovered by filtration following HTC.

In other reactions, hydrochars were first oven dried and then rehydrated with the desired amount of water to investigate the effects of water on the reaction.

Table 6.3. Characterization of carbonized solids used in TC-IST

Parameter	Hydrochar	
	A	B
Carbonization Temperature (°C)	220	250
Carbonization Time (min)	120	60
Total FAMES (wt.%)	46	58
Fatty acid (% of FAMES)		
C16:0	12	12
C18:0	2.3	3.9
C18:1	58	62
C18:2	25	19
C18:3	2.4	2.0
Lipid composition (wt.% of total)		
TG	51	29
DG	21	27
MG	5.6	8.5
FA	22	35

Note. The averages of replicate analyses for fatty acid methyl esters (FAMES), triglycerides (TGs), diglycerides (DGs), monoglycerides (MGs), and fatty acids (FA) are given. Standard error was less than 1% on all replicates.

### 6.3.3 Triflate-catalyzed in situ transesterification of hydrochars

Based on our understanding of oleic acid esterification, we set out to perform triflate-catalyzed IST on algal hydrochars. Carbonized solids were subjected to triflate-catalyzed IST, and the ethyl oleate yield was determined relative to the maximum theoretical amount of oleic acid present as determined by in situ acid-catalyzed transesterification using excess methanol and 5% acetyl chloride (assumed to completely (trans)esterify all lipids). Assuming FA chains of all lengths and varying degrees of unsaturation are equally likely to undergo transesterification in the presence of triflates, which was previously demonstrated (Socha and Sello, 2010), then the yield of ethyl oleate serves as an indicator of the overall conversion of lipids within carbonized solids to FAEE.

In preliminary experiments with pre-dried hydrochars at 215 °C with 1 mol% Sc(OTf)<sub>3</sub> and 15:1 EtOH:FA molar ratio for 10, 30 and 60 min, yields were 8–15% of the theoretical

maximum with or without 5 wt.% water regardless of time. When  $\text{Sc}(\text{OTf})_3$  was used at 6 mol% in 60 min reactions, yields increased substantially and reactions containing about 5 wt.% water yielded significantly more ethyl oleate than those without (cf. ~100% to 41%). This outcome suggested that in situ triflate-catalyzed transesterification was indeed possible provided an adequate amount of catalyst was present and prompted experiments utilizing wet hydrochars reacted directly following their recovery by filtration. When a wet hydrochar was reacted at 215 °C with approximately 20 mol%  $\text{Sc}(\text{OTf})_3$  and a 20:1 EtOH:FA molar ratio for 30 and 60 min, ethyl oleate yields were 50% and 76%, respectively. In these reactions, the water content was approximately 11 wt.% on a total reaction mass basis. Hexadecane recoveries in these initial exploratory experiments with hydrochars tended to be lower and more variable than in reactions containing pure oleic acid, suggesting that recovery of the product mixture in heptane may not be well suited to reactions containing carbonized solids known to be hydrophobic. With this in mind, and to avoid possible artifacts created by hexadecane acting as a co-solvent in the reaction, all subsequent work with hydrochars was performed without hexadecane in the reactor and by recovering and diluting the product mixture in ethanol.

To more readily study the impact of reaction water content, the two hydrochars selected for further experimentation (hydrochars A and B, Table 6.3) were oven dried and then rehydrated prior to reaction. The results from several reactions involving these hydrochars are given in Figure 6.5. Notably, the highest yields of ethyl oleate (~98%) were obtained when hydrochar A was reacted with stirring for 60 min at 215 °C with about 12 mol%  $\text{Sc}(\text{OTf})_3$  and no water present. When water was added to the reactor at 9 and 16 wt.% of the total reaction mixture, yields from hydrochar A decreased to 93 and 76%, respectively. In hydrochar B, ethyl oleate yield increased from 80 to 85% when the reaction time was extended from 30 to 60 min in dry reactions with stirring. With approximately 16 wt.% water present, yields in hydrochar B decreased to 59%.

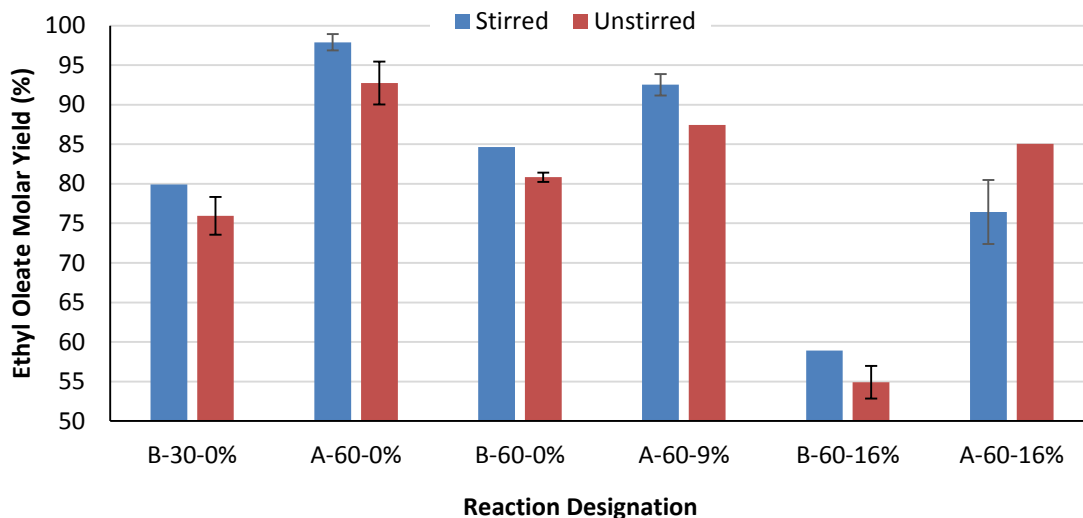


Figure 6.5. Triflate-catalyzed in situ transesterification of algal hydrochars A and B. The reaction designation given refers to the hydrochar (A or B), the time of the reaction (30 or 60 min), and the reaction water content (0%, 9%, or 16%). All reactions were carried out at 215 °C on the stirring hot plate. When accounting for the actual FA composition of each hydrochar, the average catalyst and ethanol loading in hydrochar A were  $12.6 \pm 0.3$  mol% and  $18.9 \pm 0.7$  EtOH:FA molar ratio, respectively, and  $11.4 \pm 0.5$  mol% and  $16.5 \pm 0.6$  EtOH:FA molar ratio, respectively, in hydrochar B. Error bars are given for the standard error of replicate reactions; no error bars are given for single reactions.

The data presented in Figure 6.5 suggest that both transesterification and esterification of lipids within dry carbonized solids was nearly complete under the reaction conditions investigated. As expected, water hindered the reaction and resulted in reduced ethyl oleate yields, yet it is noteworthy that yields as high as 93% could still be obtained in the presence of 9 wt.% water under these moderate conditions and ethanol loadings (~20:1 EtOH:FA molar ratio). In general, the ethyl oleate yields reported here compare favorably to those obtained by Socha and Sello (2010) in a reaction containing a 2.4:1 molar mixture of palmitic acid (90% FAME yield) and triolein (87% FAME yield) at 150 °C for 20 min with 10 mol%  $\text{Sc}(\text{OTf})_3$ , 145:1 MeOH:TG and 60:1 MeOH:FA molar ratios, and no water. Furthermore, the high conversion observed in the presence of 9 wt.% water is a considerable improvement relative to similar reactions carried out with other acid catalysts. For example, Ehimen et al. (2010) found that in situ transesterification of *Chlorella* biomass with  $\text{H}_2\text{SO}_4$  was completely inhibited in the presence of 4.8 wt.% water, and Chai et al. (2007) observed only 4% conversion of vegetable oil to FAME in the

presence of 1 wt.% water when using the heteropolyacid  $\text{Cs}_{2.5}\text{H}_{0.5}\text{PW}_{12}\text{O}_{40}$  (Chai et al., 2007). Nevertheless, considering the negative impact of water on the reaction, it may be beneficial to partially or completely dry hydrochars prior to IST or perform the reaction in stages with subsequent water removal steps.

In reactions with both hydrochars, stirring seemed to improve yields, although in at least one case with high water content, the opposite effect occurred. It is possible that the heterogeneous nature of the carbonized solids contributed to this unexpected result due to variability between the solids actually reacted and those analyzed for total lipids. It is also possible that in reactions with very high water contents, excessive mixing hinders the diffusion of ethanol into the oils contained within the carbonized solids. The transesterification reaction occurs principally in the oil phase and is therefore limited by the solubility of ethanol in oil, which is low but increases with temperature (Silva et al., 2010). With IST, mass transfer through the solid matrix surrounding the oil presents another hurdle to overcome. As of now, the exact location of lipids within carbonized solids is not well understood. Lipids within *C. protothecoides* accumulate principally as TGs within intracellular, cytoplasmic lipid bodies surrounded by a phospholipid monolayer. During HTC, the cellular structure is severely disrupted through a variety of hydrolysis, dehydration, condensation, polymerization, and aromatization reactions principally involving polysaccharides (Titirici, Thomas, Yu, et al., 2007; Libra et al., 2011). Although Heilmann et al. (2011) demonstrated that oils do not participate in char formation during HTC at 200 °C (Heilmann, Jader, Sadowsky, et al., 2011), little is known about how lipids originally present in the biomass are dispersed within carbonized solids or may be adsorbed to its surface. In studies with pure cellulose, hydrochars produced at 220-250 °C were found to consist of aggregates of microspheres with mostly hydrophilic shells and hydrophobic cores (Sevilla and Fuertes, 2009). It is likely that lipids remain adsorbed to hydrophobic components within or along the tortuous surface of carbonized algal biomass, yet it remains unclear how the reaction conditions of HTC may cause morphological and chemical changes that facilitate or hinder the diffusion of reactants

and catalysts during IST. It has been suggested that oven drying hydrochars can lead them to become more hydrophobic, which might impact the ability of ethanol to enter through micropores in the solid and access oil deposits (Libra et al., 2011).

As shown in Figure 6.5, higher yields were obtained from hydrochar A compared to hydrochar B for similar reaction conditions. Although this observation may in part be due to the high variability of the hydrochars, especially with regards to the deposition of lipids throughout a batch of solids, it may also be a reflection of the reaction conditions under which the hydrochars were produced. It is possible that the higher temperatures used to generate hydrochar B created a more hydrophobic surface structure that impeded the diffusion of ethanol. In addition, hydrochar B contained more total lipids than hydrochar A (cf. 58 vs. 46%), meaning the catalyst and EtOH:FA ratios in these reactions were slightly lower on average than those used in reactions with hydrochar A. Taken together, these data suggest a more thorough understanding of how HTC process conditions affect the performance of triflate-catalyzed IST/E of hydrochars is warranted.

#### 6.3.4 Post-reaction catalyst recovery and alcohol recycling

Catalyst recovery and reuse is an important consideration in designing any catalytic process. Socha and Sello (2010) previously demonstrated that catalyst recovery from esterification reactions was possible and that the catalyst maintained high activity through 6 cycles. However, the authors noted that catalyst recovery from transesterification reactions was more challenging due to difficulty in separating the catalyst from the glycerol byproduct remaining after evaporation of the alcohol. Although no catalyst recovery was attempted in the current work, it is noteworthy that the product mixture quickly separated into organic (ester) and alcoholic (ethanol, water, glycerol, and catalyst) phases, even in reactions containing carbonized solids (residual solids appeared at the interface and were easy to filter out). Fortunately, we expect less glycerol to be present after in situ transesterification of the hydrochar compared to reacting an equivalent amount of oil contained in the original biomass because lipid hydrolysis occurs



during HTC and glycerol is dissolved in the aqueous phase following filtration. Nevertheless, some MG, DG and TG will remain in the hydrochar as a source of glycerol, in addition to other biomass components, that could complicate recovery of the catalyst. One option to improve catalyst recovery may be to heterogenize metal triflates by attachment to a solid support.

Alcohol recycling and reuse is another key determinant of cost effective and net-energy positive biodiesel production. Because triflate catalysts are soluble in both ethanol and water, as well as highly water-tolerant, it may be advantageous to use rectified ethanol in any recycle stream to avoid the additional costs associated with producing anhydrous alcohol (Kobayashi et al., 2002). Future work should address catalyst recovery and reuse along with alcohol recycling.

#### 6.4 Conclusions

This work demonstrated the utility of  $\text{Sc}(\text{OTf})_3$  and  $\text{In}(\text{OTf})_3$  in the esterification of pure oleic acid with ethanol in the presence of water. More importantly,  $\text{Sc}(\text{OTf})_3$  was found to catalyze the in situ transesterification of lipids within carbonized algal biomass. This is the first report of which we are aware to demonstrate triflate-catalyzed IST without first extracting lipids from their biomass matrix of origin. This approach represents an opportunity for process intensification, as separate extraction and reaction steps can be combined into a single unit operation. Our work demonstrated that  $\text{Sc}(\text{OTf})_3$  is unique in its ability to catalyze transesterification in the presence of water, which is ideal when working with wet hydrochars. Overall, our preliminary findings suggest that further experimentation to optimize triflate-catalyzed transesterification is warranted, particularly with regards to catalyst recovery and reuse.

## CHAPTER 7

### ALGAL GROWTH ON THE AQUEOUS CO-PRODUCT OF HTC

#### 7.1 Backgrounds

Interest has grown in using the aqueous phase generated during hydrothermal processing of wet algal biomass as a nutrient source for producing additional algal biomass. From a strictly economic perspective, nitrogen and phosphorus fertilizers do not appear to be a major cost driver at algal production facilities today. We would contend, however, that careful nutrient management at algal bio-refineries is essential from a sustainability perspective and will only continue to become more relevant as the industry expands. Early work carried out on hydrothermal gasification (Minowa and Sawayama, 1999; Tsukahara et al., 2001), along with more recent advances in hydrothermal liquefaction (Jena et al., 2011; Biller et al., 2012), have demonstrated that certain algae are capable of growing on the dissolved nutrients in the aqueous phase co-product. In these studies, algal biomass was processed at 350 °C for varying amounts of time, the unreacted solids and bio-oil (in some cases with organic solvents) were separated, and the aqueous phase was diluted 50–500 fold to test its ability to support algal growth. In general, growth was greatest in the most dilute solutions, probably because dilution reduces the concentration of potential inhibitors such as ammonia, phenols, fatty acids, and metal catalyst residues (Minowa and Sawayama, 1999; Tsukahara et al., 2001; Jena et al., 2011; Biller et al., 2012). In cultures grown on diluted aqueous phase, however, biomass density only reached about 12% (Minowa and Sawayama, 1999), 50% (Jena et al., 2011), or 85% (Biller et al., 2012) of the density that was achieved when algae were grown on standard media. These data suggest that the presence of inhibitors and the unequal dissolution of certain nutrients into the aqueous phase, such as nitrogen, phosphorus, and trace metals, could contribute to low overall biomass yields when using aqueous phase as a growth medium.

In an effort to reduce the concentration of inhibitors generated during subcritical water hydrolysis and preserve the nutrient quality of the aqueous phase, we have focused on HTC reactions carried out near 200 °C for 15–30 min. To our knowledge, only two previous studies have tested the efficacy of the aqueous phase co-product from algal biomass treatment at this temperature as a nutrient source. Heilmann et al. (2011) noted that about 45% of the carbon, 80% of the nitrogen, and 100% of the phosphorus from the reactant biomass (*Chlamydomonas reinhardtii*) could be recovered in the aqueous phase after a 2 h reaction at 200 °C (Heilmann, Jader, Harned, et al., 2011). This extended reaction time reportedly led to the formation of nitrogen-containing Maillard-type heterocyclic compounds and piperazinediones (cyclic amino acid dimers). A 20-fold dilution of this aqueous phase was able to support growth of *C. reinhardtii* to about half the density reached when using tris-acetate-phosphate (TAP) medium. In experiments with a wild isolate of *Chlorella*, Du et al. (2012) demonstrated that growth in 50, 100, and 200-fold dilutions of aqueous phase produced after a 40 min reaction at 200 °C led to higher final biomass densities compared to cultures grown in BG-11, a medium containing no organic carbon (Du, Hu, et al., 2012). These experiments used autoclaved media in small shaker flasks that were incubated under continuous illumination for 5-day batches.

Considering that a limited amount of work has been completed with algae, it is illustrative to look to related studies carried out with other microbial biomass. The concept of solubilizing biomacromolecules that reside within biomass solids through reaction in high temperature water is not a new concept and has been applied to a variety of biomass feedstocks and wastes under various process names (He et al., 2008; Zhu et al., 2011). For example, cellulosic biomass is commonly pre-treated prior to saccharification through hydrothermolysis (Suryawati et al., 2009). Likewise, subcritical water hydrolysis has been carried out on agricultural feedstocks, such as soybean meal and rice bran (Sereewatthanawut et al., 2008; Watchararujij et al., 2008), fish meal (Zhu et al., 2008), poultry waste (Zhu et al., 2010), bovine serum albumin (Rogalinski et al., 2005), and yeast biomass (Lamoolphak et al., 2006). In general, temperatures from 200–220 °C for up to

30 min have been found to maximize protein, amino acid, and organic carbon yields in the aqueous phase, while more severe conditions (i.e., higher temperatures and/or longer reaction times) tend to result in increased decomposition of amino acids, formation of carboxylic acids (Quitain et al., 2002), and gaseous by-products. Some of these aqueous phase products were also found to be suitable growth substrates for yeast, replacing commercial yeast extracts (Lamoolphak et al., 2006; Sereewatthanawut et al., 2008). At higher temperatures (~250–350 °C), subcritical water hydrolysis is typically referred to as hydrothermal liquefaction wherein the goal is mainly to produce a bio-oil for fuel purposes. At these higher temperatures, repolymerization reactions tend to be favored over hydrolysis, resulting in the conversion of smaller, water-soluble molecules into oil-phase products (Garcia Alba et al., 2012).

Although previous studies have focused on comparing algal growth rates when cultured with various dilutions of aqueous phase and common media formulations (e.g, TAP or BG-11), here we focus on the productivity of a two-stage growth system in which a nutrient-replete seed culture (stage 1) is used to inoculate larger production reactors that receive aqueous phase (stage 2). In this system, the dilution of the aqueous phase is intrinsically determined because all the biomass harvested from the second stage is reacted to produce aqueous phase that is returned to that stage. We note that this approach differs from what many in the field refer to as a two-stage cultivation strategy involving a nutrient-replete stage for biomass growth and a nutrient-deficient stage for lipid accumulation. A model biomass (*Nannochloropsis oculata*) was reacted at various conditions to identify the optimal combination of reaction temperature and time that results in high lipid yields and nutrient partitioning to the aqueous phase co-product (Section 3.3.6, pg. 64). A unique bi-culture of a marine microalgae and a cyanobacteria developed in our laboratory was grown in bubble column reactors (BCRs) to study how C, N, and P liberated from the biomass during HTC could be recycled for algal growth. The effects of media recycling and nutrient supplementation, as well as the design of a production facility to limit contamination and maximize productivity, are discussed.

## 7.2 Materials and Methods

### 7.2.1 Culture conditions

A bi-culture of a marine green algae and cyanobacteria, tentatively identified as *Nannochloris* and *Synechocystis*, respectively, was developed in our lab by stressing an open raceway culture of *Nannochloropsis oculata* with high concentrations of trace metals. The mixed culture was grown in a modified f/2 media containing brackish water (27 g/L Instant Ocean salt mix, Spectrum Brands) fortified with N (25-200 mg/L urea), P (50 mg/L  $\text{NaH}_2\text{PO}_4 \cdot 2\text{H}_2\text{O}$ ), trace metals (1 mL stock solution/L final media), and vitamins (1 mL stock solution/L final media). The trace metal stock solution contained the following salts dissolved in 0.01 N  $\text{H}_2\text{SO}_4$  (mg/L):  $\text{Na}_2\text{EDTA} \cdot 2\text{H}_2\text{O}$  (4360),  $\text{FeCl}_3 \cdot 6\text{H}_2\text{O}$  (3150),  $\text{MnCl}_2 \cdot 4\text{H}_2\text{O}$  (180),  $\text{ZnSO}_4 \cdot 7\text{H}_2\text{O}$  (22),  $\text{CuSO}_4 \cdot 5\text{H}_2\text{O}$  (10),  $\text{CoCl}_2 \cdot 6\text{H}_2\text{O}$  (10),  $\text{Na}_2\text{MoO}_4 \cdot 2\text{H}_2\text{O}$  (6.3). The vitamin stock solution contained thiamin HCl (200 mg/L), vitamin B<sub>12</sub> (5 mg/L), and biotin (5 mg/L). Aqueous phase and various amounts of the nutrient supplements in the f/2 media were used in different growth experiments, as described in Section 7.3. In some experiments, a seed culture (0.4 to 1 L) was diluted to the 4-L working volume of the BCRs with freshly prepared brackish water while in others spent media recovered after centrifugation was used for dilution to study the impact of continuous media recycling. Finally, when using aqueous phase in the BCRs, Antifoam A concentrate (Sigma, 1-5 mg/L final concentration) was used to reduce foaming.

Cultures were maintained in 4-L polystyrene BCRs (12.2 cm diameter x 50 cm tall) illuminated on a 14:10 h light:dark cycle with fluorescent bulbs ( $\sim 300 \mu\text{mol}/\text{m}^2\text{-sec}$ ) and stirred at 60 rpm. The BCRs were sparged with 2.5 L/min air containing  $\sim 1\%$   $\text{CO}_2$  during the light hours or air during the dark hours. Each day a 14.5-mL sample was removed and centrifuged (5,000 RCF x 5 min), and the cell-free supernatant was retained for analysis. The pH in the supernatant was measured immediately and then typically samples were frozen and maintained at  $-4^\circ\text{C}$ . The pellet was washed with distilled  $\text{H}_2\text{O}$  and transferred to a pre-dried, pre-weighed glass tube where it was dried ( $65^\circ\text{C}$  for at least 24 h), allowed to cool in a desiccator, and then weighed. The solids in the glass tube were used for lipid

analysis, as described in Section 7.2.4 and sent to a third-party laboratory (Micro-Analysis, Inc.) for elemental analysis with a CHN analyzer.

### 7.2.2 Hydrothermal carbonization (HTC)

All carbonization reactions with wet algal biomass were carried out in 316 stainless steel (SS) reactors fashioned from Swagelok parts (2 caps and 1 port connector). When biomass grown in BCRs was not yet available, we used *N. oculata* biomass (~32% total solids as delivered) supplied by Reed Mariculture Inc. in carbonization experiments. This material was special ordered to be free of any preservatives and was stored frozen prior to use. Once the BCRs were fully functional, centrifugation was used to harvest biomass for HTC reactions. Typically, harvested biomass was immediately reacted to produce aqueous phase that could be recycled to the BCRs. Previously frozen or freshly harvested biomass was diluted to ~15% total solids with distilled water and loaded by mass into the Swagelok reactors (28 mL total volume) such that the reactor headspace was less than 10% of the total reactor volume under reaction conditions.

Once loaded, reactors were immersed in a preheated, isothermal fluidized sand bath for the desired amount of time and then promptly removed and cooled in water. Upon cooling, the reactors were emptied into 50-mL centrifuge tubes, and 25 mL of distilled water were used to rinse the reactor housing. The reaction mixture was centrifuged (10,000 RCF x 5 min) to pellet the hydrochar, and the supernatant (i.e., aqueous phase) was transferred to a new tube. The solids were rinsed with 5 mL of distilled H<sub>2</sub>O, briefly vortexed, and centrifuged again prior to drying (65 °C for 24 h). The wash water was combined with the aqueous phase and the total volume of aqueous phase was diluted to 50 mL with distilled H<sub>2</sub>O. Typically, multiple HTC reactions were pooled to produce enough diluted aqueous phase for growth experiments involving 4 BCRs, with some material being frozen for analysis.

The solids from each reaction were analyzed to determine the solids yield (g dry hydrochar/g dry biomass reacted), the lipid retention in the hydrochar (g lipid in hydrochar/g lipid in biomass reacted), and the elemental composition (C, H, N measured by Micro Analysis Inc.).

### 7.2.3 Media and aqueous phase analysis

The cell-free supernatants taken from BCR samples and the aqueous phase samples were analyzed as described in Section 3.2.2. The C, N, and P contents of the aqueous phase were determined by difference from the masses and elemental composition of the feedstock and hydrochar. As previously discussed, because processing of *N. oculata* biomass at even harsher conditions (250 °C) resulted in <1 wt % of the biomass converted into gas-phase products (Valdez et al., 2012), we assume that any C, N, and P not retained in the hydrochar becomes dissolved in the aqueous phase. Regrettably, our attempt to directly analyze the C, N, and P content in the brackish culture water of the BCRs over time was not successful. The use of Hach kits and the TOC machine did not provide reliable data in the brackish water matrix. Another attempt to use a micro-scale total nitrogen analysis (potassium persulfate digestion with UV detection) was equally disappointing. Similarly, the salt content of the BCR samples prevented their direct analysis by Fourier transform ion cyclotron mass spectrometry (FT-ICR-MS). Because biomass density was determined regularly and several samples were analyzed for their elemental analysis, we were able to estimate the amount of N removed from the BCR culture media. For example, if biomass density increased from 0.2 to 1 g/L over the course of 5 days and the elemental analysis of the biomass at the end of the experiment showed an N content of 9%, we estimated that 72 mg of N were removed from 1 L of media ( $0.8 \text{ g/L new biomass} \times 9\% \text{ N} = 72 \text{ mg/L N assimilated from the media and into the biomass}$ ). This analysis assumes that an insignificant amount of N is utilized for cell maintenance and neglects how the elemental composition of the biomass may have changed over time. Nevertheless, without being able to directly measure N and P uptake from the media, we

felt this approximation was useful to determine the fraction of N in the aqueous phase that was bio-available.

#### 7.2.4 Analysis of lipids within algal biomass and hydrochars

Lipids from all classes in algal biomass and carbonized solids were simultaneously extracted and catalytically transesterified to determine the total lipid content, as described previously in Section 2.2.6.

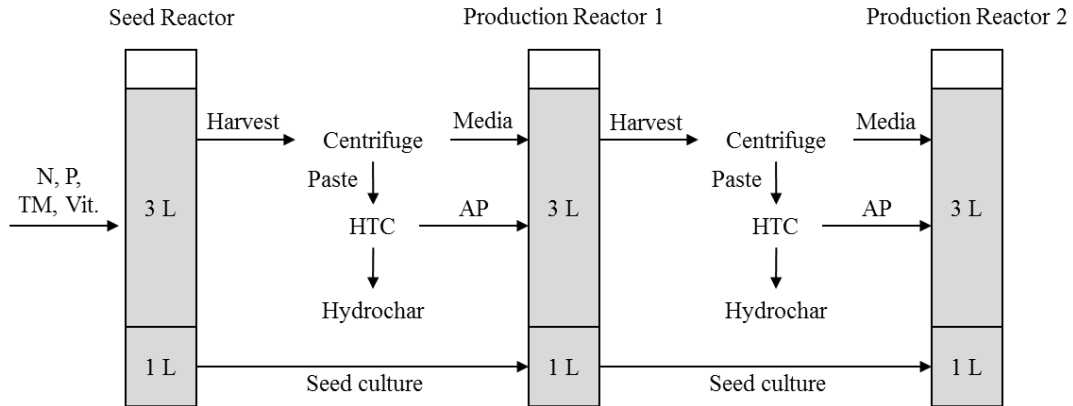
### 7.3 Results and Discussion

#### 7.3.1 Culture description and preliminary experiments

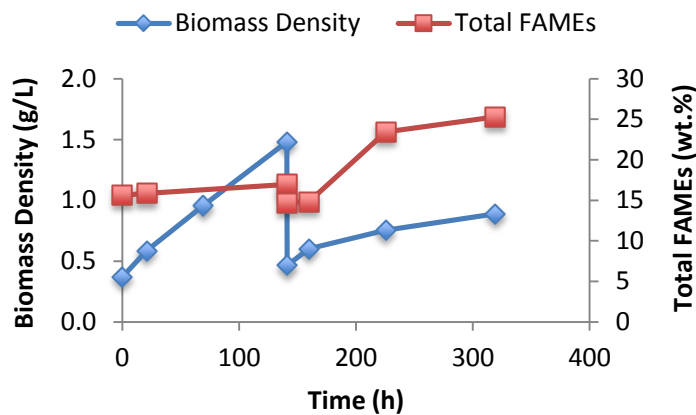
Several growth experiments were carried out to determine the biomass and lipid productivity of a two-stage production system. We utilized a bi-culture that developed over time in our lab by stressing an outdoor open pond culture of *Nannochloropsis* with excessive metals (Section 2.1.4, pg. 14). The metal-tolerant species that emerged as stable members of the photosynthetic community were tentatively identified using light microscopy, anecdotal evidence from the pond operators, and literature values for the fatty acid profile of each species (Table 2.4). Both species have been shown to consume organic nutrients in both the light and dark (Thomas, 1966; Yang et al., 2002; Park et al., 2012), leading us to hypothesize that this multi-species community would be able to consume a greater variety of dissolved organic nutrients in the aqueous phase relative to what one organism could utilize alone. Several preliminary experiments were performed to demonstrate the stability of this bi-culture over time and ascertain appropriate concentrations of N and P in the f/2 media to support growth to about 1 g/L biomass density.



a)



b)



c)



d)



Figure 7.1. (a) Schematic of the repeat batch growth system utilized in this experiment. A 4-L bubble column reactor containing a 5-day old N-replete culture (grown on f/2 media with 93 mg/L N as urea, 11 mg/L P, 1x trace metals (TM) and vitamins) served as the seed reactor. A 1-L portion of the seed reactor was transferred to the first production reactor while the remaining 3 L were centrifuged to a paste and reacted to produce aqueous phase (AP, middle row of Table 7.1) for the first batch (0-141 h). At hour 141, 1 L of the first production reactor was transferred to a second production reactor while the remaining 3 L were centrifuged to a paste and reacted to produce AP (last row, Table 7.1) for the second batch (142-320 h). The liquid liberated by the centrifugation of both 3-L harvests was recycled without any pretreatment to the production BCRs and a small amount of make-up saltwater was added to bring the initial volume of each BCR to 4 L. (b) Biomass density and total lipid content over time in repeat batches containing aqueous phase. At the conclusion of the second batch (320 h), 50 mL of the culture were centrifuged at 5000 RCF for 5 min (c) to observe non-algal material which appeared on top of the green pellet. This orange material was tentatively identified as bacteria and yeast cells and was compared to a pellet obtained by centrifuging 50 mL of a 6-day old seed reactor containing f/2 control media.

In one preliminary experiment, we sought to demonstrate that media recycling and repetitive use of cultures grown on aqueous phase could be reliably carried out in our laboratory BCRs (Figure 7.1). We grew N-rich biomass in f/2 media containing 93 mg/L N as urea to produce a seed culture and aqueous phase for production BCRs. One liter of this culture was reserved as a seed for the experiment, while 3 L were harvested to produce paste for the HTC reaction (Table 3.7). The media liberated during centrifugation was returned to the BCR, most likely supplying a small amount of leftover N and P. The aqueous phase was added (Table 7.1, middle row) and biomass growth and lipid content were tracked for almost 6 days (Figure 7.1b). During this time, biomass density increased steadily at an average rate of 7.9 mg/L-h while the lipid content remained steady at around 16% FAMES. Three liters of this culture were then harvested to produce additional paste for HTC (Table 3.7), leaving 1 L behind as seed for the second batch. Again, the 3 L of spent media liberated during harvesting were returned to the BCR along with the aqueous phase (Table 7.1, last row).

Table 7.1. C, N, and P content in the aqueous phase co-product<sup>a</sup> from hydrothermal carbonization (mg in aqueous phase per 1 g dry weight reacted)

Sample	C	N	P
<i>N. oculata</i> <sup>b</sup>	223	39	5.3
BCR-grown biomass (N-replete)	192	45	5.5
BCR-grown biomass (aqueous phase)	190	20	5.5

Notes. <sup>a</sup> Aqueous phase nutrient content determined by difference from the masses and elemental composition of the reactant feedstock and hydrochar product. Biomass P content and hydrochar P retention were assumed to be 0.9% and 43%, respectively, for all samples although it was only measured for the reaction containing *N. oculata*. All data were obtained from reactions containing about 23 g of paste (~15% solids) reacted at 200 °C for 15 min.

As shown in Figure 7.1b, the biomass density increased over time in the second batch, albeit more slowly than in the first batch, but the lipid content climbed to 25% by the end of the experiment. Notably, the fatty acid profile of the biomass changed as lipids accumulated over time, as evidenced by comparing the columns in lower half of Table 3.7. These data show an increase in the percentage of oleic acid (C18:1), which is commonly associated with triglycerides in cytoplasmic oil bodies in green algae, and a decline in the percentage of linolenic acid (C18:3), which is commonly found in polar

membrane lipids (Harwood and Jones, 1989; Thompson, 1996). This effect was even more pronounced at the conclusion of the second batch (320 h) when the lipid content was at a maximum. Most likely, biomass growth slowed and lipid accumulation occurred as a result of N limitation in the media because no supplemental N was added beyond what was in the aqueous phase. Based on the amount of new biomass generated during the second batch, its N content, and amount of N in the aqueous phase this BCR received, we estimate that about 75% of the N in the aqueous phase was utilized. It is also possible that the culture was inhibited due to refractory components in the aqueous phase or recycled media that became more concentrated in the second batch, although we have no direct evidence to support or refute this theory. In one case, spent media could reportedly be recycled up to four times in a *Nannochloropsis* culture with no apparent effects on productivity (Quinn et al., 2012). Another possibility is that non-algal contamination, which was observed both microscopically as well as in an orange layer that appeared above the green algae pellet during centrifugation (Figure 7.1c,d), diminished growth rates through competition for nutrients, increased shading of photosynthetic cells, and/or the secretion of inhibitory substances. Because the BCRs were not operated under sterile conditions and the aqueous phase was rich in organic nutrients, it is not surprising that after more than 13 days, a variety of mostly heterotrophic contaminants (e.g. bacteria and yeast) were found in this culture.

Based on these results, we hypothesized that a two-stage production process would permit better control of contamination (Figure 7.2). In the first stage, a seed culture is grown in brackish water containing synthetic media components such as urea and sodium phosphate. The majority of this culture serves as the seed for several larger production reactors, while a fraction remains in the seed reactor to produce material for the next batch. The production reactors are filled to capacity with brackish water or recycled media from the previous harvest as well as aqueous phase derived from processing the previous harvest. Because the aqueous phase typically contains about ~50-60% of the N and P of the reactant biomass and we seek to achieve roughly the same harvest density

on each batch (~1 g/L), we expect that some supplemental N and P would be required in the production reactors. We envision that this supplemental N and P could be delivered directly to the production reactors at the time of seeding, perhaps by dissolving the chemicals in the aqueous phase prior to its addition, or be contained within the seed culture by formulating a high-strength medium for the first stage. This two-stage growth process, which relies on repeat-batch and batch-processing, will likely afford better culture stability and more flexible harvest scheduling (i.e., batch time could readily be changed to account for diurnal and seasonal variability) compared to a continuous system. The impact on overall lipid productivity of supplemental N, P, and other media components, as well as media recycling and aqueous phase dosing, were therefore investigated.

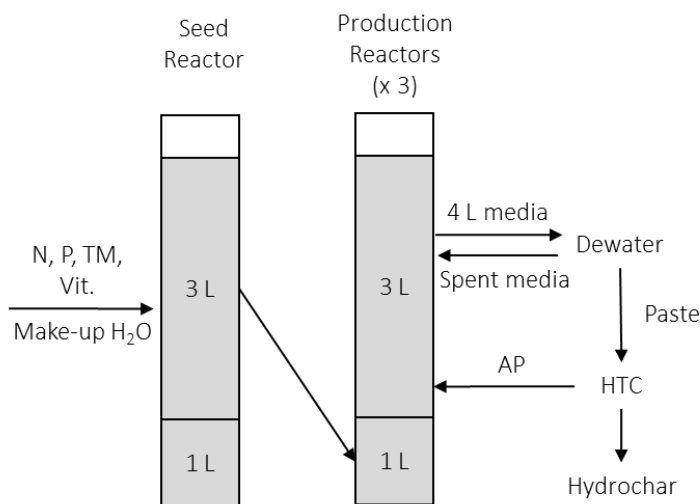


Figure 7.2. Schematic of proposed two-stage growth system with one repeat batch seed reactor and three batch or fed-batch production reactors. In this illustration, 75% of the seed reactor is used to seed three production reactors at 25% of their total volume while 25% of the seed reactor is retained to produce new seed material. These amounts are used here for illustration; in reality the percentages may vary. The seed reactor receives synthetic media components (N, P, trace metals (TM), and vitamins), along with make-up H<sub>2</sub>O to account for evaporative losses. The production reactors are initially filled with brackish water to their maximum volume (4 L), operated until the biomass density is about 1 g/L, and then the entire 4-L volume is harvested. The biomass is dewatered to produce a paste for HTC, which yields the aqueous phase (AP) co-product that is returned to the production reactors along with the spent media for subsequent batches. Additional nutrients can be added to the production reactors directly or by formulating a high strength medium for use in the seed reactor.

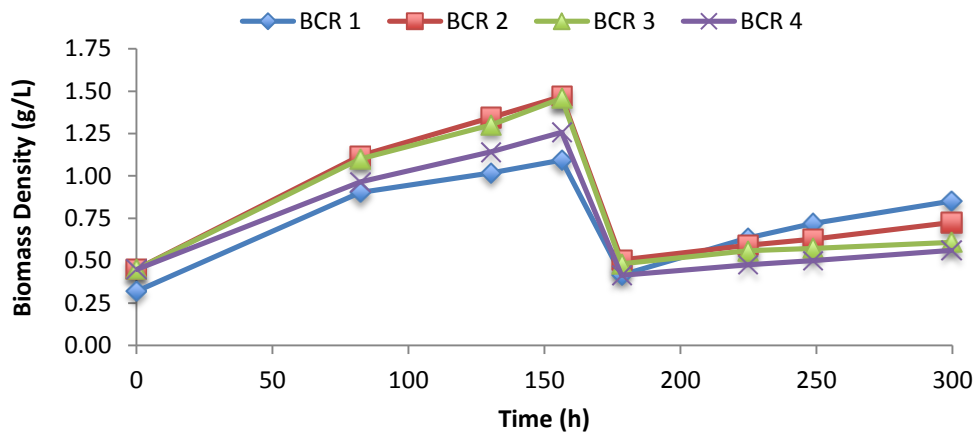
### 7.3.2 Biomass and lipid productivity with model aqueous phase

After these initial experiments, we next compared growth in the f/2 control media with growth in three treatments containing aqueous phase and various amounts of media supplements (Figure 7.3). Because there was not sufficient biomass from a previous harvest to produce aqueous phase for this experiment, commercially available *N. oculata* was reacted (200 °C for 15 min) to produce aqueous phase (Table 7.1, top row). Each 4-L BCR was setup with a 1-L seed culture from a previous batch along with 3 L brackish water containing various amounts of N, P, trace metals, vitamins, and aqueous phase. BCR 1 contained the complete f/2 medium with 17.5 mg/L N as urea, 11.2 mg/L P, and the normal amount of trace metals and vitamins. BCR 2 contained the complete f/2 media but with half the amount of N and P as BCR 1 plus 50 mL of aqueous phase. BCR 3 contained brackish water with 8.8 mg/L N as urea, 50 mL of aqueous phase, and no other media components. A final treatment (BCR 4) contained fresh brackish water with 50 mL of aqueous phase. Each reactor received the same volume of aqueous phase, corresponding to the amount generated from harvesting and reacting 4 L of a 1 g/L culture, and was estimated to add 234 mg/L C, 41 mg/L N, and 5.5 mg/L P to the initial media. In this experiment, BCR 1 represented the first stage of an algal biorefinery that we envision producing the seed culture for production reactors (BCRs 2-4).

As shown in Figure 7.3a, all treatments containing aqueous phase grew faster than the control media up until hour 156, when the cultures were diluted to study the effect of higher per-cell irradiance on lipid accumulation. Most likely, aqueous phase led to higher growth rates and final densities by providing a source of organic nitrogen and as well as carbon that supported mixotrophic growth (Liang et al., 2009; Gim et al., 2013). This outcome is similar to a recent report in which *Nannochloris* was found to grow significantly faster in f/2 media supplemented with yeast extract compared to f/2 media without organic nutrients (Park et al., 2012). Notably, there was very little difference in biomass density over time between the two treatments receiving aqueous phase plus supplemental N (BCRs 2 and 3), suggesting that the addition of P, vitamins, and trace

metals was not necessary to support growth at these levels. This is likely because the aqueous phase provides some of these nutrients and because added vitamins are superfluous in a mixed culture containing algae, cyanobacteria, and bacteria (Droop, 2007). There was, however, a noticeable effect of the supplemental N; the treatment that received only aqueous phase (BCR 4) grew to a slightly lower density by 156 hours compared to aqueous phase-supplemented cultures receiving extra urea.

a)



b)

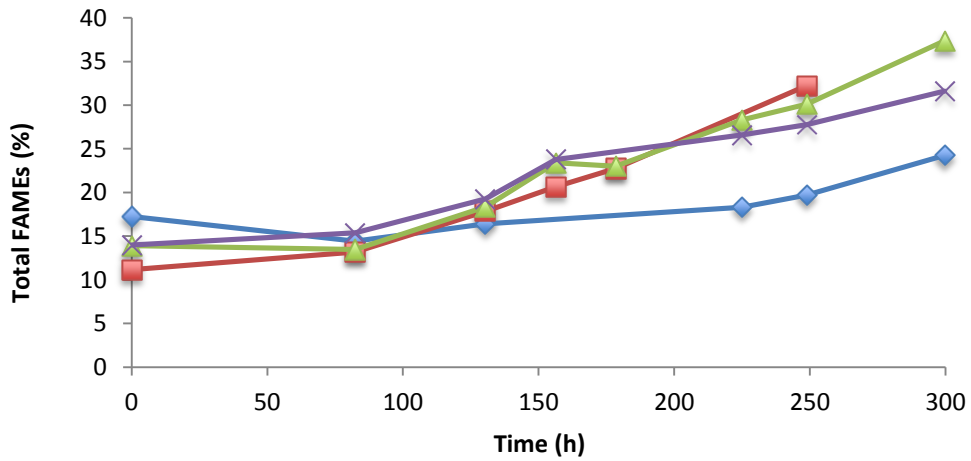


Figure 7.3. Biomass density (a) and lipid content (b) over time in cultures containing control media or aqueous phase with and without supplemental nutrients. Bubble column reactors (BCRs) contained 4-L total culture volume with the following components: (1) f/2 media with 17.5 mg/L N as urea and 11 mg/L P; (2) f/2 media with 8.75 mg/L N as urea, 5.5 mg/L P, and 50 mL of aqueous phase; (3) 8.75 mg/L N as urea and 50 mL of aqueous phase; (4) 50 mL of aqueous phase. Aqueous phase was generated by reacting *N. oculata* biomass at 200 °C for 15 min. Cultures were diluted 1:4 at 156 hours to increase irradiance per cell. Lipid data for BCR 2 at 300 h was not available.

Based on the amount of N estimated to be in the initial media, the amount of new biomass generated, and the elemental composition of this biomass, we estimated the amount of N uptake that occurred during the first 156 hours of growth (Table 7.2). In the control reactor (BCR 1), which did not contain aqueous phase, about 0.8 g/L of new biomass containing about 2.3% N was generated by 156 hours. If we assume that all the N in this new biomass was taken up from the media, we estimate that slightly more than all the urea initially present was consumed. Most likely, this minor overestimation is due to error associated with preparing the media, which could have led to slightly more urea being present initially, or error associated with determining the biomass density and its elemental composition. The complete utilization of N in the media was also apparent as the culture lost its green color and turned bright yellow by the third day. This process, termed chlorosis, is known to occur when N becomes limiting and the cell scavenges its internal N-rich components, such as green chlorophyll (Gossauer and Engel, 1996). Similar observations were recorded for *Nannochloropsis* grown in nutrient-limited media in outdoor photobioreactors (Rodolfi and Zittelli, 2009).

Table 7.2. Media N content, biomass growth, and N uptake for the growth experiment shown in Figure 7.3 (up to 156 hours)

Metric	BCR 1	BCR 2	BCR 3	BCR 4
Initial media N content from aqueous phase (mg/L)	0.0	41.0	41.0	41.0
Initial media N content from urea (mg/L)	17.5	8.8	8.8	0.0
New biomass (g/L)	0.8	1.0	1.0	0.8
Biomass N content at 156 hrs (wt.%) <sup>a</sup>	2.31	3.05	2.99	2.86
Estimated N uptake (mg/L)	17.9	31.1	30.1	23.2
Estimated N uptake (% of total)	102	62	61	56
Estimated N uptake (% of N in aqueous phase) <sup>b</sup>	-	54	52	56

Note. a Biomass N content measured by elemental analysis using CHN analyzer (Micro-Analysis, Inc.). b Estimated N uptake as a percentage of the N in the aqueous phase assumes that all urea present in the initial media was completely utilized and any remaining N assimilated into biomass was supplied by the aqueous phase.

In the BCRs that received aqueous phase, if we assume that any supplemental urea was utilized entirely, then about 52-56% of the N in the aqueous phase was incorporated into cell mass (Table 7.2). These cultures demonstrated signs of N limitation at 156 hours,

evidenced by yellowing (Figure 7.4) and some lipid accumulation (Figure 7.3b), even though the total N present in BCRs 2-4 could theoretically support 1.4 to 1.7 g/L of new biomass growth assuming 3% N in the biomass. These data suggest that only about 50-60% of the total N in the aqueous phase was utilized by the culture during this time period. We corroborated the elemental analysis of the aqueous phase N content presented in Table 7.1 by using Hach kits to measure both the total nitrogen and ammonia-N present and found that about 54% of the total N in the aqueous phase used in this experiment was in the form of inorganic ammonia (Table 3.10). Taken together, these data suggest that the algae readily consumed the inorganic N fraction of the aqueous phase during this 6.5-day cultivation.



Figure 7.4. Bubble column reactors (BCRs) in a nutrient replete state (green) and nutrient-deprived state (yellow).

With regards to the lipid content up to 156 hours, there was a slight accumulation of lipids in all treatments, with those receiving the most supplemental N having the lowest lipid content (Figure 7.3b). In the cultures with aqueous phase, the lipid content increased from about 15% to 23% total FAMES. In the control media, the lipid content fluctuated from 15 and 19%. At hour 156, each treatment was diluted by harvesting 3 L and refilling the BCR. In the case of BCR 1, new f/2 media was added exactly as was done at the beginning of the experiment. For the three other treatments, fresh brackish water was added with no other media ingredients. Following dilution, biomass density increased only very slightly in all treatments except for the control BCR, which doubled in density



over the course of about 120 hours. This difference was expected because the control reactor received the complete f/2 media.

In the case of the reactors receiving aqueous phase, the most growth occurred in BCR 2, the reactor receiving half the N and P of the control reactor as well as the full complement of f/2 trace metals and vitamins. Following the dilution event, the biomass in all four reactors accumulated lipids, most likely as a result of higher irradiance per cell and nutrient limited conditions. Although the control reactor remained green until the end of the experiment and received extra N and P, its lipid content increased to 24% at the conclusion of the experiment. This suggests that even without nitrogen limitation, increased irradiance can lead to higher lipid content as cells seek an electron sink to manage excess photons (Hu et al., 2008). In the cultures receiving aqueous phase, lipid accumulation was significantly greater than the control BCR, with the highest lipid content of 37% being achieved in the BCR that received only aqueous phase and extra urea. These data are interesting as a comparison to what might be achievable in outdoor cultures exposed to substantially more light than our laboratory BCRs. Overall, it is likely that lipid productivity throughout this work was limited by the fluorescent lighting available. In the roughly 6 days leading up to the dilution event, lipid productivity was highest in the reactors receiving aqueous phase (i.e. 1.6, 1.8, 1.5 mg/L-h for BCRs 2, 3 and 4). In comparison, the lipid productivity of the control reactor was about half, or 0.8 mg/L-h.

### 7.3.3 Biomass and lipid productivity with self-generated aqueous phase, media recycling, and various seed volumes

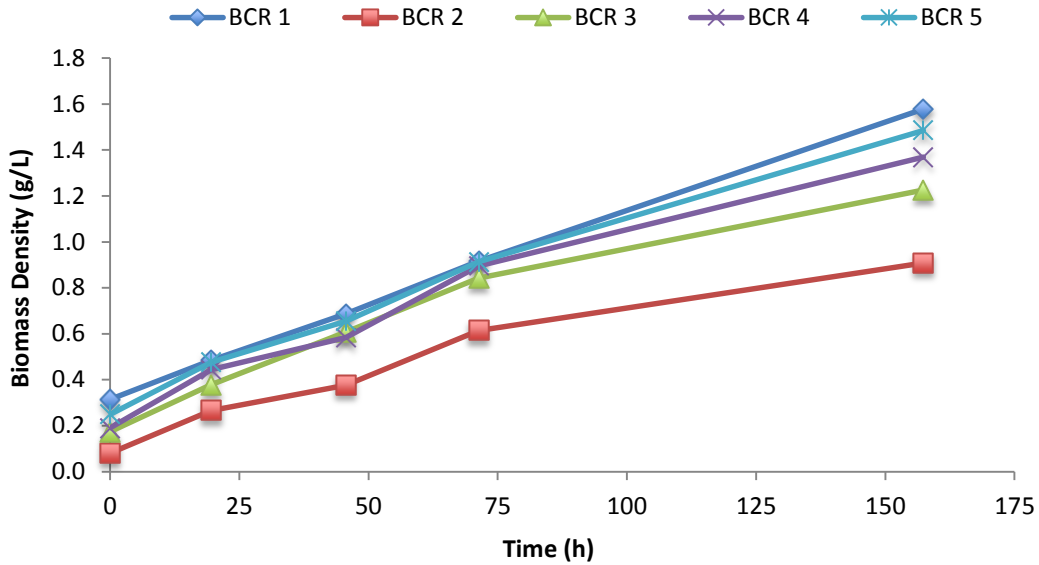
Given the success of the previous experiment, which utilized an external source of algae to produce aqueous phase, we next repeated these experiments with aqueous phase co-product from hydrothermal treatment of the algae produced in our own BCRs. Although using aqueous phase produced by reacting lipid-rich biomass grown on aqueous phase is ideally how we envision the production reactors operating, the nature of our experimental setup limited our ability to produce such biomass in large enough quantities

for subsequent studies. Our first experiments (Figure 7.1), however, demonstrated that growth on aqueous phase produced from N-rich (~9%) and N-poor (~3%) biomass can support a similar amount of biomass when normalized for its N content. As a result, four BCRs were setup again with f/2 media containing 93 mg/L N as urea to produce biomass for HTC reactions. Density in these reactors increased from about 0.3 g/L to 1.1 g/L over the course of 90 h while lipid content in the quickly growing cells remained roughly constant at about 10%. The average biomass and lipid productivity over the 90-h period was  $8.5 \pm 0.8$  and  $0.72 \pm 0.06$  mg/L-h, respectively. The biomass present at 90 h was used as a seed culture for four production reactors as well as another seed reactor (Figure 7.5). The remaining material was centrifuged to produce a paste that was reacted at 200 °C for 15 min to make aqueous phase.

In this experiment, we sought to study the effect of media recycling and seed culture size in the second stage production reactors that are grown with aqueous phase and then completely harvested after 3-5 days. As with earlier experiments, the total culture volume of all the BCRs was initially 4 L. The new seed reactor (BCR 1) received 1600 mL of seed culture and 2400 mL of complete f/2 media (46 mg/L N as urea). The production reactors (BCRs 2-5) received either 400 or 800 mL of seed culture to serve as a 10% or 20% inoculum, respectively. To fill the reactors to 4 L, BCRs 2 and 3 received fresh brackish water while BCRs 4 and 5 received recycled media from the previous harvest. This recycled media probably contained some additional N and P as well as cells that were not removed by centrifugation. Unlike previous experiments, in this one aqueous phase was added to BCRs 2-5 in a fed-batch process such that one third of the total aqueous phase dose was given on the first night and on each of the two evenings thereafter. The total amount of aqueous phase given to each BCR corresponded to harvesting and reacting 4 L of culture at about 0.85 g/L density, which was equivalent to adding 164 mg/L C, 31 mg/L N, and 4 mg/L P to each BCR. This strategy was adopted to reduce the concentration of excess organic carbon that may promote contamination, to preferentially supply carbon

at night to promote heterotrophic growth and reduce biomass losses to respiration, and to limit the concentration of inhibiting compounds, should any be present.

a)



b)

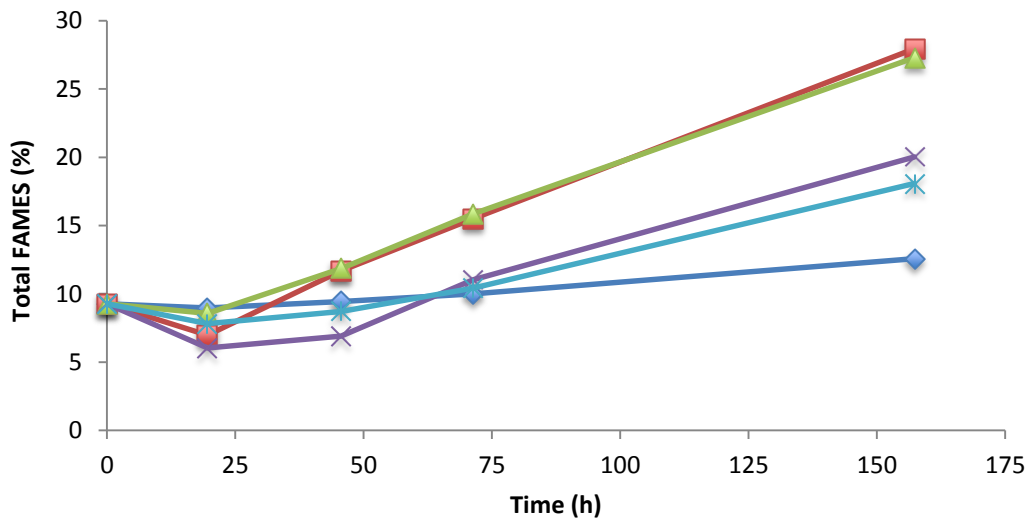


Figure 7.5. Biomass density (a) and lipid content (b) over time in cultures containing control media or aqueous phase with various seed sizes and recycled media. Bubble column reactors (BCRs) contained 4 L total culture volume with the following components: 1) f/2 media with 46 mg/L N as urea and 11 mg/L P; 2) 800-mL seed with fresh brackish water and aqueous phase; 3) 400-mL seed with fresh brackish water and aqueous phase; 4) 800-mL seed with recycled media and aqueous phase; 5) 400-mL seed with recycled media and aqueous phase. Aqueous phase was generated by reacting BCR-grown N-replete biomass at 200 °C for 15 min.

As shown in Figure 7.5a, biomass density increased over time in all cultures, with the least growth observed in BCR 2. This reactor received the least amount of seed culture, so lower densities were expected. In a true production system, we envision ponds containing aqueous phase running for only about 3-5 days, but here we took daily observations for 3 days and then allowed the cultures to continue to grow until day 6 in an effort to observe more distinct changes between them. As expected, the cultures that received recycled media reached a higher density than those receiving fresh brackish water, most likely as a result of the excess urea present and the additional biomass that was not pelleted by centrifugation. Although all reactors were, in effect, supplemented with some amount of urea and f/2 media components from the seed culture, BCR 4 and 5 was supplemented more due to the recycled media. These data suggest that recycling media for this length of time (about 250 h) does not present a significant detriment due to the build-up of inhibitors. In addition, the densities achieved in BCR 2 and 3, which contained fresh brackish water, point to the importance of determining a suitable inoculum size to reduce the time until harvest densities are reached. The 20% inoculum reached 0.84 g/L after 3 days compared to 0.6 g/L for the 10% inoculum. The difference in density after 3 days among different seed culture sizes was much less pronounced in the reactors receiving recycled media, mostly likely as a result of the additional biomass present in the media.

The lipid content in each culture increased over time after a slight initial decline (Figure 7.5b). Notably, the two cultures receiving fresh brackish water and the two cultures receiving recycled media had very similar lipid contents, with the former being higher than the latter as a result of reduced nutrient content in the media. After 3 days, BCRs 2 and 3 contained about 16% lipids whereas BCRs 4 and 5 contained about 11% total FAMES. As expected, the control reactor containing f/2 maintained a lipid content around 10% up until day 3, after which point it increased slightly to 12.5%. As shown in Table 7.3, lipid productivity was highest in BCR 3, which contained fresh brackish water and 20% inoculum. Lipid productivity increased from 1.6 (3 days) to 2.0 (6 days) suggesting that it

may be advantageous to run production reactors for longer than 3 days in order to achieve higher densities and lipid content. A similar correlation between batch length, biomass density, and lipid content has previously been reported for *Nannochloropsis* (Quinn et al., 2012).

Table 7.3 Biomass and Lipid Productivities (mg/L-h) for Growth Experiments in Figure 7.6

Metric	Bubble Column Reactor				
	1	2	3	4	5
Biomass Productivity					
0 to 71 h	8.4	7.5	9.4	9.9	9.3
0 to 157 h	8.0	5.3	6.7	7.5	7.8
Lipid Productivity					
0 to 71 h	0.8	1.2	1.6	1.2	1.0
0 to 157 h	1.0	1.6	2.0	1.7	1.6

#### 7.3.4 Scale up modeling

The data collected throughout this work were used to create a production model for an algal biorefinery producing about 3,800 m<sup>3</sup> (or 1,000,000 gallons) of biodiesel per year (Table 7.4). The model assumes there are two stages for biomass production: the first is the seed reactor that operates in repeat-batch mode to generate material for the second stage production reactors. Based on the results obtained from growth on f/2 media with urea and no organic carbon sources (BCR 1 in Figure 7.5a and Table 7.3) and growth on aqueous phase (BCR 3 in Figure 7.5a and Table 7.3), biomass productivities of 8 and 7 g/m<sup>3</sup>/h were chosen for the first and second stages of the model, respectively. At this rate, 90% of the seed reactor can be harvested every 5 days at about 1 g/L biomass density. In the production reactors, the seed culture is diluted (1:5) and then grown for 5 days until the density of 1 g/L is reached. This target biomass density was chosen because it appears to be achievable in open pond cultures, although it may be possible to reach significantly higher densities in photobioreactors (Quinn et al., 2012). Production reactors also receive the aqueous phase co-product arising from the HTC of the previous harvest. We envision a large-scale HTC reactor would process biomass paste continuously or semi-continuously, likely in a tubular reactor using scraped-surface heat exchangers. As previously mentioned, because aqueous phase is rich in organic material, these

production reactors are at a higher risk for contamination. To manage this risk, we assume that the entire volume of the production reactor will be harvested every 5 days. It may also be necessary to briefly disinfect the production reactors prior to beginning the next batch.

Table 7.4. Production model for algal biorefinery using two-stage growth scheme to produce about 1,000,000 gallons of biodiesel annually

Metric	Units	Seed reactors	Production reactors
Total culture volume	m <sup>3</sup>	62,500	281,250
Batch inoculum	m <sup>3</sup>	6,250	56,250
Batch length	h	120	120
Average biomass productivity	g/m <sup>3</sup> /h	8	7
Biomass density at harvest	kg/m <sup>3</sup>	1	1
Lipid content at harvest	% d.w.	10	20
Biomass production	MT/harvest	-	300
	MT/yr	-	18,600
Oil production	MT/harvest	-	60
	MT/yr	-	3,700
Biodiesel production	MT/yr	-	3,400
	m <sup>3</sup> /yr	-	3,800

Note. This model assumes that 90% of the volume of the seed reactor is transferred to the production reactors every 5 d to provide a 20% inoculum and that the entire contents of the production reactors are harvested at the end of each 5 d batch. It is assumed that 63 batches can occur per year in a location with ideal climatic conditions. The overall yield of biodiesel from algal oil is assumed to be 90% and biodiesel is assumed to have a density of 0.88 kg/L. Numbers rounded for clarity.

If both the seed and production reactors (345,750 m<sup>3</sup>) are taken to be 25 cm deep raceway ponds (0.25 m<sup>3</sup>/m<sup>2</sup>), then the total area required for cultivation is 137 ha. Based on the values shown in Table 7.4 for the annual lipid productivity, we estimate about 27 MT/year of lipid can be produced per hectare of pond in a location permitting year-round operation. At 20% lipid content in the harvested biomass, this amount is equivalent to about 37 g/m<sup>2</sup>-day average annualized biomass productivity. If we assume that the mass yield of biodiesel on lipids is 90% (due to losses during HTC and/or transesterification) and the fuel has a density of 0.88 kg/L, this equates to about 28 m<sup>3</sup> biodiesel/ha-yr (or 3,000 gal biodiesel/acre-yr). This value is roughly half of recent estimates for best-case lipid productivities, which ranged from 40.7 to 53.2 m<sup>3</sup> oil/ha-yr depending on location (Weyer

et al., 2010), but is about 50% higher than the open-pond productivity of 25 g/m<sup>2</sup>-day typically estimated for 20-cm deep ponds (Davis et al., 2011).

In general, our estimates for annual lipid production are higher than those from recent studies collected from large-scale marine cultures carried out in outdoor photobioreactors, but do not appear unreasonable. For example, Rodolfi et al. (2009) estimated that a two-stage growth system, in which 22% of the volume was devoted to nutrient sufficient growth and the remaining volume to lipid accumulation under nutrient deprivation, could yield 16-30 tons lipids/ha-yr depending on the latitude (Rodolfi and Zittelli, 2009). In a similar work with *Nannochloropsis* in vertical photobioreactors, Quinn et al. (2012) demonstrated average and peak lipid productivity of 7.04 and 21.1 or 13.1 and 36.3 m<sup>3</sup>/ha-yr for *N. oculata* and *N. salina*, respectively, in batches lasting between 3 and 26 days repeated over the course of 2 years (Quinn et al., 2012). These repeat batches began with media containing 70 mg/L N as NaNO<sub>3</sub> and 11.4 mg/L P and were carried out until biomass density reached 2-3 g/L and the nitrogen in the media was exhausted. The peak productivities were recorded near the summer solstice (about June 20-22 each year), pointing to the significant impact that seasonal variability plays on lipid production.

There are several reasons that our experimental biomass and lipid productivity data, when extrapolated to a large-scale facility, are higher than previously measured systems and cannot be directly compared. First and foremost, our data was collected in 4-L BCRs operating indoors under artificial illumination at near constant ambient temperatures. As a result, it likely overpredicts the productivity that could be achieved in outdoor cultures and neglects the seasonal variability that would occur at most locations outside equatorial latitudes. Moreover, it is known that data collected from a single photobioreactor are not representative of the productivity of multiple systems due to shading from adjacent systems (Quinn et al., 2012).

On the other hand, this work is the first to report the productivity of a mixed community containing both a green algae and cyanobacteria that was grown in the presence of dissolved organic materials produced by hydrothermal carbonization. Recent work has demonstrated that in some cases, an algal polyculture will yield more biomass than even its most productive species, a phenomena known as transgressive overyielding (Cardinale et al., 2011). It is also well known that mixotrophic cultures, which can utilize solar energy as well as dissolved organic compounds, typically demonstrate higher productivity than purely phototrophic or heterotrophic systems (Liang et al., 2009). This is particularly true in the case of cyclic autotrophic/heterotrophic cultures, in which a carbon source is added at the start of the dark period (Ogbonna and Tanakaah, 1998; Yang et al., 2000). Nevertheless, the increased risk of contamination associated with adding organic carbon to an outdoor pond, along with the desire to capture the energy value of this carbon to create on-site heat and power, may incentivize the use of catalytic hydrothermal gasification or related technologies that can process the aqueous phase prior to its addition to the pond (Frank, Elgowainy, et al., 2012; Frank, Han, et al., 2012). In this case, because dissolved carbon is converted into methane gas, one would expect very little additional benefit in productivity from mixotrophy relative to purely photosynthetic growth, but the aqueous phase would still serve to recycle N, P, and other nutrients. Our preliminary life-cycle assessment suggests that definitively capturing the energy value of the carbon in the aqueous phase helps improve the fossil energy ratio of the biodiesel produced and can likely eliminate the need to import electricity and natural gas for on-site operations.

#### 7.4 Conclusions

This work demonstrated that a marine bi-culture containing a green microalgae and a cyanobacteria can be grown as a biodiesel feedstock using nutrients liberated from its own biomass during hydrothermal carbonization. By dissolving biomass C, N, and P components into an aqueous phase co-product in such a way that these nutrients are bioavailable, while simultaneously producing a lipid-rich hydrochar that can be converted



into biodiesel, HTC can play a critical role in making algal biorefineries more sustainable. The use of aqueous phase must be appropriately managed to prevent unwanted contamination and optimize its utilization. By using a two-stage approach, where a clean seed culture is used to inoculate larger ponds receiving aqueous phase, our data suggest that very high lipid productivities can be achieved relative to cultures grown on only inorganic media components. Future work should focus on long-term studies with multiple batches to determine if there are negative consequences to continual media recycling, such as the buildup of recalcitrant organics that do not get consumed, and expand this work to more species or multi-species mixtures to identify those most capable of growth on aqueous phase and recycled media. Finally, consideration should be given to catalytic hydrothermal gasification and other processes that may be able to remove dissolved C and convert organic N and P compounds into readily available inorganic forms prior to recycling the aqueous phase to the algae ponds.

## CHAPTER 8

### THE ENERGY BALANCE OF ALGAL BIODIESEL PROCESSES

#### 8.1 Background

The purpose of this chapter is to address the overall energy balance of various pathways for algal biofuel production. Previous chapters have examined how feedstock characteristics and reaction conditions can impact the outcome of HTC and IST; here, we focus on how these processes fit into the broader strategy for maximizing the benefit of algae-derived fuels. We have attempted to place the experimental work carried out within the context of the on-going national dialogue regarding the sustainability of algal biofuels by quantifying the mass and energy balances for a hypothetical biorefinery capable of producing 5 billion gallons per year (BGY) of biodiesel. This production volume was chosen as it would replace about 20% of the petroleum diesel used in the US and is also consistent with recent work carried out by a consortium of national laboratories (ANL et al., 2012). Although a variety of unit operations have been proposed in the academic literature, here we compare our approach of HTC followed by SC-IST to wet hexane extraction and oil transesterification for the production of biodiesel.

It is important to recognize that algal biofuels can encompass a variety of liquid and gaseous fuels. The primary motivation for the work presented here was the production of a liquid transportation fuel, namely biodiesel. Biodiesel was chosen because it can readily replace low sulfur diesel in existing engines (i.e., B20), reduces most criteria air pollutants, and is the most prevalent commercially available biofuel today besides corn ethanol. Since the inception of this work, however, interest has grown in another liquid biofuel called renewable diesel. Instead of transesterification to convert TGs into FAME or FAEE, catalytic hydrotreating involving high pressure H<sub>2</sub> gas and sulfided mixed oxide catalysts such as NiMo and CoMo can be used to produce fully hydrocarbon, non-oxygenated biofuels (e.g., Neste Oil's NExBTL Renewable Synthetic Diesel and UOP/Eni Ecofining's Green Diesel) (Holmgren, 2007; Fernandes and Nestle Oil, 2008; Lestari et al.,

2009; Smith et al., 2009). This process has a significant advantage over transesterification in that fuel quality can be tuned using process conditions, rather than being determined by the FA profile of the harvested biomass, but it requires large amounts of H<sub>2</sub> and almost certainly necessitates shipment of extracted algae oil to a petroleum refinery. Most US refineries will not process less than 10,000 barrels/day of a new feedstock and because this quantity of oil is far beyond what any extant algae facility can produce today, hydrotreating of algal oils has been more of an academic curiosity than a commercial reality (Dr. Brian Goodall, personal communication). Because biodiesel can be produced and sold on a small scale, yet is also a viable a feedstock for hydrotreating, we decided to pursue transesterification for biodiesel production in our experimental and modeling work.

Although the focus of our experimental work on fuel conversion focused on biodiesel, the reality is that processing algae containing a typical lipid content of 10% to 25% results in more energy output in the form of gaseous fuels than liquids. Biogas, which is a mixture of roughly 60% CH<sub>4</sub> and 40% CO<sub>2</sub>, can be produced by anaerobically digesting lipid-extracted materials or subjecting them to catalytic hydrothermal gasification (CHG). The biogas can then be combusted to produce heat and electricity, which helps reduce, and in some cases totally eliminate, the need for imported electricity and natural gas. Although frequently modeled as a component of algal biorefineries in the academic literature, anaerobic digestion suffers from several drawbacks, including a sensitivity to N-rich feedstocks, the requirement for a long retention time (20-30 days), and the production of fugitive CH<sub>4</sub> emissions. Typically, the effluent of the digester is separated into liquid and solids fractions, with the liquids being returned to the algae pond and the solids being transported offsite to be applied to farmland. By exporting the digested solids, a significant amount of N and P is removed from the biorefinery and there is a high likelihood for the release of nitrous oxide (N<sub>2</sub>O), a potent greenhouse gas. By one accounting, the fugitive CH<sub>4</sub> and N<sub>2</sub>O emissions can account for up to 14% and 23%, respectively, of the whole pathway's greenhouse gas emissions (Frank, Han, et al., 2012).

Finally, the liquid fraction of the digestate, which has been estimated to contain 80% and 50% of the N and P of the original biomass, respectively, also contains a variety of organic and inorganic compounds, as well as plentiful amounts of bacteria and other microorganisms, which some research suggests may complicate its use as a nutrient source (Levine et al., 2011). As a result of these limitations, interest has grown in CHG as a promising alternative to anaerobic digestion for helping increase the energy self-sufficiency of algal biorefineries and improve nutrient recycling.

CHG involves the reaction of organic materials in hot, compressed water (~350 °C) in the presence of a catalyst to produce biogas. The technology was pioneered by the Pacific Northwest National Laboratory under the guidance of Douglas Elliott (Elliott, 2008) and was recently licensed to Genifuel Corporation. In the latest life-cycle assessment work by Argonne National Labs, it is assumed that 99% of the C in the influent material to the CHG reactor can be converted to biogas, and 95% and 90% of the influent N and P, respectively, can be recovered in the aqueous effluent (Frank, Han, et al., 2012). The N is present almost exclusively in the ammonia form while P is recovered from an apatite precipitate after reaction with sulfuric acid. In addition, the fugitive emissions of methane are assumed to be 0.2%, compared to 2% for the anaerobic digestion pathway. Although we did not carry out any experimental work with CHG, its long history in the literature with a variety of organic feedstocks suggests it is suitable for processing both the aqueous phase arising from HTC, the lipid-extracted hydrochar remaining after IST, and any lipid-extracted algae arising from a wet hexane extraction process. As will become apparent, the ability of CHG to convert nearly all non-oil C into biogas while providing for very high rates of nutrient recycling is a significant benefit to the biorefinery's energy balance.

The model we present here borrows heavily from recent efforts to integrate the life-cycle assessment work done by Argonne National Lab and the techno-economic assessment carried out by the National Renewable Energy Lab with the Resource Assessment by the Pacific Northwest National Lab (ANL et al., 2012). The goal of these efforts was to produce

a harmonized model that assessed the nation's ability to produce 5 BGY of renewable diesel. Based on modeling work that showed where freshwater algae production was likely to be most successful, as judged by the confluence of high irradiance year-round, overall water availability, and low net water losses due to evaporation, this harmonized model predicted that 446 farms of 4,850 ha each (4,050 ha pond surface area each) would be required to meet the 5 BGY target. These farms would likely be scattered along coastal regions on the Gulf of Mexico and produce biomass with an average annual productivity of 13.2 g/m<sup>2</sup>-d, or about half the value of earlier life-cycle assessments (25 g/m<sup>2</sup>-day). The model also assumed that the biomass would have a 25% lipid content, corresponding to 1,120 gal/acre of renewable diesel annually when factoring in the efficiencies of harvesting (95%) and lipid extraction (85.5%) as well as the yield of hydrotreating (78-85 wt.%). In the baseline model, the minimum product selling price was determined to be \$19.60/gal renewable diesel with a cost of production of \$9.85/gal. This techno-economic assessment highlighted that capital costs account for about 70% of the diesel selling price and suggested that improvements in biomass productivity along with lower-cost production systems (e.g., unlined ponds) could help reduce costs substantially.

The harmonized model presented by these national labs is the result of substantial work on the part of countless individuals throughout government, academia, and industry. As a result, its findings represent the most cohesive and complete picture we have today of the environmental and economic costs associated with algal biofuel production on a large scale. Because neither HTC nor IST has been considered in this model or any previously published life-cycle assessment work, we sought to determine how these two unit operations would compare with the currently modeled processes. Due to limited resources, a complete accounting of the greenhouse gas emissions and a full techno-economic assessment for the HTC and IST processes are beyond the scope of this work. Instead, we focus on the mass and energy inputs and outputs of each unit operation within the algal biorefinery to quantitatively examine the costs and benefits associated with incorporating these two processes.

In an effort to be consistent with the Greenhouse Gases, Regulated Emissions, and Energy Use in Transportation (GREET) Model developed by Argonne National Laboratory, we considered the fuel production and use pathway in two segments: well to pump (WTP) and pump to wheels (PTW). The entire pathway is referred to as well to wheels (WTW). In the case of algal biofuels, we define WTP to include biomass production in ponds, dewatering, processing (i.e. HTC or lipid extraction), and fuel production. Because our work examined the production of biodiesel, which offsets the use of petroleum diesel, the GREET model's data for low sulfur diesel served as a comparison. The latest figures estimate that the WTP fossil energy consumption for LS diesel is about 200,150 BTU/mmBTU (DOE, 2012). Because the energy content of LS diesel is entirely fossil fuel derived, the PTW consumption of fossil energy is 1,000,000 BTU/mmBTU (note: 1 mmBTU = 1,000,000 BTU). Therefore, the WTW fossil energy ratio (FER) for LS diesel, which is defined as the energy output per unit of fossil energy input, is about 0.83. In contrast, algal biofuels, like all plant-derived biofuels, tend to have a much larger WTP energy input compared to LS diesel, but have no PTW emissions because the C in the combusted fuel is assumed to be biogenic. As a result, biofuels typically achieve FERs greater than unity, which means more useful energy is gained from these fuels than went into their production. Our goal was to determine the FER of algal biofuels produced with different technology choices and compare this to other fuel choices.

## 8.2 Methodology and model descriptions

### 8.2.1 Process overview

The mass and energy balances for a hypothetical biodiesel production facility capable of producing 5 BGY were determined using a model constructed in Microsoft Excel. A simplified process flow diagram is present in Figure 8.1. The major productivity assumptions in the model are presented in Table 8.1, which also lists the source or a brief explanation for the chosen value. Like the harmonized model described in Section 8.1, we assume algae are produced in open raceway ponds located near the Gulf of Mexico

and can achieve an annual average productivity of 13.2 g/m<sup>2</sup>-d. As this rate, about 10.5% of the pond is harvested each day. In addition, we assume evaporation occurs at a rate of 2,190 m<sup>3</sup>/ha-yr, based on estimates determined using the climatic conditions of this area. Biomass production involves supplying N and P fertilizers, assumed to be urea and diammonium phosphate, respectively, as well as CO<sub>2</sub>, which is assumed to be transported by pipeline. The biomass is assumed to contain 25% lipids, 25% protein, and 50% carbohydrate at the time of harvest, corresponding to an elemental composition of about 52% C, 8% H, 4% N, 35% O, and 1% P (Table 8.2). These values are in line with our experimental data for biomass containing 25% lipids. The elemental composition of the remaining process materials is given in Table 8.2 and reflects the yields of each element given in Table 8.3.

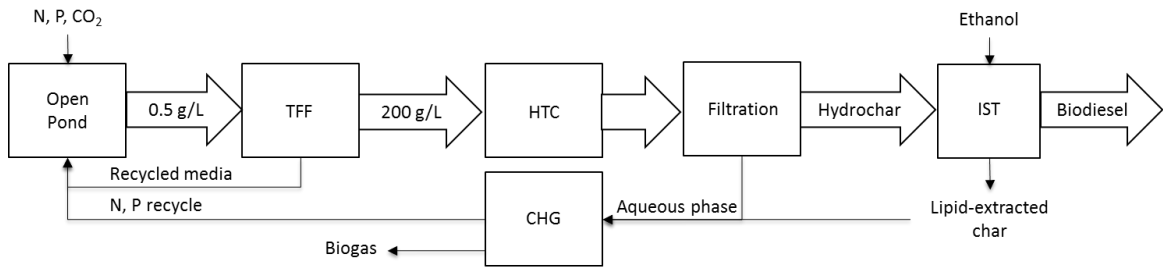


Figure 8.1. Simplified process flow diagram.

Table 8.1. Model productivity assumptions and land requirements

Metric	Units	Value	Notes and Sources
Annual average biomass productivity	g/m <sup>2</sup> -d	13.2	ANL et al., 2012
Annual average biomass productivity	MT/ha-y	48.2	Calculation
Biomass oil content	%	25%	ANL et al., 2012 and our data
Algae oil (100% theoretical)	MT/ha-y	12.0	Calculation
Yield of biodiesel on algae oil	w/w	0.98	98% yield in HTC; 95% yield in SC-IST, 105% weight conversion from TG to BD
Annual average biodiesel production	MT/ha-y	11.8	Calculation
Annual average biodiesel production	m <sup>3</sup> /ha-y	13.4	Calculation based on 0.88 kg/L density
Target biodiesel production	m <sup>3</sup> /yr	1.89E+07	5 BGY equivalent
Total pond surface area required	ha	1,414,551	Calculation

Table 8.2. Elemental composition and estimated energy content of process materials

Material	Element (wt.%)					Energy Content (MJ/kg) <sup>b</sup>
	C	H	N	O <sup>a</sup>	P	
Dry algal biomass	51.8	7.9	4.0	35.3	0.9	22.0
Dry hydrochar	57.0	7.9	3.2	31.1	0.7	24.8
Dissolved solids in aqueous phase	46.6	7.9	4.8	39.5	1.1	19.4
Biodiesel	77.1	12.2	0.0	10.7	0.0	41.0
Lipid extracted hydrochar	37.9	4.0	6.3	50.5	1.4	16.6
CH <sub>4</sub> in biogas from CHP	75.0	25.0	0.0	0.0	0.0	55.0

Notes. <sup>a</sup> The oxygen content of each material was calculated by difference on an ash-free basis. <sup>b</sup> The higher heating value of each material was estimated using the elemental composition of C, H, and N by the formula suggested by Friedl et al. (2005), with the exception of the biodiesel. The elemental composition of the biodiesel was assumed to be equivalent to ethyl oleate and its heat of combustion was taken to be just slight higher than the 40.5 MJ/kg that the GREET model uses for methyl ester biodiesel.

Table 8.3. Elemental yields

Element	Yield in Hydrochar from Biomass	Yield in Lipid-Extracted Char from Hydrochar
C	0.55	0.34
H	0.5	0.25
N	0.4	1
P	0.4	1

Notes. Based on our experimental data.

### 8.2.2 Process description and energy input assumptions

In this section we describe the major unit operations and the energy input associated with each. These values are summarized in Table 8.4. Algal growth requires electricity to run paddlewheels, pump water, and transport CO<sub>2</sub>, as well as the embodied energy in N and P fertilizers. Although previous models have incorporated a three-step dewatering process involving flocculation, dissolved air flotation, and centrifugation, we have modeled the use of tangential flow filtration (TFF) to concentrate algal biomass from 0.5 g/L in the pond harvest to 60 g/L. TFF involves pumping the algae-water mixture through pressurized membranes that remove water and dissolved solids, resulting in concentration of the algal biomass. Pall Corporation has pioneered work with TFF for algae harvesting and supplied electricity consumption information from a pilot-scale installation in Europe. Although the energy required for concentration using TFF is slightly



higher than the values assumed in the GREET model for flocculation and dissolved air flotation (which yields a similar 6% solids mixture), this approach has two major advantages: first, biomass is completely retained during TFF whereas 5% is assumed lost during flocculation and dissolved air flotation; and second, the liberated water is sterile and free of flocculants so it can be returned the pond free of contaminants. Following concentration to 6% solids, the slurry is further dewatered with a centrifuge to 20% solids, just as in the GREET model.

Table 8.4. Process energy input assumptions

Metric	Units	Value	Notes and Sources
<b>Growth</b>			
Off-site water pumping	MJ/m <sup>3</sup>	0.44	ANL et al., 2012
On-site water pumping	MJ/m <sup>3</sup>	0.09	ANL et al., 2012
Paddlewheels	MJ/ha-yr	63,072	ANL et al., 2012
CO <sub>2</sub> transport	MJ/MT CO <sub>2</sub>	76.3	ANL et al., 2012
CO <sub>2</sub> required	MT/MT biomass	2.5	Assumes 75% efficiency in uptake
N fertilizer (urea, N)	MJ/kg	65.4	EcoInvent Database
P fertilizer (Daqueous phase, P)	MJ/kg	4.8	EcoInvent Database
<b>Dewatering</b>			
Tangential Flow Filtration	MJ/m <sup>3</sup>	1.368	Doug Dilillo, personal communication
Centrifuge	MJ/kg biomass	0.0684	Frank et al. (2012)
<b>HTC</b>			
Reaction (200 °C x 15 min)	MJ/MT biomass	840	Calc. from reaction model
Filtration	MJ/MT hydrochar	3.0	Doug Dilillo, personal communication
Drying char	MJ/MT biomass	840	85% efficient dryer (2.65 MJ/kg H <sub>2</sub> O)
<b>SC-IST</b>			
Reaction	MJ/MT biomass	425	Calc. from reaction model
Filtration	MJ/MT LEC	3.0	Doug Dilillo, personal communication
Desolventize LECs	MJ/kg EtOH	0.98	85% efficient dryer
Ethanol	MJ/kg EtOH	21	Calc. from 27.3 MJ/kg and 1.3 FER
<b>CHG + Biogas Combustion</b>			
Reaction	MJ/MT biomass	1295	Calc. from reaction model
Efficiency to Electricity	%	33	ANL et al., 2012
Efficiency to Thermal	%	43	ANL et al., 2012

The 20% solids slurry is then reacted by HTC or subjected to high pressure homogenization and hexane extraction to remove lipids. HTC involves a 15 min reaction at 200 °C in a pressurized reactor, yielding a wet hydrochar (50% solids yield, 40%

moisture content) and an aqueous phase product containing 45%, 60%, and 60% of the C, N, and P of the original biomass. Based on our experimental work, we assume that 98% of lipids are retained in the hydrochar product. The HTC reaction mixture is filtered using a centrifugal discharge filter (Pall Corporation), and 95% of the moisture in the wet hydrochar is evaporated on the filter elements by the addition of hot air. We assume that like most high temperature industrial processes, suitable heat integration will permit recovery of 75% of the thermal energy required to perform HTC. For example, hydrothermal upgrading, a commercial-scale process for hydrothermal liquefaction, reportedly achieves 75% thermal efficiency (Goudriaan et al., 2000). For the drying process, however, we have assumed no heat recovery is involved. The aqueous phase collected from HTC is assumed to be reacted by CHG, during which 95% of its C content is removed in the form of biogas. Likewise, we assume that 95% of the N and P in the aqueous phase will be recovered in a usable form from the CHG effluent.

In contrast, for the lipid extraction process described by the GREET model (Table 8.5), the 20% solids slurry is passed through a high-pressure homogenizer to lyse cells and then contacted by a volume of hexane equivalent to 5 times its volume. Following some time allowed for extraction, the organic and aqueous layers are then separated by centrifugation and the organic layer is heated to remove hexane. Some hexane is assumed to be lost (5.2 g/g biomass) and the overall efficiency of both steps is assumed to be 85.5%. The aqueous phase, which contains a small amount of entrained hexane and the lipid extracted biomass is then assumed to be reacted by CHG, yielding biogas and an aqueous effluent that contains 95% of the N and P of the original biomass.

Table 8.5. Homogenization, extraction, and transesterification process assumptions

Metric	Units	Value
Homogenization + Hexane Extraction		
Homogenizer electricity	MJ/MT biomass	734.4
Extraction electricity	MJ/kg oil	0.2484
Extraction heat	MJ/kg oil	11.16
Lost hexane	MJ/kg	61.3833
Transesterification		
Methanol	MJ/kg MeOH	35.4
Heat	MJ/kg BD	11.160
Electricity	MJ/kg BD	0.2484

Note. Values taken from the harmonized GREET model (ANL, 2012).

Next, the dry hydrochar and the extracted algae oil are reacted to produce biodiesel. In our model, the hydrochar is reacted with supercritical ethanol at 270°C. In the GREET model, the algae oil is subjected to traditional transesterification using methanol, as described in Table 8.5. In the case of SC-IST, we assume no energy is required for ethanol recycling because relatively low amounts of ethanol are used (5:1 EtOH:FA ratio, equivalent to about 0.4 EtOH:solids) and azeotropic ethanol is flashed off from the hot reactor effluent. The energy required to heat the ethanol, hydrochar, and water present was calculated using Aspen Plus, and the performance of the flash drum to separate ethanol was confirmed. Also, we again assume that 75% of the energy input to SC-IST of the hydrochar is recovered. The biodiesel yield from SC-IST is assumed to be 95% and there is a 105% theoretical mass yield based on the molar conversion of 1 TG to 3 FAEE. The traditional transesterification process is assumed to be 99% efficient based on the GREET model. Both processes will require some form of cleanup step where N, P, and unreacted glycerides are removed from the biodiesel, and we assume this involves membrane filtration with only negligible pumping costs. In the case of the biodiesel produced from the hydrochar, we assume the membrane retentate would be combined with the lipid-extracted hydrochar and any glycerol co-product and reacted by CHG. Although not specified, we assume the values for energy input for transesterification in the GREET model account for all the steps required to convert raw algae oil into road-ready biodiesel. Finally, for the energy input to the CHG process, we assume that all parts

of the algae biomass that did not become biodiesel are reacted as a 20% solids mixture at 350 °C.

### 8.3 Results and Discussion

#### 8.3.1 Mass and energy flow of product streams

The mass and energy flows for the model algal biorefinery we created are presented in Table 8.6. In order to produce about 5 BGY of diesel (equivalent to about 16.7 million MT/yr), about 68.2 million MT of algal biomass is required. Notably, roughly equal amounts of C (equivalent to 36% of the carbon in the original biomass) ends up in the biodiesel and the methane generated during CHG. The remainder is lost as CO<sub>2</sub> in the biogas as well as a small fraction that remains in the aqueous effluent of the CHG reactor (which we excluded from our analysis). In terms of N and P, our model assumes the hydrochar contains about 40% of the N and P in the original biomass, but because both the aqueous phase from HTC and the lipid-extracted char following SC-IST are processed by CHG, about 95% of the N and P is captured and recycled to the pond. The remainder is assumed lost, either to volatilization or some other process (e.g., precipitation during CHG).

When considering the energy content of each material, it is noteworthy that the final biodiesel product contains the equivalent of 46% of the energy content in the original biomass whereas the methane contains about 63%. These two numbers sum to greater than 100% due to the addition of ethanol, which adds to the energy content of the biodiesel. So although the purpose of the algal biorefinery was ostensibly to create liquid fuels, in reality more than half of the solar energy captured by the algae was converted into a gaseous fuel used to produce on-site heat and power. This is analogous to how sugarcane bagasse is combusted as a solid fuel to power ethanol refineries in Brazil. Because liquid fuels have more value than solid fuels used in stationary generators (cf. 0.25¢/MJ for coal to 3¢/MJ for diesel based on 2013 prices in the US), it is desirable from a financial perspective to increase the lipid content of the algae as much as possible to

shift the final product blend towards liquid fuels. However, as Frank et al. (2012) pointed out in their analysis on hydrothermal liquefaction, if the yield of liquid fuels increases at the expense of the ability to produce heat and power on-site, the greenhouse gas emissions associated with the liquid fuel can rise significantly as grid energy is imported. In their analysis, this tipping point occurred when the yield of bio-oil exceeded 0.4 g/g-biomass.

Table 8.6. Mass flows in model algal biorefinery for 5 BGY biodiesel production (baseline case)

Material	Millions of MT/yr				Percent of biomass (%)			Total Energy MJ/yr x 10 <sup>10</sup>
	Total	C	N	P	C	N	P	
Dry algal biomass	68.2	35.3	2.7	0.6	-	-	-	150
Dry hydrochar	34.1	19.4	1.1	0.2	55	40	40	85
Dissolved solids in aqueous phase	34.1	15.9	1.6	0.4	45	60	60	66
Biodiesel	16.7	12.8	0.0	0.0	36	0	0	68
Lipid extracted hydrochar	17.4	6.6	1.1	0.2	19	40	39	29
Methane in biogas	17.1	12.8	0.0	0.0	36	0	0	95

### 8.3.2 Energy inputs, generation, and FER

The process we have modeled has the potential to produce algal biofuels with a positive net energy ratio. A summary of the energy use and generation is presented in Table 8.7, and a graphical representation of the contribution of each unit operation to the total energy demand for the baseline case is given in Figure 8.2. For the interested reader, a detailed breakdown of the energy inputs for the baseline case is given in Table 8.8. Table 8.7 also includes three additional cases which illustrate the sensitivity of the model to biomass productivity, lipid content and nutrient recycling.

This modeling effort suggests that a well-integrated algal biorefinery can actually produce more energy than it requires. As shown in Table 8.7, a surplus of thermal energy is generated by the CHG process in all cases examined, thereby obviating the use of natural gas. It is noteworthy that our baseline model predicts that almost 2.5-fold more heat is produced by CHG than is required for HTC, SC-IST, and CHG itself. We assume, as Frank

et al. (2012) did, that this excess heat is unrecoverable, but we note that there may be opportunities to use it to heat ponds (especially during winter) and thereby improve productivity (Frank, Elgowainy, et al., 2012). In contrast, electricity demand is slightly higher than the supply from biogas combustion in the baseline case, thereby requiring electricity from the national grid that has substantial upstream energy inputs (3.03 MJ total energy/MJ consumed) as well as associated greenhouse gas emissions. Although this is a very small amount of electricity in the baseline case, it has a more significant impact when the biomass contains 50% lipids and there is less material available to produce on-site heat and power through CHG. As discussed above, although there are economic incentives to shift the product stream toward liquid fuels, there is an environmental trade-off due to increased amounts of imported energy. One way to mitigate this would be to co-locate renewable electricity generation (e.g., wind turbines or solar panels) with algae farms to utilize non-fossil fuel resources to meet power demands.

Table 8.7. Summary of energy use and generation

Metric	Energy (kJ/MJ biodiesel)			
	Baseline Case	Higher Productivity (25 g/m <sup>2</sup> -d)	Higher oil content (50%)	Less nutrient recycling (50%)
Total on-site energy consumed				
Electrical energy	461	398	230	461
Thermal energy	268	268	127	268
Off-site energy consumed	95	95	86	215
Total on-site generation				
Electricity	460	460	189	460
Heat	599	599	246	599
FER (biodiesel only)	10.1	10.5	4.7	4.6

Note. No fertilizer credit is given for N and P leaving the algal biorefinery; it is considered lost.

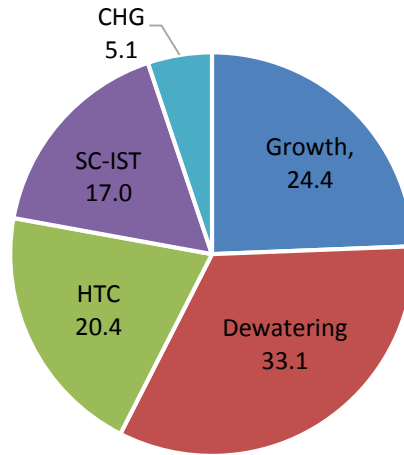


Figure 8.2. Summary of energy use as a percentage of the total energy consumed

The data in Table 8.7 can be used to calculate the FER for the algal biodiesel. In addition to the grid electricity required, the energy inputs for fertilizers and ethanol cannot be offset by on-site generation. In our baseline model, because nutrient recovery from CHG was so high (95%), fertilizer demand was low and only accounted for less than 2% of total energy demand. Ethanol consumed by the biodiesel reaction, however, resulted in about 10% of total energy demand. Overall, our baseline model predicts that algal biodiesel can be produced with a FER of about 10.1, meaning more than 10 times more energy is gained from its use than went into its production. In the case where productivity is higher (25 g/m<sup>2</sup>-d), there is a slight improvement in FER due to reduced electricity demands associated with growing the algae (e.g., paddlewheel mixing). With a higher lipid content, the FER drops by almost half due to increased demand for grid electricity, even though there is a slight decline in fertilizer use. Finally, a similar reduction in FER is observed when nutrient recycling is only 50% due to the high demand for N and P fertilizers. Note however, that our model does not allocate fertilizer credits to any N and P that does not return to the ponds; instead, we considered the fertilizer value of the material lost.

Table 8.8. Detailed summary of process energy inputs

Metric	Energy input (kJ/MJ biodiesel)	Percentage of total on-site energy used (%)
<b>Growth</b>		
Off-site water pumping	2.0	0.2
On-site water pumping	35.9	4.4
Paddlewheels	131	15.8
CO <sub>2</sub> transport	19.0	2.3
N fertilizer (urea, N)	13.1	1.6
P fertilizer (DAP, P)	0.21	0.0
Sum	201	24.4
<b>Dewatering</b>		
Tangential Flow Filtration	273	33.1
Centrifuge	0.01	0.0
Sum	273	33.1
<b>HTC</b>		
Reaction (200 °C x 15 min)	83.8	10.2
Filtration	0.1	0.0
Drying char	83.8	10.2
Sum	168	20.4
<b>SC-IST</b>		
Reaction	42.4	5.1
Filtration	0.1	0.0
Desolventize LECs	15.8	1.9
Ethanol	81.7	9.9
Sum	198	17.0
<b>CHG</b>		
Reaction	42.4	5.1

These FER data are within the range typically reported for algal biofuels but considerably higher than the latest assessment presented by the consortia of national labs, which estimated a FER of 1.5 (ANL et al., 2012). Frank et al. (2012) estimated that the lipid extraction pathway would produce renewable diesel with a FER of about 3.5 compared to 2.5 for hydrothermal liquefaction (Frank, Elgowainy, et al., 2012). For reference, the latest iteration of the GREET model estimates a FER of 5.4 for soy-based biodiesel and 2.1 for E85 (85% ethanol and 15% gasoline blend). In all cases, these biofuels outperform low sulfur diesel, which has a FER of 0.8. Although FER is an important metric to consider, future analysis should more carefully assess the greenhouse gas emissions associated with algal biofuel production. Because the fuel-conversion step contributes only a minor



amount in a biofuel's lifecycle greenhouse gas emissions, this analysis was not performed here; however, work by Frank et al. (2012) has shown that algal biofuels can significantly reduce greenhouse gas emission compared to low sulfur diesel, and we expect HTC and SC-IST to only improve those metrics.

### 8.3.3 Comparison to traditional wet hexane extraction and transesterification process

In comparison to the traditional wet hexane extraction and transesterification process, the combination of HTC and SC-IST compares favorably. As shown in Table 8.9, these two processes together consume about 769 kJ/MJ biodiesel in comparison to 366 kJ/MJ biodiesel for both HTC and SC-IST (Table 8.8). This suggests that the processes developed through our experimental work have the ability to cut algae oil processing energy costs in half. On the one hand, this could be considered a substantial benefit, but on the other hand, this could be considered a relatively insignificant accomplishment considering that most of the energy required for extraction and transesterification is thermal energy that is produced in surplus anyhow. Nevertheless, by obviating the use of hexane, there is likely to be a reduction in noxious air pollution and overall lesser dependence on fossil energy inputs. Although a full techno-economic assessment is beyond the scope of this work, and the cost of oil transesterification or hydrotreating is typically less than 10% of the overall production cost per gallon of the final biodiesel product (ANL et al., 2012), it is possible that HTC and SC-IST may offer a lower cost alternative to hexane extraction and traditional transesterification.

Table 8.9. Energy required for traditional wet hexane extraction and transesterification

Metric	Energy input (kJ/MJ biodiesel)
Homogenization + Hexane Extraction	
Homogenizer electricity	81
Extraction electricity	6.9
Extraction heat	309
Lost hexane	8.8
Sum	407
Transesterification	
Methanol	84
Heat	272
Electricity	6.1
Sum	362

## 8.4 Conclusions

The modeling work presented in this chapter describes a hypothetical algal biorefinery capable of producing 5 BGY of biodiesel. Using assumptions gathered from the literature and our own experimental work, we determined that it is possible to produce net energy positive biodiesel from algae. In particular, we demonstrated that the combination of HTC and SC-IST can significantly reduce the energy associated with algal biodiesel processing compared to wet hexane extraction and transesterification. Although we performed experimental work to better understand the growth and processing of algal biomass, as well as develop new tools for in situ transesterification, several key technologies required to make this facility a reality are not yet commercially viable. In our opinion, the most important unit operation is actually the one we studied least: catalytic hydrothermal gasification. Without the ability to convert the non-lipid fraction of algae into usable energy and recycle a very high percentage of the N and P required in the process, algal biorefineries will struggle to remain net energy positive and fertilizer demand will far outpace global supply as the industry grows. In our experimental work, the aqueous phase from HTC was fed directly to algal reactors as a nutrient source instead of being first processed by CHG to remove the carbon and convert organic nutrients into inorganic forms. Although we suspect so, we were unable to collect conclusive evidence that the organic carbon fraction of the aqueous phase was utilized by growing algae and incorporated into new biomass. Considering that every species is likely to differ in the forms of organic carbon it can utilize and that excess carbon in an open pond will invite contamination, the use of CHG to remove this carbon and convert it into energy is a prudent decision. Future work should focus more intently on various strategies to process the non-lipid fraction of microalgae in an effort to improve the energy balance and reduce the fertilizer requirements associated with algal biofuel production.

## CHAPTER 9

### SUMMARY AND ENGINEERING SIGNIFICANCE

Microalgae hold great promise for biofuels, but efforts to commercialize liquid transportation fuels from this feedstock have been stymied by the high costs associated with biomass production and processing. As technology improves, costs diminish, and this nascent industry begins to expand, a more significant hurdle will be faced: access to land, water, and fertilizers in sufficient quantities to support large-scale production. In an effort to both reduce processing costs and utilize resources wisely, our work focused on the development of a novel processing strategy consisting of hydrothermal carbonization and in situ transesterification. We demonstrated that algal biomass can be effectively reacted in subcritical water to yield a hydrochar that retains nearly all of the lipids and that these lipids can be converted through IST into biodiesel. A significant benefit of the HTC process, beyond reducing the amount of solids to be processed by IST in half, is the generation of an aqueous phase co-product containing a majority of the N and P in the reactant biomass. Through growth experiments with a unique marine bi-culture, we demonstrated that the aqueous phase co-product can support algal growth, thereby diminishing the amount of synthetic fertilizers that an algal biorefinery would require.

Our work on HTC at temperatures around 200 °C and relatively short times (15–30 min) demonstrated that this process can effectively liberate 50-60% of the biomass N and P to the aqueous phase while retaining nearly all of the lipids in a solid that is easy to separate by centrifugation or filtration. Although we initially explored higher temperatures (220–250 °C) in an effort to hydrolyze intracellular lipids, thereby making them more amenable to supercritical transesterification, the increased energy demands for HTC at these temperatures and the reduced lipid retention we observed outweigh this benefit. Although some fuel-conversion strategies may be able to process wet hydrochars as they exist following separation from the aqueous phase, others will require drying. By reducing the amount of solids, liberating intracellular water, and improving

dewaterability, HTC can significantly reduce the energy required to produce a dry, oil-bearing solid. Moreover, because the solid hydrochar can readily be stored and transported, it may be most logical to carry out HTC on individual algae farms and then process large quantities of hydrochar at a centralized facility.

With regards to fuel conversion, our work was the first to study the IST of algal hydrochars. We assessed three different methods of IST in an attempt to achieve high biodiesel yields with the least amount of ethanol. Our work with both sub- and supercritical ethanol demonstrated the importance of choosing reaction conditions so as to limit the thermal degradation of unsaturated esters. For feedstocks with a fatty acid profile suitable for biodiesel, such as *Chlorella*, and for which moisture is naturally present, supercritical ethanol (275 °C) was found to be an ideal reaction medium for uncatalyzed IST. At lower temperatures (215 °C), we observed that rare-earth metal triflates were effective catalysts for IST and also showed a high tolerance for feedstock moisture; however, difficulty in catalyst recovery will likely complicate scale-up of this process. Finally, mineral acid-catalyzed IST, the process most similar to what is done today to make biodiesel on a commercial scale, was also capable of converting nearly all hydrochar lipids into biodiesel but required a very large excesses of ethanol. Because ethanol recycling is a major energy burden in biodiesel processing, this process is probably most applicable to feedstocks such as *Nannochloropsis* that have both high-value oils (e.g., EPA) as well as FAs suitable for biodiesel. In the case of all three IST processes, additional work could focus on physical hydrochar pre-treatments, such as milling, as well as the use of co-solvents to help improve yields and reduce alcohol loadings. Although the high temperature and pressure environment required for SC-IST poses some engineering challenges, it presents considerable advantages relative to catalyzed reactions that warrant its further investigation.

Our experimental work on HTC and IST was complemented by a modeling effort that highlighted how these two processes could significantly reduce the energy associated

with biomass processing and fuel conversion compared to the approach of wet hexane extraction and traditional transesterification. Perhaps, more importantly, this modeling work pointed to the significant energy burden associated with synthetic fertilizers and the importance of nutrient recycling. Although our work with the aqueous phase co-product of HTC demonstrated that a majority of the N and P was in an inorganic form and readily bioavailable, we recognize that our approach alone would never be able to achieve the very high rates of nutrient recycling required for truly large-scale deployment of algal biofuels. Future work should focus on technologies, such as catalytic hydrothermal gasification, that are capable of converting the non-lipid fraction of algal biomass into usable forms of N and P fertilizer while also capturing the energy value of associated with this material. Although our work suggested that improved biomass productivities due to growth on organic carbon sources in the aqueous phase co-product are possible, the risk of contamination in an outdoor pond setting and the lost opportunity to produce on-site heat and power most likely outweigh this benefit.

Overall, the work presented here provides a foundation of engineering knowledge and scientific understanding regarding subcritical hydrothermal processing of algal biomass and in situ transesterification of algal hydrochars upon which we hope others can build. Given the changing climate, our ability to supply large volumes of alternative fuels to the transportation sector cannot expand soon enough. With the myriad private, public, and government entities researching algal biofuels, we hope that our work helps push the field one-step closer to commercialization in a manner cognizant of the resource limitations our society faces.

## APPENDIX A.

Table A1. Triflate-catalyzed oleic acid esterification.

Run No.	Temp. (°C)	Time (min)	Catalyst (mol %)	EtOH:FA molar ratio	H <sub>2</sub> O (wt.%)	H <sub>2</sub> O:FA molar ratio	C <sub>ao</sub> (mol/L)	Ethyl Oleate Yield (%)
1	175	25	0.9	8.9	0.0	0.0	1.2	95.3
2	175	25	8.1	8.3	0.0	0.0	1.2	92.3
3	192.5	25	1.4	15.1	11.5	8.2	0.7	92.1
4	175	25	8.5	1.9	0.0	0.0	2.3	90.9
5	192.5	25	5.4	14.6	2.6	1.7	0.7	90.6
6	175	5	7.9	8.5	0.0	0.0	1.2	89.4
7	150	45	2.1	19.9	3.0	2.3	0.6	89.3
8	215	5	8.9	1.9	0.0	0.0	2.3	88.3
9	150	45	9.4	9.3	2.3	1.1	1.0	86.7
10	215	25	0.9	1.6	0.0	0.0	2.4	86.1
11	235	5	9.5	9.9	2.3	1.2	0.9	85.8
12	175	25	1.0	1.7	0.0	0.0	2.4	85.0
13	192.5	5	5.5	15.9	11.2	8.3	0.6	84.7
14	175	25	8.8	8.1	9.9	3.9	1.2	84.4
15	192.5	25	5.9	14.9	11.4	8.2	0.7	83.7
16	192.5	25	5.4	10.2	13.4	7.7	0.8	83.0
17	175	5	8.4	1.5	0.0	0.0	2.4	82.9
18	215	25	9.0	9.1	0.0	0.0	1.2	82.7
19	195	15	5.2	5.6	4.8	1.5	1.5	81.7
20	175	25	8.2	1.7	8.7	1.9	2.2	81.7
21	192.5	25	9.9	20.2	9.9	8.8	0.5	81.4
22	150	45	11.3	21.5	15.5	15.4	0.5	81.0
23	215	25	0.8	8.7	10.0	3.8	1.1	80.9
24	215	25	8.5	8.7	9.4	3.8	1.1	80.3
25	215	5	1.0	9.3	0.0	0.0	1.2	80.2
26	215	5	6.8	9.2	0.0	0.0	1.2	80.1
27	150	25	4.9	14.8	11.4	8.0	0.7	79.0
28	235	45	0.7	10.1	2.2	1.1	0.9	78.6
29	150	5	10.5	20.0	2.8	2.3	0.6	78.5
30	192.5	25	6.0	19.7	9.9	8.6	0.5	78.5
31	235	5	9.9	19.8	15.4	15.0	0.5	78.4
32	215	5	9.0	1.8	9.1	2.1	2.2	76.3
33	192.5	25	5.1	15.0	18.7	14.8	0.6	76.1
34	215	25	9.0	1.9	8.4	1.9	2.2	75.1
35	235	45	1.4	19.9	15.8	15.1	0.5	71.6
36	235	25	5.2	15.1	11.9	8.9	0.6	69.4

---

37	195	15	5.0	5.3	4.6	1.4	1.5	68.7
38	215	5	9.4	9.6	9.5	4.1	1.0	67.0
39	175	5	7.7	1.6	8.5	1.9	2.2	66.2
40	175	5	1.0	8.8	0.0	0.0	1.2	65.9
41	235	5	1.7	9.8	22.0	13.8	0.8	63.9
42	195	15	5.0	5.7	4.7	1.5	1.5	63.9
43	175	5	8.0	7.7	9.1	3.4	1.2	61.3
44	150	45	1.3	10.0	22.8	14.1	0.8	60.7
45	175	25	1.0	8.2	9.0	3.3	1.2	60.2
46	215	5	0.8	1.7	0.0	0.0	2.4	53.3
47	150	5	1.6	8.0	2.8	1.2	1.1	52.0
48	175	5	0.9	2.0	0.0	0.0	2.3	47.0
49	215	5	0.7	8.9	9.5	3.7	1.1	45.3
50	175	25	0.9	1.7	9.1	1.9	2.2	38.9
51	215	5	0.9	1.9	8.8	1.8	2.2	26.3
52	150	5	10.0	10.3	21.7	14.2	0.8	21.5
53	175	5	0.8	1.7	8.6	1.7	2.2	15.2
54	150	5	1.1	21.0	16.4	15.6	0.5	10.1
55	175	5	0.9	8.9	9.3	3.6	1.1	4.6

---

Table A2. Response surface regression analysis of triflate-catalyzed oleic acid esterification

Term	Coefficient (coded)	Coefficient (uncoded)	SE Coef	T	P
Constant	81.919	-208.592	3.496	23.435	0
Temp	4.075	1.96525	3.198	1.274	0.211
Time	8.902	5.63736	3.901	2.282	0.029
Catalyst	5.911	15.1058	3.376	1.751	0.089
Ethanol Ratio	5.503	6.44176	3.737	1.472	0.15
Water	-6.109	-12.2312	4.267	-1.432	0.161
Temp*Temp	-6.578	-0.0036418	5.627	-1.169	0.251
Time*Time	-10.387	-0.0259669	5.353	-1.94	0.061
Catalyst*Catalyst	-4.906	-0.174668	6.552	-0.749	0.459
Ethanol Ratio*Ethanol Ratio	-6.111	-0.0611134	5.35	-1.142	0.261
Water*Water	4.916	0.0378301	5.191	0.947	0.35
Temp*Time	-14.659	-0.0172454	3.548	-4.131	0
Temp*Catalyst	-10.03	-0.0445281	3.809	-2.633	0.013
Temp*Ethanol Ratio	-7.159	-0.0168439	5.053	-1.417	0.166
Temp*Water	18.051	0.0372574	4.553	3.964	0
Time*Catalyst	-13.989	-0.131974	3.608	-3.878	0
Time*Ethanol Ratio	-8.332	-0.0416599	4.692	-1.776	0.085
Time*Water	13.935	0.0611204	4.195	3.322	0.002
Catalyst*Ethanol Ratio	-10.284	-0.194029	4.568	-2.251	0.031
Catalyst*Water	11.702	0.193677	4.56	2.566	0.015
Ethanol Ratio*Water	9.623	0.08	7.317	1.315	0.197

Note.  $R^2=86.7\%$ . Regression analysis performed with Minitab using the data in Table S1. This analysis also corresponds to the response surfaces in Fig. 1.



## REFERENCES

1. Adhami, L., Griggs, B., Himebrook, P., Taconi, K., 2009. Liquid–liquid extraction of butanol from dilute aqueous solutions using soybean-derived biodiesel. *Journal of the American Oil Chemists' Society* 86, 1123–1128.
2. Alenezi, R., Leeke, G., Santos, R., Khan, A., 2009. Hydrolysis kinetics of sunflower oil under subcritical water. *Chemical Engineering Research and Design* 87, 867–873.
3. Alves, S.P., Cabrita, A.R.J., Fonseca, A.J.M., Bessa, R.J.B., 2009. Effect of a purification step and the type of internal standard used on fatty acid determination of grass and maize silages. *Journal of Agricultural and Food Chemistry* 57, 10793–10797.
4. Anandarajah, K., Mahendrapurumal, G., Sommerfeld, M., Hu, Q., 2012. Characterization of microalga *Nannochloropsis* sp. mutants for improved production of biofuels. *Applied Energy* 96, 371–377.
5. Anitescu, G., Deshpande, A., Tavlarides, L., 2008. Integrated technology for supercritical biodiesel production and power cogeneration. *Energy & Fuels* 22, 1391–1399.
6. ANL, NREL, PNNL, 2012. Renewable diesel from algal lipids: an integrated baseline for cost, emissions, and resource potential from a harmonized model. ANL/ESD/12-4; NREL/TP-5100-55431; PNNL-21437. Argonne, IL: Argonne National Laboratory; Golden, CO: National Renewable Energy Laboratory; Richland, WA: Pacific Northwest National Laboratory.
7. Arnell, N.W., Lowe, J. a., Brown, S., Gosling, S.N., Gottschalk, P., Hinkel, J., Lloyd-Hughes, B., Nicholls, R.J., Osborn, T.J., Osborne, T.M., Rose, G. A., Smith, P., Warren, R.F., 2013. A global assessment of the effects of climate policy on the impacts of climate change. *Nature Climate Change* 3, 512–519.
8. Bacovsky, D., Ludwiczek, N., Ognissanto, M., Wörgetter, M., 2013. Status of advanced biofuels demonstration facilities in 2012: A report to IEA Bioenergy Task 39. Available Online: <http://www.task39.org/Publications.aspx>.
9. Berdeaux, O., Fournier, V., Lambelet, P., Dionisi, F., Sébédio, J.L., Destailats, F., 2007. Isolation and structural analysis of the cyclic fatty acid monomers formed from eicosapentaenoic and docosahexaenoic acids during fish oil deodorization. *Journal of Chromatography A* 1138, 216–224.

10. Biller, P., Ross, A.B., Skill, S.C., Lea-Langton, A., Balasundaram, B., Hall, C., Riley, R., Llewellyn, C., 2012. Nutrient recycling of aqueous phase for microalgae cultivation from the hydrothermal liquefaction process. *Algal Research* 1, 70–76.
11. Bligh, E., Dyer, W., 1959. A rapid method for total lipid extraction and purification. *Canadian Journal of Biochemistry and Physiology* 37, 911–917.
12. Boudreau, T.M., Hill, G. a., 2006. Improved ethanol–water separation using fatty acids. *Process Biochemistry* 41, 980–983.
13. Broch, A., Hoekman, S.K., Unnasch, S., 2013. A review of variability in indirect land use change assessment and modeling in biofuel policy. *Environmental Science & Policy* 29, 147–157.
14. Cardinale, B.J., Matulich, K.L., Hooper, D.U., Byrnes, J.E., Duffy, E., Gamfeldt, L., Balvanera, P., O'Connor, M.I., Gonzalez, A., 2011. The functional role of producer diversity in ecosystems. *American Journal of Botany* 98, 572–592.
15. Carrapiso, A., García, C., 2000. Development in lipid analysis: some new extraction techniques and in situ transesterification. *Lipids* 35, 1167–1177.
16. Carvalho, A.P., Meireles, L. a, Malcata, F.X., 2006. Microalgal reactors: a review of enclosed system designs and performances. *Biotechnology Progress* 22, 1490–1506.
17. Chai, F., Cao, F., Zhai, F., Chen, Y., Wang, X., Su, Z., 2007. Transesterification of vegetable oil to biodiesel using a heteropolyacid solid catalyst. *Advanced Synthesis & Catalysis* 349, 1057–1065.
18. Changi, S., Pinnarat, T., Savage, P.E., 2011. Modeling hydrolysis and esterification kinetics for biofuel processes. *Industrial & Engineering Chemistry Research* 50, 3206–3211.
19. Chen, C.-H., Chen, W.-H., Chang, C.-M.J., Lai, S.-M., Tu, C.-H., 2010. Biodiesel production from supercritical carbon dioxide extracted jatropha oil using subcritical hydrolysis and supercritical methylation. *The Journal of Supercritical Fluids* 52, 228–234.
20. Chen, C.-Y., Yeh, K.-L., Aisyah, R., Lee, D.-J., Chang, J.-S., 2011. Cultivation, photobioreactor design and harvesting of microalgae for biodiesel production: A critical review. *Bioresource Technology* 102, 71–81.
21. Cheng, Y., Zhou, W., Gao, C., Lan, K., Gao, Y., Wu, Q., 2009. Biodiesel production from Jerusalem Artichoke (*Helianthus tuberosus* L.) tuber by heterotrophic

- microalgae *Chlorella protothecoides*. *Journal of Chemical Technology Biotechnology* 84, 777–781.
22. Chisti, Y., 2007. Biodiesel from microalgae. *Biotechnology Advances* 25, 294–306.
  23. Christie, W.W., 1989. *Gas Chromatography and Lipids: A Practical Guide*. The Oily Press, Bridgewater, Somerset.
  24. Clarens, A.F., Resurreccion, E.P., White, M. a, Colosi, L.M., 2010. Environmental life cycle comparison of algae to other bioenergy feedstocks. *Environmental Science & Technology* 44, 1813–9.
  25. Converti, A., Casazza, A.A., Ortiz, E.Y., Perego, P., Del Borghi, M., 2009. Effect of temperature and nitrogen concentration on the growth and lipid content of *Nannochloropsis oculata* and *Chlorella vulgaris* for biodiesel production. *Chemical Engineering and Processing Process Intensification* 48, 1146–1151.
  26. Cordell, D., Drangert, J.-O., White, S., 2009. The story of phosphorus: global food security and food for thought. *Global Environmental Change* 19, 292–305.
  27. D’Ippolito, S., Yori, J.C., Iturria, M.E., Pieck, C.L., Vera, C.R., 2007. Analysis of a two-step, noncatalytic, supercritical biodiesel production process with heat recovery. *Energy* 21, 339–346.
  28. Danquah, M.K., Ang, L., Uduman, N., Moheimani, N., Forde, G.M., 2009. Dewatering of microalgal culture for biodiesel production: Exploring polymer flocculation and tangential flow filtration. *Journal of Chemical Technology Biotechnology* 84, 1078–1083.
  29. Davis, R., Aden, A., Pienkos, P.T., 2011. Techno-economic analysis of autotrophic microalgae for fuel production. *Applied Energy* 88, 3524–3531.
  30. Davis, S.J., Cao, L., Caldeira, K., Hoffert, M.I., 2013. Rethinking wedges. *Environmental Research Letters* 8, 011001.
  31. Deshpande, a, Anitescu, G., Rice, P. a, Tavlarides, L.L., 2010. Supercritical biodiesel production and power cogeneration: technical and economic feasibilities. *Bioresource Technology* 101, 1834–1843.
  32. Dickinson, N., Bolin, K., Overstreet, E., Dooley, B., 2006. Slurry dewatering and conversion of biosolids to a renewable fuel (US patent application 2006/0096163).
  33. Doan, T.T.Y., Obbard, J.P., 2012. Enhanced intracellular lipid in *nannochloropsis* sp. via random mutagenesis and flow cytometric cell sorting. *Algal Research* 1, 17–21.

34. Dodds, E.D., McCoy, M.R., Rea, L.D., Kennish, J.M., 2005. Gas chromatographic quantification of fatty acid methyl esters: flame ionization detection vs. electron impact mass spectrometry. *Lipids* 40, 419–428.
35. DOE, 2012. The greenhouse gases, regulated emissions, and energy use in transportation model (rev. 1). Available Online [accessed 3-15-13]: <http://greet.es.anl.gov/>.
36. Droop, M.R., 2007. Vitamins, phytoplankton and bacteria: symbiosis or scavenging? *Journal of Plankton Research* 29, 107–113.
37. Du, Z., Hu, B., Shi, A., Ma, X., Cheng, Y., Chen, P., Liu, Y., Lin, X., Ruan, R., 2012. Cultivation of a microalga *Chlorella vulgaris* using recycled aqueous phase nutrients from hydrothermal carbonization process. *Bioresource Technology* 126, 354–7.
38. Du, Z., Mohr, M., Ma, X., Cheng, Y., Lin, X., Liu, Y., Zhou, W., Chen, P., Ruan, R., 2012. Hydrothermal pretreatment of microalgae for production of pyrolytic bio-oil with a low nitrogen content. *Bioresource Technology* 111, 13–18.
39. Ehimen, E. a, Sun, Z.F., Carrington, C.G., 2010. Variables affecting the in situ transesterification of microalgae lipids. *Fuel* 89, 677–684.
40. EIA, 2011. International energy outlook 2011. Available Online: [www.eia.gov/forecasts/ieo](http://www.eia.gov/forecasts/ieo).
41. EIA, 2013. Monthly energy review. Available Online [accessed 3-15-13]: <http://www.eia.gov/totalenergy/data/monthly/#renewable>.
42. Elliott, D., 2008. Catalytic hydrothermal gasification of biomass. *Biofuels, Bioproducts and Biorefining* 2, 254–265.
43. EnerTech Environmental Inc., 2013. Rialto slurrycarb® facility. Available Online [accessed 3-15-13]: <http://enertech.com/facilities/sitedevelopments/rcrf.html>.
44. European Committee for Standardization, 2003. Standard EN14105: Determination of free and total glycerol and mono-, di-, and triglyceride content.
45. Fernandes, N., Nestle Oil, 2008. The next generation of biofuels experiences from the world's leading producer, in: *Low Carbon Fuels 2008*. Sacramento, CA.
46. Folch, J., Lees, M., Sloane-Stanley, G., 1957. A simple method for the isolation and purification of total lipids from animal tissues. *J Biol Chem* 497–509.

47. Fournier, V., Juanéda, P., Destailats, F., Dionisi, F., Lambelet, P., Sébédio, J.-L., Berdeaux, O., 2006. Analysis of eicosapentaenoic and docosahexaenoic acid geometrical isomers formed during fish oil deodorization. *Journal of Chromatography A* 1129, 21–28.
48. Frank, E.D., Elgowainy, A., Han, J., Wang, Z., 2012. Life cycle comparison of hydrothermal liquefaction and lipid extraction pathways to renewable diesel from algae. *Mitigation and Adaptation Strategies For Global Change* 18, 137–158.
49. Frank, E.D., Han, J., Palou-Rivera, I., Elgowainy, A., Wang, M.Q., 2012. Methane and nitrous oxide emissions affect the life-cycle analysis of algal biofuels. *Environmental Research Letters* 7, 014030.
50. Friedl, A., Padouvas, E., Rotter, H., Varmuza, K., 2005. Prediction of heating values of biomass fuel from elemental composition. *Analytica Chimica Acta* 544, 191–198.
51. Funke, A., Ziegler, F., 2010. Hydrothermal carbonization of biomass: a summary and discussion of chemical mechanisms for process engineering. *Biofuels, Bioproducts and Biorefining* 4, 160–177.
52. Gao, C., Zhai, Y., Ding, Y., Wu, Q., 2010. Application of sweet sorghum for biodiesel production by heterotrophic microalga *Chlorella protothecoides*. *Applied Energy* 87, 756–761.
53. Garcia Alba, L., Torri, C., Samorì, C., Van der Spek, J., Fabbri, D., Kersten, S.R. a., Brilman, D., 2012. Hydrothermal treatment (HTT) of microalgae: evaluation of the process as conversion method in an algae biorefinery concept. *Energy & Fuels* 26, 642–657.
54. Gim, G.H., Kim, J.K., Kim, H.S., Kathiravan, M.N., Yang, H., Jeong, S.-H., Kim, S.W., 2013. Comparison of biomass production and total lipid content of freshwater green microalgae cultivated under various culture conditions. *Bioprocess and Biosystems Engineering*.
55. Golueke, C., Oswald, W., 1965. Harvesting and processing sewage-grown planktonic algae. *Journal Water Pollution Control Federation* 37, 471–498.
56. Gomiero, T., Paoletti, M.G., Pimentel, D., 2009. Biofuels: efficiency, ethics, and limits to human appropriation of ecosystem services. *Journal of Agricultural and Environmental Ethics* 23, 403–434.
57. Gossauer, A., Engel, N., 1996. Chlorophyll catabolism — structures, mechanisms, conversions. *Journal of Photochemistry and Photobiology B: Biology* 32, 141–151.

58. Goudriaan, F., Beld, B. Van De, Boerefijn, F.R., Bos, G.M., Naber, J., Wal, S. van der, Zeevalkink, J., 2000. Thermal efficiency of the HTU<sup>®</sup> process for biomass liquefaction, in: *Progress in Thermochemical Biomass Conversion*. pp. 1312–1325.
59. Gouveia, L., Oliveira, A.C., 2009. Microalgae as a raw material for biofuels production. *Journal of Industrial Microbiology Biotechnology* 36, 269–274.
60. Green, D., Perry, R., 2008. *Perry's Chemical Engineer's Handbook*, 8th ed. McGraw-Hill, New York, NY.
61. Griffiths, M.J., Harrison, S.T.L., 2009. Lipid productivity as a key characteristic for choosing algal species for biodiesel production. *Journal of Applied Phycology* 21, 493–507.
62. Gui, M.M., Lee, K.T., Bhatia, S., 2009. Supercritical ethanol technology for the production of biodiesel: process optimization studies. *The Journal of Supercritical Fluids* 49, 286–292.
63. Guillard, R.L., 1975. Culture of phytoplankton for feeding marine invertebrates, in: Smith, W., Chanley, M. (Eds.), *Culture of Marine Invertebrate Animals*. Springer US, pp. 29–60.
64. Guiotoku, M., Rambo, C.R., Hansel, F. a., Magalhães, W.L.E., Hotza, D., 2009. Microwave-assisted hydrothermal carbonization of lignocellulosic materials. *Materials Letters* 63, 2707–2709.
65. Guschina, I.A., Harwood, J.L., 2006. Lipids and lipid metabolism in eukaryotic algae. *Progress In Lipid Research* 45, 160–186.
66. Haar, L., Gallagher, J., Kell, G., 1984. *NBS/NRC Steam Tables: Thermodynamic and Transport Properties and Computer Programs for Vapor and Liquid States of Water in SI Units*. Hemisphere Publishing Corporation.
67. Haas, M.J., Scott, K.M., 2006. Moisture removal substantially improves the efficiency of in situ biodiesel production from soybeans. *Journal of the American Oil Chemists Society* 84, 197–204.
68. Haas, M.J., Scott, K.M., Foglia, T.A., Marmer, W.N., 2007. The general applicability of in situ transesterification for the production of fatty acid esters from a variety of feedstocks. *Journal of the American Oil Chemists Society* 84, 963–970.
69. Haas, M.J., Scott, K.M., Marmer, W.N., Foglia, T.A., 2004. In situ alkaline transesterification: an effective method for the production of fatty acid esters from vegetable oils. *Journal of the American Oil Chemists Society* 81, 83–89.

70. Haas, M.J., Wagner, K., 2011a. Simplifying biodiesel production: the direct or in situ transesterification of algal biomass. *European Journal of Lipid Science and Technology* 113, 1219–1229.
71. Haas, M.J., Wagner, K.M., 2011b. Substrate pretreatment can reduce the alcohol requirement during biodiesel production via in situ transesterification. *Journal of the American Oil Chemists' Society* 88, 1203–1209.
72. Handler, R.M., Canter, C.E., Kalnes, T.N., Lupton, F.S., Kholiqov, O., Shonnard, D.R., Blowers, P., 2012. Evaluation of environmental impacts from microalgae cultivation in open-air raceway ponds: analysis of the prior literature and investigation of wide variance in predicted impacts. *Algal Research* 1, 83–92.
73. Hara, A., Radin, N.S., 1978. Lipid extraction of tissues with a low-toxicity solvent. *Analytical Biochemistry* 90, 420–426.
74. Harwood, J., Jones, A., 1989. Lipid metabolism in algae. *Advances In Botanical Research* 16, 1–53.
75. He, H., Sun, S., Wang, T., Zhu, S., 2007a. Transesterification kinetics of soybean oil for production of biodiesel in supercritical methanol. *Journal of the American Oil Chemists' Society* 84, 399–404.
76. He, H., Wang, T., Zhu, S., 2007b. Continuous production of biodiesel fuel from vegetable oil using supercritical methanol process. *Fuel* 86, 442–447.
77. He, W., Li, G., Kong, L., Wang, H., Huang, J., Xu, J., 2008. Application of hydrothermal reaction in resource recovery of organic wastes. *Resources, Conservation and Recycling* 52, 691–699.
78. Heilmann, S.M., Davis, H.T., Jader, L.R., Lefebvre, P.A., Sadowsky, M.J., Schendel, F.J., Von Keitz, M.G., Valentas, K.J., 2010. Hydrothermal carbonization of microalgae. *Biomass and Bioenergy* 34, 875–882.
79. Heilmann, S.M., Jader, L.R., Harned, L.A., Sadowsky, M.J., Schendel, F.J., Lefebvre, P.A., Von Keitz, M.G., Valentas, K.J., 2011. Hydrothermal carbonization of microalgae ii. fatty acid, char, and algal nutrient products. *Applied Energy* 88, 3286–3290.
80. Heilmann, S.M., Jader, L.R., Sadowsky, M.J., Schendel, F.J., Von Keitz, M.G., Valentas, K.J., 2011. Hydrothermal carbonization of distiller's grains. *Biomass and Bioenergy* 35, 2526–2533.

81. Holliday, R.L., King, J.W., List, G.R., 1997. Hydrolysis of vegetable oils in sub- and supercritical water. *Industrial & Engineering Chemistry Research* 36, 932–935.
82. Holmgren, J., 2007. Refining biorenewables with the uop / ENIecofining™ process, in: UOP Technical Conference. Kananaskis, Alberta, Canada.
83. Hu, Q., Sommerfeld, M., Jarvis, E., Ghirardi, M., Posewitz, M., Seibert, M., Darzins, A., 2008. Microalgal triacylglycerols as feedstocks for biofuel production: Perspectives and advances. *The Plant Journal* 54, 621–639.
84. Huang, H., Yuan, X., Zeng, G., Wang, J., Li, H., Zhou, C., Pei, X., You, Q., Chen, L., 2011. Thermochemical liquefaction characteristics of microalgae in sub- and supercritical ethanol. *Fuel Processing Technology* 92, 147–153.
85. Huang, H.-J., Ramaswamy, S., Tschirner, U.W., Ramarao, B. V., 2008. A review of separation technologies in current and future biorefineries. *Separation and Purification Technology* 62, 1–21.
86. Huber, G., Iborra, S., Corma, A., 2006. Synthesis of transportation fuels from biomass: chemistry, catalysts, and engineering. *Chemical Reviews* 106, 4044–4098.
87. Illman, A., Scragg, A., Shales, S., 2000. Increase in chlorella strains calorific values when grown in low nitrogen medium. *Enzyme and Microbial Technology* 27, 631–635.
88. Imahara, H., Minami, E., Hari, S., Saka, S., 2008. Thermal stability of biodiesel in supercritical methanol. *Fuel* 87, 1–6.
89. Index Mundi, 2013a. Soybean oil price. Available Online [accessed 3-15-13]: [Http://www.indexmundi.com/commodities/?commodity=soybean-oil](http://www.indexmundi.com/commodities/?commodity=soybean-oil).
90. Index Mundi, 2013b. Sugar price. Available Online [accessed 3-15-13]: [Http://www.indexmundi.com/commodities/?commodity=sugar](http://www.indexmundi.com/commodities/?commodity=sugar).
91. IPCC, 2012. Renewable energy sources and climate change mitigation: special report of the Intergovernmental Panel on Climate Change. Cambridge University Press, Cambridge, MA.
92. Ishihara, K., Kubota, M., Kurihara, H., Yamamoto, H., 1996. Scandium trifluoromethanesulfonate as an extremely active lewis acid catalyst in acylation of alcohols with acid anhydrides and mixed anhydrides. *Journal of Organic Chemistry* 61, 4560–4567.



93. Janaun, J., Ellis, N., 2010. Perspectives on biodiesel as a sustainable fuel. *Renewable and Sustainable Energy Reviews* 14, 1312–1320.
94. Javanmardian, M., Palsson, B., 1991. High-density photoautotrophic algal cultures: design, construction, and operation of a novel photobioreactor system. *Biotechnology and Bioengineering* 38, 1182–1189.
95. Jena, U., Vaidyanathan, N., Chinnasamy, S., Das, K.C., 2011. Evaluation of microalgae cultivation using recovered aqueous co-product from thermochemical liquefaction of algal biomass. *Bioresource Technology* 102, 3380–3387.
96. Johnson, L., 1997. Theoretical, comparative, and historical analyses of alternative technologies for oilseeds extraction, in: *Technology and Solvents for Extracting Oilseeds and Nonpetroleum Oil*. AOCS Press, Champaign, IL, pp. 4–47.
97. Johnson, M.B., Wen, Z., 2009. Production of biodiesel fuel from the microalga *Schizochytrium limacinum* by direct transesterification of algal biomass. *Energy & Fuels* 23, 5179–5183.
98. Jorquera, O., Kiperstok, A., Sales, E.A., Embiruçu, M., Ghirardi, M.L., 2010. Comparative energy life-cycle analyses of microalgal biomass production in open ponds and photobioreactors. *Bioresource Technology* 101, 1406–13.
99. Jung, S., Maurer, D., Johnson, L.A., 2009. Factors affecting emulsion stability and quality of oil recovered from enzyme-assisted aqueous extraction of soybeans. *Bioresource Technology* 100, 5340–5347.
100. Kamio, E., Sato, H., Takahashi, S., Noda, H., Fukuhara, C., Okamura, T., 2007. Liquefaction kinetics of cellulose treated by hot compressed water under variable temperature conditions. *Journal of Materials Science* 43, 2179–2188.
101. Kasim, N.S., Tsai, T.-H., Gunawan, S., Ju, Y.-H., 2009. Biodiesel production from rice bran oil and supercritical methanol. *Bioresource Technology* 100, 2399–2403.
102. Kessler, E., 1976. Comparative physiology, biochemistry, and the taxonomy of *Chlorella* (chlorophyceae). *Plant Syst. Evol.* 125, 129–138.
103. Kessler, E., 1982. Physiological and biochemical contributions to the taxonomy of the genus *prototheca*. iii. Utilization of organic carbon and nitrogen compounds. *Arch Microbiol* 132, 103–106.
104. Kessler, E., Huss, V.A., 1992. Comparative physiology and biochemistry and taxonomic assignment of the *Chlorella* (chlorophyceae) strains of the culture collection of the university of texas at austin. *Journal of Phycology* 28, 550–553.

105. Khozin-Goldberg, I., Boussiba, S., 2011. Concerns over the reporting of inconsistent data on fatty acid composition for microalgae of the genus *Nannochloropsis* (eustigmatophyceae). *Journal of Applied Phycology* 23, 933–934.
106. King, J., Holliday, R., List, G., 1999. Hydrolysis of soybean oil. in a subcritical water flow reactor. *Green Chemistry* 261–264.
107. King, J.W., Srinivas, K., 2009. Multiple unit processing using sub- and supercritical fluids. *The Journal of Supercritical Fluids* 47, 598–610.
108. Kita, K., Okada, S., Sekino, H., Imou, K., Yokoyama, S., Amano, T., 2010. Thermal pre-treatment of wet microalgae harvest for efficient hydrocarbon recovery. *Applied Energy* 87, 2420–2423.
109. Kiwjaroun, C., Tubtimdee, C., Piumsomboon, P., 2009. Lca studies comparing biodiesel synthesized by conventional and supercritical methanol methods. *Journal of Cleaner Production* 17, 143–153.
110. Knothe, G., 2005. Dependence of biodiesel fuel properties on the structure of fatty acid alkyl esters. *Fuel Processing Technology* 86, 1059–1070.
111. Knothe, G., 2009. Improving biodiesel fuel properties by modifying fatty ester composition. *Energy Environmental Science* 2, 759–766.
112. Kobayashi, S., Sugiura, M., Kitagawa, H., Lam, W.W., 2002. Rare-earth metal triflates in organic synthesis. *Chem. Rev.* 102, 2227–2302.
113. Kocsisová, T., Juhasz, J., Cvengroš, J., 2006. Hydrolysis of fatty acid esters in subcritical water. *European Journal of Lipid Science and Technology* 108, 652–658.
114. Kruse, A., Dinjus, E., 2007. Hot compressed water as reaction medium and reactant 2. degradation reactions. *The Journal of Supercritical Fluids* 41, 361–379.
115. Kumar, S., Gupta, R.B., 2008. Hydrolysis of microcrystalline cellulose in subcritical and supercritical water in a continuous flow reactor. *Industrial & Engineering Chemistry Research* 47, 9321–9329.
116. Kusdiana, D., Saka, S., 2001. Kinetics of transesterification in rapeseed oil to biodiesel fuel as treated in supercritical methanol. *Fuel* 80, 693–698.
117. Kusdiana, D., Saka, S., 2004a. Effects of water on biodiesel fuel production by supercritical methanol treatment. *Bioresource Technology* 91, 289–295.

118. Kusdiana, D., Saka, S., 2004b. Two-step preparation for catalyst-free biodiesel fuel production. *Applies Biochemistry and Biotechnology* 113-116, 781–791.
119. Lamoolphak, W., Goto, M., Sasaki, M., Suphantharika, M., Muangnapoh, C., Prommuag, C., Shotipruk, A., 2006. Hydrothermal decomposition of yeast cells for production of proteins and amino acids. *Journal of Hazardous Materials* 137, 1643–8.
120. Lapuerta, M., Armas, O., García-Contreras, R., 2009. Effect of ethanol on blending stability and diesel engine emissions. *Energy & Fuels* 23, 4343–4354.
121. Lardon, L., Hélias, A., Sialve, B., Steyer, J.-P., Bernard, O., 2009. Life-cycle assessment of biodiesel production from microalgae. *Environmental Science & Technology* 43, 6475–6481.
122. Lascaray, L., 1952. Industrial fat splitting. *Journal of the American Oil Chemists' Society* 29, 362–366.
123. Lee, J., Yoo, C., Jun, S., Ahn, C., Oh, H., 2010. Comparison of several methods for effective lipid extraction from microalgae. *Bioresource Technology* 101, S75–S77.
124. Lepage, G., Roy, C., 1986. Direct transesterification of all classes of lipids in a one-step reaction. *Journal of Lipid Research* 27, 114–120.
125. Lepage, G., Roy, C.C., 1984. Improved recovery of fatty acid through direct transesterification without prior extraction or purification. *Journal of Lipid Research* 25, 1391–1396.
126. Lestari, S., Mäki-Arvela, P., Beltramini, J., Lu, G.Q.M., Murzin, D.Y., 2009. Transforming triglycerides and fatty acids into biofuels. *ChemSusChem* 2, 1109–1119.
127. Levine, R.B., Bollas, A. a, Durham, M.D., Savage, P.E., 2012. Triflate-catalyzed (trans)esterification of lipids within carbonized algal biomass. *Bioresource Technology* 111, 222–9.
128. Levine, R.B., Bollas, A., Savage, P.E., 2013. Process improvements for the supercritical in situ transesterification of carbonized algal biomass. *Bioresource Technology* 136, 556–564.
129. Levine, R.B., Costanza-Robinson, M.S., Spatafora, G. a, 2011. *Neochloris oleoabundans* grown on anaerobically digested dairy manure for concomitant nutrient removal and biodiesel feedstock production. *Biomass and Bioenergy* 35, 40–49.

130. Levine, R.B., Pinnarat, T., Savage, P.E., 2010. Biodiesel production from wet algal biomass through in situ lipid hydrolysis and supercritical transesterification. *Energy & Fuels* 24, 5235–5243.
131. Lewis, T., Nichols, P., McMeekin, T., 2000. Evaluation of extraction methods for recovery of fatty acids from lipid-producing microheterotrophs. *Journal of Microbiological Methods* 43, 351–352.
132. Li, X., Xu, H., Wu, Q., 2007. Large-scale biodiesel production from microalga *Chlorella protothecoides* through heterotrophic cultivation in bioreactors. *Biotechnology and Bioengineering* 98, 764–771.
133. Li, Y., Horsman, M., Wang, B., Wu, N., Lan, C.Q., 2008. Effects of nitrogen sources on cell growth and lipid accumulation of green alga *Neochloris oleoabundans*. *Applied Microbiology and Biotechnology* 81, 629–636.
134. Liang, Y., Sarkany, N., Cui, Y., 2009. Biomass and lipid productivities of *Chlorella vulgaris* under autotrophic, heterotrophic and mixotrophic growth conditions. *Biotechnology Letters* 31, 1043–1049.
135. Libra, J., Ro, K., Kammann, C., Funke, A., 2011. Hydrothermal carbonization of biomass residuals: a comparative review of the chemistry, processes and applications of wet and dry pyrolysis. *Biofuels* 2, 89–124.
136. Liu, Z.-Y., Wang, G.-C., Zhou, B.-C., 2008. Effect of iron on growth and lipid accumulation in *Chlorella vulgaris*. *Bioresource Technology* 99, 4717–22.
137. Lynam, J.G., Coronella, C.J., Yan, W., Reza, M.T., Vasquez, V.R., 2011. Acetic acid and lithium chloride effects on hydrothermal carbonization of lignocellulosic biomass. *Bioresource Technology* 102, 6192–9.
138. Lynam, J.G., Toufiq Reza, M., Vasquez, V.R., Coronella, C.J., 2012. Effect of salt addition on hydrothermal carbonization of lignocellulosic biomass. *Fuel* 99, 271–273.
139. Madras, G., Kolluru, C., Kumar, R., 2004. Synthesis of biodiesel in supercritical fluids. *Fuel* 83, 2029–2033.
140. Marchetti, J.M., Miguel, V.U., Errazu, a. F., 2008. Techno-economic study of different alternatives for biodiesel production. *Fuel Processing Technology* 89, 740–748.

141. Marshall, W., Franck, E., 1981. Ion product of water substance, 0-1000 °C, 1-10,000 bars: new international formulation and its background. *J. Phys. Chem. Ref. Data* 10, 295–304.
142. Marulanda, V.F., Anitescu, G., Tavlarides, L.L., 2010a. Investigations on supercritical transesterification of chicken fat for biodiesel production from low-cost lipid feedstocks. *The Journal of Supercritical Fluids* 54, 53–60.
143. Marulanda, V.F., Anitescu, G., Tavlarides, L.L., 2010b. Biodiesel fuels through a continuous flow process of chicken fat supercritical transesterification. *The Journal of Supercritical Fluids* 253–260.
144. Mazzieri, V.A., Vera, C.R., Yori, J.C., 2008. Adsorptive properties of silica gel for biodiesel refining. *Energy & Fuels* 4281–4284.
145. McCurry, J., 2009. Automated standard and sample preparation for multiple gas chromatographic analyses of biodiesel. Agilent Technologies Application Note. Available Online: <http://www.chem.agilent.com/Library/applications/5990-3781EN.pdf>.
146. McLarnon-Riches, C., Rolph, C., 1998. Effects of environmental factors and metals on selenastrum capricornutum lipids. *Phytochemistry* 49, 1241–1247.
147. Miao, X., Wu, Q., 2004. High yield bio-oil production from fast pyrolysis by metabolic controlling of chlorella protothecoides. *Journal of Biotechnology* 110, 85–93.
148. Miao, X., Wu, Q., 2006. Biodiesel production from heterotrophic microalgal oil. *Bioresource Technology* 97, 841–846.
149. Miller, S.A., 2010. Minimizing land use and nitrogen intensity of bioenergy. *Environmental Science & Technology* 44, 3932–3939.
150. Mills, V., Jiclain, H.I.C., 1949. Fat hydrolysis. *Industrial and Engineering Chemistry* 41, 1982–1985.
151. Minami, E., Saka, S., 2006. Kinetics of hydrolysis and methyl esterification for biodiesel production in two-step supercritical methanol process. *Fuel* 85, 2479–2483.
152. Minowa, T., Sawayama, S., 1999. A novel microalgal system for energy production with nitrogen cycling. *Fuel* 78, 1213–1215.

153. Molina Grima, E., Belarbi, E.-H., Ación Fernández, F.G., Robles Medina, a, Chisti, Y., 2003. Recovery of microalgal biomass and metabolites: process options and economics. *Biotechnology Advances* 20, 491–515.
154. Moquin, P.H.L., Temelli, F., 2008. Kinetic modeling of hydrolysis of canola oil in supercritical media. *Journal of Supercritical Fluids* 45, 94–101.
155. Moura, J.M.L.N., Campbell, K., Mahfuz, a, Jung, S., Glatz, C.E., Johnson, L., 2008. Enzyme-assisted aqueous extraction of oil and protein from soybeans and cream de-emulsification. *Journal of the American Oil Chemists' Society* 85, 985–995.
156. Neyens, E., Baeyens, J., 2003. A review of thermal sludge pre-treatment processes to improve dewaterability. *Journal of Hazardous Materials B98*, 51–67.
157. Nichols, B.W., James, a T., Breuer, J., 1967. Interrelationships between fatty acid biosynthesis and acyl-lipid synthesis in *Chlorella vulgaris*. *The Biochemical Journal* 104, 486–496.
158. Nickerson, C., Ebel, R., Borchers, A., Carriazo, F., 2011. Major uses of land in the united states, 2007 (economic information bulletin no. EIB-89). Available Online: <http://www.ers.usda.gov/publications/eib-economic-information-bulletin/eib89.aspx#.Uav0IEDVCKI> 67.
159. O'Grady, J., Morgan, J., 2011. Heterotrophic growth and lipid production of *Chlorella protothecoides* on glycerol. *Bioprocess and Biosystems Engineering* 34, 121–5.
160. Ogbonna, J.C., Tanakaah, H., 1998. Cyclic autotrophic/heterotrophic cultivation of photosynthetic cells : a method of achieving continuous cell growth under light/dark cycles. *Bioresource Technology* 65, 65–72.
161. Orfield, N., Levine, R., Keoleian, G., Miller, S., Savage, P., 2013. Growing algae for biodiesel on direct sunlight or sugars: a comparative life cycle assessment. (submitted, under review).
162. Pacala, S., Socolow, R., 2004. Stabilization wedges: solving the climate problem for the next 50 years with current technologies. *Science* 305, 968–72.
163. Park, S., Choi, Y., Kim, E., Park, W., Kim, C., Yang, J., 2012. Serial optimization of biomass production using microalga *Nannochloris oculata* and corresponding lipid biosynthesis. *Bioprocess Biosyst. Eng.* 35, 3–9.
164. Patil, P.D., Gnaneswar, V., Mannarswamy, A., Cooke, P., Munson-mcgee, S., Nirmalakhandan, N., Lammers, P., Deng, S., 2011. Optimization of microwave-

- assisted transesterification of dry algal biomass using response surface methodology. *Bioresource Technology* 102, 1399–1405.
165. Patil, P.D., Gnaneswar, V., Mannarswamy, A., Deng, S., Cooke, P., Munson-mcgee, S., Rhodes, I., Lammers, P., Nirmalakhandan, N., 2011. Optimization of direct conversion of wet algae to biodiesel under supercritical methanol conditions. *Biore* 102, 118–22.
  166. Perez-Garcia, O., Escalante, F., 2011. Heterotrophic cultures of microalgae: metabolism and potential products. *Water Research* 45, 11–36.
  167. Perretti, G., Motori, A., Bravi, E., Favati, F., Montanari, L., Fantozzi, P., 2007. Supercritical carbon dioxide fractionation of fish oil fatty acid ethyl esters. *Journal of Supercritical Fluids* 40, 349–353.
  168. Peterson, A., Vogel, F., Lachance, R., Froling, M., Antal, M., Tester, J., 2008. Thermochemical biofuel production in hydrothermal media: a review of sub-and supercritical water technologies. *Energy & Environmental Science* 1, 32–65.
  169. Pinnarat, T., Savage, P.E., 2008. Assessment of noncatalytic biodiesel synthesis using supercritical reaction conditions. *Ind. Eng. Chem. Res.* 47, 6801–6808.
  170. Pinnarat, T., Savage, P.E., 2010. Noncatalytic esterification of oleic acid in ethanol. *The Journal of Supercritical Fluids* 53, 53–59.
  171. Pinto, E., Sigaud-Kutner, T., Leitao, M., Okamoto, O., Morse, D., Colepicolo, P., 2003. Heavy metal-induced stress in algae. *J. Phycol.* 1018, 1008–1018.
  172. Pinto, J.S.S., Lanças, F.M., 2006. Hydrolysis of corn oil using subcritical water. *J. Braz. Chem. Soc.* 17, 85–89.
  173. Piorreck, M., Baasch, K., Pohl, P., 1984. Biomass production, total protein, chlorophylls, lipids and fatty acids of freshwater green and blue-green algae under different nitrogen regimes. *Phytochemistry* 23, 207–216.
  174. Quesada-Medina, J., Olivares-Carrillo, P., 2011. Evidence of thermal decomposition of fatty acid methyl esters during the synthesis of biodiesel with supercritical methanol. *The Journal of Supercritical Fluids* 56, 56–63.
  175. Quinn, J.C., Yates, T., Douglas, N., Weyer, K., Butler, J., Bradley, T.H., Lammers, P.J., 2012. Nannochloropsis production metrics in a scalable outdoor photobioreactor for commercial applications. *Bioresource Technology* 117, 164–171.

176. Quitain, A.T., Faisal, M., Kang, K., Daimon, H., Fujie, K., 2002. Low-molecular-weight carboxylic acids produced from hydrothermal treatment of organic wastes. *Journal of Hazardous Materials* 93, 209–20.
177. Ratledge, C., Cohen, Z., 2008. Microbial and algal oils: do they have a future for biodiesel or as commodity oils? *Lipid Technology* 20, 155–160.
178. Rebacz, N.A., Savage, P.E., 2010. Hydration of 1-phenyl-1-propyne in high-temperature water with catalysis by water-tolerant lewis acids. *Ind. Eng. Chem. Res.* 49, 535–540.
179. Richmond, A., Cheng-Wu, Z., 2001. Optimization of a flat plate glass reactor for mass production of *Nannochloropsis* sp . outdoors. *Journal of Biotechnology* 85, 259–269.
180. Riha, V., Brunner, G., 2000. Separation of fish oil ethyl esters with supercritical carbon dioxide. *The Jour* 17, 55–64.
181. Rittmann, B., 2008. Opportunities for renewable bioenergy using microorganisms. *Biotechnology and Bioengineering* 100, 203–212.
182. Rodolfi, L., Zittelli, G.C., 2009. Microalgae for oil: strain selection, induction of lipid synthesis and outdoor mass cultivation in a low-cost photobioreactor. *Biotechnology and Bioengineeringen* 102, 100–112.
183. Rodríguez-Ruiz, J., Belarbi, E.-H., Sánchez, J., Alonso, D., 1998. Rapid simultaneous lipid extraction and transesterification for fatty acid analyses. *Biotechnology Techniques* 12, 689–691.
184. Rogalinski, T., Herrmann, S., Brunner, G., 2005. Production of amino acids from bovine serum albumin by continuous sub-critical water hydrolysis. *The Journal of Supercritical Fluids* 36, 49–58.
185. Roncarati, A., Meluzzi, A., Acciarri, S., Tallarico, N., Melotti, P., 2004. Fatty acid composition of different microalgae strains (*Nannochloropsis* sp., *Nannochloropsis oculata* (droop) Hibberd, *Nannochloris atomus* Butcher and *Isochrysis*). *Journal of the World Aquaculture Society* 35, 401–411.
186. Rosenthal, A., Pyle, D., Niranjana, K., 1998. Simultaneous aqueous extraction of oil and protein from soybean: mechanisms for process design. *Food and Bioproducts Processing: Transactions Of The Institution Of Chemical Engineers, Part C* 76, 224–230.



187. Rubio-Rodríguez, N., Beltrán, S., Jaime, I., De Diego, S.M., Sanz, M.T., Carballido, J.R., 2010. Production of omega-3 polyunsaturated fatty acid concentrates: a review. *Innovative Food Science and Emerging Technologies* 11, 1–12.
188. Santos, C., Ferreira, M., Lopes da Silva, T., Gouveia, L., Novais, J., Reis, A., 2010. A symbiotic gas exchange between bioreactors enhances microalgal biomass and lipid productivities: taking advantage of complementary nutritional modes. *Journal of Industrial Microbiology Biotechnology* 38, 909–917.
189. Savage, P., Levine, R., Huelsman, C., 2010. Hydrothermal processing of biomass, in: Crocker, M. (Ed.), *Thermochemical Conversion of Biomass to Liquid Fuels and Chemicals*. Royal Society of Chemistry, pp. 190–219.
190. Sawangkeaw, R., 2010. A review of laboratory-scale research on lipid conversion to biodiesel with supercritical methanol (2001–2009). *The Journal of Supercritical Fluids* 55, 1–13.
191. Schenk, P.M., Thomas-Hall, S.R., Stephens, E., Marx, U., Mussnug, J., Posten, C., Kruse, O., Hankamer, B., 2008. Second generation biofuels: high-efficiency microalgae for biodiesel production. *Bioenergy Research* 1, 20–43.
192. Searchinger, T., Heimlich, R., Houghton, R.A., Dong, F., Elobeid, A., Fabiosa, J., Tokgoz, S., Hayes, D., Yu, T.-H., 2008. Use of U.S. croplands for biofuels increases greenhouse gases through emissions from land-use change. *Science* 319, 1238–40.
193. Sereewatthanawut, I., Prapintip, S., Watchirarujj, K., Goto, M., Sasaki, M., Shotipruk, A., 2008. Extraction of protein and amino acids from deoiled rice bran by subcritical water hydrolysis. *Bioresource Technology* 99, 555–61.
194. Sevilla, M., Fuertes, A.B., 2009. Chemical and structural properties of carbonaceous products obtained by hydrothermal carbonization of saccharides. *Chem. Eur. J.* 15, 4195–203.
195. Sevilla, M., Maciá-Agulló, J.A., Fuertes, A.B., 2011. Hydrothermal carbonization of biomass as a route for the sequestration of CO<sub>2</sub>: chemical and structural properties of the carbonized products. *Biomass and Bioenergy* 35, 3152–3159.
196. Shahidi, F., Wanasundara, N., 1998. Omega-3 fatty acid concentrates: nutritional aspects and production technologies. *Trends In Food Science & Technology* 9, 230–240.
197. Sheehan, J., Dunahay, T., Benemann, J., Roessler, P., 1998. A look back at the U.S. Department of Energy's Aquatic Species Program: Biodiesel from algae. US Department Of Energy's Office of Fuels Development. NREL/TP-580-24190.

198. Shen, Y., Yuan, W., Pei, Z., Mao, E., 2010. Heterotrophic culture of *Chlorella protothecoides* in various nitrogen sources for lipid production. *Appl. Biochem. Biotechnol* 160, 1674–84.
199. Sheng, J., Vannela, R., Rittmann, B.E., 2012. Disruption of *Synechocystis* PCC 6803 for lipid extraction. *Water Science & Technology* 65, 567–573.
200. Silva, A.S., Sanaiotti, G., Lanza, M., Follegatti-Romero, L.A., Meirelles, A.J.A., Batista, E.A.C., 2010. Mutual solubility for systems composed of vegetable oil + ethanol + water at different temperatures. *J. Chem. Eng. Data* 55, 440–447.
201. Silva, C., Weschenfelder, T.A., Rovani, S., Corazza, F.C., Corazza, M.L., Dariva, C., Oliveira, J.V., 2007. Continuous production of fatty acid ethyl esters from soybean oil in compressed ethanol. *Industrial & Engineering Chemistry Research* 46, 5304–5309.
202. Smith, B., Greenwell, H.C., Whiting, A., 2009. Catalytic upgrading of tri-glycerides and fatty acids to transport biofuels. *Energy* 2, 262–271.
203. Socha, A., Sello, J., 2010. Efficient conversion of triacylglycerols and fatty acids to biodiesel in a microwave reactor using metal triflate catalysts. *Organic & Biomolecular Chemistry* 8, 4753–4756.
204. Stamenković, O., Veličković, A., Veljković, V., 2011. The production of biodiesel from vegetable oils by ethanolysis: current state and perspectives. *Fuel* 90, 3141–3155.
205. Stubbins, A., Spencer, R.G.M., Chen, H., Hatcher, P.G., Mopper, K., Hernes, P.J., Mwamba, V.L., Mangangu, A.M., Wabakanghanzi, J.N., Six, J., 2010. Illuminated darkness: molecular signatures of congo river dissolved organic matter and its photochemical alteration as revealed by ultrahigh precision mass spectrometry. *Limnology and Oceanography* 55, 1467–1477.
206. Suryawati, L., Wilkins, M.R., Bellmer, D.D., Huhnke, R.L., Maness, N.O., Banat, I.M., 2009. Effect of hydrothermolysis process conditions on pretreated switchgrass composition and ethanol yield by SSF with *Kluyveromyces marxianus* IMB4. *Process Biochemistry* 44, 540–545.
207. Takagi, M., Watanabe, K., Yamaberi, K., Yoshida, T., 2000. Limited feeding of potassium nitrate for intracellular lipid and triglyceride accumulation of *Nannochloris* sp. UTEX LB1999. *Appl. Microbiol. Biotechnol.* 54, 112–117.
208. Takeda, H., 1991. Sugar composition of the cell wall and the taxonomy of *Chlorella* (Chlorophyceae). *Journal of Phycology* 27, 224–232.

209. Thomas, W., 1966. Effects of temperature and illuminance on cell division rates of three species of tropical oceanic phytoplankton. *Journal of Phycology* 2, 17–22.
210. Thompson, G., 1996. Lipids and membrane function in green algae. *Biochimica Et Biophysica Acta* 1302, 17–45.
211. Titirici, M., Thomas, A., Antonietti, M., 2007. Back in the black: hydrothermal carbonization of plant material as an efficient chemical process to treat the CO<sub>2</sub> problem? *New Journal of Chemistry* 31, 787–789.
212. Titirici, M.M., Thomas, A., Yu, S., Mu, J., Antonietti, M., 2007. A direct synthesis of mesoporous carbons with bicontinuous pore morphology from crude plant material by hydrothermal carbonization. *Chem. Mater.* 19, 4205–4212.
213. Tsukahara, K., Kimura, T.A.E., Minowa, T., Sawayama, S., Yagishita, T., Inoue, S., Hanaoka, T., Usui, Y., 2001. Microalgal cultivation in a solution recovered from the low- temperature catalytic gasification of the microalga. *Journal of Bioscience and Bioengineering* 91, 311–313.
214. Ulberth, F., Gabernig, R.G., Schrammel, F., 1999. Flame-ionization detector response to methyl, ethyl, propyl, and butyl esters of fatty acids. *Journal of the American Oil Chemists' Society* 76, 263–266.
215. US Department of Energy, 2011. U.s. billion-ton update: biomass supply for a bioenergy and bioproduct industry. R.D. Perlack and B.J. Stokes (Leads), ORNL/TM-2011/224. Oak Ridge National Laboratory, Oak Ridge, TN. 227.
216. USDA, 2013a. Agricultural baseline projection tables. Available Online [accessed 3-15-13]:  
<http://usda.mannlib.cornell.edu/MannUsda/viewDocumentInfo.do?documentID=1192>.
217. USDA, 2013b. Fertilizer use and price. Available Online [accessed 3-15-13]:  
<http://www.ers.usda.gov/data-products/fertilizer-use-and-price.aspx#26718>.
218. USDA, 2013c. Feed grains: yearbook tables. Available Online [accessed 3-15-13]:  
<http://www.ers.usda.gov/data-products/feed-grains-database/feed-grains-yearbook-tables.aspx>.
219. Valdez, P.J., Nelson, M.C., Wang, H.Y., Lin, X.N., Savage, P.E., 2012. Hydrothermal liquefaction of *Nannochloropsis* sp.: systematic study of process variables and analysis of the product fractions. *Biomass and Bioenergy* 46, 317–331.

220. Van Kasteren, J., Nisworo, A., 2007. A process model to estimate the cost of industrial scale biodiesel production from waste cooking oil by supercritical transesterification. *Resources, Conservation and Recycling* 50, 442–458.
221. Varma, M., Deshpande, P., Madras, G., 2010. Synthesis of biodiesel in supercritical alcohols and supercritical carbon dioxide. *Fuel* 89, 8–13.
222. Vieitez, I., Alckmin, I., Castilhos, F. De, Oliveira, J.V., Grompone, M.A., Jachmanián, I., 2011. Stability of ethyl esters from soybean oil exposed to high temperatures in supercritical ethanol. *The Journal of Supercritical Fluids* 56, 265–270.
223. Vieitez, I., Silva, C. da, Alckmin, I., Borges, G., Corazza, F., Oliveira, J., Grompone, M., Jachmanian, I., 2008. Effect of temperature on the continuous synthesis of soybean esters under supercritical ethanol. *Energy & Fuels* 23, 558–563.
224. Vieitez, I., Silva, C. da, Borges, G., Corazza, F., Oliveira, J., Grompone, M., Jachmanian, I., 2008. Continuous production of soybean biodiesel in supercritical ethanol-water mixtures. *Energy & Fuels* 22, 2805–2809.
225. Wahlen, B.D., Willis, R.M., Seefeldt, L.C., 2011. Biodiesel production by simultaneous extraction and conversion of total lipids from microalgae, cyanobacteria, and wild mixed-cultures. *Bioresource Technology* 102, 2724–2730.
226. Wang, Y., Wang, X., Liu, Y., Ou, S., Tan, Y., Tang, S., 2009. Refining of biodiesel by ceramic membrane separation. *Fuel Processing Technology* 90, 422–427.
227. Warabi, Y., Kusdiana, D., Saka, S., 2004. Reactivity of triglycerides and fatty acids of rapeseed oil in supercritical alcohols. *Bioresource Technology* 91, 283–287.
228. Watchararuji, K., Goto, M., Sasaki, M., Shotipruk, A., 2008. Value-added subcritical water hydrolysate from rice bran and soybean meal. *Bioresource Technology* 99, 6207–13.
229. Weyer, K., Bush, D., Darzins, A., Willson, B., 2010. Theoretical maximum algal oil production. *Bioenerg. Res.* 3, 204–213.
230. Widjaja, A., Chien, C., Ju, Y., 2009. Study of increasing lipid production from fresh water microalgae *Chlorella vulgaris*. *Journal of the Taiwan Institute of Chemical Engineers* 40, 13–20.
231. Witt, U., Koske, P., Kuhlmann, D., Lenz, J., Nellen, W., 1981. Production of *Nannochloris* sp. (Chlorophyceae) in large-scale outdoor tanks and its use as a food organism in marine aquaculture. *Aquaculture* 23, 171–181.

232. Wu, F., Wang, J., Chen, W., Shuai, S., 2009. A study on emission performance of a diesel engine fueled with five typical methyl ester biodiesels. *Atmospheric Environment* 43, 1481–1485.
233. Xiong, W., Gao, C., Yan, D., Wu, C., Wu, Q., 2010. Double CO<sub>2</sub> fixation in photosynthesis – fermentation model enhances algal lipid synthesis for biodiesel production. *Bioresource Technology* 101, 2287–2293.
234. Xiong, W., Li, X., Xiang, J., Wu, Q., 2008. High-density fermentation of microalga *Chlorella protothecoides* in bioreactor for microbio-diesel production. *Appl. Microbiol. Biotechnol.* 78, 29–36.
235. Xu, H., Miao, X., Wu, Q., 2006. High quality biodiesel production from a microalga *Chlorella protothecoides* by heterotrophic growth in fermenters. *Journal of Biotechnology* 126, 499–507.
236. Yamaberi, K., Takagi, M., Yoshida, T., 1998. Nitrogen depletion for intracellular triglyceride accumulation to enhance liquefaction yield of marine microalgal cells into a fuel oil. *Journal of Marine Biotechnology* 6, 44–48.
237. Yan, S., Dimaggio, C., Mohan, S., Kim, M., Salley, S.O., Ng, K.Y.S., 2010. Advancements in heterogeneous catalysis for biodiesel synthesis. *Top. Catal.* 53, 721–736.
238. Yan, W., Acharjee, T.C., Coronella, C.J., Va, V.R., 2009. Thermal pretreatment of lignocellulosic biomass. *Environmental Progress & Sustainable Energy* 28, 435–440.
239. Yan, W., Hastings, J., Acharjee, T., Coronella, C.J., Vásquez, V., 2010. Mass and energy balances of wet torrefaction of lignocellulosic biomass. *Energy & Fuels* 24, 4738–4742.
240. Yang, C., Hua, Q., Shimizu, K., 2000. Energetics and carbon metabolism during growth of microalgal cells under photoautotrophic, mixotrophic and cyclic light-autotrophic/dark-heterotrophic conditions. *Biochemical Engineering Journal* 6, 87–102.
241. Yang, C., Hua, Q., Shimizu, K., 2002. Integration of the information from gene expression and metabolic fluxes for the analysis of the regulatory mechanisms in *synechocystis*. *Applied Microbiology and Biotechnology* 58, 813–22.
242. Zhang, S., Wang, Z., Xu, S., 2007. Optimization of the aqueous enzymatic extraction of rapeseed oil and protein hydrolysates. *Journal of the American Oil Chemists' Society* 84, 97–105.

243. Zhang, X., Hu, Q., Sommerfeld, M., Puruhito, E., Chen, Y., 2010. Harvesting algal biomass for biofuels using ultrafiltration membranes. *Bioresource Technology* 101, 5297–5304.
244. Zhou, D., Zhang, S., Fu, H., Chen, J., 2012. Liquefaction of macroalgae *enteromorpha prolifera* in sub-/supercritical alcohols: direct production of ester compounds. *Energy & Fuels* 26, 2342–2351.
245. Zhu, G., Zhu, X., Fan, Q., Wan, X., 2011. Recovery of biomass wastes by hydrolysis in sub-critical water. *Resources, Conservation and Recycling* 55, 409–416.
246. Zhu, G.-Y., Zhu, X., Wan, X.-L., Fan, Q., Ma, Y.-H., Qian, J., Liu, X.-L., Shen, Y.-J., Jiang, J.-H., 2010. Hydrolysis technology and kinetics of poultry waste to produce amino acids in subcritical water. *Journal of Analytical and Applied Pyrolysis* 88, 187–191.
247. Zhu, X., Zhu, C., Zhao, L., Cheng, H., 2008. Amino acids production from fish proteins hydrolysis in subcritical water. *Chinese Journal of Chemical Engineering* 16, 456–460.
248. Zittelli, G.C., Lavista, F., Bastianini, A., Rodolfi, L., Vincenzini, M., Tredici, M.R., 1999. Production of eicosapentaenoic acid by *Nannochloropsis* sp. cultures in outdoor tubular photobioreactors. *Journal of Biotechnology* 70, 299–312.